Light-Driven Molecular Motors and Switches in Confined Environments

Gábor London

The work described in this thesis was carried out at the Stratingh Institute for Chemistry, University of Groningen, The Netherlands.

The work described in this thesis was financially supported by NanoNed.

Printed by: Ipskamp Drukkers B.V. Enschede, The Netherlands

RIJKSUNIVERSITEIT GRONINGEN

Light-Driven Molecular Motors and Switches in Confined Environments

Proefschrift

ter verkrijging van het doctoraat in de
Wiskunde en Natuurwetenschappen
aan de Rijksuniversiteit Groningen
op gezag van de
Rector Magnificus, dr. E. Sterken,
in het openbaar te verdedigen op
vrijdag 23 september 2011
om 11.00 uur

door

Gábor London

geboren op 31 mei 1983
te Szeged, Hongarije

Promotor:	Prof. dr. B. L. Feringa
Beoordelingscommisie:	Prof. dr. A. J. M. Driessen
	Prof. dr. J. G. Roelfes
	Prof. dr. P. Rudolf

ISBN: 978-90-367-5081-3 (printed version)
ISBN: 978-90-367-5082-0 (electronic version)

Anyukának, Apukának
Márinak, Gyereknek

Table of contents

Chapter 1 Controlling wetting and mass-transport with monolayers of photoresponsive molecular switches **1**
1.1 Introduction 2
1.2 Theoretical background 3
1.2.1 Surface energy and surface tension 3
1.2.2 Wetting 4
1.3 Photochromic compounds for control of surface energy 8
1.3.1 Azobenzenes 8
1.3.2 Spiropyrans 8
1.3.3 Dithienylethenes 9
1.3.4 Stilbenes 10
1.3.5 Other photoresponsive surfaces 10
1.4 Controlling wettability with molecular switches 11
1.4.1 Influence of functional groups 11
1.4.2 Type of surface, anchoring functional group and surface coverage 17
1.4.3 Surface roughness 20
1.5 Light-induced liquid motion on photoresponsive monolayers 24
1.5.1 Azobenzenes 24
1.5.2 Spiropyrans 26
1.5.3 Rotaxanes 26
1.6 Potential of molecular motors in surface energy control 28
1.7 The aim and outline of the thesis 31
1.8 References 32

Chapter 2 Light-driven altitudinal molecular motors: design, synthesis and characterization in solution **39**
2.1 Introduction 40
2.2 Molecular design 43
2.2.1 Previously synthesized structures 43
2.2.2 Novel design 44
2.2.3 Surface modification strategies 45
2.3 Synthesis of altitudinal molecular motors 46
2.3.1 Synthesis of molecules for direct attachment 46

2.3.2 Synthesis of molecules for interfacial reactions 52
2.4 Photochemical and thermal isomerization studies 55
2.4.1 UV-Vis spectroscopy 57
2.4.2 CD-spectroscopy 58
2.4.3 ^{1}H-NMR spectroscopy 59
2.5 Discussion 60
2.6 Conclusions 62
2.7 Experimental 63
2.8 References 74

Chapter 3 Attachment of molecular motors to inorganic surfaces 77
3.1 Introduction 78
3.2 Attachment of silane-functionalized motors to silicon and quartz surfaces 79
3.2.1 Introduction to silane-based SAMs 79
3.2.2 Attachment of a triethoxysilane-functionalized motor to silicon (Si/SiO_2) and quartz substrates 82
3.3 Assembly of molecular motors on mica surface 86
3.3.1 Surface modification and characterization 87
3.4 Functionalization of inorganic surfaces with motors containing OH-groups 92
3.5 Discussion and Conclusion 95
3.6 Experimental 97
3.7 References 100

Chapter 4 Adhesion of photon-driven molecular motors to surfaces *via* 1,3-dipolar cycloadditions: effect of interfacial interactions on molecular motion 105
4.1 Introduction 106
4.1.1 Interfacial reactions 106
4.1.2 Attachment of dialkyne-motor to azide-functionalized surfaces 107
4.2 Azide-functionalized surfaces: preparation and characterization 108
4.3 Interfacial click-reaction for motor attachment 111
4.3.1 UV-vis spectroscopy, water contact angle and ellipsometry measurements 112

4.3.2 XPS and ATR-IR measurements 115
4.4 Rotation on the surface 116
4.5 Click-reaction prior to surface modification 116
4.6 Attachment of a diazide-motor to alkyne-functionalized surfaces 118
4.7 Effect of confinement on the speed of rotary motion – kinetics on surface 121
4.7.1 Effect of surface coverage on the speed of the rotary motion 123
4.7.2 Effect of the valency of the attachment on the speed of the rotary motion 125
4.8. Interfacial click-reaction on gold surface 130
4.9 Conclusions 131
4.10 Experimental section 132
4.11 References 138

Chapter 5 Functionalized altitudinal molecular motors on surfaces 143
5.1 Introduction 144
5.2 Synthesis of functionalized molecular motors 146
5.2.1 Molecular motor with perfluoroalkyl-chain 146
5.2.2 Molecular motor with cyano-group 151
5.3 Photochemical and thermal isomerization studies in solution 153
5.3.1 UV-vis spectroscopy: perfluorobutyl motor 153
5.3.2 ^{1}H NMR-spectroscopy: perfluorobutyl-motor 155
5.3.3 UV-vis spectroscopy: cyano–motor 156
5.3.4 ^{1}H NMR-spectroscopy: cyano-motor 158
5.4 Attachment to quartz surface 159
5.4.1 Perfluoralkyl-motor on quartz 160
5.4.2 Cyano-motor on quartz 164
5.5 Discussion and conclusions 167
5.5.1 Switching of wetting properties 168
5.6 Acknowledgement 170
5.7 Experimental 170
5.8 References 185

Chapter 6 Light-induced control of protein translocation by the SecYEG complex **189**
6.1 Introduction 190
6.2 Control of protein translocation with an azobenzene photoswitch 192
6.2.1 Structural considerations and synthesis of an azobenzene switch 192
6.2.2 Incorporation of the azobenzene switch into the SecYEG protein complex 195
6.2.3 Light-induced switching inside SecYEG protein complex 196
6.2.4 Effect of isomerization on the translocation activity 197
6.3 Discussion 202
6.4 Conclusions 203
6.5 Acknowledgement 204
6.6 Experimental 204
6.7 References 208

Summary **211**

Samenvatting **215**

Összefoglaló **219**

Acknowledgement **223**

Chapter 1

Controlling wetting and mass-transport with monolayers of photoresponsive molecular switches

In this chapter recent progress on the control of surface energy in a reversible manner with light using monolayers of photoswitchable molecules is discussed. An overview on the construction of surfaces with photoregulated wettability and light-guided liquid motion is presented with particular emphasis on practical aspects of the design. The importance of the types of surfaces, functional groups, surface coverage and surface structuring will be illustrated with relevant literature examples.

1.1 Introduction

One of the major challenges in nanotechnology is to demonstrate that molecular machines[1,2] can perform useful work.[3] Inspired by the machines of the macroscopic world molecular tweezers, propellers, gears, brakes, elevators, valves, rotors and switches have been developed.[1] Additionally, it has been shown that molecular switches and motors can be used to perform different tasks in solution, such as modulation of supramolecular organization,[4,5] host-guest interactions[6], fluorescence[7] or catalysis.[8,9] However, their uncontrolled, thermal rotational and translational motion in solution sets a limitation for many possible further applications which would require more order and coherence of the molecules.

In recent years increasing attention has focused on surface immobilized systems containing molecules that are capable of undergoing reversible structural changes upon the application of external stimuli.[10-12] Confining molecules at an interface prevents Brownian motion and allows to exploit externally induced reversible structural changes in order to perform work or modify the surface properties of a material.[11,13]

Various types of external stimuli i. e., electrical, thermal, magnetic, optical and chemical, can be applied to address molecules on surfaces.[14] The use of photons is of particular interest due to the fast response times of photochemical processes and because light provides a clean, non-invasive and tunable energy input.[2,10,12]

Among the most widely explored applications of photoresponsive molecules on surfaces[11,12] are the reversible control of wettability and the induction of liquid motion on solid substrates or in microfluidic channels.[15-17]

In this chapter recent progress in reversible surface energy control by light using monolayers of photochemical molecular switches is discussed. An overview on the construction of surfaces displaying photoregulated wettability and on light-guided liquid motion is given with particular emphasis on the practical aspects of the design. The importance of the types of surfaces, functional groups, surface coverage and surface structuring will be illustrated with relevant literature examples.

1.2 Theoretical background

1.2.1 Surface energy and surface tension

Surfaces of materials have different properties compared to the bulk. The reason for this is that the components of the materials at the bulk benefit from interactions with all of their neighbors, while the ones at the interface loosing much of these stabilizing interactions and existing in a higher energy state (Figure 1a).[18]

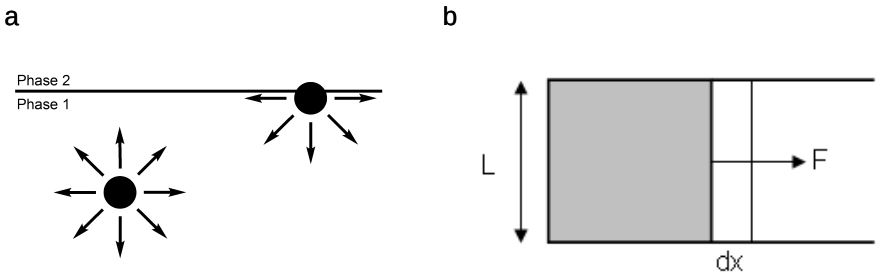

Figure 1 (a) Components at the interfacial region benefit less from stabilizing interactions with neighbors compared to components in the bulk. (b) Surface tension is measured by the normal force acting on a unit length of a line on a surface.[18]

Therefore, to bring more of the components of the material from the bulk to the surface to create more surface area requires energy input. The work (dW) required to increase the surface area by a length dx:

$$dW = \gamma \cdot dx \cdot L = \gamma \cdot dA \qquad \text{Eq 1}$$

where γ is the *surface/interfacial energy* (unit: J/m^2).

Another way to illustrate the difference between the surface and the bulk of a material is the introduction of *surface/interfacial tension*. Surface tension can be understood as a force (F) along a line of unit length (L) that is involved in stretching a film (Figure 1b). The force is parallel to the surface and perpendicular to the line.

$$F = \gamma \cdot L \qquad \text{Eq 2}$$

where γ is the surface/interfacial tension (unit: N/m).

It has to be noted that although many authors interpret surface energy and surface tension as interchangeable definitions,[19] others advocate that they are discreet and different quantities that are mathematically equivalent at equilibrium.[20]

Surfaces can be divided into two types: low energy and high energy surfaces.[18] Materials dominated by van der Waals interactions (molecular crystals of fluorocarbons or hydrocarbons), generally have lower surface energies compared to those dominated by strong chemical bonding (covalent, ionic or metallic). A high energy surface tends to adsorb materials more readily under ambient conditions.

1.2.2 Wetting

Wettability, the behavior of liquids on surfaces, is a property of solids that is important in natural systems and in a range of industrial applications.[16,21] Measurement of contact angles (CA) (θ) of liquids on solid surfaces is a common technique to determine their wettability.

When a liquid drop is placed on a solid surface it either spreads completely (complete wetting) or forms a spherical cap resting on the substrate (partial wetting) with a CA value of θ. To distinguish these two types of wetting the *spreading parameter*, *S*, is introduced (Eq 3 and 4), which measures the difference between the surface energy of the substrate when dry and wet[18]:

$$S = (E_{substrate})_{dry} - E(_{substrate})_{wet} \qquad \text{Eq 3}$$

or

$$S = \gamma_{sg} - (\gamma_{sl} + \gamma_{lg}), \qquad \text{Eq 4}$$

where γ_{sg}, γ_{sl} and γ_{lg} stand for the interfacial free energies of the solid-gas, liquid-gas and solid-liquid interfaces, respectively. When $S > 0$ the liquid spreads completely, when $S < 0$ the wetting is only partial.

The basic equation of wetting was formulated by Young in 1805.[22] *Young's equation* (Eq 5) relates the contact angle (θ) of a liquid drop on solid surface to the interfacial free energies assuming that the system is in thermodynamic equilibrium and the surface is ideal (e.g., roughness, chemical heterogeneity, surface reconstruction, swelling and dissolution are neglected) (Figure 2). The possible contact angles are ranging from 0° (complete wetting) to 180° (complete dewetting). Based on Eq 5, hydrophilic surfaces exhibit a CA of less than 90°, while in the case hydrophobic surfaces CA is higher than 90°.

$$\gamma_{sg} = \gamma_{lg} \cdot \cos\theta + \gamma_{sl} \qquad \text{Eq 5}$$

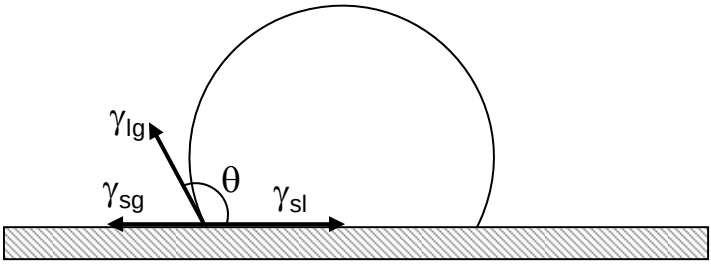

Figure 2 If a liquid does not spread completely, a drop has a CA value of θ on the surface. Young`s equation (Eq 5) is derived from the balance of forces operating on the contact line.

It has been realized[23,24] that the effect of surface roughness and chemical heterogeneity on wettability may lead to deviations from the Young-equation which assumes the surfaces to be ideal. Two models have been developed to explain the effect of these features on the apparent contact angle of liquid drops (Figure 3).[23,24]

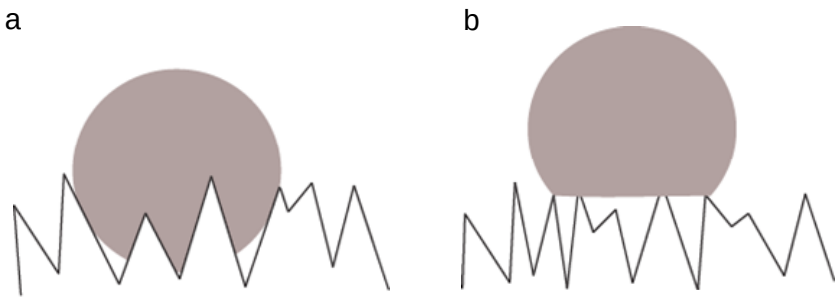

Figure 3 Wetting of rough surfaces. Wenzel-state of wetting (a) and Cassie-state of wetting (b).

The *Wenzel model*[23] describes a situation where a droplet wets a rough surface following the roughness features (Figure 3a). In this case the roughness increases the area of the solid-liquid interface by a factor *r* (surface roughness) compared to the smooth surface and amplifies the contact angle according to the expression:

$$\cos\theta^* = r \cdot \cos\theta \qquad \text{Eq 6}$$

where θ* is the apparent contact angle on the rough surface and θ is the equilibrium contact angle on an ideal surface of the same material, given by the Young-equation.

The *Cassie/Baxter model*[24] postulates that in the case of rough materials with hydrophobic surface chemistry and/or pronounced surface roughness droplets prefer to rest on top of the roughness features, with air trapped underneath (Figure 3b). The pockets of air trapped under the liquid drop can be considered as non-wetting areas of the solid/air composite surface. If φ is the fraction of the solid in contact with the liquid, the contact angle can be calculated as follows:

$$\cos\theta^* = \varphi \cdot \cos\theta + \varphi - 1 \qquad \text{Eq 7}$$

Both Wenzel's and Cassie's model are valid only if the size of the liquid drop is large compared to the roughness features. Wenzel and Cassie states of wetting can also coexist on rough surfaces depending on how the drop was deposited.[16,25]

It has to be noted, that according to recent discussion in the literature,[20,26] conditions at the three-phase (solid-liquid-gas) contact line are much more important than those under the entire droplet in determining the apparent contact angle. To take this into account, in the above equations (Eq 6 and Eq 7) the local values of r and φ in the vicinity of the contact line should be used.[27,28]

Another important feature for characterizing wettability is *contact angle hysteresis*.[29-31] It implies that when a liquid spreads and then retracts from a surface there is a difference between the advancing (θ_{adv}) and the receding (θ_{rec}) contact angles (Figure 4). In solid-liquid contacts, hysteresis has been attributed to surface roughness or chemical heterogeneity.[29-31] Due to the surface structures, kinetic barriers prevent the drops to reach the minimum-energy state described by the Wenzel and Cassie models.[32] As a result a number of static CAs are possible, representing different metastable states, depending on the droplet volume, mode of deposition, liquid evaporation or surface roughness topology.

Dynamic contact angles θ_{adv} and θ_{rec} can be measured *via* two methods (Figure 4).[18] In one method volume is added and removed from a drop while the contact angle is dynamically measured (Figure 4a). Liquid is added until the three-phase line increases in diameter, thus increasing wetting. The highest contact angle before spreading of the liquid is θ_{adv}. To measure θ_{rec} volume is removed from the

droplet until the liquid retracts. The minimum contact angle before the three-phase line decreases in diameter is θ_{rec}.

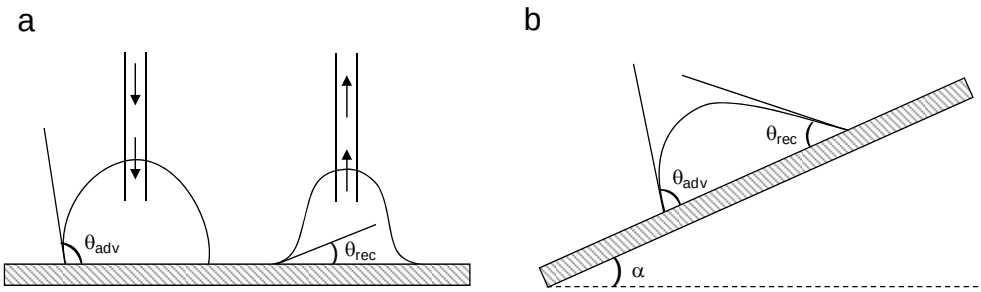

Figure 4 Methods to measure dynamic contact angles of liquids on solid surfaces. (a) Addition and removal of liquid from a droplet until the contact area begins to change. (b) Tilting a surface with a liquid droplet on top until the contact area is changing. The advancing (θ_{adv}) and receding (θ_{rec}) contact angles are the maximum and minimum contact angles, respectively, before the contact area begins to change. The contact angle hysteresis is the difference between θ_{adv} and θ_{rec}.

The other method to measure θ_{adv} and θ_{rec} of a liquid on a surface is the tilting method (Figure 4b). In this method first a sessile drop is produced while the stage is at $\alpha = 0°$. As the tilt angle (α) increases the contact angle on the downhill side (θ_{adv}) increases while the contact angle on the uphill side (θ_{rec}) decreases. At some point the drop may roll off. The maximum downhill angle and the smallest uphill angle measured prior to roll off represent the advancing and receding contact angles. The contact angle hysteresis is the difference between θ_{adv} and θ_{rec}.

Contact angle hysteresis of a liquid droplet on a solid surface is also influencing the *droplet mobility*.[29] CA hysteresis is a reflection of the activation energy required for a droplet to move on a surface from one metastable state to another. The lower the CA hysteresis (the difference between θ_{adv} and θ_{rec}), the easier the droplet moves on the surface. According to a recently suggested definition of hydrophobicity, a solid substrate that exhibit low CA with test liquids can be hydrophobic (lyophobic) if the drops move easily on its surface.[32]

1.3 Photochromic compounds for control of surface energy

1.3.1 Azobenzenes

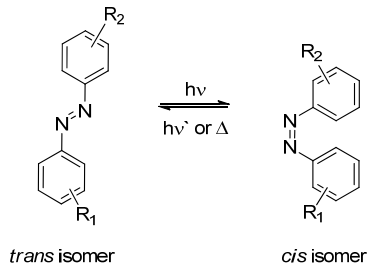

Scheme 1 Reversible photoisomerization of azobenzenes.

Azobenzenes[33](Scheme 1) are among the most frequently used photochromic units that are incorporated into molecular systems including self-assembled monolayers (SAMs),[12,15] polymers[34,35] and biomolecules[36-38] to affect and control their physical, chemical and biological properties. The origin of the popularity of azobenzenes in such applications are their relatively facile syntheses, sensitive and fatigue resistant *cis* → *trans* and *trans* → *cis* photoisomerization accompanied by large changes in size and dipole moment. A drawback of these switches is the often modest thermal stability of the less stable *cis*-isomer.

1.3.2 Spiropyrans

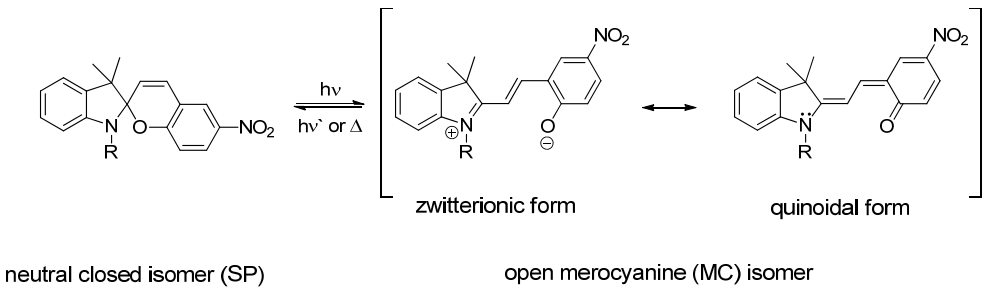

Scheme 2 Reversible photoisomerization of spiropyrans.

Spiropyrans (SPs) (Scheme 2) are molecular switches that can undergo reversible photoisomerization between a stable SP form and a metastable merocyanine (MC) form upon irradiation with UV or visible light.[39] The reversible photochemical switching between the relatively hydrophobic SP and the more polar MC forms induces a large change in molecular dipole moment. It should be noted that the zwitterionic MC form is the major contributor to the structure of the open form, since in the neutral quinoidal form the aromaticity of the oxygen-bearing ring is lost.

1.3.3 Dithienylethenes

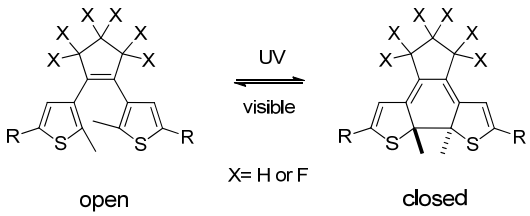

Scheme 3 Reversible photocyclization of 1,2-dithienylethenes.

1,2-Dithienylethenes (Scheme 3) undergo reversible photocyclization between an open form and a closed form by UV or visible light irradiation.[40,41] Among the photochromic compounds, dithienylethenes have excellent thermal stability of both isomers and high fatigue resistance, however, compared to azobenzenes or spiropyrans, no remarkable polarity changes are observed upon photoswitching. Despite the lack of change in dipole moment, control of the wettability of the surfaces of some thin films of dithienylethenes is still possible, due to the reversible morphological changes that occur upon irradiation with UV and visible light.[42,43,44]

1.3.4 Stilbenes

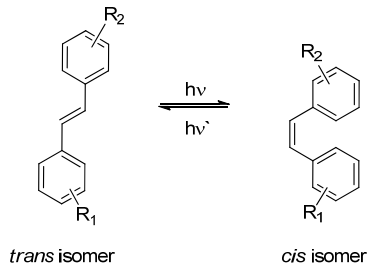

Scheme 4 Photochemical trans/cis isomerization of stilbenes.

Although the reversible *cis/trans* isomerization of stilbene (Scheme 4) and its derivatives is thoroughly studied,[45,46] their application in the construction of photoresponsive surfaces is rather limited.[47-51] Their tendency to undergo undesired photochemical side-reactions in confined environments makes them somewhat unattractive in such applications.[47,48,50]

1.3.5 Other photoresponsive surfaces

It should be noted that apart from the SAMs of the above mentioned photochromic switches there are other organic and inorganic surfaces that could be applied for light-controlled reversible surface energy modulation. These include pyrimidine-terminated monolayers[52,53] that can undergo photodimerization when irradiated with UV-light resulting in a pK_a change that can affect wettability. Alternatively, malachite green derivatives,[54] have been used to construct multi-responsive surfaces whose wettability could be controlled either by light or by pH. Furthermore, molecular switches are not only used in SAMs, but also as part of polymeric materials to modulate surface properties.[34,35,55-58] Inorganic oxide materials such as TiO_2 and ZnO, SnO also attracted much attention due to their photoinduced redox and morphological changes that can be used to achieve light-induced wettability-control of surfaces.[15] Since this summary focuses on SAMs of molecular switches/motors, the latter systems will not be discussed.

1.4 Controlling wettability with molecular switches

Controlling wettability means being able to modify a surface to turn it from non-wettable into wettable or vice versa. It can be achieved by changing surface energy, thus changing the affinity of liquids for the surface. To make hydrophilic surfaces hydrophobic, coatings of monolayers of hydrocarbons or fluorocarbons or polymers of these types of materials are used. Surfaces can be made hydrophilic by coating them with thin layers of metals or using plasma or UV/ozone treatment to generate hydrophilic groups.[18]

Attaching molecular motors and switches to surfaces provide new possibilities for wettability control. Their ability to undergo reversible changes in chemical and physical properties facilitates the fabrication of multi-functional interfaces that could allow for reversible switching from one desired function to another.

To achieve wettability control the key property is the structural change upon photoisomerization, which determines the hydrophilic and hydrophobic nature of the isomers.

Although the reversible isomerization of the switching units is crucial to realize photoregulated surface-wetting, additional design elements, such as the nature of the functional groups, types of surfaces, surface-anchoring groups, spacer-length, surface coverage, and surface-structuring has to be considered in order to create systems of practical use.

1.4.1 Influence of functional groups

1.4.1.1 Azobenzenes

It has been shown in several reports[59-62] that due to the inherent changes in polarity that accompany structural changes upon isomerization, azobenzenes can affect surface free energy in monolayer assemblies, even without an additional functional group present at the surface to ensure sufficient polarity change. Changes in water contact angle (WCA) from 2-14°[59,60,61] have been found for azobenzene monolayers upon isomerization between the less polar *trans* and the more polar *cis*-isomer.

Incorporating additional functional groups can enhance the effect of isomerization on wettability. In a study by Siewierski et al.[59] unsubstituted and *p*-pentyl-substituted azobenzene monolayers on silicon wafers were compared. They found that monolayers of *p*-pentyl-substituted azobenzenes produced WCA

changes up to 9° after photochemical switching, while unsubstituted switches showed only a difference of 4-5° between the *trans* and *cis* form. Yang et al. measured similar wettability changes for *p*-pentyl-substituted azobenzenes.[63] They found a 12.4° change in WCA upon isomerization of the azobenzenes from *trans* to *cis*. Ichimura et al. constructed monolayers of *p*-octyl-azobenzenes attached to calix[4]resorcinarene derivatives (Figure 5), which showed an 8° WCA change upon *trans* to *cis* isomerization.[64-66] This value is slightly higher than the 6° difference in the case of *p*-hexyl-azobenzenes, attached to silica surfaces by silylation as demonstrated by the same group.[64,67]

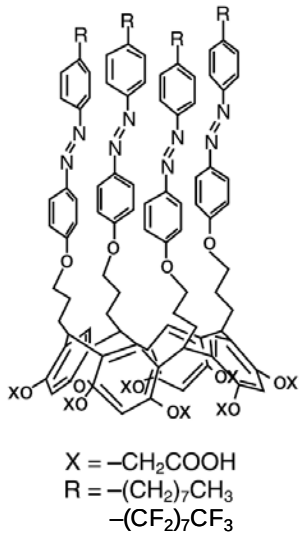

Figure 5 Azobenzene functionalized calix[4]resorcinarene derivatives used for surface energy control by Ichimura and co-workers. (Figure reproduced from ref. 65.)

Because of their low surface energy, fluorinated alkyl chains are often used as hydrophobic functional groups in azobenzenes.[62,64,68,69] In the case of short fluoroalkyl groups (CF_3, OCF_3), however, the effect of photoisomerization on flat surfaces remains modest with a WCA change of 5-6°.[62,69] Azobenzene monolayers containing longer fluoroalkyl chains were studied by Ichimura et al.[64] They found that a monolayer of calix[4]resorcinarene functionalized with *p*-perfluorooctyl-azobenzenes (Figure 5, R= $(CF_2)_7CF_3$) showed a high WCA of 104-105°. Surprisingly, however, in contrast to *p*-octylazobenzenes, upon irradiation of the

monolayer with UV-light almost no change (~ 0.5°) in contact angle was observed, although switching of the azobenzenes was shown by UV-vis spectroscopy. A possible explanation for this observation is that the fluoroalkyl chains remain exposed to the interface even after the *trans* to *cis* isomerization takes place.

There are only a limited number of studies available in the literature on azobenzenes in a non-polymer based surface assembly with hydrophilic functional groups for which WCA changes are reported upon photoisomerization of the molecules.[70,71] Demirel et al. reported the assembly of 4-(4`-aminophenylazo) benzoic acid by an interfacial reaction with an epoxysilane SAM on Si/SiO_2.[70] (Figure 6a) The resulting carboxylic acid terminated azobenzene monolayer was irradiated alternating with UV and visible light and found to undergo reversible isomerization processes with a remarkable difference in the WCA of 40° between the *trans* and the *cis* geometry of the azobenzene.

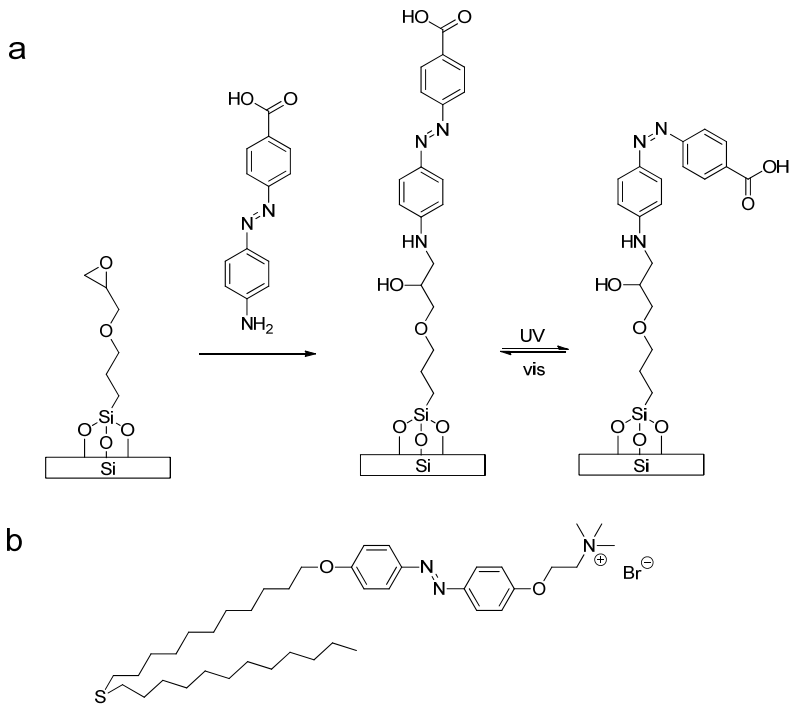

Figure 6 Azobenzenes with hydrophilic functional groups for wettability control. (a) Functionalization of epoxy-terminated SAMs with 4-(4`-aminophenylazo) benzoic acid. (b) Azobenzene containing quaternary ammonium salt assembled on a platinum electrode.

Callari et al. assembled a quaternary ammonium salt functionalized azobenzene (Figure 6b) on an ultrathin platinum electrode in order to coordinate porphyrin derivatives.[71] As part of the characterization the WCA change upon isomerization of the azobenzenes was measured, which was around 10°. The molecule used for self-assembly was a non-symmetric thioether with the azobenzene unit on one side and a dodecane chain on the other (Figure 6b), so the resulting SAM could be considered as a mixed monolayer, which is likely to influence the WCA value.

1.4.1.2 Spiropyrans

Most of the efforts towards surface wettability control with SPs[72-78] rely on the photoinduced formation of the open MC form (Scheme 5). Despite the formation of the charged species, however, the WCA changes induced by a monolayer of SPs on flat surfaces are only in the range of 5-14°,[72,74] comparable with azobenzene monolayers.

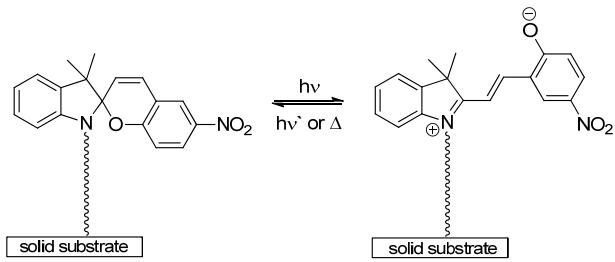

Scheme 5 Photoinduced isomerization of spyropirans on solid surfaces. Wettability control is based on the reversible formation of the zwitterionic MC-form.

1.4.1.3 Stilbenes

Although stilbene and its derivatives are a thoroughly studied group of photoswitches,[45,46] their application in the construction of photoresponsive surfaces is limited.[47-51] Their tendency to undergo undesired photochemical side-reactions (e.g. photocyclization, dimerization) in confined environments makes them somewhat unattractive in such applications.[47,48,50]

Nevertheless, functionalized stilbenes and stilbene derivatives were used to modify surface wettability. Wolf and Fox studied stilbene monolayers on gold substrates containing a cyano end-group as a hydrophilic moiety.[47,48] Upon irradiation of a surface bearing the *cis*-derivative, irreversible WCA changes of up to 15° were observed, however, surfaces modified with the *trans*-derivative

showed no change upon irradiation. Moreover, longer irradiation times led to photodimerization within the monolayer.

Gulino et al. covalently assembled stilbene derivatives on Si(100) surfaces *via* interfacial hydrosilylation containing either no substituent or a Cl-group in the *para*-position of the aromatic ring[51] (Figure 7). It was found that the surface bound molecules undergo reversible photoisomerization, without photocyclization that would limit their applicability. This stability could be due to the electron-withdrawing CN-substituent at the vinylic position (Figure 7). The reversible WCA changes reported for the H-terminated stilbenes (Figure 7, X=H) were around 5°.

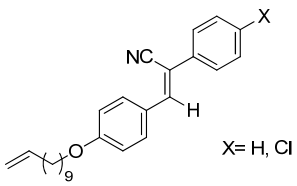

Figure 7 Stilbene-derivative used by Gulino et al.[51] for covalent monolayer formation. The lack of photocyclization observed on the surface is attributed to the electron-withdrawing CN-group at the vinylic position.

Photoswitchable surfaces based on dipyridylethylene[49] (Scheme 6) and stilbene-4,4`-dicarboxylic acid[50] on a gold surface (Figure 8) obtained *via* a non-covalent assembly approach were studied by the group of McGimpsey.

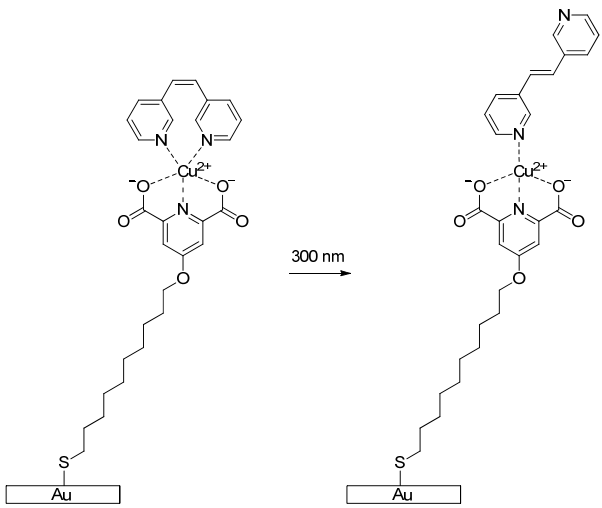

Scheme 6 Non-covalent approach for wettability control using dipyridylethylene.[49] Only *cis*-to-*trans* isomerization was observed probably due to the high packing density on gold.

Both *cis* and *trans*-dipyridylethylenes were assembled. The *cis*-dipyridylethylene based system[49] (Scheme 6) was found to undergo photochemical isomerization to the *trans*-isomer resulting in a WCA change of approximately 20°. This change, however, was found to be irreversible; *trans* → *cis* isomerization of the monolayer could not be achieved. The *trans*-isomer based assembly, however, did not undergo photoisomerization, probably due to the ordered and dense packing of the molecules which creates a steric barrier to isomerization. The possible contribution of the Cu(II)-coordination on the photochemical activity is not clear.

A similar supramolecular arrangement on a gold surface using *cis* and *trans*-stilbene-4,4`-dicarboxylic acid was constructed[50] (Figure 8). Photocontrol of wettability could not be obtained in the case of surfaces with full coverage. After irradiation of both *cis* and *trans*-stilbene functionalized surfaces with 240 and 350 nm light, respectively, no evidence of *cis*/*trans* isomerization was observed spectroscopically. Instead, the assembled films underwent irreversible chemical changes upon exposure to UV-irradiation indicated by WCA and IR measurements. This change in the chemical composition could be due to the removal of the stilbenes or more likely due to their photodimerization reaction. In a mixed monolayer assembly, however, two successful switching cycles could be achieved using both the *cis* and the *trans* isomers with a WCA change of around 25°[50] (Figure 8). Further irradiation resulted in the convergence of the measured WCAs

to an intermediate value between the WCAs exhibited by the surfaces containing pure *cis* or pure *trans* stilbenes.

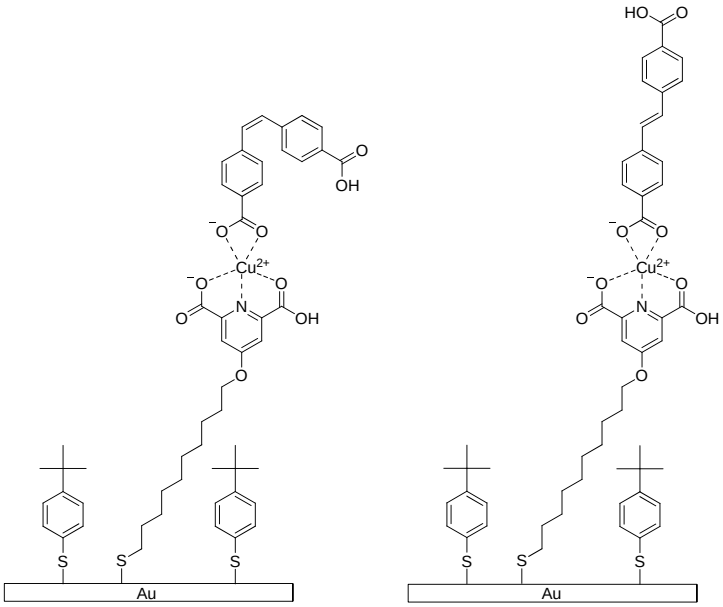

Figure 8 Non-covalent self-assembly approach for surface energy control in a mixed monolayer using *cis* and *trans* stilbene dicarboxylic acids.[50] Reversible switching of both *cis* and *trans* isomers was observed only in a mixed monolayer assembly.

1.4.2 Type of surface, anchoring functional group and surface coverage

The surface of choice, the functional groups for attachment and the surface coverage are related features and should be considered together in the design of surfaces with photocontrolled wettability. The most frequently applied materials for the preparation of SAMs are gold films and silicon wafers containing a SiO_2 overlayer.[79] Silicon-based surfaces, however, have advantages over gold which makes them more popular in the construction of photoresponsive monolayers. Importantly, the formation of a strong covalent bond between silicon substrates and organic molecules allows the preparation of robust monolayers that tolerate harsh conditions[79-81] (*i. e.* sonication in a range of organic solvents or water, high temperatures *etc*.). Additionally, silicious materials facilitate the analysis of the resulting monolayers with a range of routine characterization techniques such as UV-vis, CD and IR-spectroscopy. Compared to Si-based materials, monolayers on

gold based on Au-S bonding have somewhat lower thermal[82] and photochemical[83,84] stability.

It is noted, however, that, possibly due to the difficulties with purification of alkoxysilane and chlorosilane compounds,[59,61,85] the application of interfacial reactions[86,87] are increasingly used to attach photoswitches to silicon based substrates.[59,61,63,67-70,73-75,88] In this approach a well-defined, dense monolayer with a terminal functional group is formed, which is then reacted with a second molecule containing a photochromic unit with an appropriate functional group. Most of the synthetically useful surface reactions are performed on monolayers containing terminal carboxyl, amino, hydroxyl, alkyne or azide groups.[86,87] Terminal carboxyl, amino and hydroxyl groups could be modified through nucleophilic substitution reactions. Alkyne and azide terminated monolayers are suitable for modifications *via* copper-catalyzed 1,3-dipolar cycloaddition reactions which is the most widely employed of the so-called ”click” reactions.[89]

1.4.2.1 Azobenzenes

Apart from the somewhat lower thermal[82] and photochemical[83,84] stability of the Au-S bond, the major difficulty with constructing gold-based azobenzene-monolayers is that the high packing density of the molecules on the surface of this material prevents photochemical *trans* to *cis* isomerization.[90-92] To overcome this problem, either mixed monolayers[93,94] have to be assembled or bulky anchoring units[95] or substituents[96,97] should be introduced to the azobenzene structure. A method similar to mixed monolayer formation is the assembly of unsymmetrical sulfides[71] and disulfides[98-100] which provide for reduced steric interactions between the switching units. The mixed monolayer approach to achieve reversible photoisomerization on gold is receiving increased interest; however, the surface coverage may be decreased too much to be useful for photoinduced wettability control. Additionally, at higher temperatures, phase-separation of the photochromic unit and the diluent alkane thiol has been observed.[99,101]

Although most pronounced in the case of gold, the requirement for sufficient free volume for efficient *trans* ↔ *cis* isomerization is not exclusively related to gold surfaces. Several authors comment on the steric requirements of the photoisomerization regardless of the surface used.[62,64-70,95-97,102,103] Min et al. attached azobenzenes to H-terminated silicon surfaces through aryldiazonium coupling and suggested the role of phenyl rings in reducing steric constraints to the isomerization.[62] Ichimura and co-workers used the cyclic skeleton of

calix[4]resorcinarenes to attach azobenzenes (Figure 5) to ensure sufficient free volume for photoswitching on the surface.[64-66] Aoki et al. compared azobenzene films on quartz prepared through covalent attachment of alkoxysilane functionalized azobenzenes and *via* the Langmuir-Blodgett method using an amphiphilic azobenzene derivative.[67] Their results showed that the relatively loose packing of the azobenzenes attached through covalent Si-O bonds is favorable for photoisomerization, while the more rigid LB-membrane showed no switching upon irradiation. El Garah et al. carried out AFM studies on azobenzene monolayers physisorbed on mica surface[104]. It was found that the molecules underwent complete photoisomerization in the monolayers, that can be explained by the weak substrate/molecule interactions that allows the layers to reorganize and gain sufficient free volume for the isomerization step.

1.4.2.2 Spiropyrans

As for azobenzene-based assemblies, the surface density of the chromophore is an important aspect in designing SP coated photoresponsive surfaces. SPs are found to be sensitive to steric effects due to the large changes in geometry upon isomerization from the non-planar closed form to the highly extended, conjugated open form.[39,56,72,74,105] Demonstrating the importance of the surface coverage Rosario et al. compared glass surfaces covalently modified with SP *via* amide linkages with and without additional diluents.[74] When only SP was assembled the measured WCA change was 5° upon isomerization to the MC form. If the surface was modified with a mixed monolayer of SP and bulky *tert*-butyldiphenylchlorosilane (TBDS) the measured value was 13°, suggesting more effective isomerization in the less hindered environment. Dattilo et al. found similar enhancement of WCA changes in a mixed monolayer assembly on rough silicon surfaces.[72] An SP monolayer diluted with octyl-chains exhibited a 14° WCA change, 3° higher than observed for the photoactive compound at the non-diluted surface.

In addition to the steric requirements of the isomerization, the polarity of the environment also influences the photochromism.[74,88,106,107] It is known that the zwitterionic MC form is stabilized in polar environments.[107] Studies on SPs trapped in a silica matrix indicated the importance of the coexistence of polar and non-polar regions for reversible photoswitching.[106,107] These results support the more effective isomerization in mixed monolayers, where the polar MC forms are separated by apolar diluents.

1.4.2.3 Stilbenes

As already mentioned stilbenes can undergo photochemical [2+2] cycloadditions,[47-50] which is a limitation for their application in the construction of photoresponsive surfaces. Furthermore, as for azobenzenes and SPs, the isomerization of stilbenes and their derivatives is prone to steric effects due to the large geometrical changes upon isomerization. Indeed, in densely packed monolayers of stilbenes on gold surfaces, reversible *cis*/*trans* isomerizations were not observed[47-50] unless a mixed monolayer approach was used to ensure sufficient space for the isomerization and prevention of photodimerization[50] (Figure 8). Additionally, the gold substrate could potentially quench the excited state of the surface-bound switch.[48]

Remarkably, when functionalized stilbenes (Figure 7) were assembled covalently on a Si(100) surface, reversible isomerization without photodegradation or photodimerization was observed. The lack of side-reactions could be explained by the presence of an electron-withdrawing CN-substituted olefin (Figure 7) and possibly a lower coverage on the Si-surface compared to gold decreasing the propensity for dimerization.

1.4.3 Surface roughness

Although controlling superhydrophilic (WCA ~ 0°) and superhydrophobic (WCA ~ 150°) wetting is considered to be of practical use[16,21], most of the photoresponsive monolayers prepared on flat surfaces exhibit minor changes in WCA upon UV-irradiation. In naturally occuring superhydrophobic surfaces, such as the lotus leaf,[108] the back of desert beetles,[109] and the water striders,[110] two features work together: the chemical composition of the surface and the surface roughness. Taking a similar approach, the combination of photoswitches with nano- and microstructured substrates was shown to contribute to larger changes in WCAs when the surfaces were photochemically modified.

1.4.3.1 Azobenzenes

Lim et al.[68,69] prepared a nanoporous multilayer film on a silicon wafer using layer-by-layer assembly with poly(allylamine hydrochloride) (PAH) and SiO_2 nanoparticles (d ≈ 11 nm) (Figure 9a and b). The film was modified with 3-(aminopropyl)triethoxysilane (APTES) and the terminal amino groups were subsequently reacted with a carboxylic acid functionalized azobenzene (Figure 9a and b). To increase its hydrophobic character, the azobenzene was functionalized

with an OCF_3 group. Using this system it was possible to demonstrate the switching of wettability of a 9-layer film of PAH/SiO_2 decorated with azobenzenes from superhydrophobic (152 ± 3°) to superhydrophilic (< 5 ± 1°) (Figure 9c). Additionally, the minimum and maximum WCAs could be tuned by changing the number of deposited PAH/SiO_2 layers. In comparison, flat silicon surfaces modified with the same azobenzene switch exhibited only a 5(±1)° change in the WCA.[68]

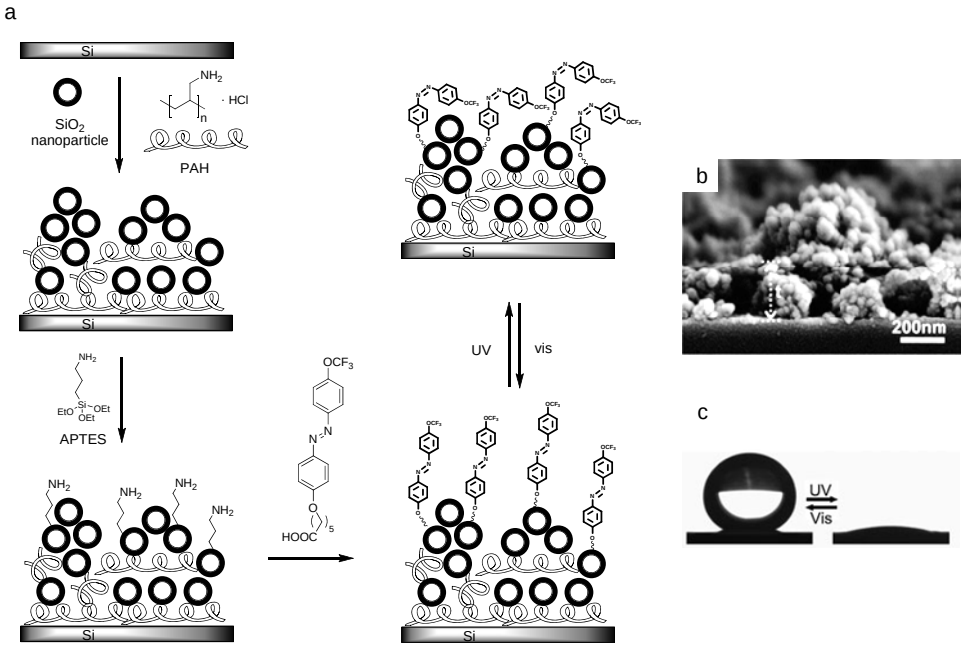

Figure 9 Attachment of azobenzene molecules to a rough surface to amplify the wettability change upon switching. (a) First, a nanoporous multilayer film was prepared on a silicon wafer *via* the layer-by-layer assembly of poly(allylamine hydrochloride) (PAH) and SiO_2 nanoparticles. The rough surface was subsequently modified with APTES. (b) Azobenzenes were attached through reaction with the terminal amino groups of APTES. The wettability could be switched between superhydrophilic and superhydrophobic upon isomerization of the azobenzenes. (c) SEM image of the substrate after nine deposition cycles of PAH/SiO_2.

The authors suggest that the reason for the enhanced wettability is twofold. First, the presence of the rough surface of the nanostructure provides a reduction in steric hindrance for the photoisomerization, which results in a large change in the surface dipole moment.[68,69] Evidence for a large change in the surface dipole moment was provided by surface potential measurements.[69] Second, the air trapped

in the inner pores of the substrate structure below a water droplet deposited on the surface contributes to the high contact angle.[24] In addition to trapped air, the presence of *trans*-azobenzenes with terminal CF_3-groups throughout the rough surface prevents the penetration of water inside the nanopores. When *trans* to *cis* photoisomerization takes place, a higher dipole moment is created within the pores. Water is then drawn into the pores due to capillary interactions[23] leading to complete wetting.

In an alternative approach a photocontrolled molecular shuttle SAM comprising an α-cyclodextrin (α-CD)/azobenzene inclusion complex bound to a rough gold surface for reversible wettability switching was developed by Wan et al[111](Scheme 7).

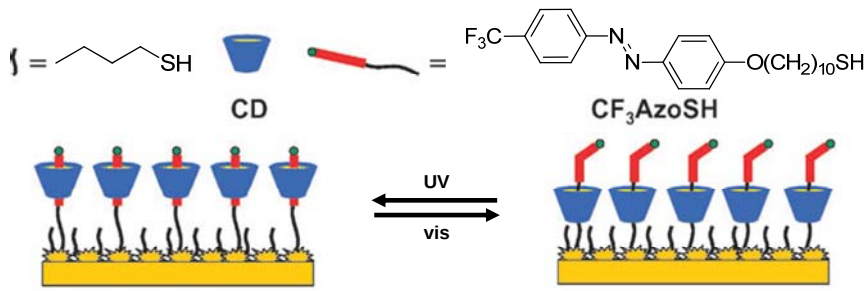

Scheme 7 Wettability control by an azobenzene/cyclodextrin complex on a rough gold surface. The use of a smooth surface resulted in only minor WCA changes. (Figure reproduced from ref. 111.)

A mixed monolayer of *n*-C_4H_9SH and the pre-formed α-CD/azobenzene complex was assembled on a rough gold surface obtained by electrodeposition. The surface exhibited a ca. 70° WCA when the azobenzenes were in the *trans* geometry. Upon UV-irradiation this value increased to 120°. The authors postulate that the reason for the lower contact angle in the initial state is that the hydrophilic α-CD moieties are exposed to the interface. UV-irradiation generates cis-azobenzenes, inducing a geometrical mismatch between the host and the guest. As a result, the hydrophilic α-CDs become buried under the switch and the effect of the hydrophopic CF_3-terminated azobenzenes becomes more pronounced at the surface. When the same system was constructed on a flat and smooth gold substrate the WCA change obtained upon photoisomerization was only about 2°, demonstrating the importance of surface roughness in achieving relatively large changes in WCA.

It is worth noting that this is the first example in which a hydrophilic → hydrophobic wettability change was associated with *trans* → *cis*

photoisomerization of azobenzenes. Usually the opposite effect is observed upon switching as the *cis* isomer is more polar than the *trans* isomer.

1.4.3.2 Spiropyrans

When porous nano- and micro-structured surfaces were combined with the photoinduced polarity change upon SP → MC isomerization, it was shown that amplification of WCA changes compared to smooth surfaces was achieved reversibly[72,73](Figure 10b vs c). Rosario et al. used Si-nanowires with diameters of 20-50 nm grown on a Si(111) substrate as a rough surface (Figure 10a). The substrate was subsequently modified by bulky *tert*-butyldiphenylchlorosilane (TBDS), perfluorooctyltrichlorosilane, and (3-aminopropyl)diethoxymethylsilane, to which the spiropyran molecules were attached covalently. Under these conditions the light-induced WCA change due to the isomerization of the SPs could be amplified compared to that on smooth surfaces.

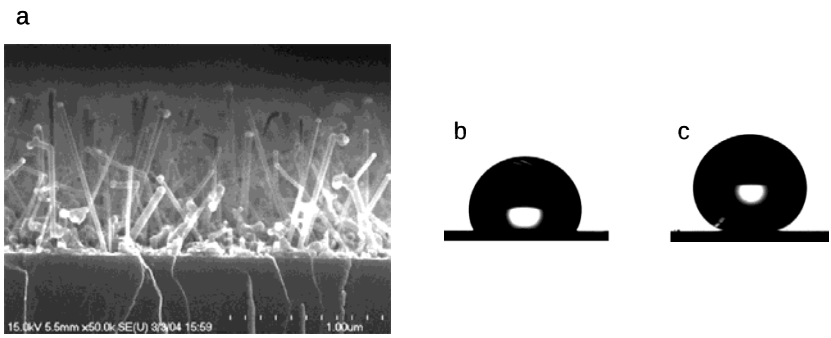

Figure 10 Modifying rough surfaces with spiropyrans results in amplified wettability switching. (a) Si-nanowires grown on a Si(111) substrate. (b) Water droplet on a smooth surface modified by spiropyrans. (c) Water droplet on a rough surface containing Si-nanowires. The presence of the nanostructure resulted in an increased water contact angle. (Figures reproduced from ref. 73.)

Dattilo et al. compared the wetting properties of flat and porous silicon surfaces coated with SPs.[72] Photoinduced SP → MC isomerization gave a 9° WCA change on a smooth surface and only a change of 11° on a porous surface. In an attempt to enhance the wettability change, both smooth and porous surfaces bearing the MC form were treated with Co(II) ions. It is know that metal ions can influence the isomerization through binding to the phenolate anion of the MC form.[112] As a result of the Co(II) ion binding the WCA change increased from 11°

to 32° in the case of the porous surface, but only a minor influence on the wettability of the smooth surface was observed.[72]

The use of molecular switches with well-defined structure and physical properties allows for the regulation of wettability through molecular level control of surface energy. Although the reversible isomerization of the switching units is the key to realize photoregulated surface-wetting, it is evident that in order to reach high level of wettability control, the effect of photoswitching has to be amplified by the combination of the photoisomerization of the molecules with appropriate functional groups, surface coverage that does not limit the isomerization and surface structuring.

1.5 Light-induced liquid motion on photoresponsive monolayers

Another phenomenon related to surface energy control is liquid motion across a suitably modified surface. In contrast to wettability control, where the surface energy of the whole substrate is reversibly altered to control its overall hydrophobic or hydrophilic nature, for liquid motion a constant surface energy gradient has to be maintained in order to achieve transport across a surface.[113] The energy gradient can be induced by concentration gradient,[113,114] electric field,[115] or thermal gradient[113,116]

It has been shown in a number of studies that solid surfaces modified with photochromic switches are suitable to initiate light-driven liquid motion.[63,65,73,117] In this case the gradient in surface energy is generated photochemically through spatially controlled structural changes accompanied with changes in dipole moment within the monolayer assembly by irradiation with light.

1.5.1 Azobenzenes

The first example of macroscopic motion of liquids on a flat solid surface modified with a monolayer of photochromic switches was demonstrated by Ichimura and co-workers.[65,66,118] They used aminosilylated silica substrates functionalized with *O*-carboxyethylated calix[4]resorcinarenes containing azobenzene units. The macrocycle calix[4]resorcinarene (Figure 5) was designed to ensure the sufficient free volume necessary for efficient isomerization of the azobenzenes. The surface energy gradient was achieved by light-induced isomerization of the azobenzenes in a spatially controlled manner. The gradient in

light-intensity was maintained by moving the light beam, which in turn continued to move the droplet. The direction of the movement could be controlled by changing the direction of the light intensity gradient. In this way the continuous movement of different liquids, such as olive oil, 1-methylnaphthalene, 1,1,2,2-tetrachloroethane and liquid crystals could be achieved (with a speed of 35 μm/s for olive oil). It should be noted, however, that no motion of droplets was observed for solvents such as water, ethylene glycol or formamide.

In the experimental setup of Ichimura et al.[65] the liquid motion originates from the imbalance of surface tension forces acting on the opposite side of the droplet due to the spatially controlled photochemical switching of the monolayer (Figure 11).

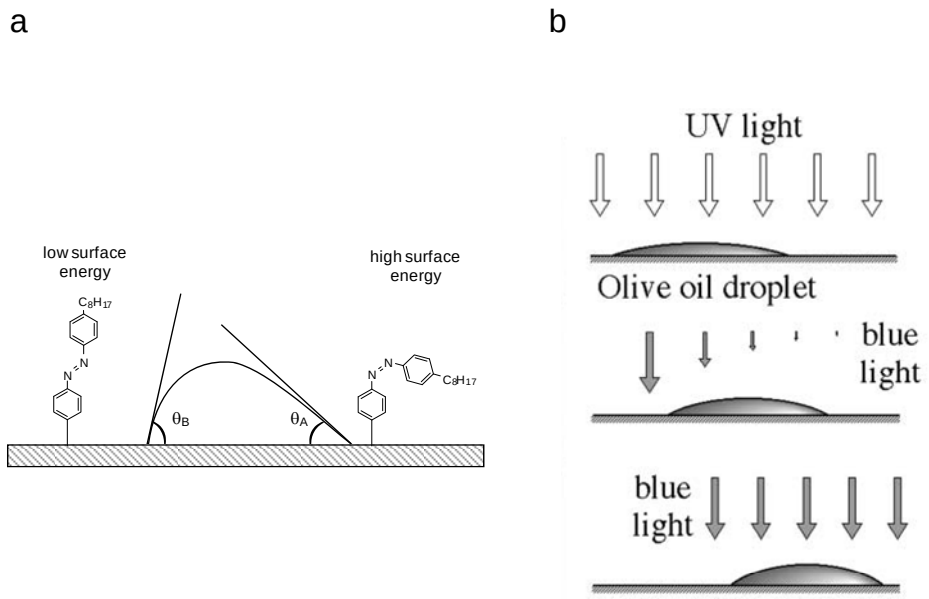

Figure 11 (a) A diagram of a liquid droplet on a gradient surface. The minimum requirement for liquid motion in response to a surface energy gradient is that the advancing contact angle (θ_A) is lower than the receding contact angle (θ_B). In the context of the azobenzene-based system of Ichimura et al.[65] the high surface energy area and the low surface energy area are *cis*-rich and *trans*-rich, respectively. (b) Schematic representation of the light-induced motion of an olive oil droplet. The droplet on a high-energy, *cis*-rich surface moves in the direction of the high-energy areas upon non-uniform irradiation at 436 nm that generates lower-surface energy, *trans*-rich regions on the surface. The advancing contact angle of the droplet on a *cis*-rich surface is higher than its receding contact angle on the *trans*- rich surface. (Figure 8b reproduced from ref. 65)

The presence of the surface energy gradient by itself, however, is not enough to ensure motion. It has to be accompanied by low contact angle hysteresis and a lack of defects that can pin the edge of the liquid drop.

If θ_A is smaller than θ_B, the drop will move towards the higher surface energy (Figure 11a). This motion will decrease the higher surface energy area and increase the lower surface energy area.[114] In the context of the described system θ_A is the advancing contact angle of the liquid on a *cis*-rich surface (θ_{adv}(cis)), while θ_B is the receding contact angle on a *trans*-rich surface (θ_{rec}(trans)). Droplets of liquids exhibiting θ_{rec}(trans) > θ_{adv}(cis) will move. If the contact angle hysteresis is higher, θ_B may become smaller than θ_A (Figure 11a). In this case the droplet will not move.

Light-induced motion of a series of different solvent droplets was demonstrated in a similar fashion by Yang et al. using azobenzenes covalently attached to a silicon wafer through an interfacial reaction with an amine-terminated monolayer.[63] The surface energy gradient was achieved by UV-light induced *trans*-to-*cis* isomerization of the azobenzenes.

1.5.2 Spiropyrans

Rosario et al. were able to induce light-driven motion of water droplets by using spiropyrans as photoswitches.[73] In previous studies the motion of water droplets was not achieved due to the large contact angle hysteresis compared to the light-induced contact angle change.[63,65] Rosario et al. were able to overcome this problem by using a rough surface in combination with spiropyrans.[73] Silicon-wires of 20-50 nm in diameter grown on a silicon wafer (Figure 10) were coated with spiropyrans resulting in a superhydrophobic surface with a decreased contact angle hysteresis and ultimately allowed for the light-guided motion of water droplets. The authors suggest that the reason for the lower hysteresis is the low surface free-energy resulting from the hydrophobic spiropyran coating and the instability of the solid-liquid-gas three-phase contact line on randomly rough surfaces.

1.5.3 Rotaxanes

SAMs of light switchable rotaxanes were recently employed for macroscopic liquid transport.[117] Leigh, Rudolf, Zerbetto et al designed a synthesized a molecular shuttle composed of a pyridine containing macrocycle and a thread with a short fluorinated chain on one side and a fumaramide moiety on the other side. A monolayer of 11-mercaptoundecanoic acid was prepared on gold in order to attach pyridine-containing rotaxanes through H-bonding (Scheme 8)[119]

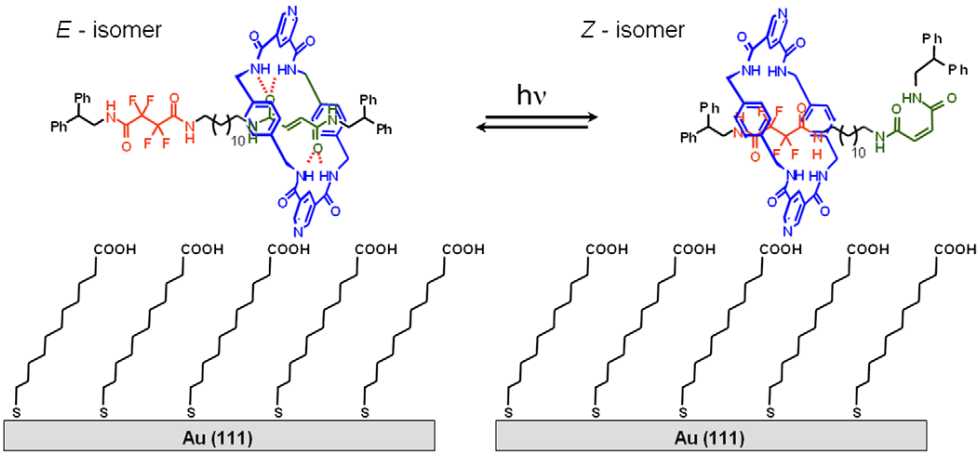

Scheme 8 Light-switchable rotaxane physisorbed on an 11-mercaptoundecanoic acid modified gold surface. In the E-isomer the fluoroalkane station is exposed making the surface polarophobic. Upon irradiation with 240-400 nm light the macrocycle is displaced, shielding the fluoroalkyl moiety, and making the surface polarophilic. The change in polarity upon isomerization was used to move liquid droplets across a surface. (Figure reproduced from ref. 117.)

In the *E*-isomer of the rotaxane the macrocycle is positioned at the fumaramide station, so the tetrafluorosuccinamide moiety at the other end of the thread is exposed. As a result the surface has an overall polarophobic nature. Upon UV-irradiation the fumaramide station undergoes isomerization generating a maleimide station (Scheme 8). As the macrocycle has a low affinity to the maleimide station it moves to the tetrafluorosuccinimide station, shielding the fluorine atoms that are responsible for the low surface energy generating a more polarophobic surface. A microlitre drop of diiodomethane was placed on this surface and irradiated with 240-400 nm light on one side of the drop and the adjacent area. As the rotaxane underwent isomerization upon irradiation it induced a surface energy gradient across the length of the drop resulting in a millimeter-scale directional transport of the liquid at speeds up to 1 μm s^{-1}. It was also found that the drop could be moved up a 12° incline.

It is noted, that the gold surfaces that were used in these experiments were prepared either on glass or on mica. The authors found that gold on mica provided a more regular surface and better ordered monolayers compared to the more rough gold on glass, making the transport of diiodomethane significantly more facile on gold deposited on mica.

In biological systems a variety of molecular motors are able to cooperate to perform macroscopic tasks.[120] Performing well-defined mechanical tasks at the molecular level with fully synthetic systems remains challenging. The systems described above are the first steps towards the construction of microreactors or lab-on-a-chip devices where the collective action of responsive molecular arrays is harnessed to perform useful work. However, in order to realize those applications some aspects of the design have to be improved. The lack of fast reversibility of the switching process is a major limitation. Although directed motion of a variety of liquids has been achieved, the range should be extended to solvents that are more relevant in practical applications (there is only one example for the manipulation of water droplets[73]) and their behavior should be better understood. Furthermore, the interaction of solutions, containing different kinds of dissolved materials, with dynamic organic surfaces should be studied as well.

1.6 Potential of molecular motors in surface energy control

Molecular motors based on overcrowded alkenes are a unique group of organic molecules that are able to convert light energy into repetitive unidirectional rotation and are highly promising in photon-driven systems.[121,122]

The unidirectional rotary cycle of these molecular motors consists of two photochemical *cis*/*trans* isomerization, each followed by a thermal rearrangement step. The rotary cycle of a so-called 'second generation molecular motor',[123,124] is depicted in Scheme 9. In second generation motors the two halves (the rotor and the stator) connected by a central double bond, the axis of the rotation, are structurally different (Figure 12).

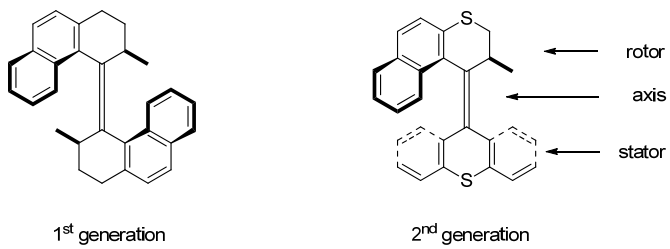

Figure 12 Examples of 1st and 2nd generation molecular motors.

In the rotary cycle (Scheme 9) the stable form adopts a non-planar shape to minimize the steric crowding around the tetrasubstituted central alkene. The substituent at the stereogenic centre adopts a pseudo-axial conformation in order to avoid steric interaction with the lower half. In the first step of the cycle the stable form of the motor undergoes a photochemical isomerization generating the unstable form in which the methyl substituent at the stereogenic centre is forced to adopt a conformationally unfavored pseudo-equatorial orientation. This conformational strain is released as the molecule undergoes a thermal helix inversion step, which leaves the stereogenic methyl group in a favored, pseudo-axial conformation. Repeating the photochemical and thermal steps complete the 360° rotation of the upper part relative to the lower part. The unidirectionality of the process is ensured by the irreversibility of the thermal steps.[125]

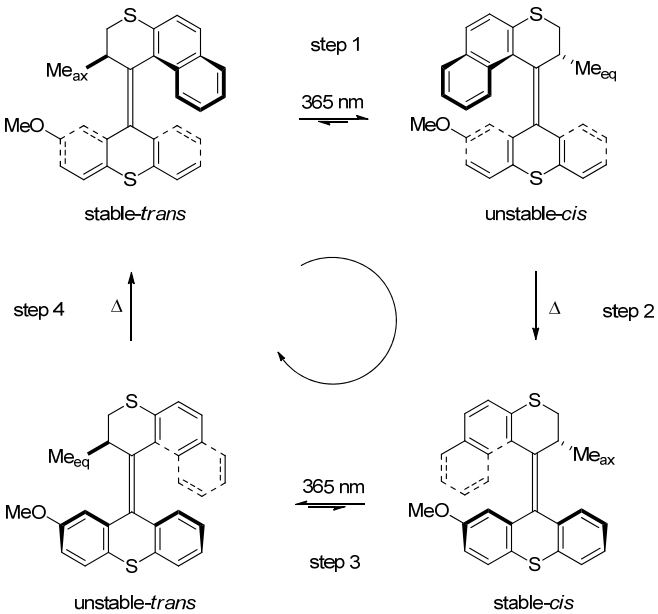

Scheme 9 Unidirectional rotary cycle of 2nd generation molecular motors.

Extensive research regarding the synthesis and thermal isomerization time-scales of a wide range of motors has led to a better understanding of how the motor's structure affects its kinetic properties. It has laid the foundations for a

general paradigm regarding the effect of substituents and ring size on the speed of the rotary motion.[126]

While it is important to study molecular motors in solution to understand their mechanism of operation, it seems that molecular machinery has limited use in practical applications in solution due to their uncontrolled thermal motion.[3,10-12] This initiated research efforts towards the construction of molecular systems where the Brownian motion is tackled and the rotary motion of the motors could be harnessed to perform useful tasks. These efforts resulted in the construction of the first systems where molecular rotary motors were interfaced with the macroscopic world in the form of self-assembled monolayers on quartz, silicon and gold surfaces[127,128] (Figure 13). In these assemblies the relative rotary motion of the two halves converted to absolute rotation of one of the halves, setting the stage to utilize the collective motion of an array of rotary motors to perform work.

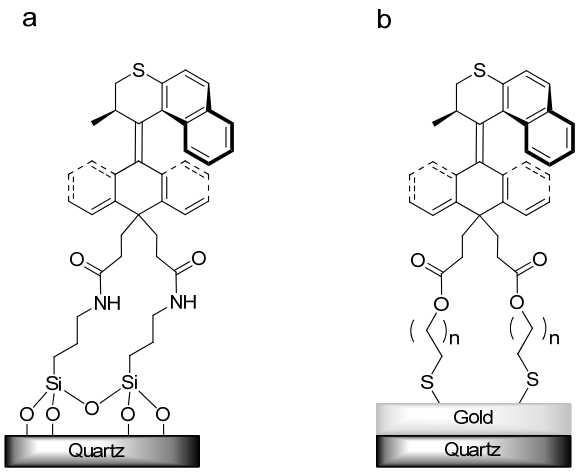

Figure 13 Azimuthal molecular motors on quartz (a) and semitransparent gold on quartz (b) surfaces. The rotary motion is preserved upon attachment to solid substrates.

The surface-bound rotary motors shown in Figure 13 have an azimuthal orientation: their axis is perpendicular to the surface. However, another type of orientation can be distinguished being altitudinal, in which the axis of rotation is parallel to the surface (Figure 14).

Molecular motors rotating in altitudinal orientation relative to a surface may have a larger impact on the construction of functional interfaces compared to the

azimuthal versions. It is easy to envision altitudinal motors bearing different functional groups which could be exposed at or buried below the interface upon isomerization. As a result of repetitive isomerization steps, reversible control over wettability, adhesion, friction or transport might be gained.

The ability of molecular motors to undergo controlled unidirectional rotation while attached to solid surfaces, and the wide range of speeds at which they are capable of rotating make them attractive candidates not only to control surface properties but also to control the motion of nano- or micrometer scale adsorbed materials.

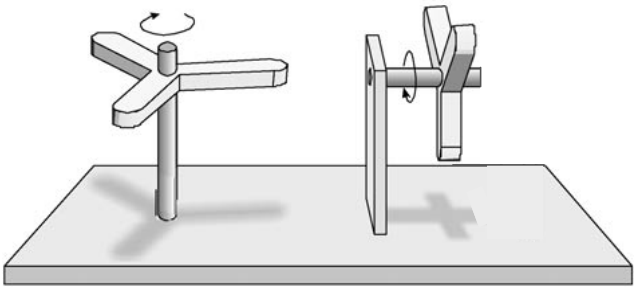

Figure 14 Schematic representation of azimuthal (left) and altitudinal (right) rotary motion. In azimuthal rotation the axis of rotation is perpendicular, while in altitudinal rotation it is parallel to the surface. (Figure adapted from ref. 11.)

1.7 The aim and outline of the thesis

This thesis deals with the synthesis of light-driven molecular motors and switches and their dynamic behavior in confined environments. The major goal is the synthesis and monolayer formation of altitudinal rotary motors, in order to construct functional interfaces with the possibility to control wettability, adhesion or transport. Confining such molecules at interfaces potentially allows for gaining control over different interfacial phenomena through the control of (sub)molecular motion.

In chapter 2 the design, synthesis and photochemical characterization of molecular motors potentially capable of altitudinal rotation on solid surfaces is described. In order to broaden the range of methods available for surface functionalization with molecular motors, the molecules are synthesized with

various functional groups that allows for attachment to solid surfaces under different conditions.

In chapter 3 the focus is on the functionalization and subsequent photochemical characterization of inorganic Si-based surfaces with altitudinal motors containing terminal alkoxysilane and alcohol functional groups. Attempts to modify chemically inert, atomically flat mica surfaces are also described.

Chapter 4 deals with the attachment of altitudinal motors bearing terminal alkyne and azide functional groups to surfaces *via* interfacial 1,3-dipolar cycloadditions. The problem of the valency of attachment is addressed and the effect of confinement on the molecular motion is examined.

In chapter 5 the primary aim is to synthesize altitudinal molecular motors with functional groups on the rotor half in order to affect surface energy. The synthesis and physico-chemical properties of motors with a perfluorobutyl chain and a cyano group are described. Preliminary results regarding the effect of functional groups on surface wettability upon, attachment of the motors to quartz *via* a 1,3-dipolar cycloaddition, are presented.

Chapter 6 describes a collaborative effort to interface photoswitches with biological systems. Azobenzene switches were synthesized and confined in the inner space of a transmembrane protein complex in order to reversibly photoregulate protein transport across the channel.

1.8 References

(1) Kay, E. R.; Leigh, D. A.; Zerbetto, F. *Angew. Chem. Int. Ed.* **2007**, *46*, 72-191.
(2) Saha, S.; Stoddart, J. F. *Chem. Soc. Rev.* **2007**, *36*, 77-92.
(3) Browne, W. R.; Feringa, B. L. *Nature Nanotechnology* **2006**, *1*, 25-35.
(4) de Jong, J. J. D.; Lucas, L. N.; Kellogg, R. M.; van Esch, J. H.; Feringa, B. L. *Science* **2004**, *304*, 278-281.
(5) Wang, J. B.; Kulago, A.; Browne, W. R.; Feringa, B. *J. Am. Chem. Soc.* **2010**, *132*, 4191-4196.
(6) Takeuchi, M.; Ikeda, M.; Sugasaki, A.; Shinkai, S. *Acc. Chem. Res.* **2001**, *34*, 865-873.
(7) Yun, C.; You, J.; Kim, J.; Huh, J.; Kim, E. *J. Photochem. Photobiol. C* **2009**, *10*, 111-129.
(8) Wang, J. B.; Feringa, B. L. *Science* **2011**, *331*, 1429-1432.

(9) Sud, D.; Norsten, T. B.; Branda, N. R. *Angew. Chem. Int. Ed.* **2005**, *44*, 2019-2021.
(10) Browne, W. R.; Feringa, B. L. *Annu. Rev. Phys. Chem.* **2009**, *60*, 407-428.
(11) Balzani, V.; Credi, A.; Venturi, M. *Chem. Phys. Chem.* **2008**, *9*, 202-220.
(12) Katsonis, N.; Lubomska, M.; Pollard, M. M.; Feringa, B. L.; Rudolf, P. *Prog. Surf. Sci.* **2007**, *82*, 407-434.
(13) Robertus, J.; Browne, W. R.; Feringa, B. L. *Chem. Soc. Rev.* **2010**, *39*, 354-378.
(14) Bunker, B. C. *Mater. Sci. Eng. R* **2008**, *62*, 157-173.
(15) Wang, S. T.; Song, Y. L.; Jiang, L. *J. Photochem. Photobiol. C* **2007**, *8*, 18-29.
(16) Dorrer, C.; Ruhe, J. *Soft Matter* **2009**, *5*, 51-61.
(17) Xin, B. W.; Hao, J. C. *Chem. Soc. Rev.* **2010**, *39*, 769-782.
(18) de Gennes, P. G.; Brochard-Wyart, F.; Quere, D. *Capillarity and Wetting Phenomena;* Springer Verlag: **2004**.
(19) Adamson, A. W.; Gast, A. P. *Physical Chemistry of Surfaces;* Wiley Interscience: New York, **1997**.
(20) Gao, L. C.; McCarthy, T. J. *Langmuir* **2009**, *25*, 14105-14115.
(21) Sun, T. L.; Feng, L.; Gao, X. F.; Jiang, L. *Acc. Chem. Res.* **2005**, *38*, 644-652.
(22) Young, T. *Phil. Trans. R. Soc. London* **1805**, *95*, 65-87.
(23) Wenzel, R. N. *Ind. Eng. Chem.* **1936**, *28*, 988-994.
(24) Cassie, A. B. D.; Baxter, S. *Trans. Farad. Soc.* **1944**, *40*, 0546-0550.
(25) Spori, D. M.; Drobek, T.; Zurcher, S.; Ochsner, M.; Sprecher, C.; Muehlebach, A.; Spencer, N. D. *Langmuir* **2008**, *24*, 5411-5417.
(26) Gao, L. C.; McCarthy, T. J. *Langmuir* **2007**, *23*, 3762-3765.
(27) McHale, G. *Langmuir* **2007**, *23*, 8200-8205.
(28) Nosonovsky, M. *Langmuir* **2007**, *23*, 9919-9920.
(29) Gao, L. C.; McCarthy, T. J. *Langmuir* **2006**, *22*, 6234-6237.
(30) Chen, Y. L.; Helm, C. A.; Israelachvili, J. N. *J. Phys. Chem.* **1991**, *95*, 10736-10747.
(31) Schwartz, A. M. *J. Colloid. Interface Sci.* **1980**, *75*, 404-408.
(32) Chen, W.; Fadeev, A. Y.; Hsieh, M. C.; Oner, D.; Youngblood, J.; McCarthy, T. J. *Langmuir* **1999**, *15*, 3395-3399.
(33) Rau, H. In *Photoisomerization of azobenzenes;* Rebek, J. F., (Ed.); Photochemistry and Photophysics; CRC Press: Boca Raton, **1990**.
(34) Seki, T. *Polym. J.* **2004**, *36*, 435-454.

(35) Barrett, C. J.; Mamiya, J. I.; Yager, K. G.; Ikeda, T. *Soft Matter* **2007**, *3*, 1249-1261.
(36) Willner, I. *Acc. Chem. Res.* **1997**, *30*, 347-356.
(37) Woolley, G. A. *Acc. Chem. Res.* **2005**, *38*, 486-493.
(38) Bonardi, F.; London, G.; Nouwen, N.; Feringa, B. L.; Driessen, A. J. M. *Angew. Chem. Int. Ed.* **2010**, *49*, 7234-7238.
(39) Bertelson, R. C. In Brown, G. H., (Ed.); Photochromism; Wiley-Interscience: New York, **1971**.
(40) Feringa, B. L., (Ed.); *Molecular Switches;* Wiley VCH: Weinheim: **2001**.
(41) Irie, M. *Chem. Rev.* **2000**, *100*, 1685-1716.
(42) Uchida, K.; Izumi, N.; Sukata, S.; Kojima, Y.; Nakamura, S.; Irie, M. *Angew. Chem. Int. Ed.* **2006**, *45*, 6470-6473.
(43) Uchida, K.; Nishikawa, N.; Izumi, N.; Yamazoe, S.; Mayama, H.; Kojima, Y.; Yokojima, S.; Nakamura, S.; Tsujii, K.; Irie, M. *Angew. Chem. Int. Ed.* **2010**, *49*, 5942-5944.
(44) Uyama, A.; Yamazoe, S.; Shigematsu, S.; Morimoto, M.; Yokojima, S.; Mayama, H.; Kojima, Y.; Nakamura, S.; Uchida, K. *Langmuir* **2011**, *27*, 6395-6400.
(45) Görner, H.; Kuhn, H. J. In Neckers, D. C., Volman, D. H. and von Bünau, G., (Eds.); *Advances in Photochemistry*; John Wiley & Sons, Inc.: **1995**; Vol. 19, pp 1-117.
(46) Waldeck, D. H. *Chem. Rev.* **1991**, *91*, 415-436.
(47) Wolf, M. O.; Fox, M. A. *J. Am. Chem. Soc.* **1995**, *117*, 1845-1846.
(48) Wolf, M. O.; Fox, M. A. *Langmuir* **1996**, *12*, 955-962.
(49) Cooper, C. G. F.; MacDonald, J. C.; Soto, E.; McGimpsey, W. G. *J. Am. Chem. Soc.* **2004**, *126*, 1032-1033.
(50) Driscoll, P. F.; Purohit, N.; Wanichacheva, N.; Lambert, C. R.; McGimpsey, W. G. *Langmuir* **2007**, *23*, 13181-13187.
(51) Gulino, A.; Lupo, F.; Condorelli, G. G.; Fragala, M. E.; Amato, M. E.; Scarlata, G. *J. Mater. Chem.* **2008**, *18*, 5011-5018.
(52) Abbott, S.; Ralston, J.; Reynolds, G.; Hayes, R. *Langmuir* **1999**, *15*, 8923-8928.
(53) Patra, A.; Ralston, J.; Sedev, R.; Zhou, J. F. *Langmuir* **2009**, *25*, 11486-11494.
(54) Jiang, Y. G.; Wan, P. B.; Smet, M.; Wang, Z. Q.; Zhang, X. *Adv. Mater.* **2008**, *20*, 1972-1977.
(55) Ercole, F.; Davis, T. P.; Evans, R. A. *Polymer Chem.* **2010**, *1*, 37-54.

(56) Smets, G. *Pure Appl. Chem.* **1972**, *30*, 1-24.
(57) Seki, T. *Bull. Chem. Soc. Jpn.* **2007**, *80*, 2084-2109.
(58) Such, G.; Evans, R. A.; Yee, L. H.; Davis, T. P. *J. Macromol. Sci. Polym. Rev.* **2003**, *C43*, 547-579.
(59) Siewierski, L. M.; Brittain, W. J.; Petrash, S.; Foster, M. D. *Langmuir* **1996**, *12*, 5838-5844.
(60) Hamelmamm, F.; Heinzmann, U.; Siemling, U.; Bretthauer, F.; der Bruggen, J. V. *Appl. Surf. Sci.* **2004**, *222*, 1-5.
(61) Delorme, N.; Bardeau, J. F.; Bulou, A.; Poncin-Epaillard, F. *Langmuir* **2005**, *21*, 12278-12282.
(62) Min, M.; Bang, G. S.; Lee, H.; Yu, B. C. *Chem. Commun.* **2010**, *46*, 5232-5234.
(63) Yang, D.; Piech, M.; Bell, N. S.; Gust, D.; Vail, S.; Garcia, A. A.; Schneider, J.; Park, C. D.; Hayes, M. A.; Picraux, S. T. *Langmuir* **2007**, *23*, 10864-10872.
(64) Ichimura, K.; Oh, S. K.; Fujimaki, M.; Matsuzawa, Y.; Nakagawa, M. *J. Inclusion Phenomena Macrocycl. Chem.* **1999**, *35*, 173-183.
(65) Ichimura, K.; Oh, S. K.; Nakagawa, M. *Science* **2000**, *288*, 1624-1626.
(66) Oh, S. K.; Nakagawa, M.; Ichimura, K. *J. Mater. Chem.* **2002**, *12*, 2262-2269.
(67) Aoki, K.; Seki, T.; Suzuki, Y.; Tamaki, T.; Hosoki, A.; Ichimura, K. *Langmuir* **1992**, *8*, 1007-1013.
(68) Lim, H. S.; Han, J. T.; Kwak, D.; Jin, M. H.; Cho, K. *J. Am. Chem. Soc.* **2006**, *128*, 14458-14459.
(69) Lim, H. S.; Lee, W. H.; Lee, S. G.; Lee, D.; Jeon, S.; Cho, K. *Chem. Commun.* **2010**, *46*, 4336-4338.
(70) Demirel, G. B.; Dilsiz, N.; Cakmak, M.; Caykara, T. *J. Mater. Chem.* **2011**, *21*, 3189-3196.
(71) Callari, F. L.; Sortino, S. *J. Mater. Chem.* **2007**, *17*, 4184-4188.
(72) Dattilo, D.; Armelao, L.; Fois, G.; Mistura, G.; Maggini, M. *Langmuir* **2007**, *23*, 12945-12950.
(73) Rosario, R.; Gust, D.; Garcia, A. A.; Hayes, M.; Taraci, J. L.; Clement, T.; Dailey, J. W.; Picraux, S. T. *J. Phys. Chem. B* **2004**, *108*, 12640-12642.
(74) Rosario, R.; Gust, D.; Hayes, M.; Jahnke, F.; Springer, J.; Garcia, A. A. *Langmuir* **2002**, *18*, 8062-8069.
(75) Vlassiouk, I.; Park, C. D.; Vail, S. A.; Gust, D.; Smirnov, S. *Nano Lett.* **2006**, *6*, 1013-1017.

(76) Athanassiou, A.; Lygeraki, M. I.; Pisignano, D.; Lakiotaki, K.; Varda, M.; Mele, E.; Fotakis, C.; Cingolani, R.; Anastasiadis, S. H. *Langmuir* **2006**, *22*, 2329-2333.
(77) Anastasiadis, S. H.; Lygeraki, M. I.; Athanassiou, A.; Farsari, M.; Pisignano, D. *J. Adhes. Sci. Technol.* **2008**, *22*, 1853-1868.
(78) Joseph, G.; Pichardo, J.; Chen, G. F. *Analyst* **2010**, *135*, 2303-2308.
(79) Ulman, A. *Chem. Rev.* **1996**, *96*, 1533-1554.
(80) Aswal, D. K.; Lenfant, S.; Guerin, D.; Yakhmi, J. V.; Vuillaume, D. *Anal. Chim. Acta* **2006**, *568*, 84-108.
(81) Ciampi, S.; Harper, J. B.; Gooding, J. J. *Chem. Soc. Rev.* **2010**, *39*, 2158-2183.
(82) Chandekar, A.; Sengupta, S. K.; Whitten, J. E. *Appl. Surf. Sci.* **2010**, *256*, 2742-2749.
(83) Lee, S. H.; Lin, W. C.; Kuo, C. H.; Karakachian, M.; Lin, Y. C.; Yu, B. Y.; Shyue, J. J. *J. Phys. Chem. C* **2010**, *114*, 10512-10519.
(84) Rieley, H.; Kendall, G. K.; Zemicael, F. W.; Smith, T. L.; Yang, S. H. *Langmuir* **1998**, *14*, 5147-5153.
(85) Sekkat, Z.; Wood, J.; Geerts, Y.; Knoll, W. *Langmuir* **1996**, *12*, 2976-2980.
(86) Haensch, C.; Hoeppener, S.; Schubert, U. S. *Chem. Soc. Rev.* **2010**, *39*, 2323-2334.
(87) Li, J.; Thiara, P. S.; Mrksich, M. *Langmuir* **2007**, *23*, 11826-11835.
(88) Rosario, R.; Gust, D.; Hayes, M.; Springer, J.; Garcia, A. A. *Langmuir* **2003**, *19*, 8801-8806.
(89) Kolb, H. C.; Finn, M. G.; Sharpless, K. B. *Angew. Chem. Int. Ed.* **2001**, *40*, 2004-2021.
(90) Evans, S. D.; Johnson, S. R.; Ringsdorf, H.; Williams, L. M.; Wolf, H. *Langmuir* **1998**, *14*, 6436-6440.
(91) Gustina, D.; Markava, E.; Muzikante, I.; Stiller, B.; Brehmer, L. *Adv. Mater. Opt. Electro.* **1999**, *9*, 245-251.
(92) Wang, R.; Iyoda, T.; Jiang, L.; Tryk, D. A.; Hashimoto, K.; Fujishima, A. *J. Electroanal. Chem.* **1997**, *438*, 213-219.
(93) Kumar, A. S.; Ye, T.; Takami, T.; Yu, B. C.; Flatt, A. K.; Tour, J. M.; Weiss, P. S. *Nano Lett.* **2008**, *8*, 1644-1648.
(94) Yasuda, S.; Nakamura, T.; Matsumoto, M.; Shigekawa, H. *J. Am. Chem. Soc.* **2003**, *125*, 16430-16433.

(95) Muzikante, I.; Gerca, L.; Fonavs, E.; Rutkis, M.; Gustina, D.; Markava, E.; Stiller, B.; Brehmer, L.; Knochenhauer, G. *Mater. Sci. Eng. C* **2002**, *22*, 339-343.
(96) Han, M. N.; Honda, T.; Ishikawa, D.; Ito, E.; Hara, M.; Norikane, Y. *J. Mater. Chem.* **2011**, *21*, 4696-4702.
(97) Han, M.; Ishikawa, D.; Honda, T.; Ito, E.; Hara, M. *Chem. Commun.* **2010**, *46*, 3598-600.
(98) Tamada, K.; Akiyama, H.; Wei, T. X. *Langmuir* **2002**, *18*, 5239-5246.
(99) Tamada, K.; Akiyama, H.; Wei, T. X.; Kim, S. A. *Langmuir* **2003**, *19*, 2306-2312.
(100) Qune, L. F. N. A.; Akiyama, H.; Nagahiro, T.; Tamada, K.; Wee, A. T. S. *Appl. Phys. Lett.* **2008**, *93*.
(101) Ishida, T.; Yamamoto, S.; Mizutani, W.; Motomatsu, M.; Tokumoto, H.; Hokari, H.; Azehara, H.; Fujihira, M. *Langmuir* **1997**, *13*, 3261-3265.
(102) Tanaka, T.; Ogino, H.; Iwamoto, M. *Langmuir* **2007**, *23*, 11417-11420.
(103) Nakagawa, M.; Watase, R.; Ichimura, K. *Chem. Lett.* **1999**, , 1209-1210.
(104) El Garah, M.; Palmino, F.; Cherioux, F. *Langmuir* **2010**, *26*, 943-949.
(105) Bunker, B. C.; Kim, B. I.; Houston, J. E.; Rosario, R.; Garcia, A. A.; Hayes, M.; Gust, D.; Picraux, S. T. *Nano Lett.* **2003**, *3*, 1723-1727.
(106) Hori, T.; Tagaya, H.; Nagaoka, T.; Kadokawa, J.; Chiba, K. *Appl. Surf. Sci.* **1997**, *121*, 530-533.
(107) Tagaya, H.; Nagaoka, T.; Kuwahara, T.; Karasu, M.; Kadokawa, J.; Chiba, K. *Micropor. Mesopor. Mater.* **1998**, *21*, 395-402.
(108) Neinhuis, C.; Barthlott, W. *Annals of Botany* **1997**, *79*, 667-677.
(109) Parker, A. R.; Lawrence, C. R. *Nature* **2001**, *414*, 33-34.
(110) Gao, X. F.; Jiang, L. *Nature* **2004**, *432*, 36-36.
(111) Wan, P. B.; Jiang, Y. G.; Wang, Y. P.; Wang, Z. Q.; Zhang, X. *Chem. Commun.* **2008**, 5710-5712.
(112) Byrne, R. J.; Stitzel, S. E.; Diamond, D. *J. Mater. Chem.* **2006**, *16*, 1332-1337.
(113) Brochard, F. *Langmuir* **1989**, *5*, 432-438.
(114) Chaudhury, M. K.; Whitesides, G. M. *Science* **1992**, *256*, 1539-1541.
(115) Mugele, F.; Baret, J. C. *J. Phys. Cond. Mat.* **2005**, *17*, R705-R774.
(116) Brzoska, J. B.; Brochardwyart, F.; Rondelez, F. *Langmuir* **1993**, *9*, 2220-2224.

(117) Berna, J.; Leigh, D. A.; Lubomska, M.; Mendoza, S. M.; Perez, E. M.; Rudolf, P.; Teobaldi, G.; Zerbetto, F. *Nature Materials* **2005**, *4*, 704-710.
(118) Oh, S. K.; Nakagawa, M.; Ichimura, K. *Mol. Crys. Liquid Cryst.* **2000**, *345*, 635-640.
(119) Cecchet, F.; Rudolf, P.; Rapino, S.; Margotti, M.; Paolucci, F.; Baggerman, J.; Brouwer, A. M.; Kay, E. R.; Wong, J. K. Y.; Leigh, D. A. *J. Phys. Chem. B* **2004**, *108*, 15192-15199.
(120) Schliwa, M., (Ed.); *Molecular Motors;* Wiley VCH, Weinheim: **2004**.
(121) Koumura, N.; Zijlstra, R. W. J.; van Delden, R. A.; Harada, N.; Feringa, B. L. *Nature* **1999**, *401*, 152-155.
(122) Feringa, B. L. *J. Org. Chem.* **2007**, *72*, 6635-6652.
(123) Koumura, N.; Geertsema, E. M.; Meetsma, A.; Feringa, B. L. *J. Am. Chem. Soc.* **2000**, *122*, 12005-12006.
(124) Koumura, N.; Geertsema, E. M.; van Gelder, M. B.; Meetsma, A.; Feringa, B. L. *J. Am. Chem. Soc.* **2002**, *124*, 5037-5051.
(125) Geertsema, E. M.; van der Molen, S. J.; Martens, M.; Feringa, B. *Proc. Natl. Acad. Sci. U. S. A.* **2009**, *106*, 16919-16924.
(126) Pollard, M. M.; Klok, M.; Pijper, D.; Feringa, B. L. *Adv. Funct. Mater.* **2007**, *17*, 718-729.
(127) Pollard, M. M.; Lubomska, M.; Rudolf, P.; Feringa, B. L. *Angew. Chem. Int. Ed.* **2007**, *46*, 1278-1280.
(128) Carroll, G. T.; Pollard, M. M.; van Delden, R.; Feringa, B. L. *Chem. Sci.* **2010**, *1*, 97-101.

Chapter 2

Light-driven altitudinal molecular motors: design, synthesis and characterization in solution

In this chapter the design, synthesis and physico-chemical characterization of light-driven molecular motors suitable for attachment to solid surfaces are presented. The molecules are designed in such way that they could potentially undergo altitudinal rotary motion (the axis of rotation is parallel to the surface) while bound to solid substrates.[*]

[*] Part of this chapter has been published:
London, G.; Carroll, G. T.; Landaluce, T. F.; Pollard, M. M.; Rudolf, P.; Feringa, B. L. *Chem. Commun.* **2009**, 1712-1714.

2.1 Introduction

The major goal of attaching rotary molecular motors to solid surfaces is to prevent their uncontrolled Brownian translational and rotational motion present in solution and to be able to harness their collective rotary action to perform work.[1-3] It has been shown that light-driven molecular motors (Figure 1a) preserve their rotary function while attached to gold nanoparticles in solution[4,5] (Figure 1b). Although this work represents an important step towards incorporating molecular motors into systems for applications, the nanometer size particles are still affected heavily by Brownian motion. Moreover, the photochemical properties of the motors could be to some extent influenced by the gold. In order to minimize Brownian motion azimuthal molecular motors (the axis of rotation is perpendicular to the surface) (Figure 2, left) were attached to macroscopic quartz, silicon[6] and semi-transparent gold surfaces[7] (Figure 1c, d). The systems were shown to undergo photochemical and thermal isomerisation while bound to the surfaces, thus transforming the relative rotation of the two halves of the motors in solution (Figure 1a) to absolute azimuthal rotation of the rotor part.

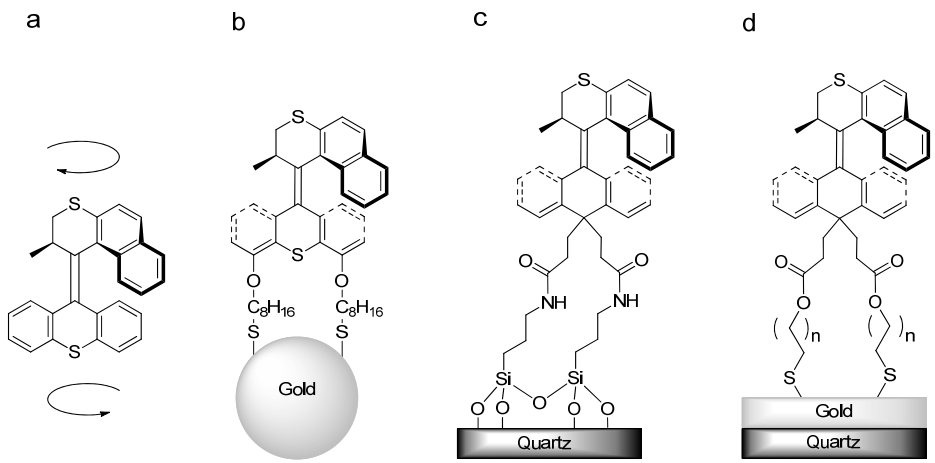

Figure 1 Transformation of the relative unidirectional rotation of the two halves of a molecular motor in solution (a) into controlled azimuthal rotation of the upper half relative to the lower half upon attachment to gold nanoparticles (b), quartz and silicon (c) and semi-transparent gold on quartz (d) surfaces.

Two-point attachment was preferred over one-point attachment in the systems described above, since it is expected that it would prevent the molecules from undergoing uncontrolled motion around a single-bond.

Azimuthal assemblies, although their importance is unambiguous in demonstrating the feasibility of absolute rotation in monolayer films, are somewhat limited towards applications aimed at controlling surface properties or applying a force that might change the coordinates of an adsorbate.

In comparison with azimuthal systems, altitudinal rotary motors (the axis of rotation is parallel to the surface) (Figure 2, right) may provide better control over surface properties including wettability, adhesion, friction and thickness due to the larger positional displacement of molecular subunits relative to the surface upon rotation.

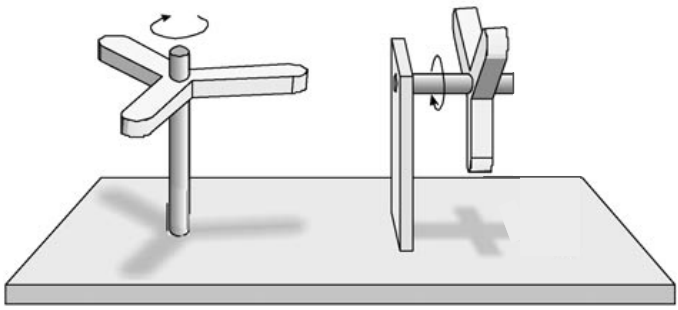

Figure 2 Left: Azimuthal rotation - the rotary axis is perpendicular to the surface; Right: Altitudinal rotation - the rotary axis is parallel to the surface. (Picture adapted from ref. 2.)

The concept of controlled molecular scale altitudinal rotation on solid surfaces was demonstrated first by Michl and co-workers.[8-10] They reported the synthesis of a series of molecules which could possibly function as unidirectional altitudinal molecular rotary motors (Figure 3). Although their unidirectional rotation has not been realized experimentally, molecular dynamics calculations suggest that it can be induced either thermally or by an oscillating electric field.

Stable submonolayers of first generation non-polar and dipolar rotors **2.1** and **2.2** were assembled on gold surfaces and imaged by STM.[8] The assembly of second generation triptycene-based non-polar and dipolar (**2.3**, X= H and F, respectively) rotors, however, was not successful, possibly due to the inadequate adhesion to the gold surface.[9] The construction of rotor **2.4** via metal-ion mediated self-assembly of coordination ligands is remarkable,[11] however, there are two main challenges to

overcome in order to attach them to solid surfaces: charge compensation and introduction of surface binding groups.

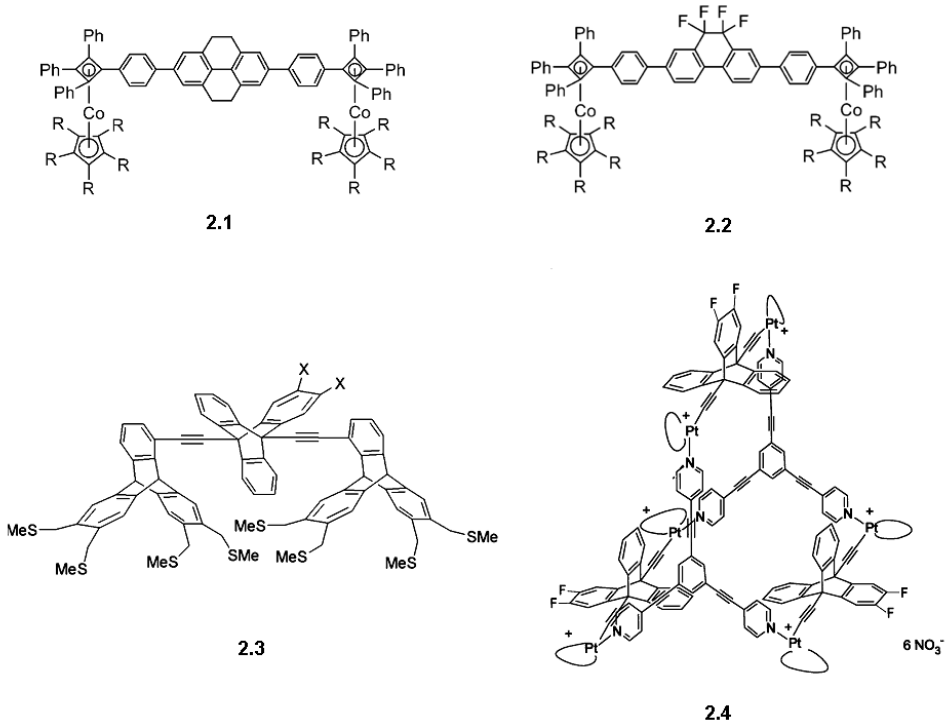

Figure 3 Potential altitudinal rotors reported by Michl and co-workers.[8-10]

Despite the potential of altitudinal rotary motors in future applications including responsive/smart surfaces and molecular electronic devices, absolute altitudinal rotary motion has not yet been realized experimentally.

In this chapter the design and synthesis of molecules potentially capable for light-driven altitudinal rotation on solid surfaces and their basic photochemical properties in solution are discussed.

2.2 Molecular design

2.2.1 Previously synthesized structures

Parallel to the development of surface bound molecular motors rotating in an azimuthal manner relative to the surface,[6] synthetic efforts have been made towards altitudinal rotary systems.[12,13] In order to achieve altitudinal rotation the linkers bearing the surface-anchoring functional groups ("legs") were displaced from the C4 and C5 or C10 positions to C2 and C3 (Figure 4).

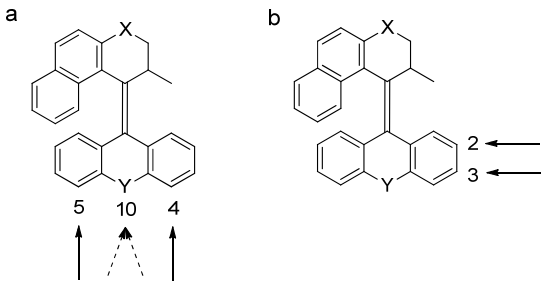

Figure 4 Azimuthal (a) and altitudinal (b) substitution pattern on second generation molecular motors.

Altitudinal motors prepared previously in our group, analogous to their azimuthal counterparts, were designed to be very slow to facilitate the analysis of their rotary cycle both in solution and on the surface. Motors bearing thiochromene upper halves are known to be slow and were chosen as the upper half in earlier designs,[12,13] while thioxanthone and fluorenone derivatives were chosen as the lower halves (Figure 5).

The general drawback of these designs is that the functionalized lower halves are not readily accessible, requiring multistep syntheses.[12,13] Additionally, considering further research towards functionalized motors of this kind, modification of upper halves containing 3-ring systems would be laborious.[14,15]

Photochemical characterization was carried out only in the case of motor **2.6**.[12] It revealed that irradiation at 254 nm results in the formation of a photostationary state containing both *cis* and *trans* unstable forms that makes the motor less attractive for future development.

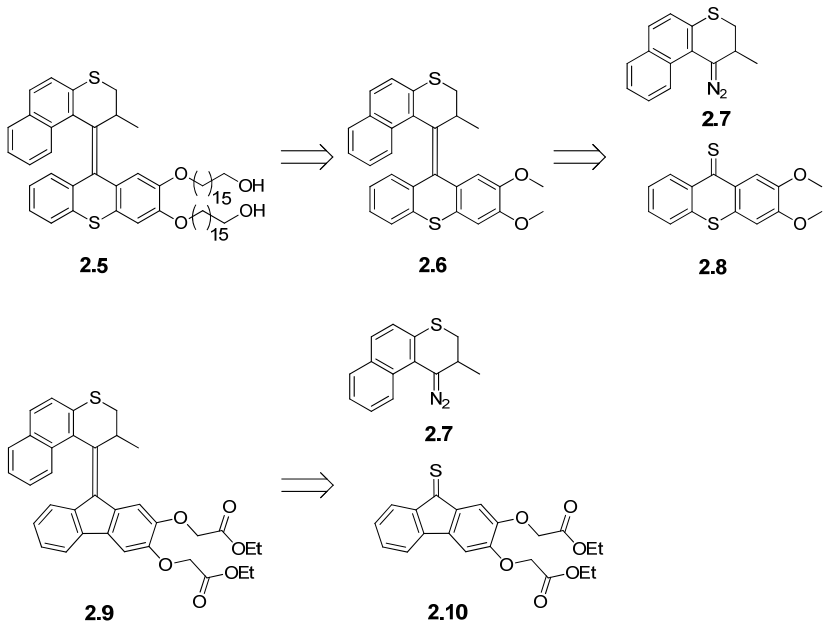

Figure 5 Previously synthesized potential altitudinal motors **2.5**[12] and **2.9**[13] and their retrosynthetic scheme.

2.2.2 Novel design

The motors used in our studies are based on a simplified structure developed recently.[16] This structure is based on a fluorene lower half as the rotor part and a substituted phenyl ring upper half as the stator part of the motor (Figure 6). Using phenyl ring-based upper halves facilitate the synthesis of highly functionalized molecular motors by avoiding the need to functionalize the naphthyl-ring systems used previously that requires lengthy syntheses.[14,15] As a lower half, fluorene is a convenient choice as it is easily available in its symmetric form and its mono-functionalized versions are relatively easily accessible also.

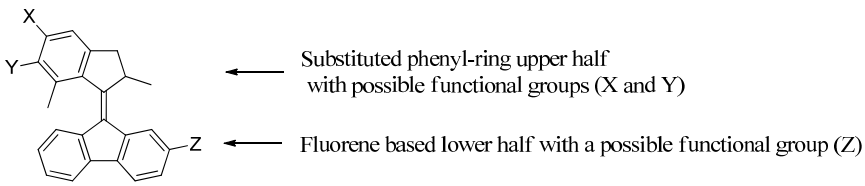

Figure 6 Novel design of altitudinal motors based on substituted phenyl-ring upper half.

Although the molecular design allows for the synthesis of molecular motors with a functionalized rotor part, in initial studies the focus will be on motors containing a symmetric fluorene ring system as the lower half because the synthesis is more straightforward and it eliminates the need to distinguish between *cis* and *trans* isomers.

2.2.3 Surface modification strategies

In the design of the molecules to be used, the nature of the surfaces should be taken into account. The molecules have to contain appropriate functional groups to be able to anchor to the outermost layer of the solid substrate.

Two attachment methods were considered for monolayer formation of molecular motors: (i) direct attachment and (ii) attachment through interfacial reactions (Figure 7) to quartz and silicon surfaces. In the case of *direct attachment* the molecules, bearing suitable functional groups, react with the outermost layer of the solid surface, an inorganic material[17,18] while in the case of *interfacial reactions,* the molecules react with the terminal functional groups of a pre-deposited organic monolayer.[19-21]

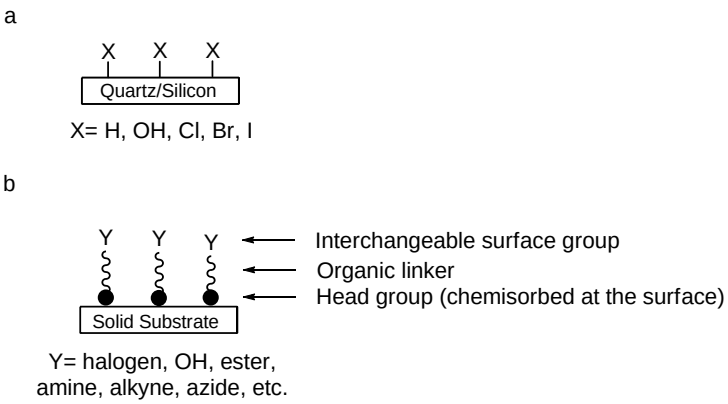

Figure 7 Solid surfaces to attach molecules *via* (a) direct attachment or (b) interfacial reaction.

Commonly used functional groups for direct attachment of molecules to hydroxylated or halogenated surfaces (e.g., aluminium-oxide, silicon-oxide, quartz, glass) are organosilicon derivatives[22] (Figure 7a). An inherent limitation of these compounds is the relatively high reactivity of the surface anchor group $–SiX_3$ (X= Cl or O-alkyl) making it incompatible with many desired functionalities that may be present in the molecule. A possible way to overcome this disadvantage is the formation of precursor monolayers with suitable terminal functional groups for further modification *via* interfacial reactions[19-21] (Figure 7b). The ability to tune the terminal functionalities of the precursor monolayers makes it possible to attach molecules with a wider variety of functional groups.

The functionalization of solid surfaces with light-driven molecular rotary motors is limited to only a few examples.[6,7] Moreover, studies regarding the effects of confinement on the physical and chemical properties of the surface-bound assemblies remain unexplored. Our initial goal was to test both kinds of attachment strategies and understand whether or not the surface-confined motors undergo rotary motion.

2.3 Synthesis of altitudinal molecular motors

2.3.1 Synthesis of molecules for direct attachment

One of the commonly used functional groups for direct attachment of molecules to solid surfaces are organosilicon derivatives. Another attractive way for direct surface-functionalization is the reaction of terminal alcohols with chlorinated quartz surfaces (Scheme 1). It was reported that molecules containing primary alcohol units readily react with glass surfaces activated with thionyl chloride.[23]

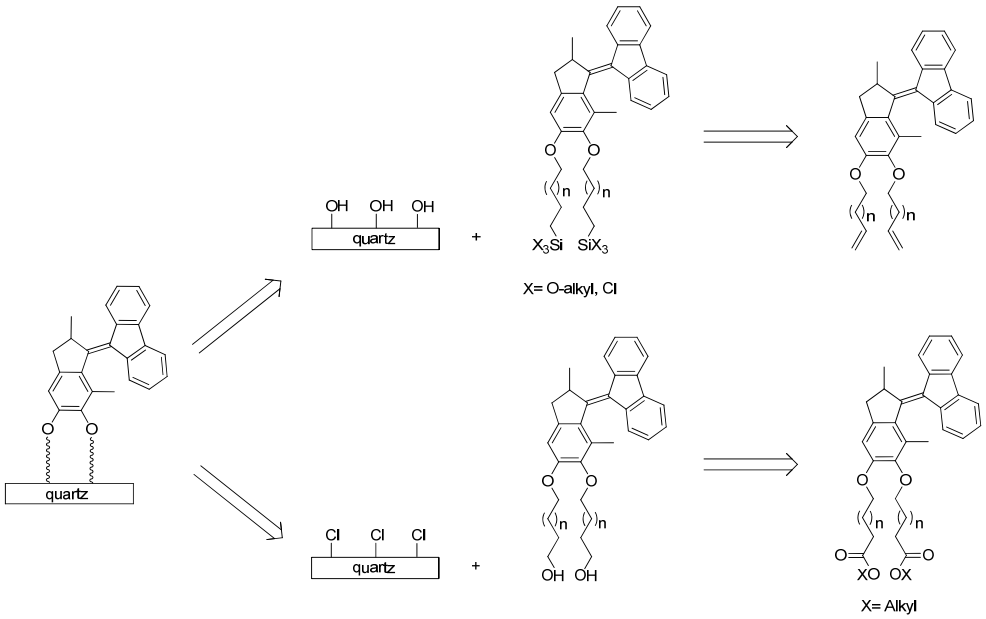

Scheme 1 Possible ways to attach molecular motors to solid surfaces *via* the direct attachment strategy.

A convenient way to introduce chloro- or alkoxysilane functional groups to a molecule is the hydrosilylation of terminal olefins. To perform this functionalization, molecular motor **2.20** (Scheme 4**)** containing two terminal alkenes was synthesized.

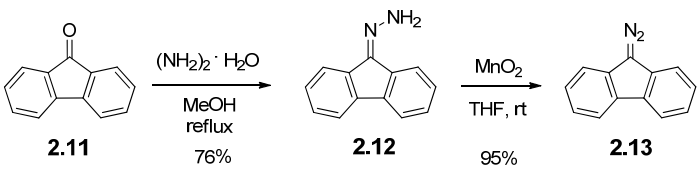

Scheme 2 Synthesis of the lower-half diazo compound **2.13**.

The synthesis of the lower half (Scheme 2) started from fluorenone, which was reacted with hydrazine monohydrate in methanol solution to give the corresponding hydrazone **2.12.** Conveniently, **2.12** was crystallized from the reaction mixture by addition of water to the hot solution followed by cooling to rt.

Hydrazone **2.12** was then treated with MnO_2 in THF yielding diazo-fluorenone **2.13** as a bench-stable, red crystalline material.

The first step in the synthesis towards the upper half containing double-bond terminated legs was a one pot two-step Friedel-Crafts acylation/Nazarov-cyclization reaction[16,24] between 2,3-dimethoxytoluene and acrylic acid (Scheme 3), which yielded ketone **2.15**.

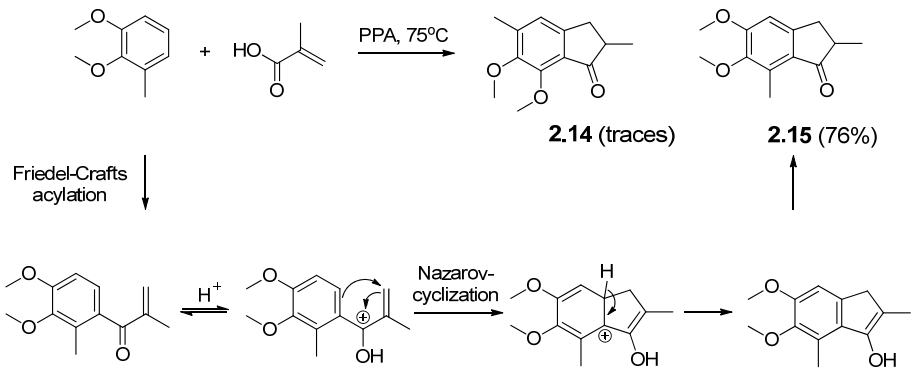

Scheme 3 The one pot two-step Friedel-Crafts acylation/Nazarov-cyclization reaction with the mechanism of the Nazarov-cyclization step.

Structural considerations based on the substitution pattern of the aromatic starting material suggested two regioisomers, **2.14** and **2.15,** as possible products, however only one product was formed,[25] which was found to be the desired ketone **2.15** as confirmed by 2D ^{1}H NMR (NOESY) spectroscopy.

The methoxy groups of ketone **2.15** were deprotected with BBr_3 to give the dihydroxy intermediate **2.16,** which was immediately functionalized further by attaching 1-bromodecene in the presence of K_2CO_3 in acetonitrile (Scheme 4). Ketone **2.17** containing the terminal alkene functional groups was converted to the corresponding thioketone **2.18** by treatment with Lawesson's reagent in toluene. Alternatively, P_2S_5 can be used for the thioketone synthesis, however, residual P_2S_5 was found to destroy the diazo compound in the next coupling step (recognizable from extensive bubbling upon the addition of a solution of the diazo compound **2.13** to the thioketone solution at room temperature). Lawesson's reagent appears to be more easily separable after the reaction, however, the formation of the thioketone requires longer reaction times in this case.

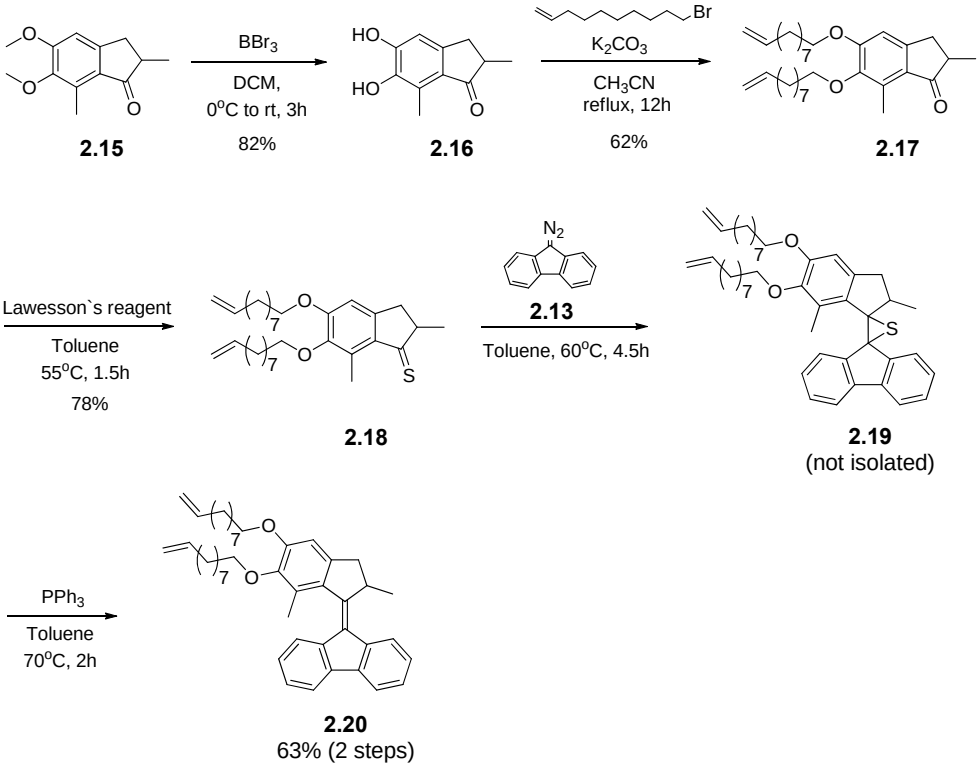

Scheme 4 Introduction of the alkene-terminated legs to upper-half ketone **2.15** and its subsequent coupling with the lower half to obtain dialkene motor **2.20**.

In the final step thioketone **2.18** was allowed to react with diazofluorene in a Barton-Kellogg reaction.[26,27] Episulfide **2.19** was formed as an intermediate in the course of the reaction which was detected by ^{1}H-NMR spectroscopy as a shift of the absorption of the aromatic proton of the thioketone from 6.76 ppm to 6.41 ppm in the episulfide. It is noted that **2.19** was not isolated; the Barton-Kellogg reaction and the subsequent desulphurization was carried out in a one-pot reaction. Alkene **2.20** was obtained from episulfide **2.19** upon addition of PPh_3 to the reaction mixture followed by stirring at 70°C for 2 h.

Compound **2.20**, bearing two terminal alkene functional groups, is suitable for the introduction of anchoring groups to attach the motor to solid surfaces (Scheme 5).

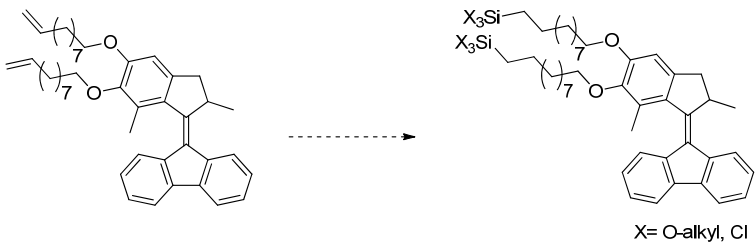

2.20 **2.21**

Scheme 5 Possible modification of dialkene-motor **2.20** to make it suitable for direct attachment to quartz/silicon surfaces.

Another possible way for direct surface-functionalization is the reaction of terminal alcohols with chlorinated quartz surfaces (Scheme 1). It has been shown that molecules containing primary alcohol units react easily with glass surfaces activated with thionyl chloride.[23] For this approach, a synthetic route to diol motor **2.27** was designed.

Dihydroxy-ketone **2.16** was transformed to ketone **2.22** by modification of the two phenolic OH-groups to introduce ester-terminated "legs". Following the synthetic sequence described for the synthesis of alkene **2.20**, compound **2.25** was obtained (Scheme 6).

In some cases upon exposure of the Barton-Kellogg-reaction mixture to prolonged heating (overnight) resulted in the spontaneous desulfurization of the episulfide, yielding not only alkene **2.25** but also a product which is possibly the result of the isomerization of the olefin (compound **2.26**). The separation of the isomerized side-product from the desired overcrowded alkene proved to be challenging. The formation of the isomerized product was not observed when the desulfurization was assisted by PPh_3.

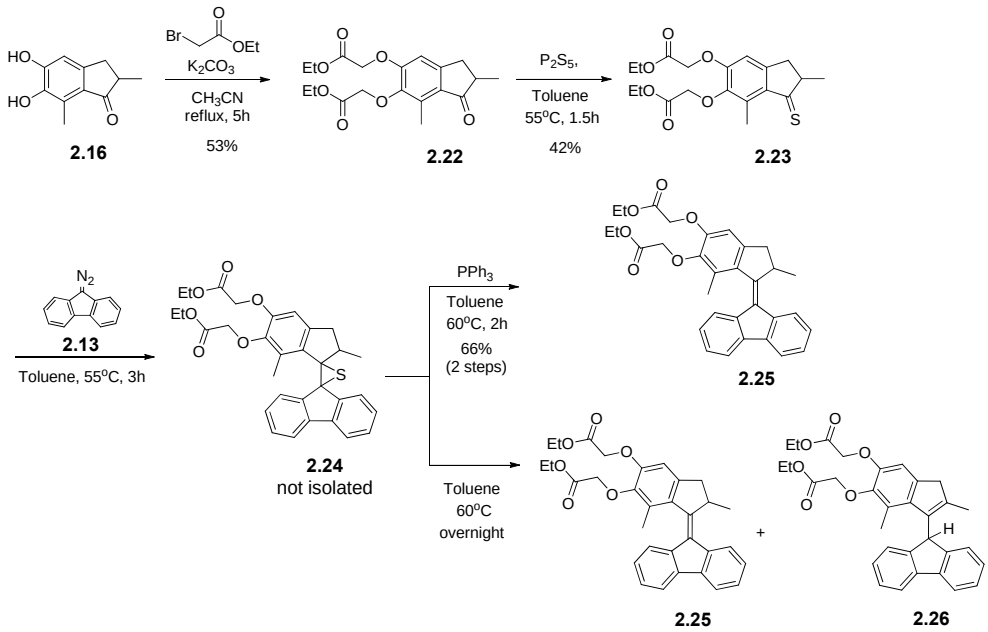

Scheme 6 Synthesis of motor **2.30** containing two ester-terminated legs.

Exposing overcrowded alkenes to reductive conditions during the course of their synthetic modifications is considered to be a critical step, which risks the reduction of the central double bond. The first attempt towards the conversion of the ester groups of **2.25** to alcohols using $LiAlH_4$ resulted in the reduction of not only the esters but also the central alkene. $LiBH_4$, however, proved to be a more selective reducing agent for the transformation (Scheme 7). Reduction of the double bond was not observed after 20 hours, which was the amount of time required to complete the reduction of the esters to primary alcohols at room temperature. Moreover, when the reduction was carried out at 40°C to decrease the reaction time (5 h), the central double bond still remained unreacted.

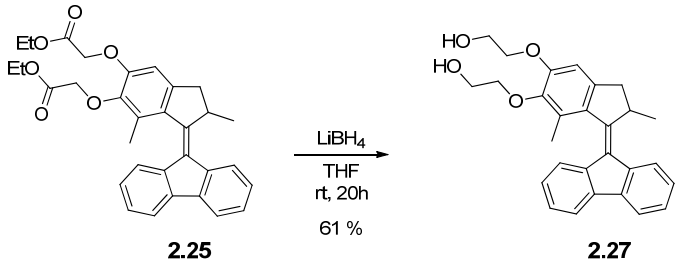

2.25 **2.27**

Scheme 7 Reduction of diester terminated motor **2.25** with $LiBH_4$ provides diol-motor **2.27** without affecting the central double bond.

2.3.2 Synthesis of molecules for interfacial reactions

Most of the synthetically useful surface reactions are performed on monolayers containing terminal carboxyl, amino, hydroxyl, alkyne or azide groups.[19-21] Terminal carboxyl, amino and hydroxyl groups could be modified through nucleophilic substitution reactions. Alkyne and azide terminated monolayers are suitable for modifications *via* copper-catalyzed 1,3-dipolar cycloaddition reactions which is the most widely employed of the so-called ”click” reactions[28] (Scheme 8).

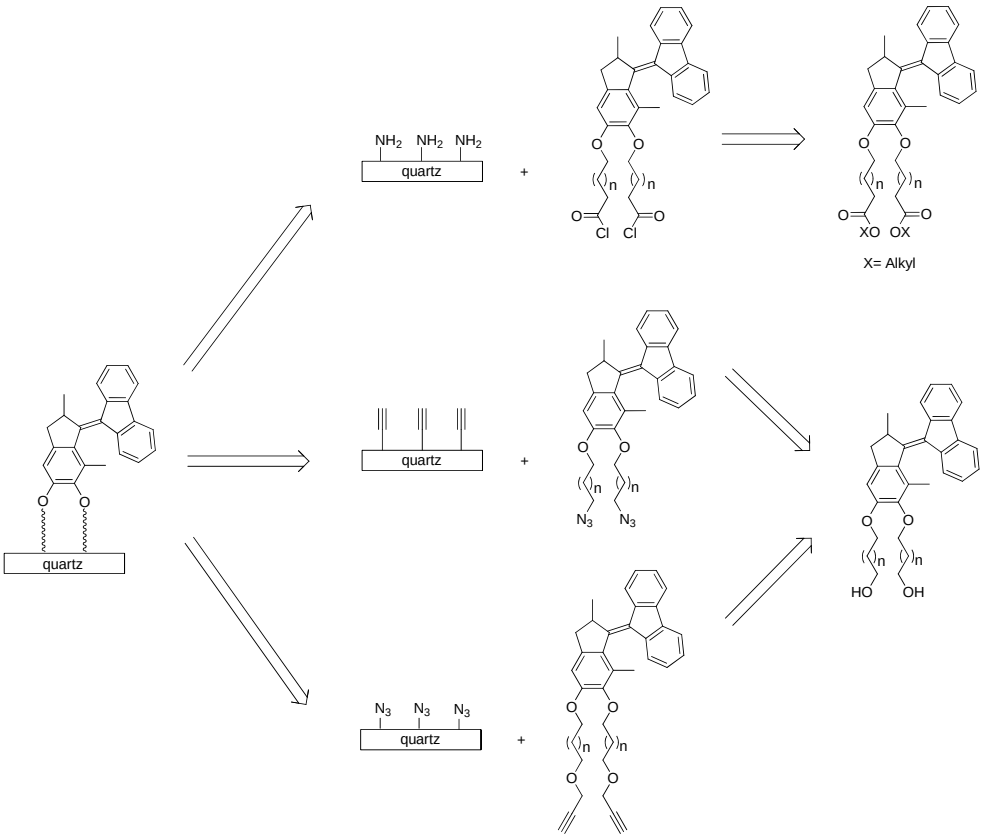

Scheme 8 Possible ways to attach molecular motors to solid surfaces *via* the interfacial reaction strategy.

It was attempted to transform diester motor **2.25** synthesized previously to its diacid chloride derivative **2.29** in order to modify amine terminated surfaces through amide-bond formation as described earlier for similar systems[6] (Scheme 9). However, the hydrolysis of the two ethyl ester groups, which is an essential step towards the surface attachement, proved to be challenging. Subjecting motor **2.25** to typical hydrolysis conditions (LiOH/EtOH at rt, KOH/MeOH/dioxane at rt), failed to provide the desired diacid derivative, yielding an inseparable mixture of products.

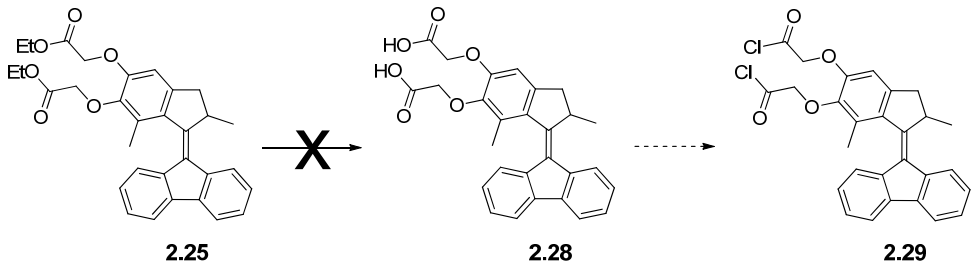

2.25 **2.28** **2.29**

Scheme 9 Attempted modification of diester-motor **2.25** to its acid chloride derivative to make it suitable for attachment to amine terminated surfaces.

Although successful hydrolysis of methyl ester containing moieties attached to molecular motors is known under the same conditions[6], in a related system the hydrolysis of esters was also not feasible.[29]

The azide-alkyne cycloaddition approach for surface modification has attracted significant interest since it fulfills several criteria required for successful interfacial reactions: (i) quantitative conversion under mild conditions, (ii) compatibility with many functional groups, (iii) no by-products.[21,30]
Molecular motors suitable for click-modification of surfaces were conveniently prepared from diol-motor **2.27** (Scheme 10).
Terminal alkyne groups, which are reactive towards azide terminated surfaces, were introduced by deprotonation of the alcohols with NaH in THF followed by alkylation with propargyl bromide.
The terminal alcohol groups of diol-motor **2.27** are also suitable to prepare a motor with terminal azides for reaction with surfaces containing alkynes. In the first step the OH-groups were converted into good leaving groups by mesylation, followed by substitution using NaN_3[31] (Scheme 10).

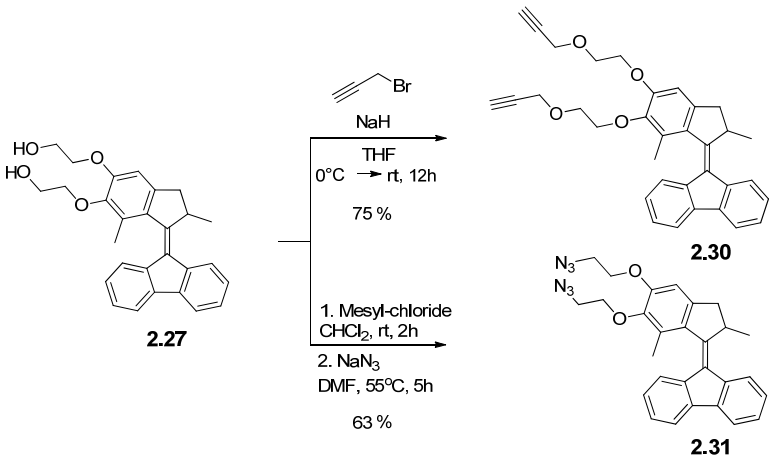

Scheme 10 Synthesis of alkyne and azide-terminated motors for interfacial 1,3-dipolar cycloadditions.

Alkylation of the dihydroxy intermediate **2.16** with propargyl bromide gives a shorter synthetic route to an alkyne terminated upper-half **2.32** (Scheme 11). Motors with this upper half have not been prepared, although the simplified synthesis can be useful, especially in the case of functionalized motors where the functional group is sensitive to reducing conditions or strong bases.

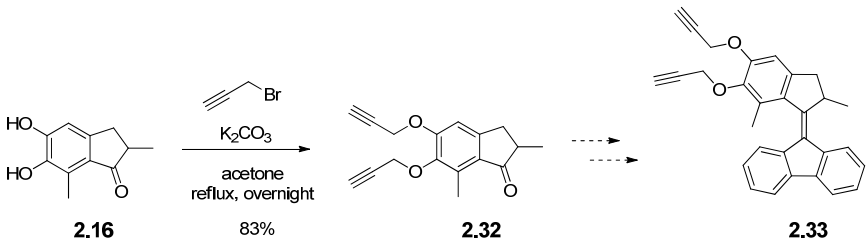

Scheme 11 A potential shorter synthesis of motor with terminal alkynes.

2.4 Photochemical and thermal isomerization studies

In comparison to previously reported and structurally similar systems,[16,32,33] motors **2.20**, **2.25**, **2.27**, **2.30** and **2.31** are anticipated to function as light-driven molecular rotary motors,[34] which involves four distinct isomerization steps in a

unidirectional fashion (Figure 8). In the rotary cycle the stable form adopts a non-planar shape to minimize the steric crowding around the tetrasubstituted central alkene. The substituent at the stereogenic centre, in order to avoid steric interaction with the lower half, adopts a pseudo-axial conformation. In the first step of the cycle the stable form of the motor undergoes a photochemical isomerization generating the unstable form in which the methyl substituent at the stereogenic centre is forced to adopt a conformationally unfavoured pseudo-equatorial orientation. This conformational strain is released as the molecule undergoes a thermal helix inversion step which leaves the stereogenic methyl group in a favoured, pseudo-axial conformation. Repeating the photochemical and thermal steps completes the 360° rotation of the upper part relative to the lower part. The unidirectionality of the process is ensured by the irreversibility of the thermal steps. Since the molecules used in our experiments have a symmetric lower-half the stable and unstable forms present are identical, which allows for easier analysis of the rotary cycle. Although the thermal *cis*/*trans* isomerization process cannot be excluded, the energy barrier in this case ($\Delta^{\ddagger}G°_2$, Figure 8) is much higher compared to the barrier of the helix inversion process ($\Delta^{\ddagger}G°_1$, Figure 8), so the latter occurs on much faster timescales.[35]

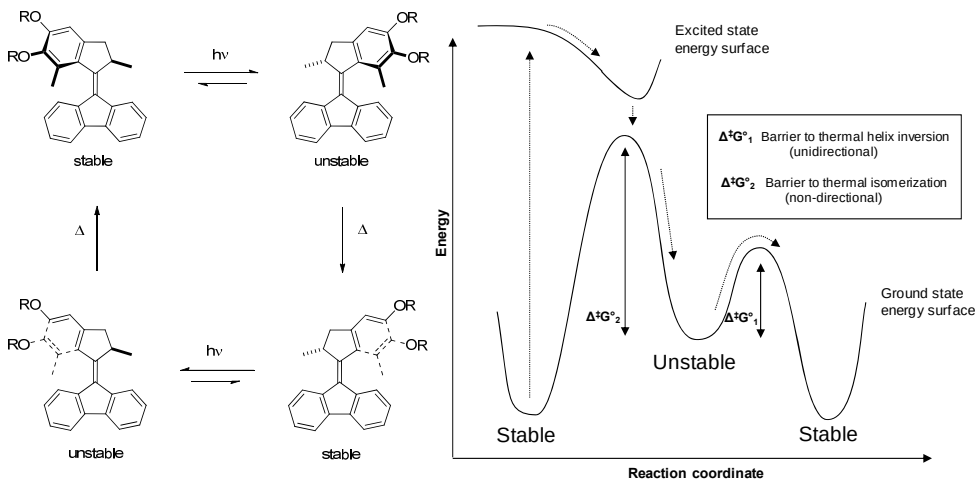

Figure 8 The four step rotary cycle and potential energy profile of light-driven molecular motors described in this chapter.

The analysis of the rotary cycle involves the observation and characterization of the higher energy intermediate forms upon irradiation of the sample at a suitable temperature with an appropriate wavelength of light.
The general techniques used to characterize the rotary cycle will be shown through the analysis of motor **2.30**.

2.4.1 UV-Vis spectroscopy

The UV-vis spectrum of a sample of **2.30** in methanol solution at 253 K has an absorption band centered at 378 nm. Irradiation (λ_{max}= 365 nm) of this sample led to a red-shift in the UV-vis absorption to a broader absorption band at 397 nm, which is consistent with the formation of the unstable isomer.[16,32] Representative UV-vis spectra for stable and unstable forms are shown in Figure 9. The sample was irradiated until no further change was observed. Allowing the solution to warm to room temperature led to a UV-vis spectrum that was identical to the spectrum of stable-**2.30,** which is consistent with the regeneration of the stable isomer through a thermal isomerization step.

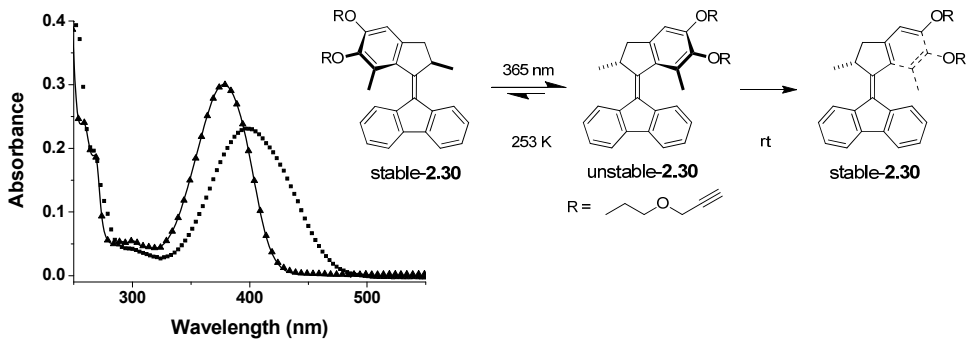

Figure 9 Representative UV-vis spectra of stable (solid line) and unstable (■) forms of **2.30** and the reversion of the UV-vis spectra to the original upon thermal helix inversion (▲).

The kinetic parameters of the thermal helix inversion of unstable-**2.30** to stable-**2.30** were determined by monitoring the change of the UV-Vis absorption at 418 nm as a function of time at different temperatures (T = 253, 258, 263, 268 K) (Figure 10 a). During the measurement of the thermal step a 380 nm cut-off filter was placed between the light source of the spectrometer and sample to eliminate photochemical processes induced by shorter wavelength light.

Based on the rate constants (k) of the first order process the Gibbs energy of activation ($\Delta^{\ddagger}G°$) could be determined using an Eyring plot (Figure 10 b) and calculated to be 83.5 kJ mol^{-1}. By extrapolation the half-life ($t_{1/2}$) of **2.30** was calculated to be 87 s at room temperature. These values are similar to those of related systems containing a fluorene moiety in their structures.[16,32]

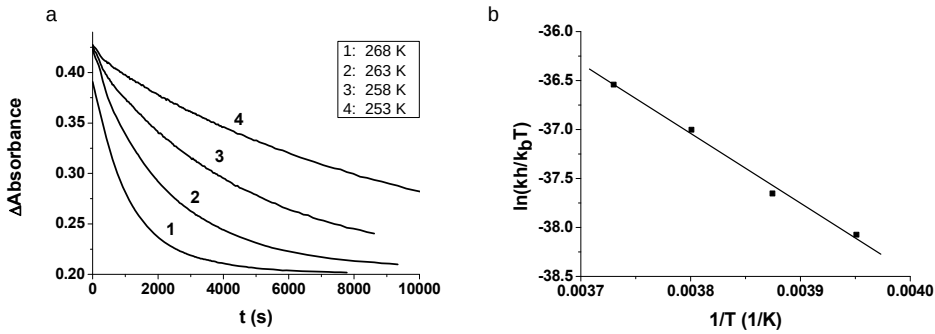

Figure 10 Thermal conversion of unstable-**2.30** to stable-**2.30** in the temperature range 253-268 K monitored by UV-vis spectroscopy in methanol solution (a) and the corresponding Eyring plot based on these data (b).

2.4.2 CD-spectroscopy

Upon irradiation of enantiopure alkene **2.30** with UV-light (λ_{max}=365 nm), *cis*/*trans* isomerization yields unstable-**2.30** which adopts a geometry that may be described as "pseudo-enantiomeric" in that it possesses approximately mirror-image molecular helicity.[36] The pseudo-enantiomeric nature of the stable and unstable forms of **2.30** allows for further study of the rotary cycle through CD spectroscopy. Separation of the enantiomers of diol-motor **2.27** was achieved by HPLC using chiral stationary phase (Chiralpak AD, heptane : isopropanol 95 : 5) This compound was alkylated with propargyl bromide yielding enantiopure (2`*R*)-(*P*)-**2.30**. A methanol solution of the enantiopure **2.30** was irradiated at $\lambda_{max}$=365 nm at -20°C to record the spectra of the unstable form at the photostationary state. Irradiation of (2`*R*)-(*P*)-**2.30** resulted in the inversion of the major absorption bands in the CD spectrum indicating a change in the molecular helicity (Figure 11). Allowing the sample to warm to room temperature regenerated the original CD spectrum of (2`*R*)-(*P*)-**2.30** indicating a reversal to the initial helicity.

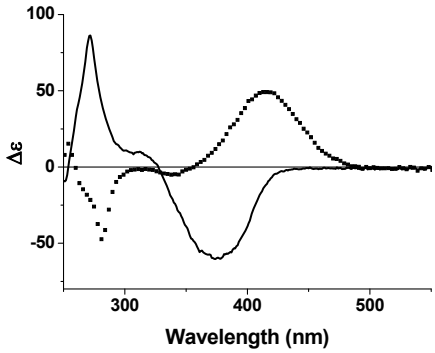

Figure 11 CD spectra of enantiopure **2.30** (1.98×10^{-4} M in MeOH) (solid line) and the inversion of the major CD bands upon UV-irradiation (■) indicating the change in molecular helicity.

2.4.3 ^{1}H-NMR spectroscopy

The different isomers formed during the rotary cycle were also characterized with ^{1}H-NMR spectroscopy (Figure 12). Irradiation (λ_{max}= 365 nm) of a solution of stable-**2.30** was performed in CD_2Cl_2 at -50°C until no further change was observed. The formation of the unstable form was followed by the appearance of a new set of absorptions upon irradiation. Characteristic changes are the upfield shift of the singlet absorption of the methyl group at the benzylic position from 2.08 (Figure 12a, CH_{3a}) to 1.93 ppm (Figure 12b, CH_{3b}) and the downfield shift of the doublet absorption of the stereogenic methyl group from 1.26 (Figure 12a, CH_{3ax}) to 1.44 ppm (Figure 12b, CH_{3eq}). The latter shift is consistent with the conformational change from the preferred pseudo-axial to the less stable pseudo-equatorial orientation upon photoisomerization in which the stable isomer is converted to the unstable form. Previously reported systems showed comparable changes in chemical shifts.[16,32]

The relative integration of the absorptions from the two isomers revealed a photostationary state of unstable-**2.30** to stable-**2.30** with a ratio of 3 : 1. Allowing the sample to warm to room temperature regenerated the original NMR-spectrum which is consistent with the selective thermal isomerization step taking place.

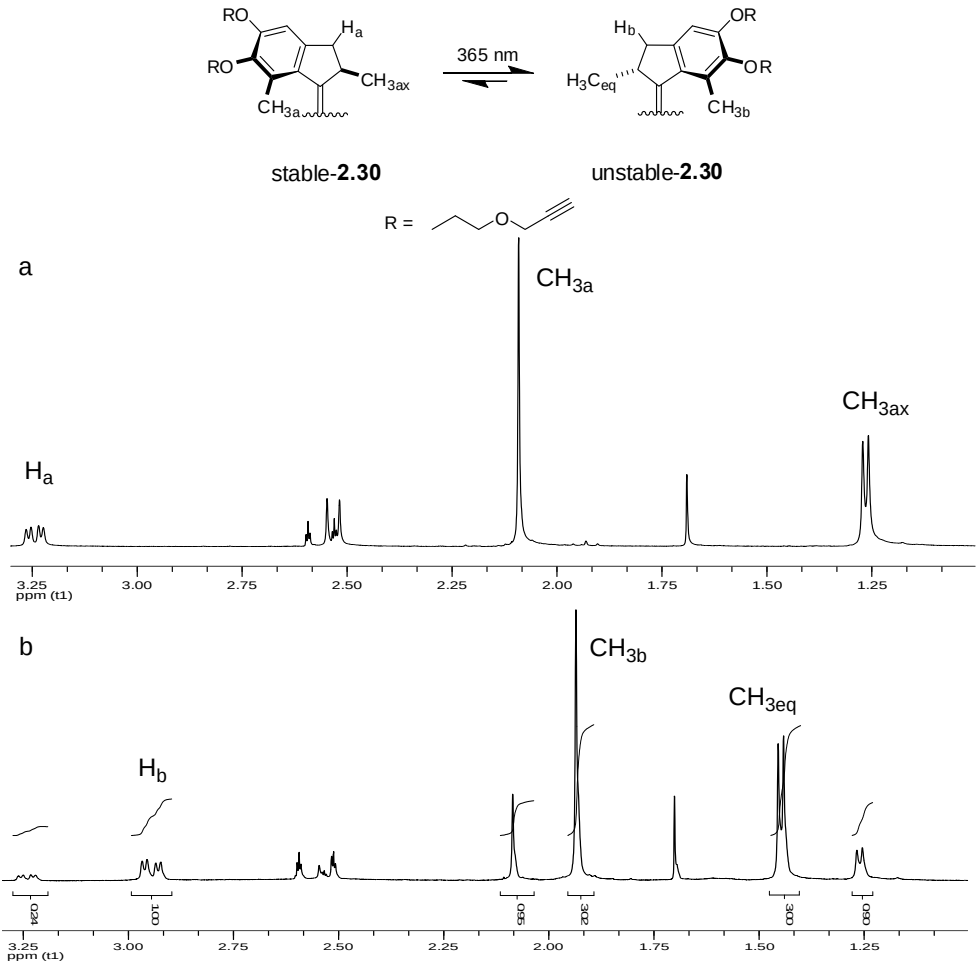

Figure 12 ^{1}H NMR spectra of stable-**2.30** in CD_2Cl_2 solution (a) and the appearance of a new set of absorptions corresponding to the unstable form upon irradiation at λ_{max} = 365 nm at -50°C (b). (Spectra were taken at -55°C.)

2.5 Discussion

The physico-chemical results obtained for the basic motor structures described in this chapter are summarized in Table 1. The data obtained are in good agreement with those of previously reported related systems[16,32] (Table 2). The introduction of the electron donating groups led to a modest red-shift of the UV-vis absorption (for motor **2.34** the major absorption band is centered at 360 nm), similarly to previous

observations.[37] Additionally, the substituents do not have a major effect on the thermal isomerization step as the half-lives obtained are comparable to those of reported for related systems[16,32] (Table 2). In the case of dialkene motor **2.20** poorer photo stationary state (PSS) composition was found compared to the other motors presented in this chapter. A possible explanation for this observation is the sensitivity of the photochemical equilibrium to the combination of the substituent and solvent.[37] It has been reported earlier, that in the case of a motor, bearing a methoxy substituent in direct conjugation with the central double bond no unstable form was detected when the irradiation was performed in dichloromethane solvent. In contrast, using toluene or hexane a slight excess of the unstable form was observed.[37] However, for further conclusions on the precise solvent effect the solvent dependence of the PSS composition of **2.20** should be measured.[16]

Table 1 Gibbs energy of activation ($\Delta^{\ddagger}G°$), half-life time ($t_{1/2}$), PSS composition and the position of the maximum of the longer wavelength absorption band (λ_{max}) for the stable form and the PSS-mixture of motors **2.20**, **2.25**, **2.27**, **2.30**, **2.31**.

Motor	$\Delta^{\ddagger}G°$ (20°C)[a] [kJ mol^{-1}]	$t_{1/2}$ (20°C) [s]	PSS (-50°C)[c] (stab : unstab)	λ_{max} (-20°C)[a] [nm] stable (PSS)
2.20 (dialkene)	81.8	43[a]	2 : 1	379 (397)
2.25 (diester)	80.5	25[b]	n.d.	374 (392)
2.27 (diol)	83	71[a]	1 : 6	378 (399)
2.30 (dialkyne)	83.5	87[a]	1 : 3	378 (397)
2.31 (diazide)	82.0	46[a]	1 : 2.5	376 (397)

[a] Measurements were performed in MeOH.
[b] Measurements were performed in isopentane.
[c] Measurements were performed in CD_2Cl_2.

Table 2 Gibbs energy of activation ($\Delta^{\ddagger}G°$), half-life time ($t_{1/2}$), and PSS composition of previously reported motors[16,32] **2.34** and **2.35**, which are structurally similar to motors described in this chapter

	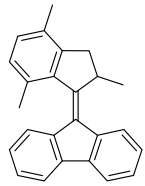 **2.34**	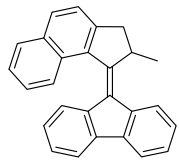 **2.35**
$t_{1/2}$ (s)	15	190
$\Delta^{\ddagger}G°$ (kJ/mol)	79	85
PSS (stab : unstab)	1 : 3	1 : 3

2.6 Conclusions

Molecular motors designed for altitudinal rotation on solid surfaces were successfully synthesized and characterized. Ketone **2.16**, containing vicinal phenolic hydroxyl groups, proved to be a very useful intermediate for the introduction of a variety of functional groups, making the molecules suitable for attachment to different kinds of solid substrates. The photochemical characterization of the functionalized motors revealed that their rate of rotation and PSS-composition is comparable to previously reported motors with similar structural features.[16,32] Additionally, although these are the fastest motors designed for surface attachment to date, they are slow enough for convenient characterization of the rotary cycle while attached to surfaces without the need of using inconveniently low or high temperatures during measurements.

All the motors presented are bearing a symmetric fluorene ring-system as the rotor part to facilitate the establishment of reproducible and robust surface attachment strategies using the simplest design possible. Furthermore, the symmetric lower half allows for a more facile characterization of the rotary cycle of surface-bound motors.

2.7 Experimental

2.7.1 General remarks

Reagents were purchased from Aldrich, Acros, Merck or Fluka and were used as provided unless otherwise stated. All solvents used were reagent grade and were dried and distilled before use according to standard procedures. Air- and moisture-sensitive liquids and solutions were transferred via syringe or stainless steel cannula. Organic solutions were concentrated by rotary evaporation 30–40 °C. Flash column chromatography was performed as described by Still et al.[38]
Chromatography: silica gel, Merck type 9385 230-400 mesh. TLC: silica gel 60, Merck, 0.25 mm, impregnated with a fluorescent indicator (254 nm).
Mass spectra (HRMS) were recorded on an AEI MS-902. Melting points were recorded on a Büchi B-545 melting point apparatus and are uncorrected. ^{1}H and ^{13}C NMR spectra were recorded on a Varian VXR-300 a Varian Mercury Plus, or a Varian Inova 500 operating at 299.97, 399.93, and 499.98 MHz, respectively, for the ^{1}H nucleus, and at 75.43, 100.57 and 124.98 MHz for the ^{13}C nucleus.
Chemical shifts for protons are reported in parts per million scale (δ scale) downfield from tetramethylsilane and are referenced to residual protium in the NMR solvents $CHCl_3$: δ 7.26, $CDHCl_2$: δ 5.32, DMSO δ 2.5, CD_2HCOD δ 3.31). Chemical shifts for carbon are reported in parts per million (δ scale) downfield from tetramethylsilane and are referenced to the carbon resonances of the solvent ($CDCl_3$: δ 77.0, CD_2Cl_2: δ 53.8, DMSO-d_6: δ 39.4). Data are represented as follows: chemical shift, multiplicity (s = singlet, d = doublet, t = triplet, q = quartet, quin = quintet, m = multiplet), coupling constant in Hz, integration. Irradiation experiments were performed using a Spectroline model ENB-280C/FE lamp at λ= 365 nm, ± 30 nm. NMR samples were placed 2-3 cm from the lamp. Solution CD spectra were recorded on a JASCO J-715 spectropolarimeter using UVASOL grade methanol in a 1.0 cm quartz cell at $T \leq$ -20ºC temperature. UV spectra were obtained using Hewlet-Packard HP 8543 diode array or a Jasco V-630 spectrophotometer in a 1 cm quartz cuvette.

2.7.2 Synthesis of compounds and intermediates

(9*H*-fluoren-9-ylidene)hydrazine (2.12)

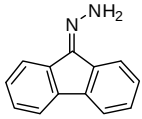

$(NH_2)_2$ x H_2O (10 mL) was added to a solution of 9*H*-fluorene-9-one (10 g, 55.5 mmol) in ethanol (150 mL) and the solution was heated at reflux for 4 h. Addition of water (5 mL) to the hot mixture followed by cooling to room temperature resulted in the precipitation of pale brown crystals (needles). The solid was filtered, washed with cold EtOH and dried on air. The product (8.17 g, 42.1 mmol, 76%) was used without further purification. ^{1}H NMR (300MHz, $CDCl_3$) δ 6.41 (br s, 2H), 7.28-7.38 (m, 3H), 7.45 (t, *J* = 7.36 Hz, 1H), 7.66 (d, *J* = 6.72 Hz, 1H), 7.76 (t, *J* = 7.8 Hz, 2H), 7.92 (d, *J* = 7.46 Hz, 1H); ^{13}C NMR (75 MHz, $CDCl_3$) δ 119.5, 120.4, 120.7, 125.4, 127.7, 127.9, 128.4, 129.6, 130.1, 137.7, 138.5, 141.2, 145.5. HRMS (ESI) calcd for $C_{13}H_{11}N_2$ 195.0917 (M^+), found 195.0918.

9-diazo-9*H*-fluorene (2.13)

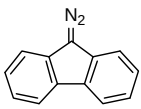

MnO_2 (5 g, 57.5 mmol) was added to a stirred solution of **2.12** (8.0 g, 41.2 mmol) in THF (60 mL), after which the colour of the solution turned to red. The mixture was stirred for an additional 1 h and then filtered over a plug of celite. Removal of the solvent under reduced pressure yielded the product as red solid (7.52 g, 39.1 mmol, 95%) which was used without further purification. ^{1}H NMR (300MHz, $CDCl_3$) δ 7.30-7.42 (m, 4H), 7.52 (d, *J* = 7.46 Hz, 2H), 7.96 (d, *J* = 7.50 Hz, 2H); ^{13}C NMR (100 MHz, $CDCl_3$) δ 119.2, 120.9, 124.4, 126.2, 131.4, 132.9.

5,6-dimethoxy-2,7-dimethyl-indane-1-one (2.15)

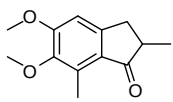

Methacrylic acid (12.9 ml, 150 mmol) and 2,3-dimethoxytoluene (12 mL, 89 mmol) were added to mechanically stirred polyphosphoric acid (30 mL), heated at 70°C. After stirring at 70°C for 3 h, the mixture was poured onto ice and stirred overnight. The water layer was extracted with EtOAc (3×50 mL). The combined organic layers were washed with aqueous $NaHCO_3$ (30 mL), water (30 mL) and brine (30 mL) and dried (Na_2SO_4). The solution was concentrated *in vacuo* and the crude product was recrystallized from *n*-heptane : EtOAc 10 : 1 to give brown crystals (13.5 g, 61.3 mmol, 76%). M.p. 106-107 °C; ^{1}H NMR (400 MHz, $CDCl_3$) δ 1.27 (d, *J* = 6.8 Hz, 3H), 2.62 (s, 3H), 2.60-2.70 (m, 2H), 3.26 (dd, *J* = 7.0, 16.8

Hz, 1H), 3.76 (s, 3H), 3.93 (s, 3H), 6.75 (s, 1H); ^{13}C NMR (APT, 125 MHz, $CDCl_3$) δ 10.5, 16.5, 34.3, 42.5, 55.7, 60.2, 105.8, 127.0, 131.8, 146.6, 151.8, 157.9, 208.8. HRMS (EI) calcd for $C_{13}H_{16}O_3$ 220.1099, found 220.1097. Elemental analysis calcd: (%) C, 70.89; H, 7.32; found: C, 70.94; H, 7.31.

5,6-dihydroxy-2,7-dimethyl-indane-1-one (2.16)

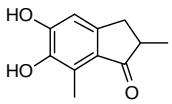

BBr_3 (1.9 ml, 20 mmol) was added slowly to a stirred solution of **2.15** (3.00 g, 13.4 mmol) in CH_2Cl_2 (10 ml) at 0°C under inert atmosphere (N_2). After 3 h at this temperature, the reaction was quenched by adding water (20 mL) slowly. The water layer was extracted with EtOAc until the water phase became colourless. The organic layer was washed with water (20 mL) and brine (20 mL), and dried (Na_2SO_4). The solvent was evaporated under reduced pressure to give the crude product as a brown solid. The solid was suspended in diethyl ether (2×20 mL) followed by filtration gave 2.10 g (10.9 mmol, 82 %) of grey powder. Mp 229.5-230.5 °C; ^{1}H NMR (500 MHz, Methanol-d_4) δ 1.20 (d, J = 7.0 Hz, 3H), 2.46 (s, 3H), 2.50 (dd, J = 3.5, 16.5 Hz, 1H), 2.54-2.61 (m, 1H), 3.18 (dd, J = 7.8, 16.8 Hz, 1H), 6.67 (s, 1H); ^{13}C NMR (APT, 100 MHz, DMSO-d_6) δ 10.3, 16.5, 33.4, 42.0, 108.9, 123.2, 125.3, 142.9, 147.2, 151.8, 208.0. HRMS (EI) calcd for $C_{11}H_{12}O_3$ 192.0786, found 192.0776. Elemental analysis calcd: (%) C, 68.74; H, 6.29; found: C, 68.37; H, 6.30.

5,6-bis(dec-9-enyloxy)-2,7-dimethyl-2,3-dihydro-1*H*-inden-1-one (2.17)

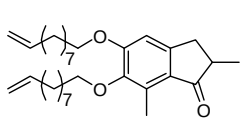

K_2CO_3 (2.5 g, 18 mmol) and 10-bromo-1-decene (2.3 mL, 11.5 mmol) were added to a solution of **2.16** (0.70 g, 3.64 mmol) in acetonitrile (30 mL) and the mixture was heated at reflux overnight. The reaction was quenched by the addition of water (50 mL). The mixture was extracted with EtOAc (3×50 mL). The combined organic layers were washed with water and brine and dried (Na_2SO_4). After the evaporation of the solvent the crude product was purified by flash chromatography (SiO_2, *n*-heptane : EtOAc = 7 : 1) to give 1.05 g (2.24 mmol, 62 %) of colourless oil. ^{1}H NMR (400 MHz, $CDCl_3$) δ 1.26 (d, J = 7.2 Hz, 3H), 1.33-1.42 (m, 16H), 1.45-1.53 (m, 4H), 1.77 (quin, J = 8.0 Hz, 2H), 1.85 (quin, J = 8.0 Hz, 2H), 2.04 ($q_{apparent}$, J = 6.8 Hz, 4H), 2.55 (s, 3H), 2.59-2.67 (m, 2H), 3.23 (dd, J = 7.6, 16.4 Hz, 1H), 3.85 (t, J = 6.4 Hz, 2H), 4.02 (t, J = 6.4 Hz, 2H), 4.91-4.92 (m, 1H), 4.93-495 (m, 1H), 4.96-4.97 (m, 1H), 5.00-5.02 (m, 1H), 5.76-5.86 (m, 2H),

6.71 (s, 1H). ^{13}C NMR (100 MHz, $CDCl_3$) δ 10.87, 16.65, 26.08, 26.11, 28.88, 28.91, 29.04, 29.10, 29.11, 29.27, 29.41, 29.46, 29.48, 30.32, 33.76, 33.78, 34.50, 42.61, 68.47, 72.99, 106.43, 114.11, 114.16, 126.95, 132.18, 139.05, 139.12, 146.06, 151.57, 157.70, 208.99. HRMS (APCI) calcd for $C_{31}H_{48}O_3$ 469.3676 (M^+), found 469, 3658 (M^+).

5,6-bis(dec-9-enyloxy)-2,7-dimethyl-2,3-dihydro-1H-indene-1-thione (2.18)

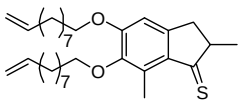

Lawesson`s reagent (202 mg, 0.5 mmol) was added to a solution of **2.17** (110 mg, 0.23 mmol) in toluene (10 ml). The mixture was heated to 75ºC for 2 h and then filtered over celite. The solid residue was washed with toluene until it became colorless. The filtrate was concentrated *in vacuo* and purified by flash chromatography (SiO_2, *n*-pentane : diethyl ether = 10 : 1) to give 86 mg (0.18 mmol, 78 %) of a purple oil . ^{1}H NMR (400 MHz, $CDCl_3$) δ 1.33-1.42 (m, 19H), 1.45-1.54 (m, 4H), 1.75-1.82 (m, 2H), 1.83-1.90 (m, 2H), 2.05 (q, *J* = 6.7 Hz, 4H), 2.70-2.75 (m, 1H), 2.73 (s, 3H), 2.97-3.05 (m, 1H), 3.32 (dd, *J* = 7.0, 17.3 Hz, 1H), 3.84 (t, *J* = 6.6 Hz, 2H), 4.06 (t, *J* = 6.4 Hz, 2H), 4.92-4.97 (m, 3H), 5.01 (s, 1H), 5.76-5.86 (m, 2H), 6.76 (s, 1H). ^{13}C NMR (APT, 100 MHz, $CDCl_3$) δ 13.1, 21.7, 26.0, 26.1, 28.8, 28.9, 29.0, 29.1, 29.2, 29.3, 29.4, 29.5, 30.2, 33.7, 33.8, 39.0, 55.3, 68.5, 73.1, 105.7, 114.1, 114.2, 134.2, 137.5, 139.0, 139.1, 146.3, 153.5, 157.5, 248.2. (1 C not observed due to overlap.) HRMS (ESI) calcd for $C_{31}H_{48}O_2S$ 485.3448 (MH^+), found 485.3627 (MH^+).

Dialkene-motor (2.20)

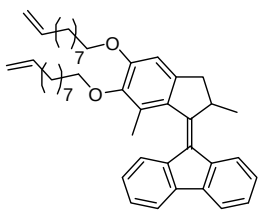

Diazofluorenone **2.13** (577 mg, 3.0 mmol) was added to a solution of thioketone **2.18** (700 mg, 1.45 mmol) in toluene (10 mL). The mixture was heated to 75ºC for 3 h. The formation of the episulfide was monitored by ^{1}H NMR spectroscopy by following the shift of the aromatic proton of the thioketone from 6.76 ppm to 6.41 ppm. PPh_3 (650 mg, 2.5 mmol) was added to the reaction mixture and it was heated for additional 2 h at 75ºC. The reaction mixture was concentrated *in vacuo.* Diethyl ether (20 mL) was added to the mixture which resulted in the precipitation of PPh_3S as yellow crystals. The precipitate was filtered and the procedure wasrepeated once more. To remove the excess PPh_3, CH_3I (1.0 mL, 16.1 mmol) was added to the ether phase and the mixture was stirred for 1 h. The resulting

precipitate was filtered. After the evaporation of the solvent the crude product was purified by flash chromatography (SiO_2, *n*-heptane : toluene = 5 : 1) to give alkene **2.20** as yellow oil which solidified to a waxy solid upon standing in the fridge (560 mg, 0.91 mmol, 63 %).
^{1}H NMR (500 MHz, $CDCl_3$) δ 1.33-1.42 (m, 19H), 1.49-1.56 (m, 4H), 1.82 (quin, *J* = 8.0 Hz, 2H), 1.88 (quin, *J* = 8.0 Hz, 2H), 2.06 (quin, *J* = 7.5 Hz, 4H), 2.18 (s, 3H), 2.53 (d, *J* = 14.5 Hz, 1H), 3.30 (dd, *J* = 5.5, 14.5 Hz, 1H), 3.92 ($q_{apparent}$, *J* = 6.5 Hz, 1H), 4.00-4.15 (m, 4H), 4.92-5.03 (m, 4H), 5.77-5.87 (m, 2H), 6.83 (s, 1H), 7.11 (t, *J* = 7.0 Hz, 1H), 7.27 (t, *J* = 7.5 Hz, 1H), 7.34-7.36 (m, 2H), 7.38 (s, *J* = 8.0 Hz, 1H), 7.76 (d, *J* = 7.5 Hz, 1H), 7.81-7.83 (m, 1H), 7.86-7.88 (m, 1H). ^{13}C NMR (125 MHz, $CDCl_3$) δ 16.33, 19.34, 26.49, 29.22, 29.39, 29.43, 29.66, 29.71, 29.77, 29.80, 29.85, 30.76, 34.09, 41.83, 45.07, 68.70, 72.99, 107.92, 114.41, 114.46, 119.36, 119.86, 123.72, 123.87, 126.63, 126.67, 126.89, 126.98, 128.77, 132.06, 133.33, 138.23, 139.35, 139.42, 139.46, 139.87, 139.99, 143.45, 145.95, 152.74, 153.76. (3 C not observed due to overlap.) HRMS (ESI) calcd for $C_{44}H_{56}O_2Na$ 639.4173, found 639.4194.

Irradiation experiment to generate unstable isomer of dialkene-motor 2.20:
Motor **2.20** (~2 mg) was dissolved in CD_2Cl_2 (~1 ml). This sample was placed in an NMR tube and irradiated with 365 nm light at -50ºC at a distance of 2-3 cm from the centre of the lamp. ^{1}H NMR spectra of the sample were taken before, during and after irradiation at -50ºC. No further changes were observed after 4 h of irradiation. The relative integration of the absorptions from the two isomers revealed a photostationary state of unstable-**2.20** to stable-**2.20** with a ratio of 1 : 2. After warming the sample to rt, only the stable form was observed by ^{1}H NMR spectroscopy.

stable-**2.20** ^{1}H NMR (500 MHz, CD_2Cl_2, -50°C) δ 1.19-1.36 (m, H), 1.37-1.50 (br m, H), 1.69-1.76 (br m, 2H), 1.76-1.84 (br m, 2H), 1.98 (br q, *J* = 6.5 Hz, 4H), 2.05 (s, 3H), 2.52 (d, *J* = 14.8 Hz, 1H), 3.23 (dd, *J* = 5.6, 14.6 Hz, 1H), 3.78 ($q_{apparent}$, *J* = 6 Hz, 1H), 3.96-4.07 (m, 4H), 4.87 (m, 2H), 4.93 (d, *J* = 5.2 Hz, 1H), 4.97 (d, *J* = 5.6 Hz, 1H), 5.73-5.83 (m, 2H), 6.85 (s, 1H), 7.10 (t, *J* = 5.9 Hz, 1H), 7.25-7.27 (m, 2H), 7.31-7.36 (m, 2H), 7.75 (d, *J* = 7.6 Hz, 1H), 7.84 (d, *J* = 6.8 Hz, 1H)
unstable-**2.20** ^{1}H NMR (500 MHz, CD_2Cl_2, -50°C) δ 1.25-1.82 (absorptions in this region could not be resolved due to overlap with remaining stable-**2.20**), 1.90 (s, 3H), 1.97-2.00 (absorptions in this region could not be resolved due to overlap with

remaining stable-**2.20**), 2.93 (dd, *J* = 5.8, 15.9 Hz, 1H), 3.37 (dd, *J* = 8.1, 16.3 Hz, 1H), 3.69 ($q_{apparent}$, *J* = 7.1 Hz, 1H), 3.90-5.82 (absorptions in this region could not be resolved due to overlap with remaining stable-**2.20**), 6.80 (s, 1H), 7.14 (t, *J* = 7.5 Hz, 1H), 7.22-7.36 (absorptions in this region could not be resolved due to overlap with remaining stable-**2.20**), 7.68 (d, *J* = 7.0 Hz, 1H) 7.75-7.85 (absorptions in this region could not be resolved due to overlap with remaining stable-**2.20**).

Diethyl 2,2'-(2,7-dimethylindane-1-one-5,6-diyl)bis(oxy)diacetate (2.22)

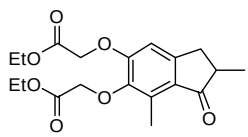

K_2CO_3 (3.5 g, 25 mmol) and ethyl bromoacetate (3.5 mL, 30 mmol) were added to a solution of **2.16** (1.96 g, 10.2 mmol) in acetonitrile (15 mL) and the mixture was heated at reflux for 5 h. The reaction was quenched by the addition of water (25 mL). The mixture was extracted with EtOAc (3 x 30 mL). The combined organic layers were washed with water (30 mL) and brine (30 mL), and dried (Na_2SO_4). After evaporation of the solvent at reduced pressure the crude product was purified by flash chromatography (SiO_2, *n*-heptane : EtOAc = 2 : 1) to give 2.84 g (7.80 mmol, 76 %) of white crystals. M.p. 81–81.5 ºC; ^{1}H NMR (400 MHz, $CDCl_3$) δ 1.27 (d, *J* = 6.8 Hz, 3H), 1.29-1.33 (m, 6H), 2.58 (dd, *J* = 4.2, 17.0 Hz, 1H), 2.63 (s, 3H), 3.23 (dd, *J* = 7.8, 16.6 Hz, 1H), 4.28 (q, *J* = 7.2 Hz, 4H), 4.66 (s, 2H), 4.73 (s, 2H), 6.62 (s, 1H); ^{13}C NMR (APT, 100 MHz, $CDCl_3$) δ 10.9, 14.0, 14.1, 16.4, 34.3, 42.6, 60.9, 61.5, 65.2, 69.4, 106.7, 128.2, 132.8, 145.1, 151.4, 155.2, 167.9, 169.2, 208.7. HRMS (EI) calcd for $C_{19}H_{24}O_7$ 364.1522, found 364.1533.

Diethyl-2,2'-(2,7-dimethyl-1-thioxo-2,3-dihydro-1H-indene-5,6-diyl)bis(oxy)diacetate (2.23)

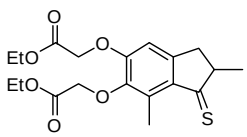

P_2S_5 (1.35 g, 3.00 mmol) was added to a solution of **2.22** (750 mg, 2.00 mmol) in toluene (10 ml). The mixture was heated to 80ºC for 1 h and then filtered over celite. The solid residue was washed with EtOAc until its colour became pale yellow. The filtrate was concentrated *in vacuo* and purified by flash chromatography (SiO_2, *n*-heptane : EtOAc = 4 : 1) to give 320 mg (0.85 mmol, 42 %) of a purple oil that solidified to a waxy solid upon standing in the fridge. (*Note*: this compound is not stable towards air or moisture and slowly decomposes to ketone **2.22**.)

^{1}H NMR (400 MHz, $CDCl_3$) δ 1.29-1.33 (m, 6H), 1.40 (d, *J* = 7.2 Hz, 3H), 2.72 (dd, *J* = 3.2, 17.2 Hz, 1H) 2.95-3.04 (m, 1H), 3.33 (dd, *J* = 6.8, 17.2 Hz, 1H), 4.28 (q, *J* = 6.8 Hz, 4H), 4.64 (s, 2H), 4.75 (s, 2H), 6.66 (s, 1H); ^{13}C NMR (APT, 100 MHz, $CDCl_3$) δ 13.2, 14.0, 21.5, 38.9, 55.5, 60.9, 61.6, 65.1, 69.5, 106.0, 134.7, 138.1, 145.3, 153.2, 154.8, 167.7, 169.1, 248.8. (1 C not observed due to overlap.) HRMS (EI) calcd for $C_{19}H_{24}O_6S$ 380.1294, found 380.1289.

Diester-motor (2.25)

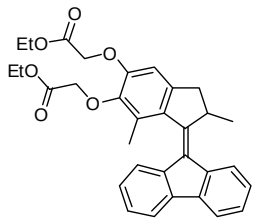

Diazofluorenone **2.13** (500 mg, 2.5 mmol) was added to a solution of **2.23** (630 mg, 1.67 mmol) in toluene (10 mL). The mixture was heated up to 55ºC for 3 h. The formation of the episulfide was monitored by ^{1}H NMR spectroscopy by following the shift of the aromatic proton of the thioketone from 6.66 ppm to 6.35 ppm. PPh_3 (650 mg, 2.5 mmol) was added to the reaction mixture and it was heated for an additional 2 h at 75ºC. The reaction mixture was concentrated *in vacuo.* EtOAc (20 mL) was added to the mixture which resulted in the precipitation of PPh_3S as yellow crystals. The precipitate was filtered and the procedure was repeated once more. After the evaporation of the solvent the crude product was purified by flash chromatography (SiO_2, *n*-heptane : EtOAc = 5 : 1) to give alkene **2.25** as yellow solid (570 mg, 1.11 mmol, 66 %). ^{1}H NMR (400 MHz, $CDCl_3$) δ 1.30-1.34 (m, 9H), 2.25 (s, 3H), 2.52 (d, *J* = 14.4 Hz, 1H), 3.28 (dd, *J* = 5.8, 14.2 Hz, 1H), 4.12 (quin, *J* = 6.2 Hz, 1H), 4.26-4.33 (m, 4H), 4.66 (d, *J* = 16.0 Hz, 1H), 4.73 (s, 2H), 4.88 (d, *J* = 16.0 Hz, 1H), 6.74 (s, 1H), 7.14 (t, *J* = 7.6 Hz, 1H), 7.28 (t, *J* = 7.4 Hz, 1H), 7.32-7.38 (m, 3H), 7.74 (d, *J* = 8.0 Hz, 1H), 7.79-7.81 (m, 1H), 7.84-7.86 (m, 1H); ^{13}C NMR (APT, 100 MHz, $CDCl_3$) δ 14.0, 14.1, 16.1, 18.8, 41.3, 44.7, 60.8, 61.3, 65.7, 69.2, 108.2, 119.0, 119.5, 123.6, 126.5, 126.6, 126.7, 126.9, 129.4, 131.9, 134.6, 137.6, 139.1, 139.4, 139. 7, 143.2, 145.0, 150.9, 151.1, 168.4, 169.5 (1 C not observed due to overlap.) HRMS (EI) calcd for $C_{32}H_{32}O_6$ 512.2199, found 512.2188.

Isomerized alkene (2.26)

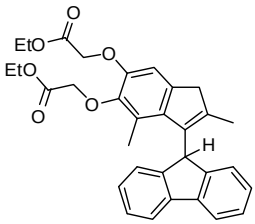

Prolonged heating of the formed episulfide during the synthesis of **2.25** resulted in spontaneous desulfurization, which yielded not only alkene **2.25** but also also a product which is suggested to be the result of the isomerization of the olefin.

^{1}H NMR (300 MHz, $CDCl_3$) δ 1.29 (t, 6H, *J*= 7.2 Hz), 1.97 (s, 3H), 2.93 (s, 3H), 3.40 (s, 2H), 4.26 (q, 4H, *J*= 7.2 Hz), 4.67 (s, 4H), 5.08 (s, 1H), 6.86 (s, 1H), 7.14-7.23 (m, 3H), 7.28-7.37 (m, 3H), 7.72 (d, 2H, *J*=7.5 Hz)

Diol-motor (2.27)

A solution of **2.25** (90 mg, 0.21 mmol) in THF (5 mL) was added to a suspension of $LiBH_4$ (22 mg, 1 mmol) in THF (3 mL) and the mixture was stirred at rt for 20 h. The reaction was quenched with aqueous HCl solution (5 mL, 0.1 M) and the mixture was extracted with EtOAc until the aqueous phase was colourless. The combined organic layers were washed with water (20 mL) and brine (20 mL) and dried (Na_2SO_4). The solvent was evaporated under reduced pressure and the crude product was recrystallized from toluene : *n*-heptane (5 : 1) to give yellow crystals (70 mg, 0.14 mmol, 67 %). M.p. 187.5-188.0ºC. ^{1}H NMR (500 MHz, DMSO-d_6) δ 1.26 (d, *J* = 6.5 Hz, 3H), 2.10 (s, 3H), 2.55 (d, *J* = 15.0 Hz, 1H), 3.24 (dd, *J* = 5.8, 14.8 Hz, 1H), 3.71 (q, *J* = 5.5 Hz, 2H), 3.80 (q, *J* = 5.5 Hz, 2H), 3.92-3.96 (m, 1H), 4.03 (quin, *J* = 6.5 Hz, 1H), 4.06-4.10 (m, 1H), 4.12-4.17 (m, 2H), 4.80 (t, *J* = 5.0 Hz, 1H, O*H*), 4.93 (t, *J* = 5.0 Hz, 1H, O*H*), 7.06 (s, 1H), 7.17 (t, *J* = 7.8 Hz, 1H), 7.26-7.31 (m, 2H), 7.35-7.40 (m, 2H), 7.83 (d, *J* = 7.0 Hz, 1H), 7.87 (d, *J* = 7.5 Hz, 1H), 7.91-7.93 (m, 1H); ^{13}C NMR (APT, 125 MHz, $CDCl_3$) δ 15.9, 18.9, 41.5, 44.8, 61.0, 62.1, 70.5, 108.0, 119.2, 119.6, 123.2, 123.7, 126.4, 126.7, 126.8, 126.9, 129.1, 131.9, 134.0, 137.8, 139.3, 139.5, 139.6, 143.9, 145.4, 151.5, 152.3. (1 C not observed due to overlap.) HRMS (EI) calcd for $C_{28}H_{28}O_4$ 428.1987, found 428.1998.

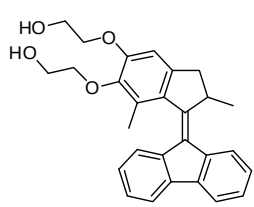

Irradiation experiment to generate unstable isomer of diol-motor 2.27:

Irradiation of diol-motor **2.27** was performed under identical conditions as dialkene-motor **2.20**, however, in this case only ~1 mg sample was used because precipitation was observed at higher concentrations from CD_2Cl_2 solution at low

temperature. The relative integration of the absorptions from the two isomers at the PSS revealed a photostationary state of unstable-**2.27** to stable-**2.27** with a ratio of 6 : 1.

stable-**2.27** ^{1}H NMR (500 MHz, -50ºC, CD_2Cl_2) δ 1.27 (d, *J* = 6.6 Hz, 3H), 2.12 (s, 3H), 2.55 (d, *J* =14.8 Hz, 1H), 3.26 (dd, *J* = 5.6, 14.8 Hz, 1H), 3.56-3.59 (m, 1H), 3.79-3.85 (m, 1H), 3.92 (br, 3H), 3.97-4.02 (m, 1H), 4.06-4.14 (m, 4H), 4.34 (t, *J* = 6.9 Hz, 1H,), 6.89 (s, 1H), 7.12 (t, *J* = 7.54 Hz, 1H), 7.24-7.29 (m, 2H), 7.32-7.37 (m, 2H), 7.76 (d, *J* = 7.6 Hz, 1H), 7.79-7.82 (m, 1H), 7.84-7.87 (m, 1H)
unstable-**2.27** ^{1}H NMR (500 MHz, -50ºC, CD_2Cl_2) δ 1.46 (d, *J* = 6.4 Hz, 3H), 1.97 (s, 3H), 2.96 (dd, *J* = 6.0, 16.4 Hz, 1H), 3.38 (dd, *J* = 8.4, 16.3 Hz, 1H), 3.52-3.54 (m, 1H), 3.75-4.13 (absorptions in this region could not be resolved due to overlap with remaining stable-**27**), 4.31 (t, *J* = 7.0 Hz, 1H), 6.83 (s, 1H), 7.10-7.36 (absorptions in this region could not be resolved due to overlap with remaining stable-**2.27**), 7.67-7.69 (m, 1H), 7.47-7.87 (absorptions in this region could not be resolved due to overlap with remaining stable-**2.27**)

Dialkyne-motor (2.30)

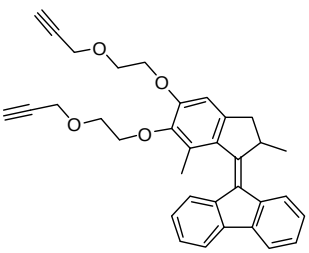

A suspension of NaH (30 mg, 1.3 mmol) in THF (3 mL) was cooled to 0ºC and a solution of **2.27** (67 mg, 0.16 mmol) in THF (7 mL) was added dropwise (under N_2 atmosphere). To this mixture propargyl bromide (50 µL, 0.45 mmol, 80 % in toluene) was added. The solution was stirred at rt for 12 h. The reaction was quenched with water (10 mL) and the mixture was extracted with EtOAc until the yellow colour of the aqueous phase had disappeared. The organic phase was washed with water (10 mL) and brine (10 mL) and dried (Na_2SO_4). The solvent was evaporated under reduced pressure and the crude product was recrystallized from *n*-heptane to give yellow crystals (55 mg, 0.11 mmol, 69 %). M.p. 138.0-139.0ºC; ^{1}H NMR (400 MHz, $CDCl_3$) δ 1.32 (d, *J* = 6.8 Hz, 3H), 2.20 (s, 3H), 2.43 (t, *J* = 2.0 Hz, 1H), 2.49 (t, *J* = 2.4 Hz, 1H), 2.53 (d, *J* = 14.8 Hz, 1H), 3.29 (dd, *J* = 5.8, 14.6 Hz, 1H), 3.91 (t, *J* = 4.6 Hz, 2H), 3.98 (t, *J* = 4.2 Hz, 2H), 4.09-4.16 (m, 2H), 4.21-4.36 (m, 3H), 4.31 (dd, *J* = 0.6, 2.2 Hz, 2H), 4.32 (dd, *J* = 0.8, 2.4 Hz, 2H), 6.84 (s, 1H), 7.11 (t, *J* = 7.4 Hz, 1H), 7.23 (t, *J* = 7.4 Hz, 1H), 7.33-7.37 (m, 3H), 7.75 (d, *J* = 7.2 Hz, 1H), 7.80-7.82 (m, 1H), 7.85-7.87 (m, 1H); ^{13}C NMR (APT, 100 MHz, $CDCl_3$) δ 16.0, 19.0, 41.5, 44.8,

58.3, 58.6, 68.00, 68.2, 69.3, 71.5, 74.5, 74.7, 108.3, 119.1, 119.6, 123.5, 123.6, 126.5, 126.5, 126.7, 128.9, 131.9, 133.8, 137.8, 139.1, 139.6, 143.2, 145.7, 152.0, 152.6. (4 C not observed due to overlap.) HRMS (EI) calcd for $C_{34}H_{32}O_4$ 504.2301, found 504.2286.

Irradiation experiment to generate unstable isomer of dialkyne motor 2.30:
Irradiation of dialkyne-motor **2.30** was performed under identical conditions as for dialkene-motor **2.20**. No further changes were observed after 5h of irradiation. The relative integration of the absorptions from the two isomers revealed a photostationary state of unstable-**2.30** to stable-**2.30** with a ratio of 3 : 1.

stable-**2.30**: ^{1}H NMR (500 MHz, -50ºC, CD_2Cl_2) δ 1.25 (d, *J* = 6.5 Hz, 3H), 2.08 (s, 3H), 2.52 (d, *J* = 15.0 Hz, 1H), 2.52 (t, *J* = 2.5 Hz, 1H), 2.58 (t, *J* = 2.5 Hz, 1H), 3.23 (dd, *J*= 5.5, 14.8 Hz, 1H), 3.76-3.85 (m, 2H), 3.92 (t, *J* = 4.0 Hz, 2H), 3.96-4.00 (m, 1H), 4.06 (quin, *J*= 6.5 Hz, 1H), 4.14-4.27 (m, 7H), 6.84 (s, 1H), 7.1 (t, *J* = 7.0 Hz, 1H), 7.23-7.27 (m, 2H), 7.30-7.35 (m, 2H), 7.74 (d, *J* = 7.5Hz, 1H) , 7.78-7.80 (m, 1H), 7.83-7.84 (m, 1H)
unstable-**2.30**: ^{1}H NMR (500 MHz, -50ºC, CD_2Cl_2) δ 1.44 (d, *J* = 6.5 Hz, 3H), 1.93 (s, 3H), 2.94 (dd, *J* = 6.0, 16.5 Hz, 1H), 2.51 (t, *J* = 2.5 Hz, 1H), 2.59 (t, *J* = 2.5 Hz, 1H), 3.37 (dd, *J* = 8.5, 16.5 Hz, 1H), 3.71-4.29 (absorptions in this region could not be resolved due to overlap with remaining stable-**2.30**), 6.80 (s, 1H), 7.09-7.35 (absorptions in this region could not be resolved due to overlap with remaining stable-**2.30**), 7.67-7.69 (m, 1H), 7.74-7.85 (absorptions in this region could not be resolved due to overlap with remaining stable-**2.30**).

Diazide-motor (2.31)

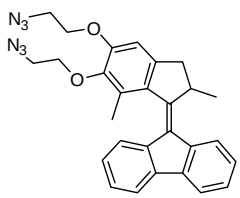

Methanesulfonyl chloride (28 µL, 0.350 mmol) was added to a mixture of diol motor **2.27** (50 mg, 0.117 mmol) and triethylamine (100 µL) in dichloromethane (5 mL) cooled to 0°C, and the solution was allowed to warm to rt. After 3 h at rt the mixture was poured on ice-cold 1 M aqueous HCl-solution (20 mL). The mixture was extracted with dichloromethane (3×20 mL), washed with saturated aqueous $NaHCO_3$-solution (2×30 mL) and dried (Na_2SO_4). After evaporation of the solvent at reduced pressure the residue was dissolved in DMF (5 mL), NaN_3 was added (46 mg, 0.7 mmol) and the mixture was stirred at 55°C for 5h. The reaction was quenched with

water (10 mL) and the mixture was extracted with EtOAc (3×10 mL). The organic phase was washed with water (20 mL) and brine (20 mL) and dried (Na_2SO_4). The solvent was evaporated at reduced pressure and the crude product was purified by flash chromatography (SiO_2, *n*-heptane : EtOAc 3 : 1) to give a yellow solid (31 mg, 0.065 mmol, 56%). ^{1}H NMR (400 MHz, CD_2Cl_2) δ 1.32 (d, *J* = 6.8 Hz, 3H), 2.20 (s, 3H), 2.57 (d, *J* = 14.4 Hz, 1H), 3.31 (dd, *J* = 5.6, 14.4 Hz, 1H), 3.62 (br, t, 2H), 3.73 (br, t, 2H), 4.10-4.17 (m, 2H), 4.19-4.30 (m, 3H), 6.90 (s, 1H), 7.14 (t, *J* = 7.6 Hz, 1H), 7.29 (t, *J* = 7.6 Hz, 1H), 7.33-7.37 (m, 3H), 7.77 (d, *J* = 8.0 Hz, 1H), 7.80-7.83 (m, 1H), 7.87-7.89 (m, 1H);
^{13}C NMR (APT, 100 MHz, $CDCl_3$) δ 15.9, 18.9, 41.5, 44.8, 50.5, 51.3, 67.4, 71.1, 108.2, 119.2, 119.6, 123.3, 123.7, 126.5, 126.7, 126.8, 127.0, 129.3, 132.1, 134.3, 137.8, 139.3, 139.6, 139.7, 143.6, 145.1, 151.4, 152.2. HRMS (EI) calcd for $C_{28}H_{26}N_6O_2$ 478.2117, found 478.2125.

Irradiation experiment to generate unstable isomer of diazide-motor 2.31:
Irradiation of diazide-motor **2.31** was performed under identical conditions as for dialkene-motor **2.20**. No further changes were observed after 6h of irradiation. The relative integration of the absorptions from the two isomers revealed a photostationary state of unstable-**2.31** to stable-**2.31** with a ratio of 5 : 2.

stable-**2.31**: ^{1}H NMR (500 MHz, -50ºC, CD_2Cl_2) δ 1.26 (d, *J* = 5.5 Hz, 3H), 2.15 (s, 3H), 2.54 (d, *J* =14.5 Hz, 1H), 3.25 (dd, *J* = 4.0, 13.8 Hz, 1H), 3.50-3.61 (br, m, 2H), 3.63-3.70 (br, m, 1H), 3.70- 3.78 (br, m, 1H), 4.01-4.12 (br, m, 2H), 4.12-4.19 (br, m, 1H), 4.19-4.28 (br, m, 2H), 6.87 (s, 1H), 7.12 (t, *J* = 7.0 Hz, 1H), 7.27 (d, *J* = 7.5 Hz, 2H), 7.31-7.38 (m, 2H), 7.76 (d, *J* = 7.0 Hz, 1H), 7.78-7.83 (m, 1H), 7.83-7.88 (m, 1H).
unstable-**2.31**: ^{1}H NMR (500 MHz, -50ºC, CD_2Cl_2) δ 1.46 (d, *J* = 5.5 Hz, 3H), 2.00 (s, 3H), 2.90 (dd, *J* = 5.5, 15.5 Hz, 1H), 3.36-3.41 (m, 1H), 3.53-4.22 (absorptions in this region could not be resolved due to overlap with remaining stable-**2.31**), 6.81 (s, 1H), 7.15 (t, *J* = 7.0 Hz, 1H), 7.23-7.35 (absorptions in this region could not be resolved due to overlap with remaining stable-**2.31**), 7.65-7.71 (m, 1H), 7.75-7.87 (absorptions in this region could not be resolved due to overlap with remaining stable-**2.31**)

2,7-dimethyl-5,6-bis(prop-2-ynyloxy)-2,3-dihydro-1*H*-inden-1-one (2.32)

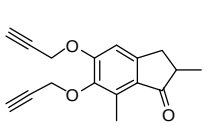

K_2CO_3 (0.83 g, 6 mmol) and propargyl bromide (80 % in toluene, 1.13 mL, 10 mmol) were added to a solution of **2.16** (0.5 g, 2.6 mmol) in acetone (10 mL). The mixture was heated at reflux overnight and then quenched by the addition of water (20 mL). The aqueous solution was extracted with EtOAc (3×20 mL). The organic phase was washed with water and brine and dried (Na_2SO_4). The solvent was evaporated at reduced pressure and the crude product was purified by recrystallization (heptane : EtOAc 4 : 1) to give pale brown crystals (0.58 mg, 2.16 mmol, 83 %). M.p. 111-112 °C. ^{1}H NMR (400 MHz, $CDCl_3$) δ 1.27 (d, J = 6.8 Hz, 3H), 2.44 (s, 1H), 2.56 (s, 1H), 2.58-2.70 (m, 2H), 2.62 (s, 3H), 3.28 (dd, J = 7.4, 16.7 Hz, 1H), 4.67 (s, 2H), 4.82 (s, 2H), 6.88 (s, 1H); ^{13}C NMR (75 MHz, CD_2Cl_2) δ 11.5, 16.6, 34.7, 43.0, 56.6, 60.1, 75.5, 76.6, 78.0, 79.6, 107.9, 128.2, 133.5, 144.9, 152.2, 155.8, 208.7. HRMS (EI) calcd for $C_{17}H_{16}O_3$ 268.1100, found 268.1085.

2.8 References

(1) Browne, W. R.; Feringa, B. L. *Nature Nanotechnology* **2006**, *1*, 25-35.

(2) Balzani, V.; Credi, A.; Venturi, M. *ChemPhysChem* **2008**, *9*, 202-220.

(3) Katsonis, N.; Lubomska, M.; Pollard, M. M.; Feringa, B. L.; Rudolf, P. *Prog. Surf. Sci.* **2007**, *82*, 407-434.

(4) van Delden, R. A.; ter Wiel, M. K. J.; Pollard, M. M.; Vicario, J.; Koumura, N.; Feringa, B. L. *Nature* **2005**, *437*, 1337-1340.

(5) Pollard, M. M.; ter Wiel, M. K. J.; van Delden, R. A.; Vicario, J.; Koumura, N.; van den Brom, C. R.; Meetsma, A.; Feringa, B. L. *Chem. Eur. J.* **2008**, *14*, 11610-11622.

(6) Pollard, M. M.; Lubomska, M.; Rudolf, P.; Feringa, B. L. *Angew. Chem. Int. Ed.* **2007**, *46*, 1278-1280.

(7) Carroll, G. T.; Pollard, M. M.; van Delden, R.; Feringa, B. L. *Chem. Sci.* **2010**, *1*, 97-101.

(8) Zheng, X. L.; Mulcahy, M. E.; Horinek, D.; Galeotti, F.; Magnera, T. F.; Michl, J. *J. Am. Chem. Soc.* **2004**, *126*, 4540-4542.

(9) Magnera, T. F.; Michl, J. *Top. Curr. Chem.* **2005**, *262*, 63-97.

(10) Horinek, D.; Michl, J. *Proc. Natl. Acad. Sci. U. S. A.* **2005**, *102*, 14175-14180.

(11) Caskey, D. C.; Wang, B.; Zheng, X. L.; Michl, J. *Collect. Czech. Chem. Commun.* **2005**, *70*, 1970-1985.
(12) Personal communication (Cristoph Stock).
(13) Personal communication (Javier Vicario).
(14) ter Wiel, M. K. J.; Feringa, B. L. *Synthesis* **2005**, 1789-1796.
(15) Qu, D. H.; Feringa, B. L. *Angew. Chem. Int. Ed.* **2010**, *49*, 1107-1110.
(16) Pollard, M. M.; Meetsma, A.; Feringa, B. L. *Org. Biomol. Chem.* **2008**, *6*, 507-512.
(17) Jingxian Yu; Shapter, J. G.; Quinton, J. S.; Johnston, M. R.; Beattie, D. A. *Phys. Chem. Chem. Phys.* **2007**, *9*, 510; 510-520; 520.
(18) Richter, C. A.; Hacker, C. A.; Richter, L. J.; Vogel, E. M. *Solid-State Electron.* **2004**, *48*, 1747-1752.
(19) Chechik, V.; Crooks, R. M.; Stirling, C. J. M. *Adv. Mater.* **2000**, *12*, 1161-1171.
(20) Haensch, C.; Hoeppener, S.; Schubert, U. S. *Chem. Soc. Rev.* **2010**, *39*, 2323-2334.
(21) Li, J.; Thiara, P. S.; Mrksich, M. *Langmuir* **2007**, *23*, 11826-11835.
(22) Ulman, A. *Chem. Rev.* **1996**, *96*, 1533-1554.
(23) Hergenrother, P. J.; Depew, K. M.; Schreiber, S. L. *J. Am. Chem. Soc.* **2000**, *122*, 7849-7850.
(24) Kaminsky, W.; Rabe, O.; Schauwienold, A. M.; Schupfner, G. U.; Hanss, J.; Kopf, J. *J. Organomet. Chem.* **1995**, *497*, 181-193.
(25) Literature examples of Friedel-Crafts acylations on structurally related aromatic compounds (3-methylanisole, 2,3-dimethylanisole) report similar selectivities as observed here. Bartoli, G. *et al*. *Tetrahedron Lett*. **2002**, *43*, 6331-6333.; Cregoe, E., J. *et al*. *J. Med. Chem.* **1986**, *28*, 825-841.; He, F. *et al*. *Synth. Commun*. **2008**, *38*, 255-264.; Smith, K. *et al*. *Org. Biomol. Chem.* **2003**, *1*, 1560-1564.
(26) Barton, D. H. R.; Willis, B. J. *J. Chem. Soc. Perkin Trans. 1* **1972**, 305.
(27) Buter, J.; Wassenaar, S.; Kellogg, R. M. *J. Org. Chem.* **1972**, *37*, 4045-4060.
(28) Kolb, H. C.; Finn, M. G.; Sharpless, K. B. *Angew. Chem. Int. Ed.* **2001**, *40*, 2004-2021.
(29) Personal communication (Jerome Vachon).
(30) Lummerstorfer, T.; Hoffmann, H. *J. Phys. Chem. B* **2004**, *108*, 3963-3966.
(31) Sasson, R.; Rozen, S. *Org. Lett.* **2005**, *7*, 2177-2179.

(32) Vicario, J.; Walko, M.; Meetsma, A.; Feringa, B. L. *J. Am. Chem. Soc.* **2006**, *128*, 5127-5135.
(33) Kazaryan, A.; Kistemaker, J. C. M.; Schafer, L. V.; Browne, W. R.; Feringa, B. L.; Filatov, M. *J. Phys. Chem. A* **2010**, *114*, 5058-5067.
(34) Koumura, N.; Zijlstra, R. W. J.; van Delden, R. A.; Harada, N.; Feringa, B. L. *Nature* **1999**, *401*, 152-155.
(35) (a) Geertsema, E. M.; van der Molen, S. J.; Martens, M.; Feringa, B. L. *Proc. Nat. Acad. Sci. U. S. A.* **2009**, *106*, 16919-16924; (b) Klok, M. PhD Thesis, University of Groningen (2009).
(36) Eliel, E. L.; Wilen, S. H. In *Stereochemistry of Organic Compounds;* Wiley, New York: 1994;
(37) Pollard, M. M.; Wesenhagen, P. V.; Pijper, D.; Feringa, B. L. *Org. Biomol. Chem.* **2008**, *6*, 1605-1612.
(38) Still, W. C.; Kahn, M.; Mitra, A. *J. Org. Chem.* **1978**, *43*, 2923-2925.

Chapter 3
Attachment of molecular motors to inorganic surfaces

In this chapter the attachment of molecular rotary motors containing triethoxysilane functional groups to quartz, silicon and mica surfaces is described. Motors containing silane coupling agents in their structure form stable molecular layers on quartz and silicon surfaces. Motors attached to these surfaces were found to undergo photochemical and thermal isomerization steps similar to those observed in solution. Additionally, successful formation of "carpets"with monomolecular thickness on atomically flat mica extending micrometer-sized length scales is presented. These "carpets" were found to undergo morphological changes upon irradiation with UV-light.

Attempts to broaden further the methods available for surface modification with molecular motors through the attachment of an alcohol-functionalized motor to chlorinated silicon surfaces were partly successful but found to be difficult to reproduce consistently.

3.1 Introduction

A major challenge in nanotechnology research is to design and use stimuli-responsive molecules to perform work.[1] One approach towards this goal is the assembly of molecules capable of undergoing controlled structural changes on a solid surface and using their collective action to induce microscopic or macroscopic movement.[2-5] It has been demonstrated that an array of responsive molecules is able to alter the wettability of a surface,[4] control the organization of liquid crystal layers[6-8] or control cell adhesion[9] *via* structural changes triggered by external stimuli. Systems that can be controlled by light are of particular interest due to its non-invasive nature, fast response times and the compatibility of light with a variety of solid materials that can be used as surfaces.[3,4]

Apart from controlling surface-properties, there is a growing interest in using these materials in novel applications such as nanomachinery[10-12] or molecular electronics.[13-15]

As silicon-based self-assembled monolayers (SAMs) have a promising future in molecular electronic devices,[16-20] and taking advantage of the development in the silicon-based integrated circuit (IC) industry, many of the assemblies containing switchable molecules are prepared on silicon-based materials. Additionally, silicon-based materials are a popular choice of solid substrates due to their relatively low price and chemical, mechanical and thermal stability. Preparation of SAMs on silicon and quartz allows for the construction of robust, covalently-bound molecular layers and facilitates their analysis with a range of routine characterization techniques such as UV-vis, CD and IR-spectroscopy.

Exploring the possibilities and limitations of self assembly of dynamic and stimuli-responsive molecular systems along with their behavior in the confined environment of a monolayer on Si-based materials is a step forward towards the realization of functional molecular devices.

Molecular motors based on overcrowded alkenes provide promising photon-driven systems.[21] Their ability to undergo controlled unidirectional rotation while attached to solid surfaces,[22-24] and the wide range of speeds at which they are capable of rotating[25-27] make them attractive candidates not only to control surface properties but also to control the motion of nano- or micrometer scale adsorbed materials.[28]

The synthesis of molecular rotary motors containing silyl ether functional groups allows for their attachment to a variety of surfaces, most notably SiO_2/Si,

glass and quartz. Other high energy surfaces that are known to allow assembly of molecules with silane-based functional groups include aluminum oxide, germanium oxide, gold, glass and mica.[29] Mica, a sheet silicate, is of particular interest because it provides an atomically flat surface, facilitating atomic force microscopy (AFM) studies of adsorbed materials and the morphology of the SAM.

3.2 Attachment of silane-functionalized motors to silicon and quartz surfaces

3.2.1 Introduction to silane-based SAMs

Robust, covalently attached SAMs of alkylchlorosilanes and alkylalkoxysilanes require Si-OH surfaces for their formation.[29] The driving force for this self-assembly is the *in situ* formation of polysiloxane, which is covalently connected to surface hydroxyl groups (Figure 1).

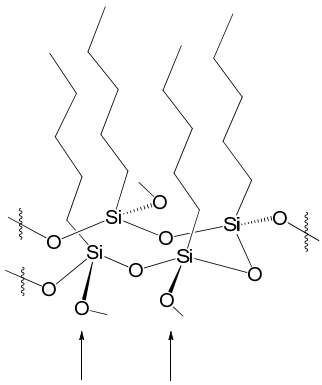

Figure 1 Schematic representation of a polysiloxane at the monolayer-substrate interface. The arrows show the Si-O bonds that either can be connected to the surface Si-OH groups or to other polysiloxane chains.

Surface modification with trialkoxysilanes has been described as a four step process[16,30] (Scheme 1). Initially, hydrolysis of the three alkoxy groups occur. Condensation of the formed silanols to oligomers follows. The oligomers then form hydrogen bonds with OH-groups at the surface of the substrate. Finally, upon drying, a covalent linkage is formed to the surface of the substrate with concomitant loss of water. Although described as a sequential process, it should be

noted that these reactions can occur simultaneously after the initial hydrolysis step. At the interface, there is usually only one bond from each silicon of the organosilane to the substrate surface.[31] The two remaining silanol groups are present either in condensed or free form. It should be noted, however, that the mechanism of monolayer formation is still a subject of debate.[29]

Water for hydrolysis may come from several sources. First, water is typically present at hydrophilic surfaces. Second, water from the atmosphere can be incorporated into the self-assembly solution. For less reactive silanes, controlled volumes of water are often added to increase the surface coverage and rate of reaction. Monolayers of alkoxysilanes or chlorosilanes do not form in the complete absence of water.[32-34]

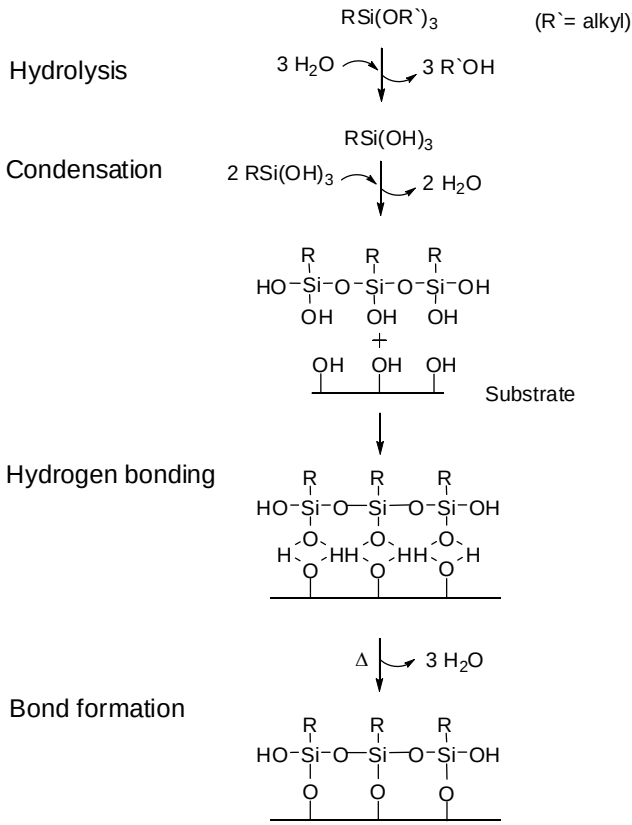

Scheme 1 Surface modification with trialkoxy silanes. The steps shown here occur simultaneously**.** (Figure is adapted from ref 29.)

High-quality SAMs of alkylchlorosilane derivatives are not simple to prepare, mainly because of the need to control carefully the amount of water present in the solution and the humidity of the environment.[29,31,35-37]

Chlorosilanes are susceptible to hydrolysis and cross-linking prior to surface adsorption. If the conditions are non-optimal (including water content, humidity, solvent, concentration and age of the chlorosilane solution) for monolayer formation, a three-dimensional network is deposited on the surface. In contrast, alkoxysilanes can be stored and used for extended periods with minimal protection from hydrolysis.

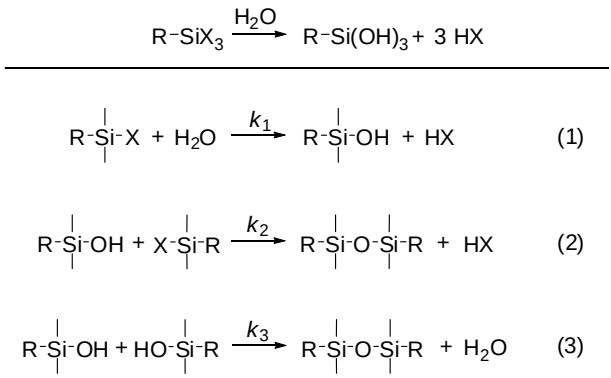

Scheme 2 Hydrolysis of trifunctional silanes.

The hydrolysis of trifunctional silanes[38] is shown in Scheme 2. It can be seen that the ability to obtain non-cross-linked silanols depends on the relative rates of reactions (1), (2) and (3). If k_2 and k_3 are small relative to k_1 it might be possible to obtain a silanetriol that would have a useful lifetime for self-assembly procedures. Alkoxysilanes are more stable towards hydrolysis than chlorosilanes.[38,39] A major reason for this is that both steps (1) and (2) in Scheme 2 result in the formation of acid when X= Cl as in the case of chlorosilanes. This acid catalyzes further reactions and ultimately leads to gel formation. Steps (1) and (2) are more exothermic for the hydrolysis of chlorosilanes than that of alkoxysilanes, which means that the activation energy for steps (1) and (2) is lower and the rate of hydrolysis may be faster for chlorosilanes.

3.2.2 Attachment of a triethoxysilane-functionalized motor to silicon (Si/SiO_2) and quartz substrates

Considering the stability issues, alkoxysilanes were chosen to explore the possibilities for the attachment of molecular motors to surfaces through silane-chemistry.

Molecules containing a triethoxysilane-moiety are known to be relatively stable towards polymerization, and a variety of these compounds is commercially available and commonly used as silane coupling agents.

Molecular motor **2.20** was synthesized (for the synthesis see Chapter 2) containing two terminal double bonds, which could be functionalized with triethoxysilane anchoring units making it suitable for attachment to quartz and silicon (Si/SiO_2) surfaces. A platinum oxide (PtO_2) catalyzed hydrosilylation reaction was chosen to convert the terminal double bonds to silanes.[40] In a previous study[40] PtO_2 was found to be an efficient hydrosilylation catalyst for terminal alkenes with highly reproducible results and easy removal of the catalyst after reaction.

It was expected that modifying the legs of motor **2.20** by means of PtO_2-catalyzed hydrosilylation using triethoxysilane would result in a sufficiently stable disilane-derivative for controlled surface modification.

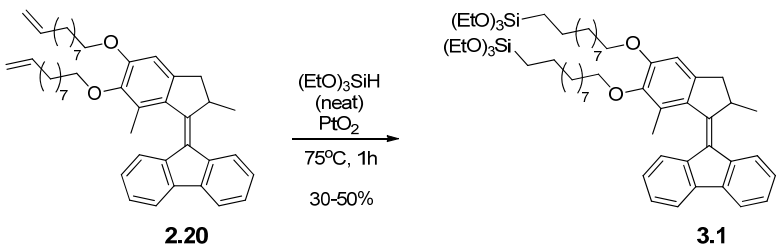

Scheme 3 PtO_2-catalyzed hydrosilylation reaction of **2.20.**

The hydrosilylation of motor **2.20** was carried out under argon atmosphere in triethoxysilane (Scheme 3). The product disilane **3.1** was found to be stable towards polymerization even during flash chromatography using silica gel as a stationary phase. Although polymerization was not observed (no precipitation or broadened absorptions in the ^1H NMR spectra were observed), partially hydrolyzed silanes were present in the crude reaction mixture and possibly form during purification as well. It is possible that the presence of free silanol groups contributes to the varying isolated yields due to their different interactions with the

stationary phase (which could also include covalent attachment) during column chromatography.

The motor with two triethoxysilane units was expected to assemble on silicon and quartz surfaces from dilute solutions. Prior to exposing the surfaces to a solution of **3.1**, substrates were cleaned for 1 h using a 3/7 ratio of 30% H_2O_2 in H_2SO_4 ('piranha') at > 90°C. (*Caution! This mixture is extremely corrosive and reactive towards organics.*) These samples were then rinsed with double distilled water (3 times) and with methanol and dried under a stream of argon. Such thorough cleaning of the substrate is a prerequisite for obtaining clean surfaces with high densities of silanol groups. Silanol groups then act as nucleation and bonding sites in the film growth process.

Since ethoxysilanes are known to be relatively stable towards hydrolysis, which may be a limitation for the formation of dense molecular layers, a chemical pretreatment method[38,39] was applied to hydrolyze the ethoxy groups of motor **3.1** to silanol groups prior to deposition on solid surfaces. This involves the treatment of **3.1** with aqueous HCl solution in THF, followed by dilution with cyclohexane. The resulting hydrolysis solution was then used for the subsequent surface modification (Scheme 4). Freshly cleaned quartz and silicon surfaces were immersed in the hydrolysis solution for 12 h. After the substrates had been removed from the solution, they were rinsed by sonication (3×2 min) in DMF, toluene and MeOH to remove physisorbed species. The resulting surfaces were dried under a stream of argon.

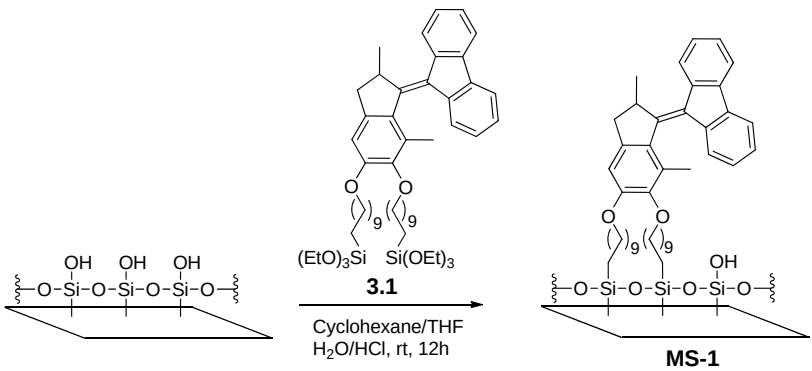

Scheme 4 Attachment of triethoxysilane-containing motor **3.1** to quartz and silicon surfaces. The ethoxysilane units are hydrolyzed prior to surface modification.

The first indication of successful surface modification was obtained by water contact angle measurements. Since bare quartz and silicon are high energy surfaces, exhibiting complete spreading of water, any modificaton with an organic group is expected to induce a change in this value. Indeed, the surfaces treated with motor **3.1** had a large increase in contact angle from complete wetting (~0°) to 87(± 2)°.

Ellipsometry was used to measure the thickness of the SAM. We obtained thickness values of 2.0 (±0.2) nm in agreement with the calculated length (geometry was optimized using molecular mechanics calculations with HyperChem 7.5; the length was calculated to 2.1 nm) of motor **3.1** indicating the formation of a well-packed monomolecular layer.

Further presence of **3.1** on the surface was confirmed by ATR-FTIR spectroscopic measurements. Chemical identification of **3.1** on the surface is evident by the appearance of the CH_2 and CH_3 stretching modes at 2855, 2927 and 2963 cm^{-1} in the IR-spectra which compares well with the IR absorptions of a bulk sample of motor **2.20** in the same region (Figure 2). Note that these stretching modes do not appear when bare Si/SiO_2 is measured.

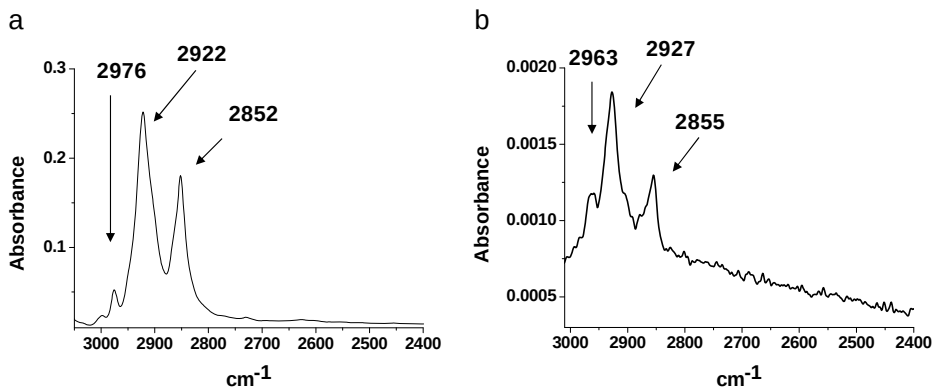

Figure 2 ATR-IR spectra of motor **2.20** (a) and **MS1** (b). The presence of the motor on the surface is evident by the appearance of the CH_2 and CH_3 stretching modes.

The UV-vis spectrum of the modified surface clearly shows the presence of the motor, which compares well to the spectrum of motor **2.20** in solution (Figure 3).

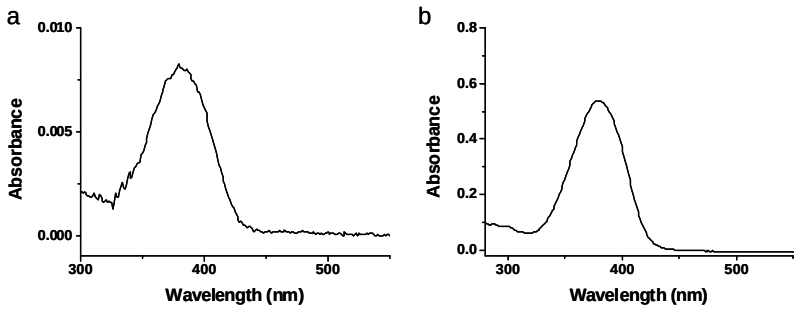

Figure 3 UV-vis spectra of a quartz surface modified with motor **3.1** (**MS1**) (a) and dialkene-motor **2.20** in MeOH (b).

As the UV-vis absorption spectrum of the modified surface is not significantly different from that observed in methanol solution for compound **2.20** (Figure 3), the UV-vis spectrum of **MS-1** could be used to estimate the surface coverage based on the assumption that the molar absorptivity (ε) of **2.20** in solution and the molar absorptivity (ε) of the motor attached to the surface are similar.[41,42] Using the Beer-Lambert law, the relation between the absorption (A) and the surface-density (Γ) of the absorbing species can be written as follows:

$$A = \varepsilon \times \Gamma \qquad \textbf{Eq. 1}$$

Taking into account that both sides of the slide are functionalized, the surface coverage density of **2.20** is estimated to be 1.4×10^{-10} mol/cm^2 for a single side, which is in agreement with the value obtained for similar monolayers of overcrowded alkenes reported recently.[43]

The UV-vis spectrum of **MS-1** was found to undergo changes upon irradiation with UV-light (365 nm, 0°C, 45 min) that correspond to photoisomerization of the attached molecular motors (Scheme 5b). The changes in the absorption spectrum are similar to that observed for **2.20** in methanol solution (365 nm, -20°C, 90 min) (Scheme 5a) indicating that the rotary function is preserved upon surface attachment.

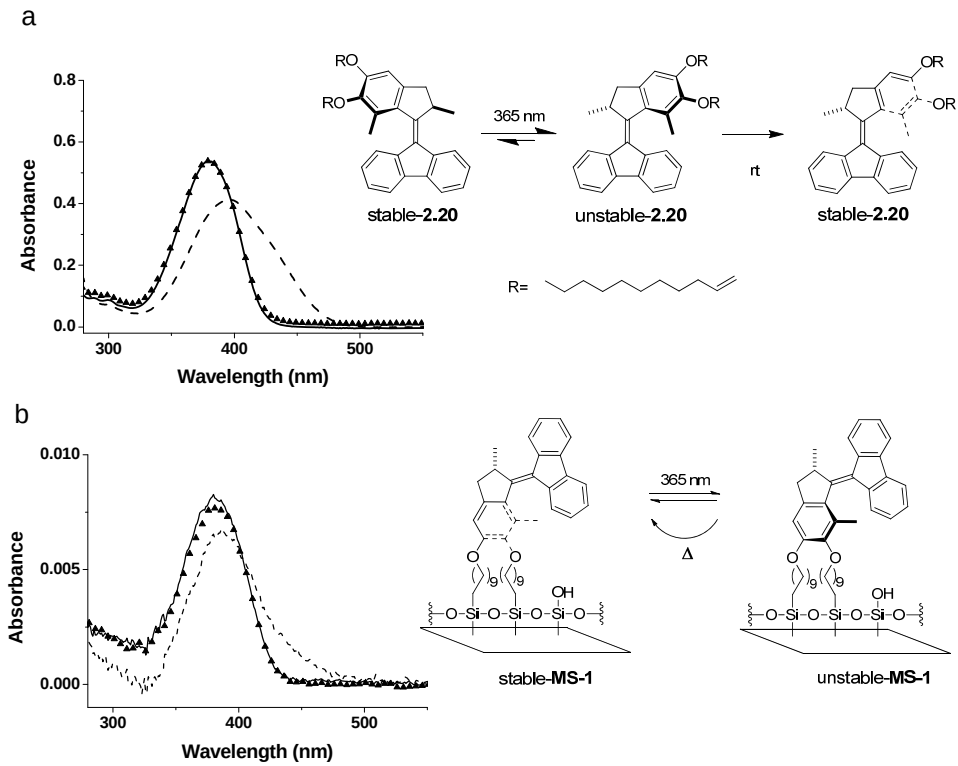

Scheme 5 (a) The stable form of **2.20** (solid line) undergoes photoisomerization (dashed line) upon irradiation with 365 nm light (methanol, -20°C). The original spectrum is restored upon warming the sample to room temperature (▲). (b) Similarly, the surface bound motor (solid line) undergoes photoisomerization upon irradiation (365 nm, 0°C) (dashed line). The reversion of the spectrum to the original indicates the thermal isomerization back to the stable form (▲).

3.3 Assembly of molecular motors on mica surface

In biological systems nature developed a variety of molecular motors, which are able to cooperate to perform macroscopic tasks.[44] Performing well-defined mechanical tasks at the molecular level with fully synthetic systems has been demonstrated,[45-48] but still remains challenging. The potential of dynamic organic surfaces through the collective action of responsive molecular arrays is highly attractive in this respect.

To achieve the maximal mechanical effect on adsorbates on top of a layer of responsive molecules, the externally induced geometrical changes of the organic

surface should be exploited equally. Substrates with atomically flat surfaces are considered to be ideal because it is uncertain how surface roughness affects the propensity for chemical conformational changes at an interface to induce motion in an adsorbate. Rougher areas may act as "roadblocks" that inhibit motion. Furthermore, application of solid surfaces with high roughness makes the visualization of adsorbed material (e.g., macromolecules) with AFM more difficult. The importance of surface-flatness was demonstrated in the visualization of stretched DNA by AFM.[49] To distinguish the adsorbate from the SAM, a smooth monolayer on an atomically flat surface is ideal.

For an attempt to use molecular rotary motors to mechanically affect adsorbed materials (e.g., polymers, macromolecules) mica was chosen as a step-free, atomically flat surface to assemble arrays of molecular motors in order to exploit their rotary motion.

It is well-established that alkyl-silanes can easily self-assemble on glass, silicon oxide and metal oxide surfaces by reaction and covalent-bond formation with the hydroxylated surface.[29] Controlling self-assembly on mica, however, is challenging because its surface is almost entirely non-functional;[50] there are few hydroxyl functionalities to provide a robust anchor. It is believed that silane monolayers adhere to mica through the formation of two-dimensional oligomeric/polymeric species in solution which anchors through any adventitious Si-OH functionality.[38,51,52]

The density of the surface-silanol groups can be increased by plasma pre-treatment of the freshly cleaved mica, which results in more robust sub-monolayers and monolayers.[53-55] Chemical pre-treatment of the substrate with water steam[52,53,56] and sodium ethoxide[57] was tested in order to generate surface-silanol groups; however, in most cases a covalent attachment of the monolayer film to the mica surface was not achieved. Although some of the mica pre-treatment methods improve the stability of the monolayers formed, they risk disruption of the atomically flat mica surface.[58]

3.3.1 Surface modification and characterization

To avoid disruption of the flat, step-free surface, the formation of a motor monolayer was attempted by using chemical pre-treatment of the monolayer-

forming material, by the hydrolysis of the trialkoxysilane groups prior to surface modification.[38,39,59]

Clean mica surfaces were prepared by cleaving the top layer by covering with scotch tape and peeling off the layer. Freshly cleaved mica surfaces were immersed in a solution containing motor **3.1** (0.1 mM), THF, cyclohexane and a small amount of aqueous HCl for 1 h (Figure 4). To generate covalent cross-links between the assembled silane units to create a more stable layer, the mica surfaces were post-baked at 120°C for 1h. Leaving out the post-baking step, however, did not affect considerably the results obtained. The importance of the post-baking step is subject to contradictory conclusions in the literature.[38,59]

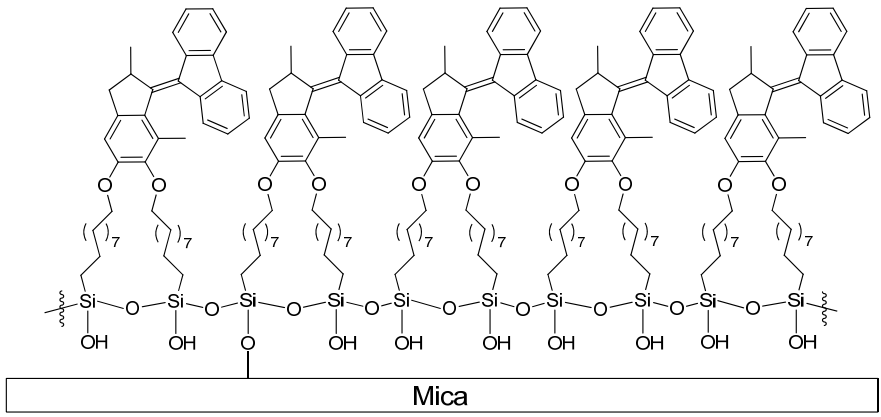

MS-2

Figure 4 Schematic representation of a layer of motor **3.1** on a mica surface. The surface of mica is almost entirely non-functional. It is believed that silane monolayers adhere through the formation of two-dimensional oligomeric/polymeric species in solution which anchors through any adventitious surface Si-OH functionality.

In contrast to silicon, mica is not ideal for ellipsometric film-thickness measurements or IR reflection spectroscopy due to its low refractive index and soft, flexible nature.[60] A detailed spectroscopic analysis of the film structure is more difficult in comparison to Si substrates. However, that atomically flat nature of the mica surface makes it ideal for AFM studies. AFM tips with a force constant of 5 N/m were used. When tips with higher force constants were used, scanning damaged the films, indicating the fragility of the physically adsorbed films. Similar observations have been previously reported.[56,57]

Representative AFM pictures are shown in Figure 5. It can be seen that the silane-containing motor molecules assemble to form micrometer size carpets on mica. The thickness of the carpets is 2-2.5 nm, which is close to the ellipsometric thickness obtained for **MS-1**.

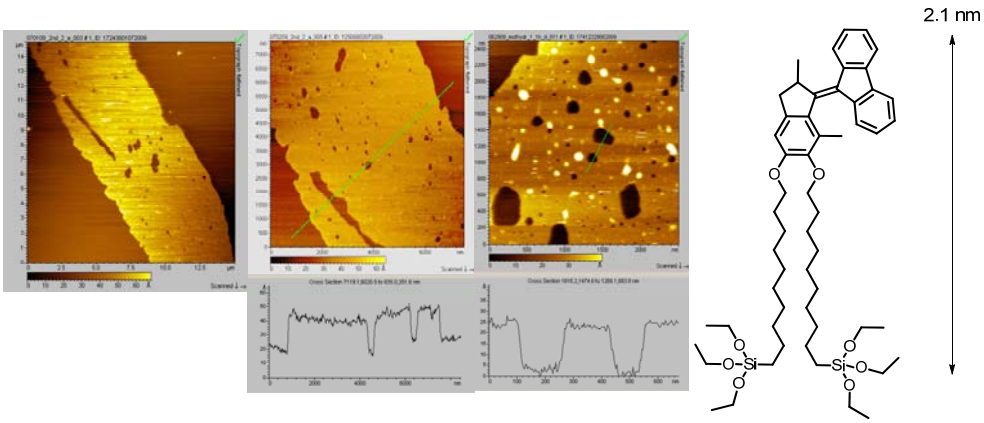

3.1

Figure 5 Representative AFM images of mica surfaces modified through the assembly of motor **3.1**. Micrometer-size carpets were found throughout the surfaces with 2-2.5 nm thicknesses, which are close to the estimated length of motor **3.1**, indicating the presence of monolayer films.

The formation of such condensed domains is consistent with the deposition, diffusion and aggregation (DDA) model described for similar systems.[56,61,62] Polymeric/oligomeric species and individual molecules adsorb onto mica from solution and can easily diffuse on the surface in order to aggregate with already deposited islands, since almost no covalent links form that could limit their mobility. In contrast to the uniform growth observed on the silanol rich silicon surface,[63] initial film growth on mica is primarily through diffusion-limited aggregation (resulting in island formation throughout the surface) while after longer immersion times the growth is limited by adsorption from solution (filling the pinholes and uncovered surface areas between the islands). Although the two growth mechanisms are mostly attributed to the presence or the lack of surface silanol groups, it has been reported that the two mechanisms may vary depending on the reaction conditions (i.e. low moisture content facilitates continuous growth while high water content facilitates the island growth mechanism).[60,64] The pinholes included in the monolayers have been observed previously and attributed to imperfect packing and monolayer reorganization processes.[56,57]

To test the effect of rotary motion on the film morphology and stability, the mica surfaces were subjected to UV irradiation (λ_{max}= 365 nm) (Figure 6).
A sample (Figure 6a) was irradiated for 35 min at rt. From the AFM images it appears that 15 min after the irradiation changes in the film structure could be observed through the appearance of new pinholes and the broadening of existing ones (Figure 6b). The samples were then left in the dark overnight (Figure 6c). Images obtained after standing overnight show that the number of pinholes increased further.

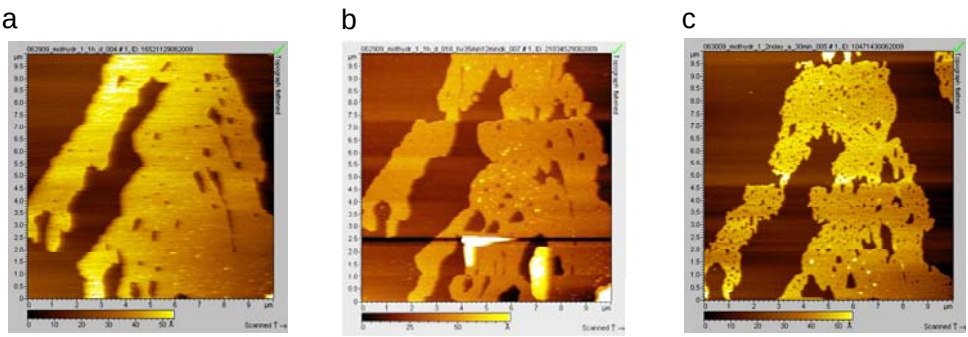

Figure 6 AFM images show the effect of UV-irradiation (365 nm, rt) on motor film morphology on mica (a) Sample without irradiation; (b) sample after 35 min irradiation; (c) sample after standing overnight in the dark at rt.

It is obvious from the AFM images that irradiation disrupts the motor layers. Major effects of the heat produced by the UV-lamp during irradiation could be excluded since post-baking at 120°C showed no considerable changes in the layer morphology. It is possible, however, that upon rotation of the rotor part of the motors the monolayer undergoes reorganization especially at the points where the cross-linking of the silane layer is incomplete. Since the layers are not considered to be covalently attached to the mica surface, Si-O-Si bonding to the surface does not prevent structural reorganization.

Comparable morphological conversions were observed in the case of azobenzene and azobenzene-based polymer films on mica[65-68] (Figure 7 and Figure 8). In one case[65] functionalized *trans*-azobenzenes were physisorbed on freshly cleaved mica from DMF solution by spincoating. Upon irradiation at 365 nm (100W, 15s, rt) some holes appeared. The authors explain the formation of the pinholes by the presence of an H-bonding network due to the amide bonds in the azobenzenes. The molecules are not easily moved apart from each other upon

isomerization because of the H-bonding between them. In contrast, when the amides were replaced by esters, only the two-dimensional expansion of the layer was observed upon irradiation under the same conditions. The lack of H-bonding allows the molecules to move apart equally upon photoisomerization.

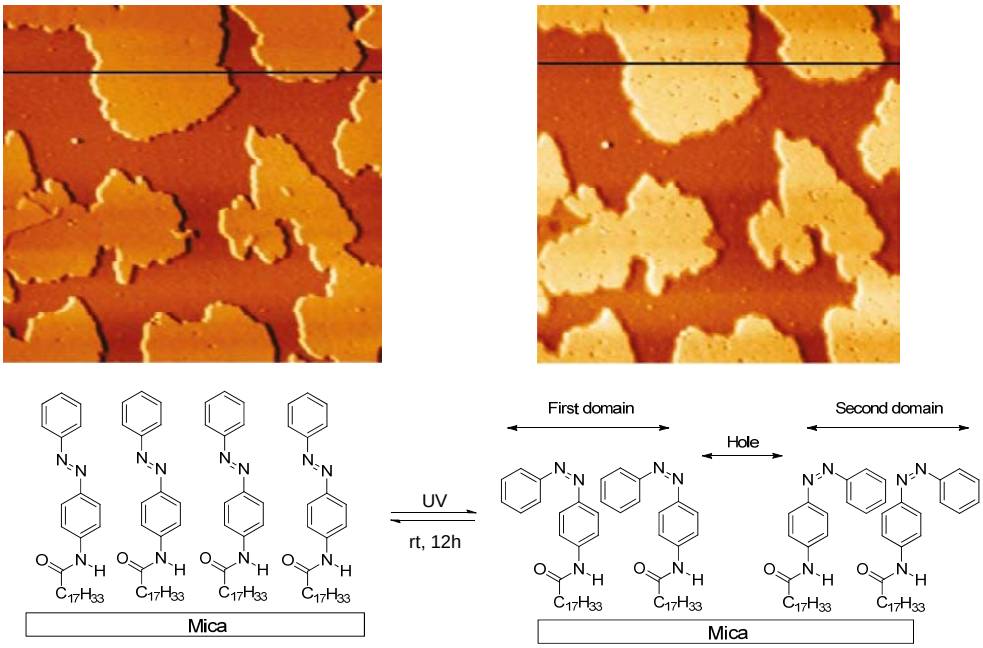

Figure 7 Irradiation (365 nm, 100W, rt, 15s) of a layer of azobenzenes physisorbed on mica surface resulted in pinhole formation. The holes form due to the presence of H-bonding between the molecules, which limits there mobility on the mica surface. (Pictures are reproduced from ref. 65.) (AFM image size: 2×2 μm.)

In another experiment[67] a monomolecular film of a poly(vinyl alcohol) derivative with azobenzene side-chains was deposited on a mica surface by the Langmuir-Blodgett technique (Figure 8). In a humidified atmosphere the authors observed the formation of a network morphology (Figure 8a) which showed a two-dimensional expansion upon irradiation at 365 nm (Figure 8b) as a result of the *trans*-to-*cis* photoisomerization. Irradiation at 436 nm produced films with dots of even size distributed on the surface (Figure 8c). The images (b) and (c) in Figure 8 were reproducible upon repeating the UV/vis irradiation cycles.

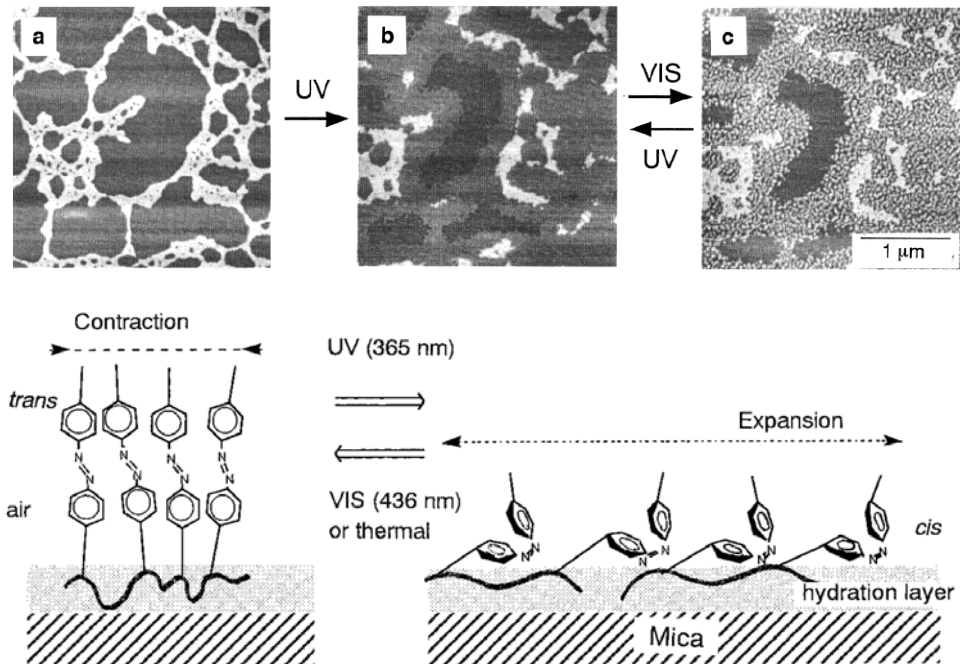

Figure 8 Irradiation of a poly(vinyl alcohol) based polymer network on a mica surface (a) at 365 nm resulted in two-dimensional expansion of the structure (b). Subsequent irradiation at 436 nm resulted in the formation of films with even-sized dots (c). The images (b) and (c) are reproducible upon repeated UV/vis irradiation cycles. (The pictures are reproduced from ref. 67.)

3.4 Functionalization of inorganic surfaces with motors containing OH-groups

Silane compounds used for surface modification of quartz or silicon can undergo side-reactions due to their hydrolytic instability. These side-reactions might lead to the formation of oligomers and polymers and ultimately result in the formation of complex surface structures and multilayered polymer films. Since alcohols cannot undergo such side-reactions, surface modification through alkoxylation is expected to form more uniform monolayers.

A number of methods have been described for attachment of alcohols to siliceous surfaces.[16, 69-71] Most involve the activation of the surface through the formation of a Si-X (X= Cl, Br, I, NEt_2) bond as the first step. A common drawback of Si-O-C bonds is their hydrolytic instability.[73] It has been shown that this can be improved

by blocking the free surface Si-X (X= Cl, Br, I) groups with hexamethyldisilazane (HMDS) following surface modification or by using alcohols with bulky backbones to sterically hinder attack by water.[74]

From the methods available we chose the one applied by Schreiber and coworkers to create microarrays for testing interactions between proteins and small molecules[69] (Scheme 6). They found that among the variety of chlorination conditions available the $SOCl_2$/DMF/THF system gives the best results. The method is attractive due to the application of bench-stable chemicals avoiding highly water sensitive or difficult-to-handle reagents such as Cl_2 or $SiCl_4$. This activation method was also used by others to modify porous silica for drug release applications.[72,75]

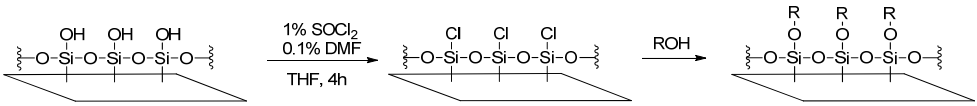

Scheme 6 Method for surface-modification with primary alcohols via surface activation with $SOCl_2$.[69]

Following the procedure reported in the literature[69] it was expected that motor **2.27** (for the synthesis see Chapter 2 or ref. 23 in this chapter) with two terminal OH-groups will readily react with chlorinated quartz surfaces (Scheme 7).

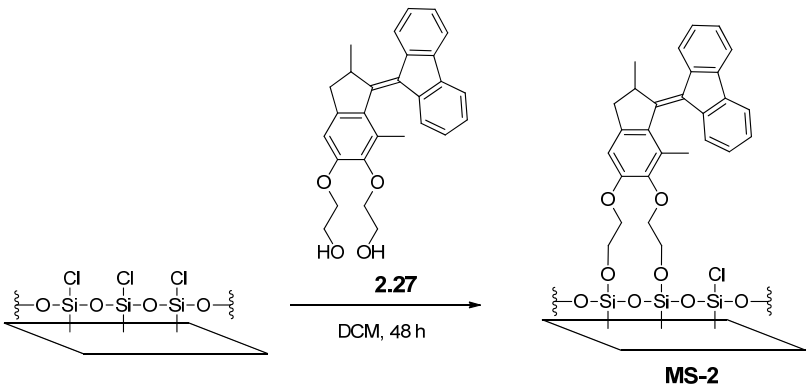

Scheme 7 Attachment of motor **2.27** to chlorinated quartz and silicon surfaces.

Chlorinated surfaces were prepared according to the procedure described by Schreiber and coworkers.[69] Piranha-cleaned quartz slides were immersed in a THF solution of $SOCl_2$ (1 %) and catalytic amount of DMF (0.1 %) for 5 h followed by rinsing with dry THF (3 times).
Slides were immersed in a DCM solution of motor **2.27** for 40-48 h then rinsed with DCM (3 times) and dried in a stream of argon.

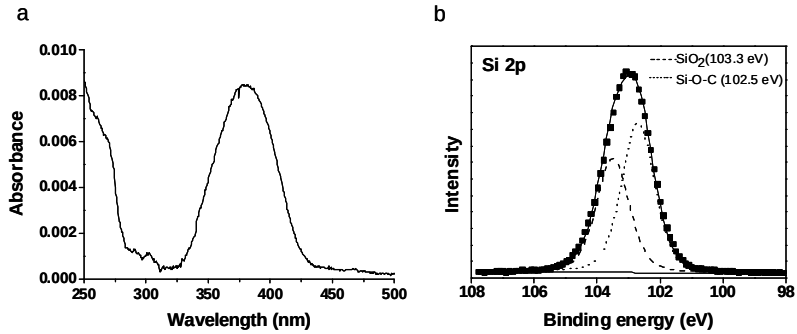

Figure 9 UV-vis (a) and XPS (b) spectra of quartz and silicon surfaces after the attachment of motor **2.27**. Although the presence of motors could be detected by these methods, the procedure for surface modification turned out to be irreproducible.

The UV-vis absorption spectrum of the slide showed the absorption spectrum expected for the motor (Figure 9a). Furthermore XPS measurements support the motor attachment also (Figure 9b). However, despite these promising initial results, the assembly was difficult to reproduce and not suitable for routine use. Further attempts to prepare motor-modified slides in this way mostly resulted in UV-vis signals only slightly above the detection limit indicating the lack of well packed monolayers.
The difficulties could be due to the hydrolytic instability of either the motor monolayer or the chlorinated surface or both.

As a control experiment assembly of 1-octadecanol on quartz was performed under identical conditions. The water contact angle of the resulting layer was around 50-60° instead of ~110°, which is the characteristic contact angle for well-packed octadecyl-monolayers.[71]
Based on these results different surface-activation methods[70,71] should be considered for the preparation of high-coverage monolayers of alcohol-functionalized molecular motors.

3.5 Discussion and Conclusion

Application of molecular motors containing silane coupling agents for surface modification is an attractive strategy to create dynamic organic surfaces. The resulting layers on quartz and silicon substrates are found to be stable towards sonication and did not degrade upon storage under ambient conditions (with the exclusion of light) over several weeks. Incorporating the trialkoxysilane groups which are prone to hydrolysis into the motor structure, however, has some disadvantages. Although alkoxysilane groups are stable towards polymerization compared to the chlorosilane derivatives, due to the lack of acid formation upon their hydrolysis, the loss of material upon purification, likely via binding to the silica/alumina stationary phase during column chromatography, is considerable. Distillation as an alternative purification method was attempted; however, it was not practical because of the small amount of material available. A possible way to reduce the loss of material upon purification is to use dialkylalkoxy silanes ($R_2(OR)SiH$) for hydrosilylation. Containing only one hydrolysis sensitive group, which is hindered to some extent by the adjacent alkyl groups, it might increase the isolated yield. A further feature of the alkoxysilanes, which has to be considered, especially in the design of functionalized versions of motors, is their incompatibility with some functional groups (e.g., carboxylic acids, amines). The presence of these groups might prevent the reproducible surface attachment by reaction/interaction with the alkoxysilane anchoring units.

Organic functionalization of non-oxidized silicon surfaces through Si-C bond formation[76] is a possible approach to avoid these interactions. Covalent attachment of 1-alkenes and 1-alkynes to hydride terminated silicon surfaces has been described, although most of them apply chemical or photochemical radical initiation, which might be incompatible with the molecular motors.[76] A recent study, however, reports a method for the assembly of 1-alkynes on H-terminated silicon surfaces without external activation, which is attractive for motor-monolayer formation (Scheme 8).[77] A disadvantage of this method, however, is that quartz cannot be functionalized in this way, making the spectroscopic characterization of rotary motion difficult.

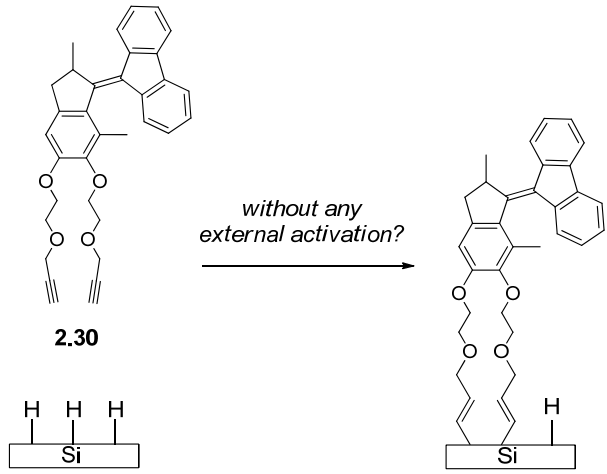

Scheme 8 The attachment of terminal alkynes to H-terminated silicon surfaces without any external activation, which could be a useful method for attachment for alkyne-functionalized molecular motors to solid surfaces.[77]

In pursuit of directional motion on dynamic interfaces through mechanical interactions, mica is considered to be a good option to manipulate and visualize nano- and micrometer scale objects due to its flat and step-free surface. Initial attempts to deposit motor layers resulted in the formation of micron scale carpets, which, however, were not stable towards irradiation and AFM imaging. The origin of this behavior is likely the lack of strong interactions between the molecular layer and the mica surface. Water plasma treatment of the substrate to generate free surface silanol groups is one possibility to overcome this problem. A different way is to exchange the potassium surface cations that usually occupy the surface of natural mica with ammonium cations,[78-80] which could be built into the motor structure.

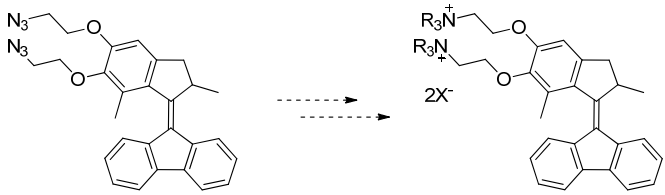

2.31

Scheme 9 Ammonium ion containing molecular motors could potentially be assembled on mica surface through an ion-exchange mechanism.

An alternative to mica is gold, which is known to have atomically flat terraces on its surface.[29] The assembly of trichlorosilanes on gold, as with mica, via two-dimensional polymer formation, has been reported.[81,82]
Using the specific interaction between gold surfaces and sulphur atoms, molecular motors containing terminal thiol or thioacetate groups could be assembled on gold.[24,83] In this case, however, the lower thermal[84] and photochemical[85,86] stability of the Au-S bond compared to silane-based systems could be a limitation for the characterization and application of the system.

3.6 Experimental

3.6.1 General remarks

Synthesis

For general remarks on the synthesis and characterization of compounds and intermediates, see Chapter 2.

Surfaces

Silicon wafers (Wafer World Inc.) containing a thin layer of SiO_2 (approximately 2 nm, exact value measured for each sample) and quartz microscope slides (UQG Optics) were cleaned with piranha (95°C, 2h) (*Caution! This mixture is extremely corrosive and reactive toward organics.*) prior to use for surface modification. Clean mica surfaces were prepared by cleaving the top layer by covering with scotch tape and peeling off the layer. Motor films were prepared following the procedure described in the literature.[38]

Contact angles were measured under ambient conditions on a Data Physics contact angle goniometer. The contact angle was calculated using software provided by the company. The contact angle was measured at three different locations on each surface and the results averaged.

Spectroscopic ellipsometry measurements were performed on a J.A. Woollam VASE ellipsometer.

ATR-IR spectra of the surfaces were obtained using a Spectrum 400 FT-IR (Perkin Elmer) equipped with a Pike Veemax II attachment and a liquid nitrogen cooled MCT detector. Spectra were taken with parallel-polarized light and an incident reflection angle of 65° while samples were in intimate contact with a germanium crystal. Background spectra were taken on Si wafers containing an SiO_2 overlayer exposed to piranha solution in the same manner as the surface-modified samples. Samples were cleaned with lens tissue immediately before measuring.

UV-vis absorption spectra were obtained using a Jasco V-630 spectrophotometer.

AFM images were obtained with a PicoScan LE (Molecular Imaging) atomic force microscope in tapping mode. Tips with a force constant of 5 N/m were used. Images were scanned at rates ranging from 1-2 lines per second.

For the X-ray photoelectron spectroscopy (XPS) measurements, the samples were introduced through a load look system into an SSX-100 (Surface Science Instruments) photoemission spectrometer with a monochromatic Al Kα X-ray source ($h\nu$=1486.6 eV). The base pressure in the spectrometer during the measurements was 10^{-10} mbar. The photoelectron takeoff angle was 37°. The energy resolution was set to 1.3 eV to minimize measuring time. XPS binding energies were referenced to the Si 2p core level set to the SiO_2 reference value of 103.0 eV.[87]

Spectral analysis included a linear background subtraction and a peak deconvolution that employed mixed Gaussian-Lorentzian functions in a least-square curve-fitting program (WinSpec) developed at the LISE, University of Namur, Belgium. For each sample, a survey scan and the C 1s, O 1s, N 1s and Si 2p narrow scan spectra were collected. The photoemission peak areas of each element, used to estimate the amount of each species on the surface, were normalized by the sensitivity factors of each element tabulated for the spectrometer used. Four different points on each sample were analyzed to check for

homogeneity of the monolayer. The same elemental compositions for all points of the sample were obtained, suggesting that all samples were homogeneous.

3.6.2 Preparation of the adsorbate films

1.25 mL of a hydrolysis solution containing 12 mg disilane motor **3.1**, 6 mL distilled THF, 31 µl double-distilled H_2O and 4 µl 37% aq. HCl was added to 25 mL cyclohexane to give a slightly hazy solution. Piranha cleaned silicon wafers and quartz slides were immersed in this solution. In the case of mica the best results were obtained when the concentration of motor **3.1** was 0.1 mM in the hydrolysis solution. In general quartz slides and silicon wafers were left immersed overnight, mica sheets were left immersed for 1 h. After the assembly quartz slides and silicon wafers were rinsed and sonicated in DMF, toluene and MeOH for 2 min each and dried under a stream of Ar. Mica sheets were immersed briefly in distilled toluene and postbaked at 120°C for 1 h.

3.6.3 Synthesis

Disilane motor (3.1)

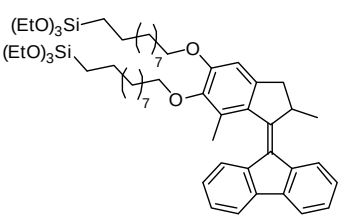

A mixture of dialkene-motor **2.20** (50 mg, 0.081 mmol) triethoxysilane (0.5 ml, 2.7 mmol) and PtO_2 (5 mg, 0.022 mmol) under inert atmosphere (Ar) was heated to 75°C for 30 min. The crude mixture was purified by column chromatography (SiO_2, heptane : EtOAc 10 : 1) to give alkene **3.1** as a yellow oil. (The isolated yields varied between 30-50%).
^{1}H NMR (400 MHz, $CDCl_3$) δ 0.61-0.67 (m, 2H), 0.89 (q, , *J*= 6.0 Hz, 2H), 1.21 (d, *J*= 4.0 Hz, 3H,), 1.25 (t, *J*= 6.8 Hz, 18H), 1.24-1.46 (broad m, 24H), 1.48-1.55 (m, 4H), 1.78-1.91 (m, 4H), 1.18 (s, 3H), 2.53 (d, *J*= 14.8 Hz, 1H), 3.29 (dd, *J*= 5.7, 14.6 Hz, 1H), 3.86 (q, *J*= 7.2 Hz, 12H), 3.99-4.15 (m, 5H), 6.83 (s, 1H), 7.11 (t, *J*= 7.5 Hz, 1H), 7.27 (t, *J*= 7.4 Hz, 1H), 7.32-7.37 (m, 2H), 7.39 (d, *J*= 7.9 Hz, 1H), 7.75 (d, *J*= 7.5 Hz, 1H), 7.79-7.82 (m, 1H), 7.86-7.89 (m, 1H). HRMS (ESI) calcd for $C_{56}H_{88}O_8Si_2Na$ 967.5910, found 967.5909.

3.7 References

(1) Browne, W. R.; Feringa, B. L. *Nature Nanotech.* **2006**, *1*, 25-35.
(2) Balzani, V.; Credi, A.; Venturi, M. *Chem. Phys.Chem.* **2008**, *9*, 202-220.
(3) Browne, W. R.; Feringa, B. L. *Annu. Rev. Phys. Chem.* **2009**, *60*, 407-428.
(4) Katsonis, N.; Lubomska, M.; Pollard, M. M.; Feringa, B. L.; Rudolf, P. *Prog. Surf. Sci.* **2007**, *82*, 407-434.
(5) Klajn, R.; Stoddart, J. F.; Grzybowski, B. A. *Chem. Soc. Rev.* **2010**, *39*, 2203-2237.
(6) Ichimura, K.; Suzuki, Y.; Seki, T.; Hosoki, A.; Aoki, K. *Langmuir* **1988**, *4*, 1214-1216.
(7) Fang, G.; Shi, Y.; Maclennan, J. E.; Clark, N. A.; Farrow, M. J.; Walba, D. M. *Langmuir* **2010**, *26*, 17482-17488.
(8) Ichimura, K. *Chem. Rev.* **2000**, *100*, 1847-1873.
(9) Robertus, J.; Browne, W. R.; Feringa, B. L. *Chem. Soc. Rev.* **2010**, *39*, 354-378.
(10) Morin, J. F.; Shirai, Y.; Tour, J. M. *Org. Lett.* **2006**, *8*, 1713-1716.
(11) Sasaki, T.; Tour, J. M. *Org. Lett.* **2008**, *10*, 897-900.
(12) Konstas, K.; Langford, S. J.; Latter, M. J. *J. Mol. Sci. Int. Ed.* **2010**, 2453-72.
(13) Pease, A. R.; Jeppesen, J. O.; Stoddart, J. F.; Luo, Y.; Collier, C. P.; Heath, J. R. *Acc. Chem. Res.* **2001**, *34*, 433-444.
(14) Peter, B. *Chimia* **2010**, *64*, 356-361.
(15) Tsujioka, T.; Irie, M. *J. Photochem. Photobiol. C* **2010**, *11*, 1-14.
(16) Aswal, D. K.; Lenfant, S.; Guerin, D.; Yakhmi, J. V.; Vuillaume, D. *Anal. Chim. Acta* **2006**, *568*, 84-108.
(17) Cerofolini, G. F.; Romano, E. *Appl. Phys. A* **2008**, *91*, 181-210.
(18) Heath, J. R. *Annu. Rev. Mater. Res.* **2009**, *39*, 1-23.
(19) Li, Q. L. *Mod. Phys. Lett. B* **2008**, *22*, 1183-1202.
(20) Perrine, K. A.; Teplyakov, A. V. *Chem. Soc. Rev.* **2010**, *39*, 3256-3274.
(21) Feringa, B. L. *J. Org. Chem.* **2007**, *72*, 6635-6652.
(22) Pollard, M. M.; Lubomska, M.; Rudolf, P.; Feringa, B. L. *Angew. Chem. Int. Ed.* **2007**, *46*, 1278-1280.
(23) London, G.; Carroll, G. T.; Landaluce, T. F.; Pollard, M. M.; Rudolf, P.; Feringa, B. L. *Chem. Commun.* **2009**, 1712-1714.
(24) Carroll, G. T.; Pollard, M. M.; van Delden, R.; Feringa, B. L. *Chem. Sci.* **2010**, *1*, 97-101.

(25) Pollard, M. M.; Klok, M.; Pijper, D.; Feringa, B. L. *Adv. Funct. Mat.* **2007**, *17*, 718-729.
(26) Klok, M.; Boyle, N.; Pryce, M. T.; Meetsma, A.; Browne, W. R.; Feringa, B. L. *J. Am. Chem. Soc.* **2008**, *130*, 10484-10485.
(27) Kulago, A. A.; Mes, E. M.; Klok, M.; Meetsma, A.; Brouwer, A. M.; Feringa, B. L. *J. Org. Chem.* **2010**, *75*, 666-679.
(28) Eelkema, R.; Pollard, M. M.; Vicario, J.; Katsonis, N.; Ramon, B. S.; Bastiaansen, C. W. M.; Broer, D. J.; Feringa, B. L. *Nature* **2006**, *440*, 163-163.
(29) Ulman, A. *Chem. Rev.* **1996**, *96*, 1533-1554.
(30) Arkles, B. *Chem. Tech* **1977**, *7*, 766-778.
(31) Krasnoslobodtsev, A. V.; Smirnov, S. N. *Langmuir* **2002**, *18*, 3181-3184.
(32) Tripp, C. P.; Hair, M. L. *Langmuir* **1992**, *8*, 1120-1126.
(33) Tripp, C. P.; Hair, M. L. *Langmuir* **1995**, *11*, 1215-1219.
(34) Carson, G. A.; Granick, S. *J. Mater. Res.* **1990**, *5*, 1745-1751.
(35) Rozlosnik, N.; Gerstenberg, M. C.; Larsen, N. B. *Langmuir* **2003**, *19*, 1182-1188.
(36) Brzoska, J. B.; Benazouz, I.; Rondelez, F. *Langmuir* **1994**, *10*, 4367-4373.
(37) Pillai, S.; Pai, R. K. *Ultramicroscopy* **2009**, *109*, 161-166.
(38) Kessel, C. R.; Granick, S. *Langmuir* **1991**, *7*, 532-538.
(39) Peanasky, J.; Schneider, H. M.; Granick, S.; Kessel, C. R. *Langmuir* **1995**, *11*, 953-962.
(40) Sabourault, N.; Mignani, G.; Wagner, A.; Mioskowski, C. *Org. Lett.* **2002**, *4*, 2117-2119.
(41) Durfor, C. N.; Turner, D. C.; Georger, J. H.; Peek, B. M.; Stenger, D. A. *Langmuir* **1994**, *10*, 148-152.
(42) Moon, J. H.; Kim, J. H.; Kim, K.; Kang, T. H.; Kim, B.; Kim, C. H.; Hahn, J. H.; Park, J. W. *Langmuir* **1997**, *13*, 4305-4310.
(43) Coleman, A. C.; Areephong, J.; Vicario, J.; Meetsma, A.; Browne, W. R.; Feringa, B. L. *Angew. Chem. Int. Ed.* **2010**, *49*, 6580-6584.
(44) Schliwa, M., (Ed.) *Molecular Motors;* Wiley VCH, Weinheim: **2004**.
(45) Berna, J.; Leigh, D. A.; Lubomska, M.; Mendoza, S. M.; Perez, E. M.; Rudolf, P.; Teobaldi, G.; Zerbetto, F. *Nature Materials* **2005**, *4*, 704-710.

(46) Huang, T. J.; Brough, B.; Ho, C. M.; Liu, Y.; Flood, A. H.; Bonvallet, P. A.; Tseng, H. R.; Stoddart, J. F.; Baller, M.; Magonov, S. *Appl. Phys. Lett.* **2004**, *85*, 5391-5393.
(47) Ichimura, K.; Oh, S. K.; Nakagawa, M. *Science* **2000**, *288*, 1624-1626.
(48) Nguyen, T. D.; Tseng, H. R.; Celestre, P. C.; Flood, A. H.; Liu, Y.; Stoddart, J. F.; Zink, J. I. *Proc. Natl. Acad. Sci. U. S. A.* **2005**, *102*, 10029-10034.
(49) Sasou, M.; Sugiyama, S.; Yoshino, T.; Ohtani, T. *Langmuir* **2003**, *19*, 9845-9849.
(50) Barrer, R. M. In *Zeolites and Clay Minerals as Sorbents;* Academic: London, 1978.
(51) Resch, R.; Grasserbauer, M.; Friedbacher, G.; Vallant, T.; Brunner, H.; Mayer, U.; Hoffmann, H. *Appl. Surf. Sci.* **1999**, *140*, 168-175.
(52) Schwartz, D. K.; Steinberg, S.; Israelachvili, J.; Zasadzinski, J. A. N. *Phys. Rev. Lett.* **1992**, *69*, 3354-3357.
(53) Malham, I. B.; Bureau, L. *Langmuir* **2009**, *25*, 5631-5636.
(54) Liberelle, B.; Banquy, X.; Giasson, S. *Langmuir* **2008**, *24*, 3280-3288.
(55) Parker, J. L.; Claesson, P. M.; Cho, D. L.; Ahlberg, A.; Tidblad, J.; Blomberg, E. *J. Colloid Interface Sci.* **1990**, *134*, 449-458.
(56) Britt, D. W.; Hlady, V. *J. Colloid Interface Sci.* **1996**, *178*, 775-784.
(57) Nakagawa, T.; Ogawa, K.; Kurumizawa, T. *Langmuir* **1994**, *10*, 525-529.
(58) Senden, T. J.; Ducker, W. A. *Langmuir* **1992**, *8*, 733-735.
(59) Xiao, X. D.; Liu, G. Y.; Charych, D. H.; Salmeron, M. *Langmuir* **1995**, *11*, 1600-1604.
(60) Vallant, T.; Brunner, H.; Mayer, U.; Hoffmann, H.; Leitner, T.; Resch, R.; Friedbacher, G. *J. Phys. Chem. B* **1998**, *102*, 7190-7197.
(61) Jensen, P.; Barabasi, A. L.; Larralde, H.; Havlin, S.; Stanley, H. E. *Phys. Rev. E* **1994**, *50*, 618-621.
(62) Jensen, P.; Barabasi, A. L.; Larralde, H.; Havlin, S.; Stanley, H. E. *Phys. Rev. B* **1994**, *50*, 15316-15329.
(63) Wasserman, S. R.; Whitesides, G. M.; Tidswell, I. M.; Ocko, B. M.; Pershan, P. S.; Axe, J. D. *J. Am. Chem. Soc.* **1989**, *111*, 5852-5861.
(64) Brunner, H.; Vallant, T.; Mayer, U.; Hoffmann, H.; Basnar, B.; Vallant, M.; Friedbacher, G. *Langmuir* **1999**, *15*, 1899-1901.
(65) El Garah, M.; Palmino, F.; Cherioux, F. *Langmuir* **2010**, *26*, 943-949.
(66) Kadota, S.; Aoki, K.; Nagano, S.; Seki, T. *Coll. Surf. A* **2006**, *284*, 535-541.
(67) Seki, T.; Kojima, J.; Ichimura, K. *Macromolecules* **2000**, *33*, 2709-2717.

(68) Seki, T.; Kojima, J. Y.; Ichimura, K. *J. Phys. Chem. B* **1999**, *103*, 10338-10340.
(69) Hergenrother, P. J.; Depew, K. M.; Schreiber, S. L. *J. Am. Chem. Soc.* **2000**, *122*, 7849-7850.
(70) Yam, C. M.; Tong, S. S. Y.; Kakkar, A. K. *Langmuir* **1998**, *14*, 6941-6947.
(71) Zhu, X. Y.; Boiadjiev, V.; Mulder, J. A.; Hsung, R. P.; Major, R. C. *Langmuir* **2000**, *16*, 6766-6772.
(72) Eckertlill, C.; Lill, N. A.; Rupprecht, H. *Coll. Polym. Sci.* **1987**, *265*, 1001-1008.
(73) Utsugi, H.; Horikoshi, H.; Matsuzawa, T. *J. Colloid Interface Sci.* **1975**, *50*, 154-161.
(74) Ossenkamp, G. C.; Kemmitt, T.; Johnston, J. H. *Langmuir* **2002**, *18*, 5749-5754.
(75) Eckertlill, C.; Lill, N. A.; Endres, W.; Rupprecht, H. *Drug Dev. Ind. Pharm.* **1987**, *13*, 1511-1532.
(76) Ciampi, S.; Harper, J. B.; Gooding, J. J. *Chem. Soc. Rev.* **2010**, *39*, 2158-2183.
(77) Scheres, L.; Giesbers, M.; Zuilhof, E. *Langmuir* **2010**, *26*, 10924-10929.
(78) Claesson, P. M.; Blom, C. E.; Herder, P. C.; Ninham, B. W. *J. Colloid Interface Sci.* **1986**, *114*, 234-242.
(79) Liu, Y. H.; Evans, D. F.; Song, Q.; Grainger, D. W. *Langmuir* **1996**, *12*, 1235-1244.
(80) Silbert, G.; Klein, J.; Perkin, S. *Faraday Discuss.* **2010**, *146*, 309-324.
(81) Finklea, H. O.; Robinson, L. R.; Blackburn, A.; Richter, B.; Allara, D.; Bright, T. *Langmuir* **1986**, *2*, 239-244.
(82) Sabatani, E.; Rubinstein, I.; Maoz, R.; Sagiv, J. *J. Electroanal. Chem.* **1987**, *219*, 365-371.
(83) van Delden, R. A.; ter Wiel, M. K. J.; Pollard, M. M.; Vicario, J.; Koumura, N.; Feringa, B. L. *Nature* **2005**, *437*, 1337-1340.
(84) Chandekar, A.; Sengupta, S. K.; Whitten, J. E. *Appl. Surf. Sci.* **2010**, *256*, 2742-2749.
(85) Lee, S. H.; Lin, W. C.; Kuo, C. H.; Karakachian, M.; Lin, Y. C.; Yu, B. Y.; Shyue, J. J. *J. Phys. Chem. C* **2010**, *114*, 10512-10519.
(86) Rieley, H.; Kendall, G. K.; Zemicael, F. W.; Smith, T. L.; Yang, S. H. *Langmuir* **1998**, *14*, 5147-5153.

(87) Mulder, J. K.; Stickle, W. F.; Sobol, P. E.; Bomben, K. D. In *Handbook of X-ray Photoelectron Spectroscopy;* Physical Electronics, Inc.: **1995**.

Chapter 4

Adhesion of photon-driven molecular motors to surfaces *via* 1,3-dipolar cycloadditions: effect of interfacial interactions on molecular motion

Molecular motors containing azide or alkyne groups were attached to alkyne or azide modified surfaces using 1,3-dipolar cycloaddition reactions. Surface-bound motors were found to undergo photochemical and thermal isomerizations consistent with unidirectional rotation in solution. Confinement at a surface was found to reduce the rate of the thermal isomerization process that was dependent on the surface coverage of the motors also. Two half-lives were calculated for the rate of thermal isomerization for surface-bound motors. Both one and two-legged motors were attached to surfaces and it was shown that the kinetics of the thermal isomerization process was not affected by the valency of attachment. This indicates that the changes in kinetics from solution to surface systems are related to interactions between the surface-bound motors.[*]

[*] This chapter has been published:
London, G.; Carroll, G. T.; Landaluce, T. F.; Pollard, M. M.; Rudolf, P.; Feringa, B. L. *Chem. Commun.* **2009**, 1712-1714.
Carroll, G. T.; London. G; Landaluce, T. F.; Rudolf, P.;Feringa, B. L. *ACS Nano* **2011**, 5, 622-630.

4.1 Introduction

The application of organic chemistry to create molecular and supramolecular systems that undergo switching processes has inspired the design of numerous systems that can be cycled between states through the application of various stimuli.[1-8] A key theme has been the construction of chemical systems that mimic dynamic functions of macroscopic machines with the ultimate goal of creating molecules that can perform useful work.[9] The utility of rotary motion in macroscopic and biological machines provides a strong motivation for studying nanoscale constructs that contain molecular components that can undergo rotary motions.[10-12] Such systems are not only interesting in terms of understanding fundamental aspects of motion at the molecular level, but also because biological systems have shown that rotary motions can be used to perform important functions. Two key examples are the ATP synthase[13,14] and the bacterial flagellum,[15] both of which use rotary motion for biological needs. These natural machines show that nanoscale rotary motors are interesting not only for academic purposes, but also indicate their potential future role in powering artificial nanomachines.[16] The potential for developing new technologies that utilize rotary motion has provided a strong impetus for understanding the physics of these biological motors as well as to develop synthetic rotors[10-12,17-28] whose chemical composition and physical properties can be tailored for a given device. In order to harness the collective motions of rotary motors to perform useful tasks, it is expected that surface-confined systems[26,29-32] will be the most relevant as these provide the opportunity to gain more order, compared to solution-phase systems and minimize Brownian motion.[33]

4.1.1 Interfacial reactions

As mentioned above, the ability to control the structure of a solid surface at the molecular level is key towards potential technological applications[34,35] and subject of extensive research.[36-39] Chemical reactions that allow for structural changes of pre-formed monolayers,[40-42] therefore, are expected to play a central role in the construction of nanoscale devices. Analyzing interfacial reactions, however, compared to their solution phase counterparts, is difficult due to the small numbers of molecules (~ few picomoles/square millimeter) present at the resulting modified interface. Because of these challenges, only a limited number of interfacial reactions have been reported.[42]

To gain control over the molecular structure of surfaces with the use of interfacial reactions there are a few criteria the reactions have to fulfill[42,43]: (i) quantitative conversion under mild conditions (atmospheric pressure and rt), (ii) compatibility with different functional groups, (iii) no reaction by-products (which might accumulate on the surface and slow down or stop the reaction). These criteria are related to the "click-chemistry" concept introduced by Sharpless[44] as "a set of powerful, virtually 100% reliable, selective reactions for the rapid synthesis of new compounds *via* heteroatom links (C-X-C)".The most widely employed of the so-called ''click"-reactions is the 1,3- dipolar cycloaddition reaction of azides with alkynes,[45] which has shown great success in many applications[46-49] including surface modification.[43,50-54] Therefore, the "click"-reaction was expected to be a useful tool for the covalent modification of surfaces with rotary molecular motors.

4.1.2 Attachment of dialkyne-motor to azide-functionalized surfaces

The two pendant azide and alkyne moieties at the stator part of modified second-generation molecular motors **2.30** and **2.31** (for the synthesis see chapter 2), allow for a general and convenient attachment to a variety of materials through a 1,3-dipolar cycloaddition. Covalent attachment of the azide or alkyne moieties of **2.30** and **2.31** to an interface likely forces the system to rotate in an altitudinal manner with the axis approximately parallel to the surface (Scheme 1), affording opportunities for controlling surface properties or the position of adsorbates.

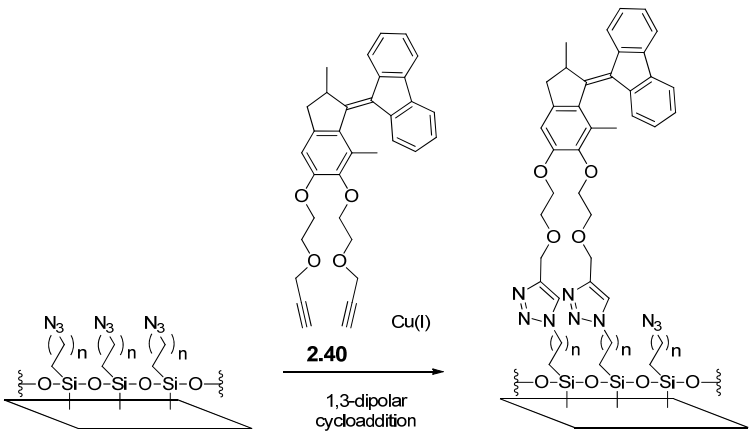

Scheme 1 Modification of an azide functionalized surface with a molecular motor via a Cu(I) catalyzed 1,3-dipolar cycloaddition reaction.

This new approach has the advantage over the previously reported method[55] (Scheme 2) in that the diazide and dialkyne readily react with a modified surface without further need to activate the molecule to a more reactive and less stable intermediate (i.e. acid chloride) before surface modification.

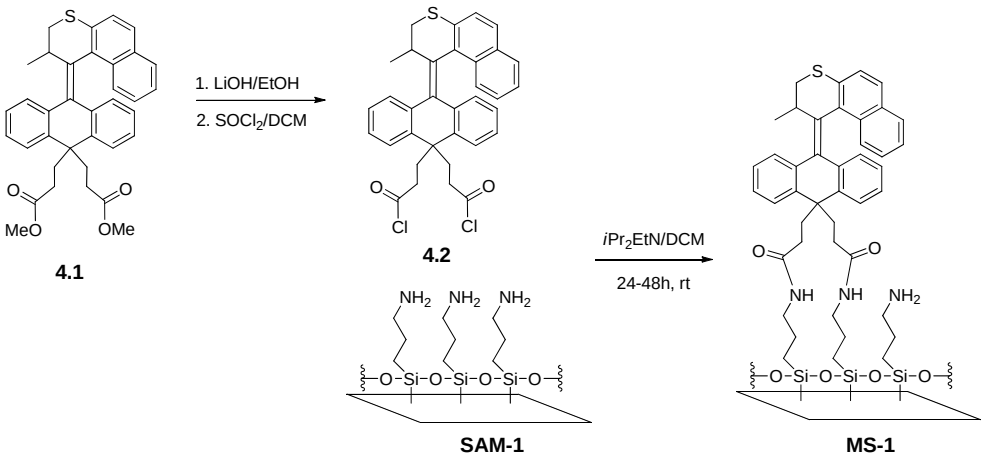

Scheme 2 Attachment of azimuthal motor **4.1** to amine functionalized surface via amide bond formation as reported earlier.[55] The procedure requires the formation of the acid chloride derivative **4.2** prior to surface modification.

In addition, the reactivity of amino groups confined to the surface is lower[40] and the preparation of aminopropylsilane surfaces raises difficulties due to polymerization/oligomerization, hydrogen bonding with surface silanol groups and hydrolytic instabilities.[56-59]

4.2 Azide-functionalized surfaces: preparation and characterization

To convert the relative rotary motion of the two halves of **2.30** in solution into a controlled altitudinal rotary motion, we prepared azide functionalized quartz slides (Scheme 3). Such surfaces have shown to be convenient substrates for interfacial 1,3-dipolar cycloaddition reactions.[43,53]

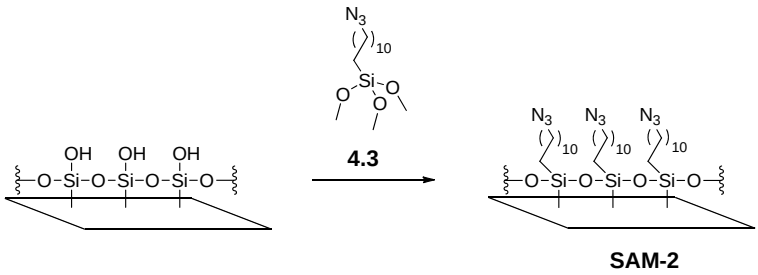

Scheme 3 Formation of azide monolayer on silicon and quartz surfaces for further modification via 1,3-dipolar cycloaddition.

The azide-terminated silane **4.3** was prepared by the reaction of 11-bromoundecyltrimethoxysilane with NaN_3 in DMF[60] (Scheme 4).

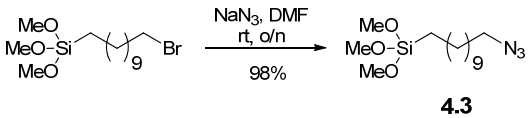

Scheme 4 Synthesis of 11-azidoundecyltrimethoxysilane.

The azide-terminated monolayer **SAM-2** was prepared by two different methods. In the first method piranha-cleaned quartz slides were immersed in a 1 mM solution of silane **4.3** in toluene for 1 day at room temperature.[43] However, a more efficient procedure for achieving a higher coverage of azide involved self-assembly from a 20:1 cyclohexane:THF solution containing a small quantity of H_2O and HCl.[61] Following the assembly process, the azide-functionalized substrates were rinsed extensively by sonication in DMF, toluene and methanol (2 min in each) and then dried under a stream of Ar. Typical water contact angles of the azide SAMs prepared by the two methods were 77º(±1º) and 83º(±1º), respectively, which are similar to those reported for other azide functionalized surfaces.[53,62,63]

Ellipsometry measurements revealed that immersion of piranha-cleaned quartz or Si/SiO_2 substrates in 1 mM solutions of compound **4.3** consistently gave organic coatings of 1.8 nm or less. The theoretical length of **4.3** is approximately 1.9 nm, consistent with a monolayer of the azide. Surfaces prepared via self-assembly from toluene showed an average thickness of 0.7 nm (±0.1 nm) while the ones prepared

using the hydrolysis method reached thicknesses up to 1.8 nm (±0.1 nm). Self-assembly in cyclohexane/THF mixture without water or acid required two days to reach a film thickness of approximately 1.7± 0.1 nm.
A given substrate showed a thickness variation of no more than 0.1 nm when multiple areas of the substrate were measured, indicating a uniform coating.

X-ray photoelectron spectroscopy (XPS) was used to further characterize the azide-modified surface (Figure 1). XPS spectra show two distinct N1s peaks due to the azide group, one positioned at 401 eV and another centered at 405 eV, with a 2:1 ratio of the peak areas. The smaller peak is assigned to the central, electron-deficient nitrogen in the azide group.[64-66]

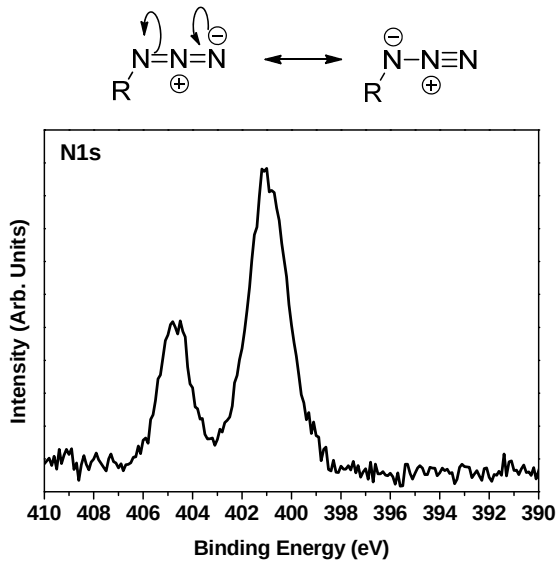

Figure 1 XPS spectrum of azide modified silicon surface **SAM-2**. The smaller peak corresponds to the central electron deficient nitrogen atom.

ATR-IR spectroscopy, performed by placing the surface in intimate contact with a germanium crystal, was used to show the presence of the azide functionality on the substrate. The distinct band at 2095 cm^{-1} clearly shows the presence of azide on **SAM-2** (Figure 2).

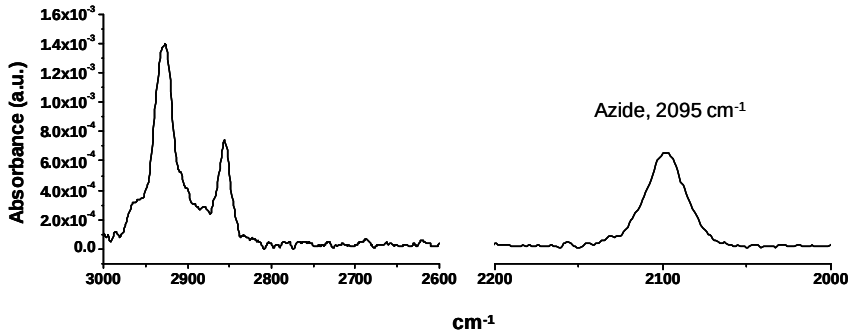

Figure 2 IR spectrum of azide modified silicon surface **SAM-2**. The distinct band at 2095 cm^{-1} clearly shows the presence of azide groups on the substrate.

Collectively, the characterization shows a highly stable and uniform coating of azide-functionalized molecules with a thickness that is consistent with a monolayer. As will be discussed below, the surface-bound azides provide a highly reactive monolayer for attaching alkyne-modified molecules.

4.3 Interfacial click-reaction for motor attachment

Motor **2.30** was grafted to the azide monolayer in DMF at room temperature by immersing the slide into a 1-2 mM solution of **2.30** containing 1 mol% $CuSO_4 \cdot 5H_2O$ and 5 mol% Na-ascorbate relative to the alkyne moieties (Scheme 5). The surfaces were rinsed by sonication for up to three minutes in DMF, H_2O and MeOH (once in each solvent) and then dried under a stream of argon.

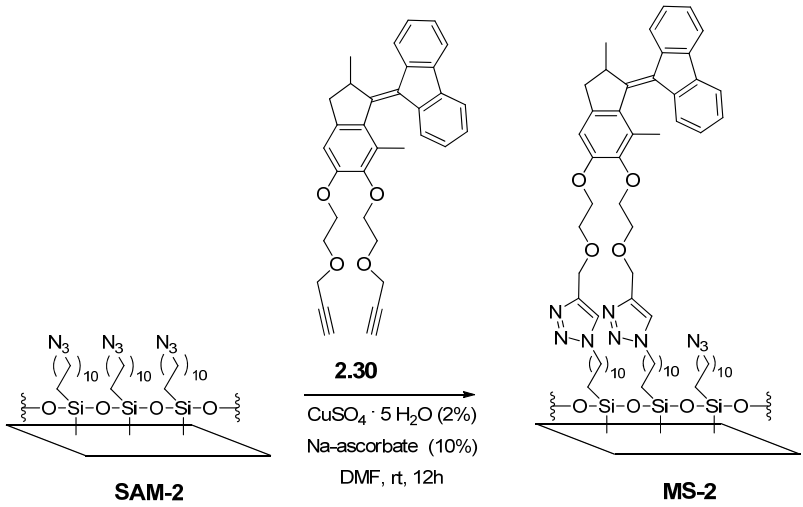

Scheme 5 Covalent attachment of motor **2.30** to azide monolayer **SAM-2**.

A range of characterization techniques were used to support the hypothesis that the motor adheres to the surface via covalent bond formation.

4.3.1 UV-vis spectroscopy, water contact angle and ellipsometry measurements

The UV-Vis spectrum of a quartz substrate shows the presence of the motor after immersion in a 1 mM solution of **2.30** in the presence of copper catalyst (Figure 3).

To show that the signal is not simply the result of insufficiently rinsing a surface coated by physisorption from solution, several control experiments were performed. If an unmodified quartz slide was immersed in a solution of **2.30**, H_2O was found to spread on the quartz with a contact angle of 3º(±1º), indicating the lack of organic coating. Immersing an azide-functionalized slide in a solution of **2.30**, which lacks the copper catalyst, did not give the UV-vis absorption of the motor, indicating that the Cu-catalyst is essential for the reaction and that non-specific adsorption of **2.30** is negligible (Figure 3).

The control experiments were performed at room temperature and at 65º C, and also for prolonged immersion times up to 5 days. These results indicate that the silane coating is chemically modified by the controlled reaction of a carefully designed molecule.

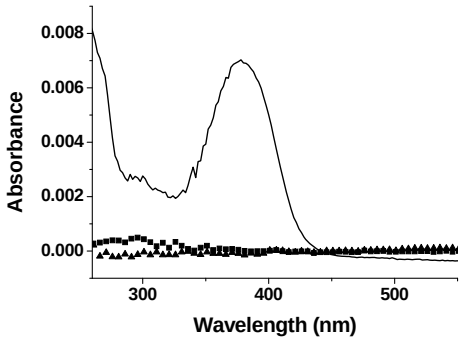

Figure 3 UV-vis absorption spectrum of **MS-2** (solid line) is similar to that of the motor in solution. Control experiments were carried out in the absence of azide functional groups (■) and in the absence of copper catalyst (▲) to show that the absorption is not the result of insufficient rinsing. (Note that the azide monolayer (**SAM-2**) was deposited from 1mM toluene solution in this case.)

As the UV-vis absorption spectrum of **2.30** on the surface is not significantly different from that observed in methanol solution, the UV-vis spectrum of **MS-2** could be used to estimate the surface coverage based on the assumption that the molar absortivity (ε) of **2.30** is the same in solution and on the surface.[67,68] Using the Beer-Lambert law, the relation between the absorption (A) and the surface-density (Γ) of the absorbing species can be written as follows:

$$A = \varepsilon \times \Gamma \qquad \textbf{Eq. 1}$$

Taking into account that both sides of the slide are functionalized, the surface coverage density of **2.30** is estimated to be 1.5×10^{-10} mol/cm^2 for a single side, which is in agreement with the value obtained for monolayers of overcrowded alkenes reported elsewhere recently.[69]

To elucidate the effectiveness of the attachment technique, the interfacial reaction was performed under different conditions. The amount of catalyst was varied from 1-5 mol % relative to the alkynes. No difference in the intensity of the resulting UV-vis absorption was observed. Likewise, performing the surface reaction at 65º C showed no difference in the intensity of the absorption.

Changing the immersion time provided a simple manner to control the surface coverage. After removing the substrate at various times followed by sonication (3 times 2 min in toluene and MeOH), the UV absorption increased with reaction time as expected for a covalent attachment to the interface (Figure 4).

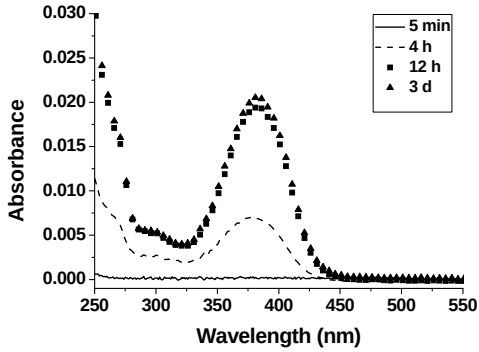

Figure 4 Attachment of **2.30** to azide modified quartz surfaces via copper-catlayzed 1,3-dipolar cycloaddition. Changes in surface coverage by time were monitored by UV-vis spectroscopy. Increase of the intensity after longer immersion times indicates higher surface coverages. (Note that the azide monolayer (**SAM-2**) was deposited using the hydrolysis method, which involves the hydrolysis of the methoxysilane groups of **4.3** prior to surface modification. This method gives higher azide-coverage which leads to higher density of motors on the surface.)

The intensity of the UV signal and the reaction time to reach saturation was dependent on the quality of the azide layer. A higher coverage of azide produced a more intense UV absorption and a longer reaction time was required to reach saturation.

The higher density of motor was also evident in a higher ellipsometric thickness. The highest ellipsometric thickness of the motor layer obtained for the highest yield of azide is approximately 1.5 nm, which is close to the calculated length of 1.55 nm if the 'leg' of **2.30** are oriented normal to the substrate.

A reduction in the H_2O contact angle from 82±1º to 65±1º upon motor attachment, probably due to the ethylene glycol 'legs' and triazole-moiety of the surface linkage, implies that the layer of motors is not so well packed as to screen the molecular components beneath the chromophore from a water droplet. Note that the H_2O contact angle of a poly (styrene) film on solid surfaces is approximately 90º.[36,70] Although not a perfect comparison, it provides a comparative value for a smooth film composed of aromatic units and aliphatic CH groups, both of which comprise the motor component of **2.30**.

The measurements clearly indicate the presence of the motor on the azide-coated surfaces, which appears to be a single layer. Covalent attachment of the motor to the surface seems the likely adhesion mechanism given the control experiments described above.

4.3.2 XPS and ATR-IR measurements

To further support the covalent attachment, XPS and ATR-IR spectroscopy was performed on surface **MS-2**.

The XPS spectrum of N1s after the reaction of the azide monolayer with the dialkyne-motor **2.30** via the 1,3-dipolar cycloaddition shows the effective disappearance of the peak at 405 eV to the level of noise (Figure 5a). The broadening of the N1s peak at 400.7 eV indicates the presence of chemically distinct nitrogen atoms (Figure 5a, lower panel). The formation of this profile of absorption is consistent with the data from analogous surface modifications.[64-66]

Additionally, the absence of Cu peaks in the XPS spectrum indicates that the washing steps removed the copper catalyst from the substrate.

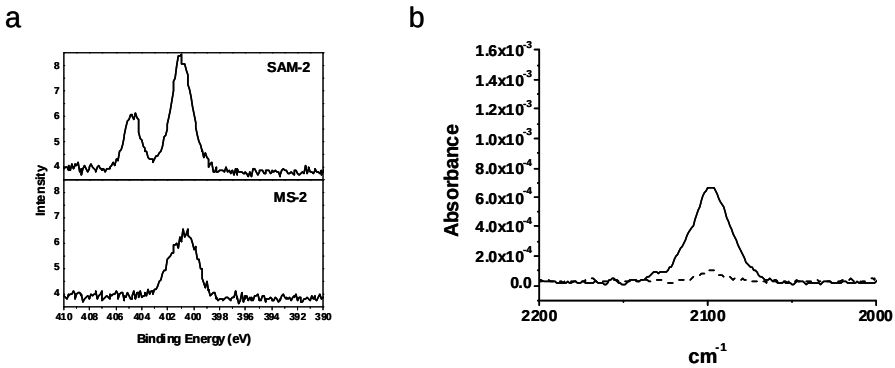

Figure 5 (a) XPS spectra of the N1s core level region of an azide functionalized silicon surface (**SAM-2**) before (upper panel) and after (lower panel) attachment of motor **2.30**; (b) IR-spectrum of an azide functionalized silica surface before (solid line) and after (dashed line) attachment of motor **2.30**. The attenuation of the azide signal indicates that the interfacial click-reaction is taking place.

As showed above, the azide signal is clearly present in the IR-spectrum of the azide modified silicon substrate. After reaction with the motor, the signal attenuates to the level of noise, providing further evidence for covalent modification of the azide layer (Figure 5b).

The combination of characterization techniques and resistance to repeated cycles of sonication and washing strongly indicates that the motors are covalently bound to the interface.

4.4 Rotation on the surface

To confirm that the rotary function of the surface-bound molecules is preserved, **MS-2** was irradiated with UV light (365 nm, 253 K, N_2 atmosphere). Irradiation of **MS-2** for 30 min led to a red shift in the long-wavelength absorption, as observed for **2.30** in solution (Figure 6). Allowing the substrate to warm to room temperature restored the original UV-vis spectrum, indicating that the thermal helix inversion regenerated stable **MS-2**. Such observations are consistent with the behaviour of **2.30** in solution. In addition, irradiation (365 nm, MeOH, rt, 30 min) of a solution of **2.30** in the presence of 11-azidoundecyltrimethoxysilane **4.3** did not cause any change in the motor structure.

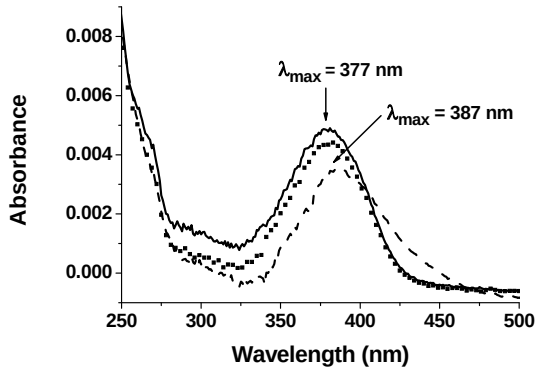

Figure 6 UV-vis spectrum of the surface bound motor **2.30** before (solid line) and after (dashed line) irradiation at λ_{max}= 365 nm. The shift in the spectrum upon irradiation and the reversion of the spectrum after standing at rt (30 min) (■) indicates that the rotary function is preserved upon surface attachment.

4.5 Click-reaction prior to surface modification

An alternative approach one may opt for is to directly assemble a silanated version of the motor **2.30**. Although such an approach appears more efficient on paper, an advantage of the interfacial 1,3-dipolar cycloaddition of the motor over the hydrolysis of a silanated motor is that multilayer formation during assembly or polymerization during storage or handling is no longer a possible undesirable outcome. Additionally, performing the reaction on the surface allows one to bypass a step of the synthesis and the accompanying purification methods. Nevertheless, we felt that it would be instructive to work with a silanated version of the motor.

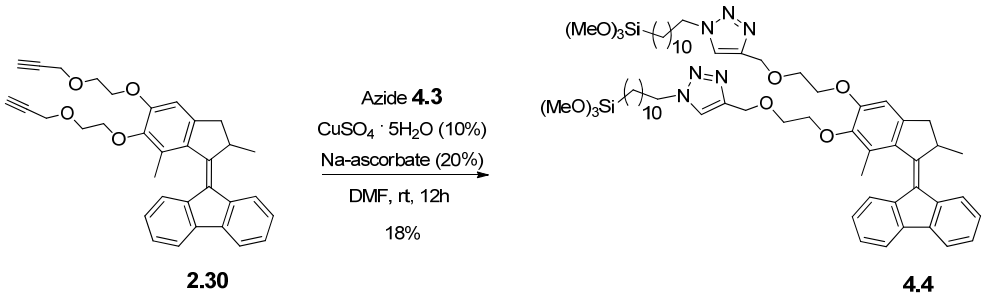

Scheme 6 The click-reaction in solution prior to surface attachment. The resulting compound **4.4** is less convenient to purify and handle and its attachment is less straightforward compared to the interfacial reaction approach.

The first attempt at forming the triazole in solution and assembling the silane **4.4** resulted in a multilayer of 77±8 nm and an H_2O contact angle of 79±3º on silicon. Polymerization of the silane was evident in the formation of a yellow particulate within 10 min of mixing a THF solution containing silane and a small amount of H_2O and HCl in cyclohexane. Scanning electron microscopy (SEM) images show what appear to be fused particle-like aggregates (Figure 7a).

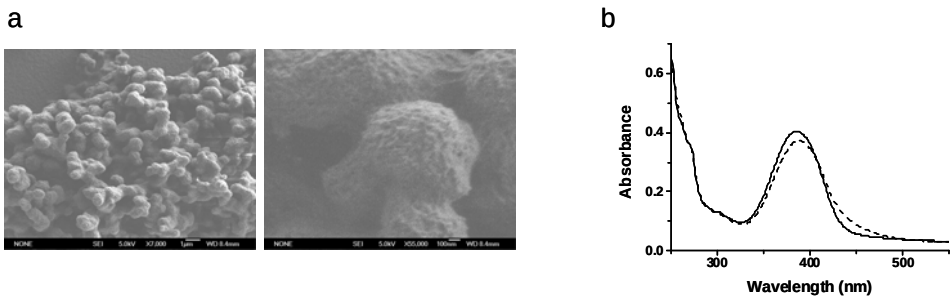

Figure 7 (a) SEM image of polymerized **4.4**. The first attempt to attach **4.4** on silicon resulted in its polymerization and multilayer formation; (b) UV-vis spectrum of the multilayer film formed from polymerized **4.4**. In spite of the polymerization the motor preserved its rotary function; the irradiation of the multilayer film (rt) (straight line) with UV-light (365 nm) resulted in a change in its UV-vis spectrum (dashed line) indicating the formation of the unstable form.

A stable coating was formed on silicon and quartz that was resistant to sonication. Irradiation of the film at room temperature with UV light produced a yellow film that faded with time as the motor underwent thermal isomerization to the stable

form. The changes in the UV-Vis spectrum (Figure 7b) correspond to the changes found in solution and for the monolayer (Figure 6). Thinner films with a thickness that corresponds to monolayer coverage could be obtained by reducing the concentration. For example, a film with an ellipsometric thickness of 1.9±0.1 nm could be obtained by assembling **4.4** from a 0.01 mM cyclohexane/THF solution containing a small amount of water and HCl (Figure 8a). Interestingly, self-assembly from THF in the absence of cyclohexane showed low coverage (0.3 nm ellipsometric thickness) (Figure 8b) and may be a result of competition with THF coordinating to the surface as has been implicated when self-assembly is attempted on mica,[61,71] although this comparison is imperfect as mica is chemically distinct and may have a different mechanism of adhesion prevention. Although the system can be somewhat intractable, it provided an additional variant to study the kinetics of isomerization as will be discussed below.

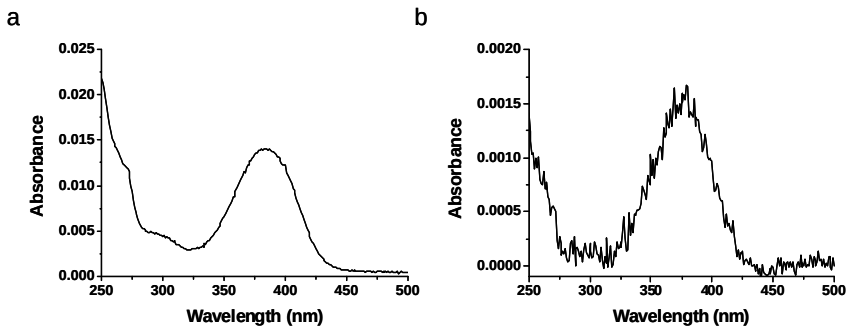

Figure 8 UV-vis absorption spectra of 4.4 assembled on quartz surfaces. (a) A layer of **4.4** with close to monolayer coverage (2.3×10^{-10} mol/cm^2) could be obtained through assembly from a 0.01 mM solution of **4.4** in cyclohexane/THF/H_2O/HCl; (b) Attempt to assemble from THF/H_2O/HCl solution resulted in poor surface coverage (0.3 nm ellipsometric thickness)

4.6 Attachment of a diazide-motor to alkyne-functionalized surfaces

To more directly probe the feasibility of two-legged attachment as well as expand and test the versatility of the interfacial reaction, the attachment of motor **2.31**, which contains two azides, was attempted to an alkyne-modified surface, **SAM-3** (Scheme 7). Quartz and silicon wafers were silanated with O-(propargyloxy)-N-(triethoxysilylpropyl)urethane which resulted in a coating with 0.8 ±0.1 nm ellipsometric thickness.

After reaction of **SAM-3** with **2.31** under the same conditions for attaching **2.30** to **SAM-2**, the thickness increased to 1.9 ±0.1 nm, measured by ellipsometry, consistent with the attachment of a layer of motor **2.31**.

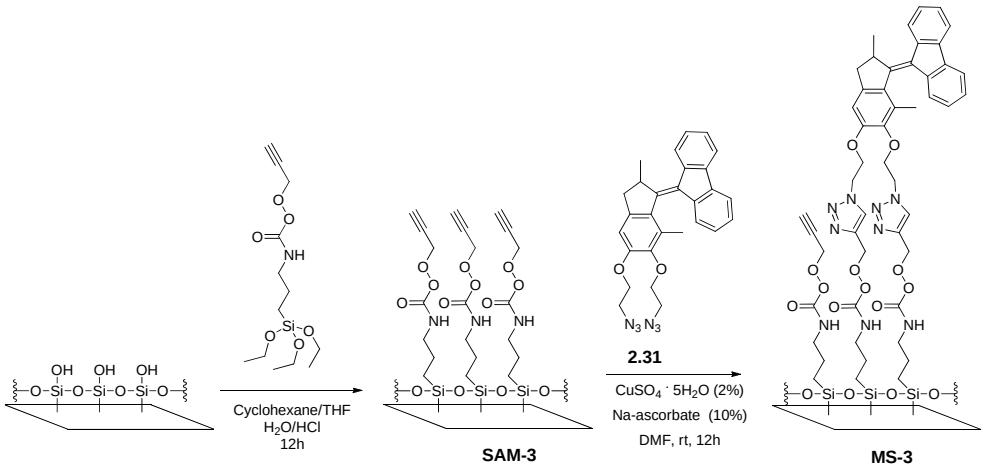

Scheme 7 Formation of alkyne terminated monolayer and the subsequent attachment of azide functionalized motor **2.31**.

The UV-Vis spectrum showed the presence of the motor on the surface only when catalyst was added to the reaction mixture (Figure 9). In the absence of catalyst or an alkyne film no motor was detected on the quartz surface. Based on the UV-vis absorption, the surface density of the motor was estimated as 2.6×10^{-10} mol/cm^2 consistent with monolayer coverage.[69] Irradiation of the resulting layer at room temperature resulted in changes in its UV-vis spectrum similar to those in solution showing that the motor preserved its rotary function upon attachment to solid surfaces.

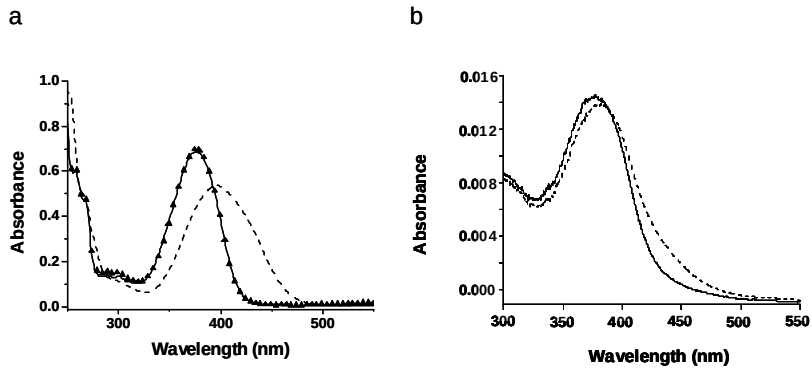

Figure 9 UV-vis spectra of (a) the stable form (solid line) and the PSS mixture (dashed line) of diazide motor **2.31** in methanol solution (irradiation at λ_{max}= 365 nm, -20°C) and (b) on the surface (irradiation at λ_{max}= 365 nm, rt).

The distinctive XPS and IR signals corresponding to azide functionality were used to probe the propensity for two-legged attachment.[31,43] Both the XPS (Figure 10a) and IR (Figure 10b) spectra show no evidence for unreacted azide supporting the conclusion that both legs of the motor react under the conditions employed.

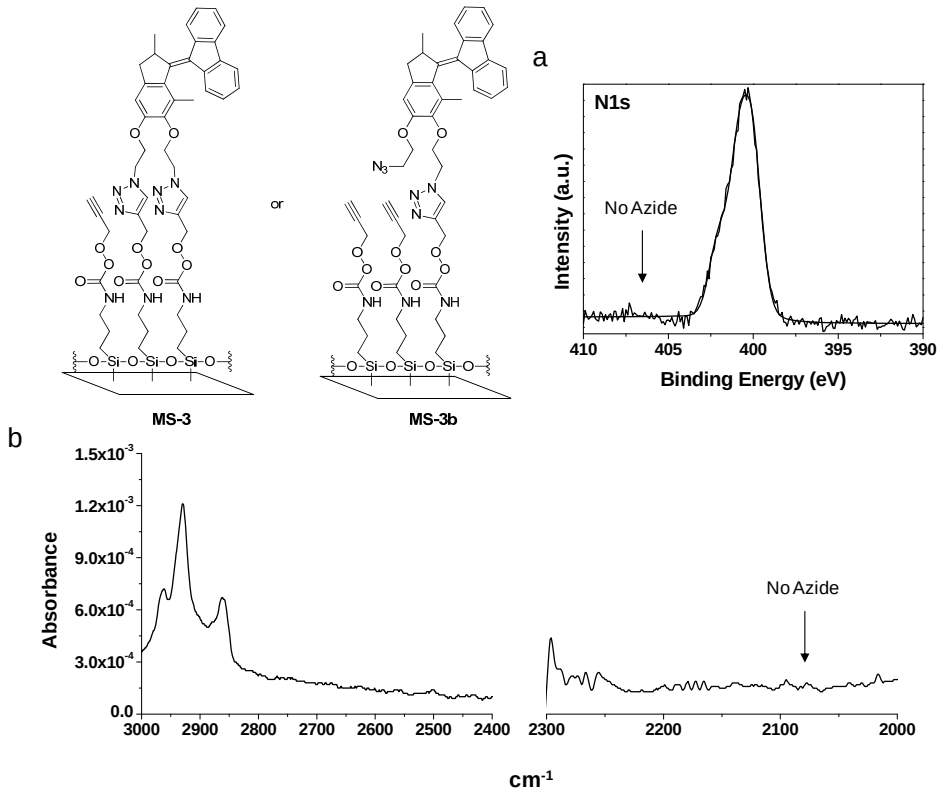

Figure 10 (a) XPS spectrum of the N1s core level region and (b) ATR-IR spectrum of surfaces functionalized with azide terminated motors **2.31**. The spectra show the lack of free azide groups, therefore, support that both 'legs' of the motor are attached to the surface.

4.7 Effect of confinement on the speed of rotary motion – kinetics on surface

As previously shown, **2.30** can undergo photochemical isomerization followed by an irreversible thermal isomerization while confined at an interface.[31] The thermal isomerization is the rate-limiting step of the rotary cycle. Understanding how the structure of the motor affects the half-life of the thermal step has been key in increasing the speed of the motor.[72] A general paradigm regarding the effect of substituents and ring size has been developed in order to design faster motors. Although much progress has been made in synthesizing motors of various speeds, confinement and intermolecular effects on the speed of rotation have previously

received little attention. In solution the thermal isomerization of **2.30** was found to proceed through a unimolecular process with a half-life of 87 s in methanol. In order to compare the surface-bound system with the solution analogue, we followed the time dependence of the changes in the UV-vis spectrum during thermal isomerization at the interface using a surface that had a coverage of approximately 50%, determined based on the intensity of its UV-vis absorption. (Figure 11).

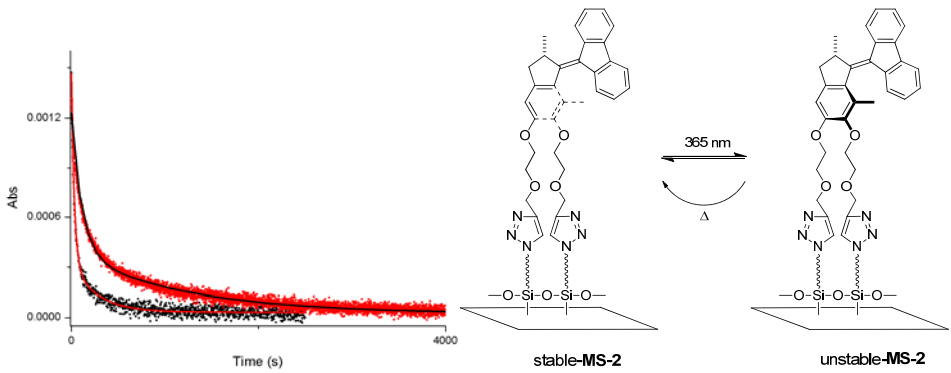

Figure 11 Thermal decay of UV-vis signal of **MS-2** (50% surface coverage) at 439 nm at 25ºC (red) and 40ºC (black). Both data sets were fit with a biexponential decay, and hence two half-lives for the rate of thermal isomerization were calculated for each temperature. The half-lives at 25º C are 110 s and 1200 s. The half-lives at 40º C are 30 s and 270 s.

In contrast to the solution experiments, fitting the thermal decay of the signal at 439 nm suggested that at least two processes occur during the thermal isomerization that have half-lives that differ by an order of magnitude at 25ºC. The first half-life had a value of approximately 110 s, consistent with the half-life of 87 s measured in MeOH solution. More striking is the extraction of a second half-life of 1200 s, making the rotary cycle of the surface-bound ensemble considerably slower than in solution.

Evidenced by the biexponential decay of the UV spectrum corresponding to the unstable form of the motor, the existence of at least two different processes is postulated. The biexponential fit may reflect environmental or configurational heterogeneities (i.e. surface roughness, defects sites, etc.) or multiple processes occurring during thermal isomerization when **2.30** is clustered and bound to a substrate. As expected, higher temperatures increase the rate of thermal isomerization on the surface (Figure 11). For example, measurements performed at

40º C gave a thermal decay for which half-lives of 30 and 270 s were obtained. Interestingly, other surface-confined systems have similarly shown a non-monoexponential decay corresponding to the kinetics of molecular conformational changes. For example, methylthiolate chemisorbed on an Ag(111) surface showed a biexponential decay for the lifetime of the first excited level of the symmetric C-H stretching mode.[73] Similarly, thin polymer films containing azobenzenes attached to side-chains have shown thermal rates that deviate from simple monoexponential behavior[74]

Regardless of the fitting procedure, it is clear that the thermal conformational change requires more time on the surface compared to solution. Based on our model of a layer of oriented motors covalently attached to a solid substrate, supramolecular interactions within a cluster of surface-bound motors seems to be the most plausible reason for the observed kinetics. The hypothesis was tested by constructing surfaces with a different coverage of motors and comparing the half-life for thermal isomerization. A potential advantage of the surface modification strategy presented herein is that better control over the density of the bound species can be obtained compared to direct self-assembly of a silane, which can assemble into dense clusters prior to surface attachment. Although the exact mechanism of interfacial 1,3-dipolar cycloadditions for small molecules is not known, it is assumed that for **2.30** self-assembly into clusters at the surface does not precede covalent bond formation. For the arguments presented below random growth of the film without pre-aggregation or self-assembly is assumed,[75] however the latter cannot be explicitly ruled out.

4.7.1 Effect of surface coverage on the speed of the rotary motion

To understand the effect of surface coverage on the kinetics of the thermal isomerization four different coverages were examined. The highest covered surface is designated as a saturation of 1.0. Using the UV-Vis absorption signal at 379 nm for detection, surfaces that had a coverage that was approximately 50% and 25% the saturation coverage (saturation factor of 0.5 and 0.25, respectively) were studied (Figure 12). Additionally, the multilayer formed by assembly of the silane **4.4** was used in order to probe a more extreme situation in which a given motor is more susceptible to axial interactions (i.e., having neighbors not only on the side, but also on the top) compared to a monolayer in which axial interactions could only

occur when deviations from our model in Scheme 5 occur (i.e. surface roughness, defects which considerably tilt the axle, adventitious impurities).

a

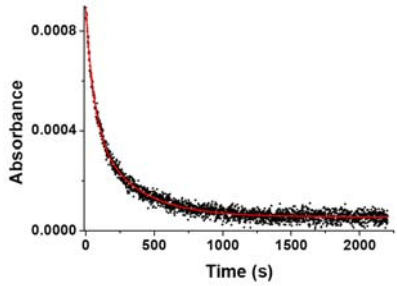

b

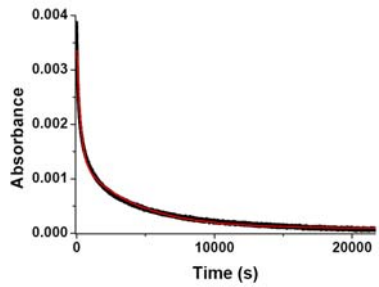

c

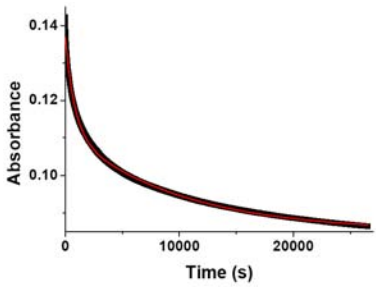

d

Saturation factor	T1(s)	T2 (s)
0.25	60	320
0.5	110	1200
1	280	4100
20	800	10000

Figure 12 Thermal decay of UV-vis signal of **MS-2** at 439 nm at 25°C at (a) 25%, (b) 100% coverage and (c) multilayer film. (d) Summary of the half-life values of surface bound motor **2.30** at different coverages.

The thermal decay curves and half-lives for the thermal isomerization are presented in Figure 12. Both the fast and slower processes show a decrease in half-life with a decrease in the surface coverage. At full coverage, the half-lives are 280 and 4100 s, considerably higher than the values found for surfaces with 50% coverage. The most drastic change occurs on going from the monomolecular layer to the multilayer prepared by polymerization of the silane. The overlayer experienced by the motors in the multilayer film has a significant effect on the motors, which not only provides support for the idea that supramolecular interactions affect the speed of the rotary cycle, but also indicates that the systems fabricated by the controlled dipolar cycloaddition do contain a reasonable degree of order as expected from chemoselective covalent bond formation of a small molecule with a surface.

4.7.2 Effect of the valency of the attachment on the speed of the rotary motion

One may consider that the two processes indicated by the biexponential fit reflect surface populations that are attached through one and two legs. If this were the case then attaching a one-legged motor would show monoexponential decay. In pursuit of understanding the valency of surface attachment on the kinetic behavior of the rotary cycle, a one-legged derivative of **2.30**, compound **4.12** was synthesized.

4.7.2.1 One-legged motor – synthesis and characterization in solution

The synthesis of the one-legged motor (Scheme 8 and Scheme 9) involves similar synthetic transformations described earlier for the two-legged motor.
The upper half was prepared starting from 3-methylanisole (Scheme 8). The previously described (see Chapter 2.) Friedel-Crafts acylation / Nazarov cyclization one-pot reaction sequence yielded the desired ketone **4.5**, but in this case the other regioisomer, **4.6**, could also be isolated.

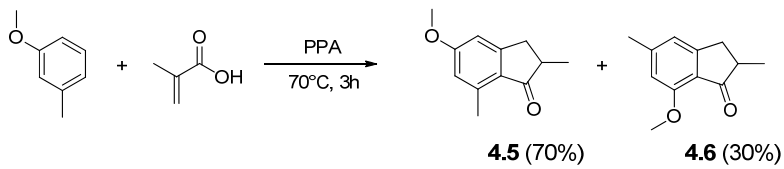

Scheme 8 Synthesis of the upper half ketone results in the formation of two regioisomers.

Deprotection of the methoxy group of ketone **4.5** with BBr_3 yielded phenol **4.7** that could be further functionalized with ethyl bromoacetate to introduce an ester terminal leg. Ketone **4.8** was converted to the corresponding thioketone with Lawesson`s reagent to react with diazofluorenone in the next step. The formation of the episulfide in the Barton-Kellogg reaction between thioketone **4.9** and diazofluorene was monitored by ^1H NMR spectroscopy by following the appearance of the upper-half aromatic protons at 6.42 ppm and 6.55 ppm. The episulfide could be desulphurized with PPh_3 yielding motor **4.10**. The reduction of the ester moiety with $LiBH_4$ afforded alcohol containing motor **4.11,** which was alkylated with propargyl bromide to introduce the terminal triple bond necessary for attachment to azide modified solid surfaces (Scheme 9).

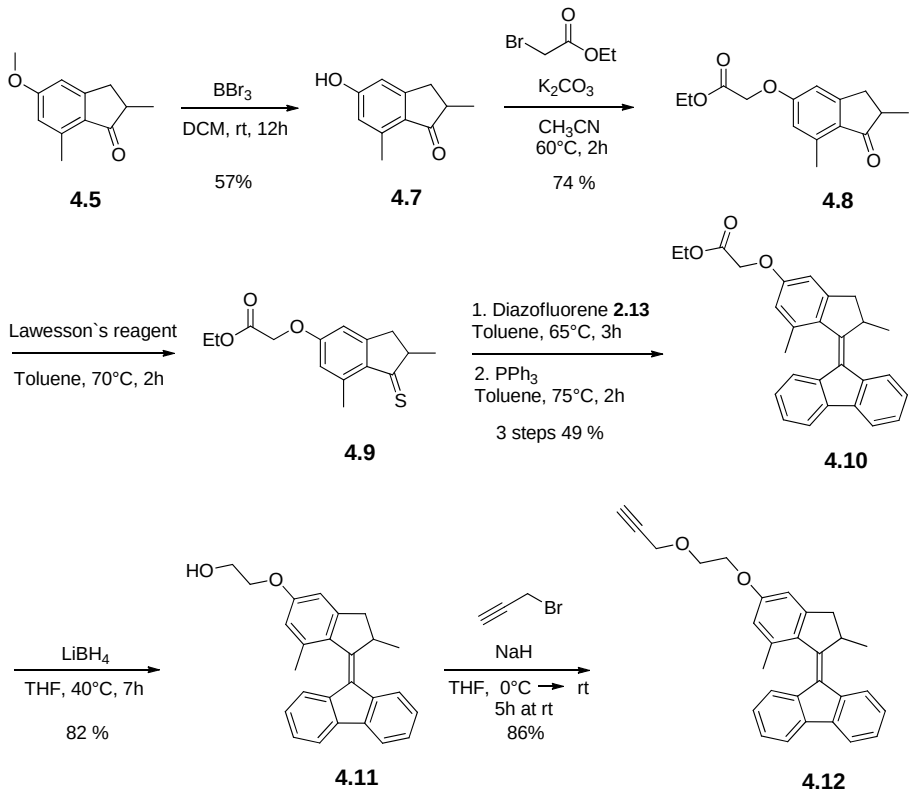

Scheme 9 Synthesis of motor **4.12** containing a single terminal triple bond for surface attachment.

The UV-vis absorption spectrum of **4.12** in methanol solution at -20°C is similar to that obtained for **2.30** under the same conditions. As expected, upon irradiation with UV-light (λ_{max}= 365 nm) the formation of the unstable form was observed as a shift of the absorption band centered at 374 nm to a broader band at 385 nm. Upon warming the sample to rt the thermal helix inversion took place as indicated by the regeneration of the original UV-vis spectra (Figure 13).

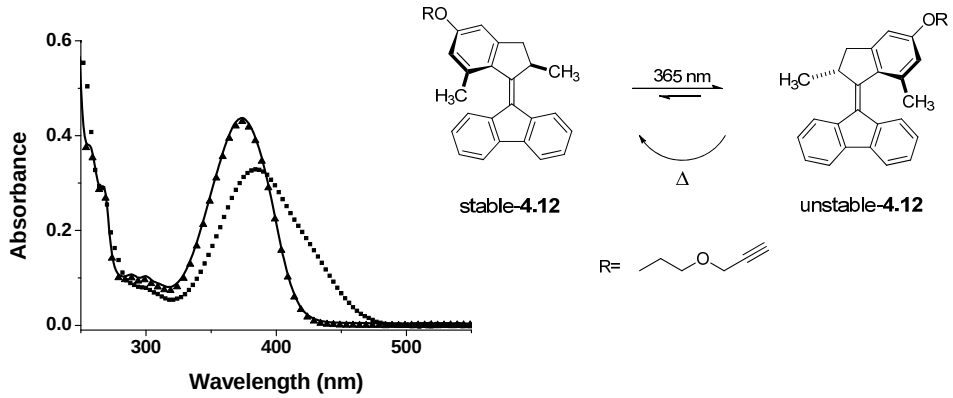

Figure 13 Upon irradiation with UV-light (365 nm, MeOH, -20°C), **4.12** (solid line) undergoes *cis*/*trans* isomerization (■) indicated by the red-shift of the original UV-vis spectrum. The original UV-vis spectrum was recovered upon heating the sample to rt (▲).

The kinetic parameters of the thermal helix inversion of unstable-**4.12** to stable-**4.12** were determined by monitoring the change of the UV-Vis absorption as a function of time at different temperatures (T = 253, 258, 263, 268 K). Using the Eyring equation, the Gibbs free energy of activation ($\Delta^{\ddagger}G°$) was calculated to be 78.4 kJ mol^{-1}. By extrapolation the half-life ($t_{1/2}$) of **4.12** at rt was calculated 11 s. ^{1}H NMR spectroscopy was used to determine the composition of the photostationary equilibrium. Irradiation of a CD_2Cl_2 solution of motor **4.12** at λ_{max}= 365 nm at -60°C resulted in a 1 : 2 ratio of stable-**4.12** : unstable-**4.12**.

4.7.2.2 One-legged motor – surface attachment

Surface attachment was carried out under similar condition to that of the dialkyne motor **2.30** (Scheme 10a). When 1 mol % of copper catalyst was used, **2.30** was found to react with the surface much faster than **4.12** as determined by the UV-vis spectrum (Scheme 10b). The UV-vis spectra reached saturation almost after 12 h for **2.30** whereas the surface reaction for **4.12** was only approximately halfway complete, requiring an additional day for full conversion. Based on the UV-vis absorption, the surface density of the motor was estimated as 3.4×10^{-10} mol/cm^2 consistent with monolayer coverage.[69]

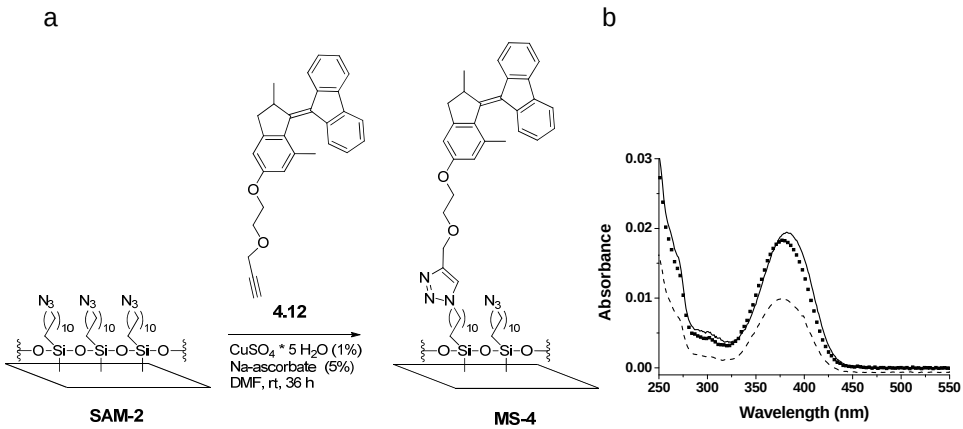

Scheme 10 (a) Attachment of **4.12** to azide functionalized surfaces. (b) UV-vis spectrum of the resulting layer (**MS-4**) taken after 12 h (dashed line) and 36 h (solid line) immersion times. UV-vis absorption of **MS-2** after 12 h immersion (■) is shown for comparison.

The successful modification of azide-functionalized quartz and silicon surfaces was supported further by similar techniques to those used for the characterization of **MS-2**. Ellipsometry measurements revealed an increment in layer thickness from 1.8± 0.1 nm for the azide to 3.0± 0.2 nm after the interfacial reaction. Furthermore, the water contact angle of the azide surface decreased from 80± 1° to 72± 0.3° following the reaction with motor **4.12**.

ATR-IR and XPS spectroscopy - performed before and after the interfacial reaction - also confirmed the attachment of **4.12** to **SAM-2**. As found for **2.30**, the azide peak in the IR spectrum disappeared. Similarly, the azide band at 405 eV in the XPS spectrum is significantly attenuated, signifying chemical transformation through the formation of a triazole moiety (Figure 14).

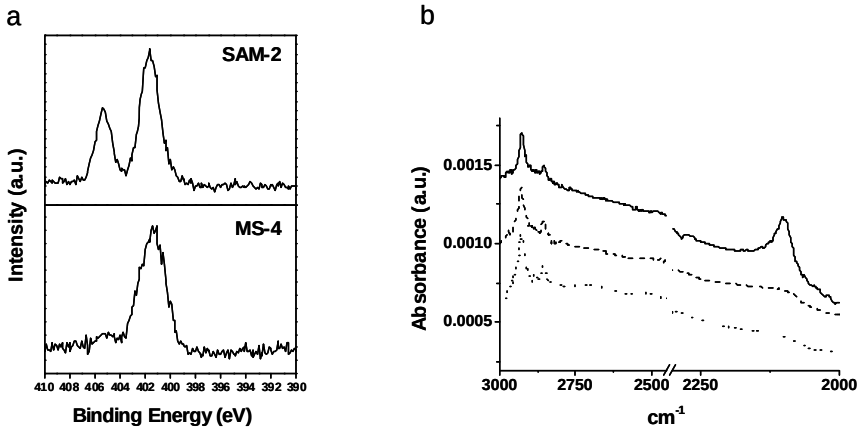

Figure 14 (a) XPS spectra of the N1s core level region of azide functionalized surface **SAM-2** before (upper panel) and after (lower panel) attachment of motor **4.12** (**MS-4**); (b) IR-spectra of azide functionalized surface **SAM-2** before (solid line) and after (dashed line) attachment of motor **4.12** (**MS-4**) A layer of two-legged alkyne motor **MS-2** (dotted line) is shown for comparison.

4.7.2.3 One-legged motor – effect of confinement on the speed of rotation

The decay of the signal at 439 nm in the UV-vis spectrum was monitored (Figure 15) following irradiation with UV-light (365 nm, rt) under the same conditions employed for **MS-2**. As found for **MS-2**, the resulting decay showed two processes, the first with a half-life of 240 s and the second with a half-life of 4500 s, similar to the values obtained for the two-legged system (Figure 12d).

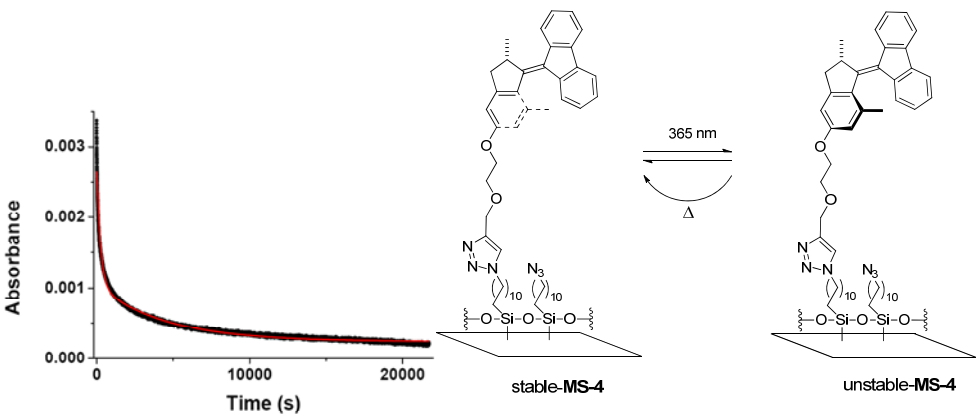

Figure 15 Thermal decay of UV signal of **MS-4** at 439 nm at 25°C at 100% coverage.

The presence of two rates for the thermal isomerization and the increased half-life of **4.12** when attached to a solid surface (**MS-4**) indicate that the kinetic behavior of the rotary cycle is more strongly affected by factors other than one or two-legged attachment. The most plausible explanation is intermolecular interactions between the surface-bound motors. Regardless of the origin of the behavior, it seems clear that confinement of a group of motors at an interface or within a film results in a considerable increase of the half-life of the rotary cycle.

4.8. Interfacial click-reaction on gold surface

The assembly and subsequent modification of azide or alkyne monolayers via click chemistry on gold surface has been described and extensively studied. It has been shown that both α,ω-azide thiols and alkyne thiols readily assemble on gold surface providing a highly covered and densely packed monolayers.[50,51,54,65,76-78]

Given the high density of the terminal functional groups, however, the interfacial click reaction is prone to steric effects. To facilitate the reaction between the surface functional groups and the reactant, diluent alkyl thiols are generally used to ensure that the azide groups are sterically unhindered for reaction. Furthermore, if the azide or alkyne terminated thiol is shorter than the diluent thiol the reaction can be inhibited.[54,65,78]

In accordance with the literature,[54,65,78] when the click reaction was performed between **2.30** and an azide functionalized gold surface the amount of motors attached was under the detection limit of XPS. However, when the reaction of **2.30** was performed using a mixed monolayer (**SAM-4**) (Scheme 11) prepared from a solution of 11-azidoundecane-1-thiol : decane thiol 1 :10 the formation of the triazole linkage could be detected. The quality of the resulting surface (amount of motors attached and the valency of attachement) is probably dependent on the distance between the azide functional groups on the diluted surface, which could be varied by the azide/diluent ratio.[79]

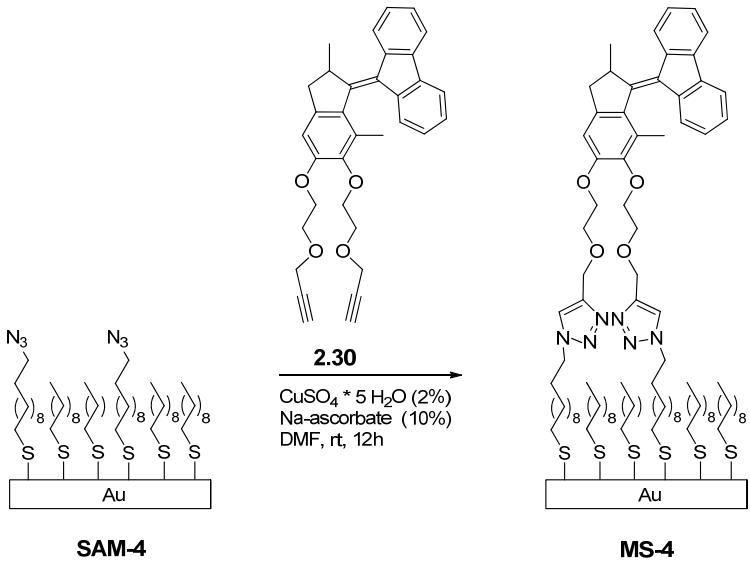

Scheme 11 The interfacial reaction between motor **2.30** and an azide terminated monolayer on gold works only in the presence of diluent alkyl-thiol. In the case of full azide-coverage no attached motor was detected.

4.9 Conclusions

The results presented here show that the Cu-catalyzed 1,3-dipolar cycloaddition reaction provides a versatile approach to attach molecular motors to surfaces. When azide motors are attached to alkyne surfaces, the absence of both XPS and IR signals corresponding to the azide strongly suggests predominantly two-legged attachment. Attachment of motors to surfaces increases the half-life of the thermal isomerization. The higher the surface coverage is the lower the speed of the rotation that is measured. Additionally, motor films attached to quartz surfaces show at least two half-lives for thermal isomerization, pointing to significant intermolecular interactions between motors, affecting rotary speed.

4.10 Experimental section

4.10.1 General remarks

For general remarks for the synthesis and characterization of compounds and intermediates, see Chapter 2.
For general remarks on surface characterization, see Chapter 3.

4.10.2 Experimental procedures for surface modification

11-Azidoundecyltrimethoxysilane monolayer on quartz
Quartz microscope slides (UQG Optics) were cut into pieces so as to fit into the measurement cell of the UV/Vis spectrometer. They were cleaned using a 3/7 ratio of 30% H_2O_2 in H_2SO_4 at >90 °C. (*Caution! This mixture is extremely corrosive and reactive toward organics.*) These samples were then rinsed with doubly destilled water (3 times) and with MeOH and dried under a stream of Ar.

Azide-terminated monolayer was prepared according to two different methods:
Method A (Assembly in toluene without pre-hydrolysis)

Piranha-cleaned quartz slides were immersed in a 1 mM solution of the silane in distilled toluene for 1 d at rt. After the assembly the slides were sonicated twice in fresh toluene and once in MeOH for 2 min each, and dried under a stream of Ar.

Method B (Assembly in cyclohexane after exposure to hydrolysis environment)

1.25 mL of a hydrolysis solution containing 0.04 g 11-azidoundecyltrimethoxy silane **4.3**, 6 ml distilled THF, 31 µl double-distilled H_2O and 4 µl 37% aq. HCl was added to 25 mL cyclohexane to give a slighty hazy solution. The piranha-cleaned quartz slides were immersed into this solution. In general slides were left immersed overnight, however, the surface modification was found to be complete within approximately 4 h. After the assembly the slides were sonicated in DMF, toluene and MeOH for 2 min each and dried under a stream of Ar.

Attaching **2.30** to azide-functionalized surfaces **SAM-2**
Compound **2.30** was grafted to the azide monolayer in DMF at room temperature by immersing the slide into a 2 mM solution of **2.30** containing 1 mol%

$CuSO_4 \cdot 5H_2O$ and 5 mol% sodium-ascorbate relative to the alkyne moieties. Although the reaction time depended on the method of preparation, the azide surface slides were typically immersed for 12 h. The modified quartz substrate or silicon wafer was sonicated in DMF, water and MeOH for 2 min each and then dried under a stream of N_2.
Higher coverages were obtained when the motor was reacted with azide surfaces prepared by *Method B*.

4.10.3 Synthesis of compounds and intermediates

11-azidoundecyltrimethoxysilane (4.3)[60]

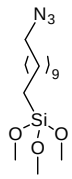

NaN_3 (130 mg, 2.0 mmol) was added to a DMF (3 mL) solution of 11-bromo undecyltrimethoxysilane (0.5 mL, 1.58 mmol). After stirring overnight at rt, the reaction was quenched with water (10 mL) and the aqueous solution was extracted with Et_2O (3x10 mL). The organic phase was washed with water (2x50 mL) and brine and dried (Na_2SO_4). The solvent was evaporated under reduced pressure to give 490.5 mg (1.55 mmol, 98%) of a pale yellow oil. The product was used without further purification. ^{1}H NMR (400 MHz, $CDCl_3$) δ 0.62-0.66 (m, 2H), 1.26 (br s, 14H), 1.36-1.40 (m, 2H), 1.59 (quin, *J*= 7.2 Hz, 2H), 3.25 (t, *J*= 6.8 Hz, 2H), 3.57 (s, 9H); ^{13}C NMR (100 MHz, $CDCl_3$) δ 9.0, 22.5, 26.6, 28.7, 29.0, 29.1, 29.3, 29.4, 33.0, 50.3, 50.4. (3 C could not observed due to overlap) HRMS (ESI) calcd for $C_{14}H_{31}N_3O_3Si$ 340.2027, found 340.2024.

Ditriazole motor (4.4)

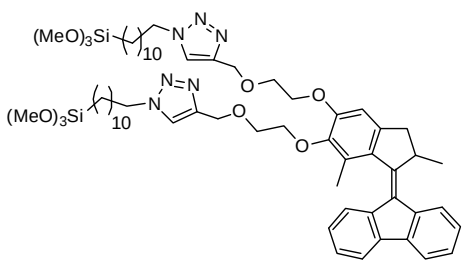

Azide-silane **4.3** (92 mg, 0.3 mmol), $CuSO_4 \cdot 5H_2O$ (2.5 mg, 0.01 mmol) and Na-ascorbate (4 mg, 0.02 mmol), each predissolved in DMF (0.5 mL), were added to a solution of dialkyne motor **2.40** (50 mg, 0.1 mmol) in DMF (5 mL). After stirring the mixture overnight at rt water (25 mL) was added. The aqueous solution was extracted with EtOAc (3x20 mL). The combined organic phase was washed with water (2x50 mL) and brine (30 mL) and dried (Na_2SO_4). The crude mixture was purified by flash chromatography (SiO_2, EtOAc) to give 21 mg of a semi-solid (0.018 mmol, 18%) which was used

immediately for surface modifications. ^{1}H NMR (400 MHz, $CDCl_3$) δ 0.61-0.65 (m, 4H), 1.21-1.43 (m, 35H), 1.80-1.89 (m, 4H), 2.18 (s, 3H), 2.52 (d, *J*= 14.4 Hz,1H), 3.28 (dd, *J*= 4.4, 14.8 Hz, 1H) 3.56 (s, 18H), 3.87-3.90 (m, 2H), 3.97 (t, *J*= 4.4 Hz, 2H), 4.20-4.35 (m, 9H), 4.76 (d, *J*= 6 Hz, 4H), 6.83 (s, 1H), 7.08 (t, *J*= 7.6 Hz, 1H), 7.32-7.35 (m, 4H), 7.51 (s, 1H, *triazole-H*), 7.60 (s, 1H, *triazole-H*), 7.74 (d, *J*= 7.6 Hz, 1H), 7.79-7.81 (m, 1H), 7.84-7.86 (m, 1H). HRMS (TOF) calcd for $C_{62}H_{94}N_6O_{10}Si_2$ 1139.6642, found 1139.6657.

5-methoxy-2,7-dimethyl-2,3-dihydro-1*H*-indene-1-one (4.5)

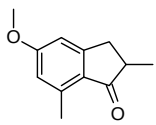

Methacrylic acid (5.2 ml, 60.5 mmol) and 3-methylanisole (5.2 ml, 40.9 mmol) were added to polyphosphoric acid (30 mL), which was stirred and heated at 70°C. After stirring at 70°C for 3 h, the mixture was poured onto ice and stirred overnight. The water layer was extracted with EtOAc (3 x 50 ml). The combined organic layers were washed with aqueous $NaHCO_3$ (30 mL), water (30 mL) and brine (30 mL) and dried (Na_2SO_4). After evaporation of the solvent the crude product was purified by flash chromatography (SiO_2, *n*-heptane : EtOAc = 3 : 1) to give 2.0 g (10.5 mmol, 26 %) of a colorless oil. ^{1}H NMR (300 MHz, $CDCl_3$) δ 1.27 (d, *J* = 7.2 Hz, 3H), 2.60 (s, 3H), 2.60-2.71 (m, 2H), 3.28 ($q_{apparent}$, *J* = 8.4 Hz, 1H), 3.84 (s, 3H), 6.63 (s, 1H), 6.70 (s, 1H); ^{13}C NMR (100 MHz, $CDCl_3$) δ 16.5, 18.2, 34.7, 42.3, 55.3, 107.3, 116.3, 127.3, 140.8, 156.9, 164.5, 208.1. HRMS (EI) calcd for $C_{12}H_{14}O_2$ 190.0994, found 190.0989.

7-methoxy-2,5-dimethyl-2,3-dihydro-1*H*-inden-1-one (4.6)

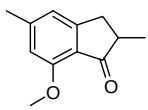

^{1}H NMR (300 MHz, $CDCl_3$) δ 1.27 (d, *J*= 7.3 Hz, 3H), 2.41 (s, 3H), 2.58-2.69 (m, 2H), 3.27 (dd, *J*= 7.6, 16.9 Hz, 1H), 3.93 (s, 3H), 6.58 (s, 1H), 6.80 (s, 1H).

5-hydroxy-2,7-dimethyl-2,3-dihydro-1*H*-indene-1-one (4.7)

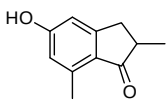

BBr_3 (0.2 ml, 2.1 mmol) was added slowly to a stirred solution of **4.5** (200 mg, 1.0 mmol) in CH_2Cl_2 (3 ml) at 0°C under inert atmosphere (N_2). The mixture was allowed to warm up to rt and stirred overnight at rt. The reaction was quenched by slow addition of water (3 mL). The aqueous layer was extracted with ethyl acetate until the water phase became colorless. The organic layer was washed with water (10 mL) and brine (10 mL), and dried (Na_2SO_4). The solvent was evaporated under reduced pressure to

give the crude product as a brown solid. The solid was suspended in diethyl ether (2×10 mL) followed by filtration to give 105 mg (0.6 mmol, 57 %) of pale brown solid. ^{1}H NMR (400 MHz, Methanol-d_4) δ 1.22 (d, J = 7.6 Hz, 3H), 2.50 (s, 3H), 2.53-2.65 (m, 2H), 3.26 ($q_{apparent}$, J = 8.4 Hz, 1H), 6.55 (s, 1H), 6.63 (s, 1H); ^{13}C NMR (100 MHz, DMSO-d_6) δ 16.3, 17.8, 33.8, 41.6, 109.6, 116.8, 125.2, 139.8, 157.1, 162.9, 206.9. HRMS (EI) calcd for $C_{11}H_{12}O_2$ 176.0837, found 176.0823.

Ethyl 2-(2,7-dimethyl-1-oxo-2,3-dihydro-1*H*-indene-5-yloxy)acetate (4.8)

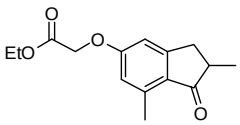

K_2CO_3 (150.0 mg, 1.1 mmol) and ethyl bromoacetate (95 µL, 0.86 mmol) were added to a solution of **4.7** (100.0 mg, 0.57 mmol) in acetonitrile (5 mL) and the mixture was heated at 60°C for 2h. The reaction was quenched by the addition of water (10 mL). The mixture was extracted with ethyl acetate (3 x 10 ml). The combined organic layers were washed with water (20 mL) and brine (20 mL), and dried (Na_2SO_4). After the evaporation of the solvent the crude product was purified by flash chromatography (SiO_2, *n*-heptane : EtOAc = 3 : 1) to afford 110.0 mg (0.42 mmol, 74 %) of white crystals. Mp 78.5-79.0 ºC; ^{1}H NMR (400 MHz, $CDCl_3$) δ 1.26 (d, J = 7.2 Hz, 3H), 1.30 (t, J=7.2 Hz, 3H), 2.59 (s, 3H), 2.62-2.68 (m, 2H), 3.27 ($q_{apparent}$, J = 8.0 Hz, 1H), 4.28 (q, J = 7.2 Hz, 2H), 4.66 (s, 2H), 6.66 (s, 2H); ^{13}C NMR (100 MHz, $CDCl_3$) δ 14.0, 16.4, 18.3, 34.5, 42.3, 61.4, 65.0, 107.9, 116.6, 128.0, 141.0, 156.9, 162.3, 168.1, 208.2. HRMS (EI) calcd for $C_{15}H_{18}O_4$ 262.1205, found 262.1200.

Ethyl 2-(2,7-dimethyl-1-thioxo-2,3-dihydro-1*H*-indene-5-yloxy)acetate (4.9)

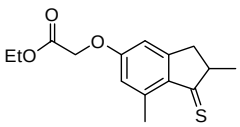

Lawesson`s reagent (465.4 mg, 1.15 mmol) was added to a solution of **4.8** (200 mg, 0.76 mmol) in toluene (10 ml). The mixture was heated at 70ºC for 3 h and filtered through a plug of celite. The solid residue was washed with toluene. The filtrate was concentrated *in vacuo* and purified by flash chromatography (SiO_2, *n*-pentane : diethyl ether = 1 : 1) to give a purple oil which was used immediately in the next step. (*Note*: this compound is not stable towards air or moisture and slowly decomposes to ketone **4.8**.) ^{1}H NMR (400 MHz, $CDCl_3$) δ 1.32 (t, J= 6.8 Hz, 3H), 1.41 (d, J= 7.2 Hz, 3H), 2.75 (s, 3H), 2.79 (d, J= 2.8 Hz, 1H), 2.98-3.06 (m, 1H), 3.37 (dd, J= 17.4, 7.2 Hz, 1H), 4.30 (q, J= 7.2 Hz, 2H), 4.69 (s, 2H), 6.69 (s, 1H), 6.74 (s, 1H).

Ester-motor (4.10)

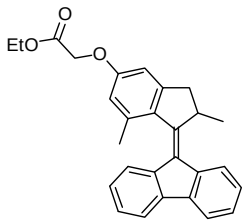

Diazofluorenone (300 mg, 1.56 mmol) was added to a solution of **4.9** in toluene (10 ml). The mixture was heated up to 65ºC for 3 h. The formation of the episulfide was monitored by ^{1}H NMR spectroscopy by following the appearance of the upper-half aromatic protons of the episulfide at 6.42 ppm and 6.55 ppm. PPh_3 (350 mg, 1.35 mmol) was added to the episulfide solution and the mixture was heated for an additional 2 h at 75ºC. The reaction mixture was concentrated *in vacuo.* Et_2O (20 ml) was added to the mixture to precipitate PPh_3S as yellow crystals. The precipitate was filtered and the procedure was repeated once more. The resulting Et_2O solution was concentrated to ~20 mL and CH_3I (0.5 ml, 8.0 mmol) was added. The mixture was stirred for 2 h at rt and the precipitate was removed by filtration. After evaporation of the solvent the crude product was purified by flash chromatography (SiO_2, *n*-heptane : ethyl acetate = 5 : 1) to give alkene **4.10** as a yellow solid (150 mg, 0.37 mmol, 49% over two steps). ^{1}H NMR (400 MHz, $CDCl_3$) δ 1.32-1.36 (m, 6H), 2.26 (s, 3H), 2.57 (d, *J* = 14.8 Hz, 1H), 3.33 (dd, *J* = 6.4, 14.8 Hz, 1H), 4.14 (quin, *J* = 5.6 Hz, 1H), 4.33 (q, *J*= 7.2 Hz, 2H), 4.69 (s, 2H), 6.71 (s, 1H), 6.81 (s, 1H), 7.14 (t, *J* = 7.6 Hz, 1H), 7.31 (t, *J* = 7.2 Hz, 1H), 7.34-7.39 (m, 3H), 7.76 (d, *J* = 7.6 Hz, 1H), 7.80-7.82 (m, 1H), 7.86-7.89 (m, 1H); ^{13}C NMR (100 MHz, $CDCl_3$) δ 14.1, 18.8, 21.6, 41.5, 44.7, 61.3, 65.4, 109.2, 114.8, 119.1, 119.6, 123.3, 123.6, 126.4, 126.5, 126.7, 126.8, 129.0, 134.0, 137.8, 138.8, 139.2, 139.5, 139.6, 149.4, 151.3, 158.9, 168.8 HRMS (EI) calcd for $C_{28}H_{26}O_3$ 410.1882, found 410.1877.

Alcohol-motor (4.11)

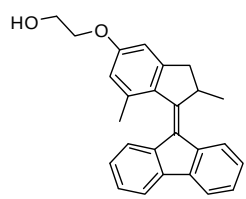

A solution of **4.10** (115 mg, 0.28 mmol) in THF (5 mL) was added to a suspension of $LiBH_4$ (20 mg, 0.52 mmol) in THF (5 mL) and the mixture was stirred at 40°C for 7 h. The reaction was quenched with aqueous HCl solution (5 mL, 0.1 M) and the mixture was extracted with EtOAc until the aqueous phase was colorless. The combined organic layers were washed with water (10 mL) and brine (10 mL) and dried (Na_2SO_4). The solvent was evaporated under reduced pressure and the crude product was purified by flash chromatography (SiO_2, *n*-heptane : ethyl acetate = 1 : 1) to give 85 mg (0.23 mmol, 82 %) yellow solid.

^{1}H NMR (400 MHz, $CDCl_3$) δ 1.32 (d, *J* = 6.8 Hz, 3H), 2.04 (t, *J* = 6 Hz, 1H O*H*), 2.25 (s, 3H), 2.58 (d, *J* = 14.4 Hz, 1H), 3.32 (dd, *J* = 6.0, 13.2 Hz, 1H), 4.01 (q, *J* = 5.2 Hz, 2H), 4.13 (quin, *J* = 6.8 Hz, 1H), 4.18 (q, *J* = 4.8 Hz, 2H), 6.72 (s, 1H), 6.83 (s, 1H), 7.15 (t, *J* = 6.4 Hz, 1H), 7.29 (t, *J* = 7.2 Hz, 1H), 7.34-7.39 (m, 3H), 7.76 (d, *J* = 7.6 Hz, 1H), 7.80-7.84 (m, 1H), 7.85-7.90 (m, 1H); ^{13}C NMR (100 MHz, $CDCl_3$) δ 18.9, 21.6, 41.5, 44.6, 61.4, 69.2, 109.1, 114.6, 119.1, 119.6, 123.3, 123.6, 126.4, 126.5, 126.7, 128.8, 133.4, 137.9, 138.8, 139.2, 139.6, 149.4, 151.6, 159.8. (2 C not observed due to overlap) HRMS (EI) calcd for $C_{26}H_{24}O_2$ 368.1776, found 368.1751.

Alkyne-motor (4.12)

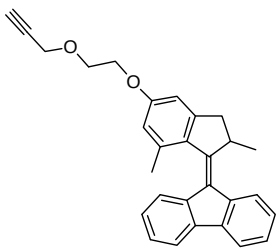

A suspension of NaH (70 mg, 1.5 mmol, 50% in oil) in THF (3 mL) was cooled to 0ºC and a solution of **4.11** (85 mg, 0.23 mmol) in THF (7 mL) was added dropwise (under N_2 atmosphere). Propargyl bromide (0.1 mL, 0.90 mmol, 80 % in toluene) was added to this mixture. The solution was stirred at room temperature for 5 h. The reaction was quenched with water (10 mL) and the mixture was extracted with EtOAc until the yellow color of the aqueous phase had disappeared. The organic phase was washed with water (10 mL) and brine (10 mL) and dried (Na_2SO_4). The solvent was evaporated under reduced pressure and the crude product was purified by flash chromatography (SiO_2, *n*-heptane : ethyl acetate = 7 : 1) to give yellow crystals (80 mg, 0.20 mmol, 86 %). ^{1}H NMR (400 MHz, $CDCl_3$) δ 1.32 (d, *J* = 6.4 Hz, 3H), 2.24 (s, 3H), 2.49 (t, *J* = 2.4 Hz, 1H), 2.57 (d, *J* = 14.8 Hz, 1H), 3.32 (dd, *J* = 6.0, 14.6 Hz, 1H), 3.96 (t, *J* = 5.2 Hz, 2H), 4.13 (quin, *J* = 6.4 Hz, 1H), 4.20-4.28 (m, 2H), 4.32 (dd, *J* = 1.2, 2.4 Hz, 2H), 6.72 (s, 1H), 6.83 (s, 1H) 7.14 (t, *J* = 8.0 Hz, 1H), 7.29 (t, *J* = 7.6 Hz, 1H), 7.33-7.39 (m, 3H), 7.76 (d, *J* = 7.6 Hz, 1H), 7.80-7.84 (m, 1H), 7.85-7.89 (m, 1H); ^{13}C NMR (100 MHz, $CDCl_3$) δ 19.9, 21.6, 41.5, 44.6, 58.5, 67.2, 68.1, 74.8, 109.1, 114.7, 119.1, 119.6, 123.3, 123.6, 126.4, 126.5, 126.70, 126.73 128.7, 133.3, 137.9, 138.8, 139.1, 139.5, 149.3, 151.8, 159.9. (2 C not observed due to overlap) HRMS (EI) calcd for $C_{29}H_{26}O_2$ 406.1933, found 406.1925.

Irradiation experiment to generate unstable isomer of motor 4.12

Molecular motor **4.12** (~2 mg) was dissolved in CD_2Cl_2 (~1 ml). The sample was placed in an NMR tube and irradiated with 365 nm light at -60º C at a distance of

2-3 cm from the centre of the lamp. ^{1}H-NMR spectra of the sample were taken before, during and after irradiation at -60º C. No further changes were observed after 6 h of irradiation, indicating that the PSS was reached. The relative integration of the absorptions from the two isomers revealed a photostationary state of unstable-**4.12** to stable-**4.12** of 2 : 1. After warming the sample to room temperature, only the stable form was observed by ^{1}H-NMR spectroscopy.

Stable-**4.12**: ^{1}H NMR (500 MHz, -60ºC, CD_2Cl_2) δ 1.29 (d, *J*= 6.5 Hz, 3H), 2.20 (s, 3H), 2.61 (d, *J* = 15 Hz, 1H), 2.64 (t, *J* = 2.0 Hz, 1H), 3.30 (dd, *J* = 5.5, 14.8 Hz, 1H), 3.92 (br, t, 2H), 4.12 (quin, *J* = 6.0 Hz, 1H), 4.18-4.21 (m, 2H), 4.31 (br, d, 2H, *J* = 1.6 Hz), 6.72 (s, 1H), 6.84 (s, 1H) 7.18 (t, *J* = 7.5 Hz, 1H), 7.31-7.36 (m, 2H), 7.37-7.41 (m, 2H), 7.81 (d, *J* = 7.5Hz, 1H), 7.84-7.86 (m, 1H), 7.89-7.90 (m, 1H)

Unstable-**4.12**: ^{1}H NMR (500 MHz, -60ºC, CD_2Cl_2) δ 1.50 (d, , *J* = 6.0 Hz, 3H), 2.04 (s, 3H), 3.00 (dd, *J* = 6, 16.3 Hz, 1H), 3.40-3.45 (m, 1H) 3.92-4.31 (absorptions in this region could not be resolved due to overlap with remaining stable-**4.12**), 6.67 (s, 1H), 6.79 (s, 1H) 7.18-7.90 (absorptions in this region could not be resolved due to overlap with remaining stable-**4.12**).

4.11 References

(1) Balzani, V.; Credi, A.; Raymo, F. M.; Stoddart, J. F. *Angew. Chem. Int. Ed.* **2000**, *39*, 3349-3391.
(2) Feringa, B. L., (Ed.); *Molecular Switches;* Wiley VCH: Weinheim: 2001.
(3) Feringa, B. L. *J. Org. Chem.* **2007**, *72*, 6635-6652.
(4) Badjic, J. D.; Balzani, V.; Credi, A.; Silvi, S.; Stoddart, J. F. *Science* **2004**, *303*, 1845-1849.
(5) Mammana, A.; D'Urso, A.; Lauceri, R.; Purrello, R. *J. Am. Chem. Soc.* **2007**, *129*, 8062-8063.
(6) Jiang, S. G.; Liu, M. H. *Chem. Mater.* **2004**, *16*, 3985-3987.
(7) Brouwer, A. M.; Frochot, C.; Gatti, F. G.; Leigh, D. A.; Mottier, L.; Paolucci, F.; Roffia, S.; Wurpel, G. W. H. *Science* **2001**, *291*, 2124-2128.
(8) Kay, E. R.; Leigh, D. A.; Zerbetto, F. *Angew. Chem. Int. Ed.* **2007**, *46*, 72-191.
(9) Browne, W. R.; Feringa, B. L. *Nat. Nano.* **2006**, *1*, 25-35.

(10) Koumura, N.; Zijlstra, R. W. J.; van Delden, R. A.; Harada, N.; Feringa, B. L. *Nature* **1999**, *401*, 152-155.
(11) Fletcher, S. P.; Dumur, F.; Pollard, M. M.; Feringa, B. L. *Science* **2005**, *310*, 80-82.
(12) Leigh, D. A.; Wong, J. K. Y.; Dehez, F.; Zerbetto, F. *Nature* **2003**, *424*, 174-179.
(13) Boyer, P. D. *Annu. Rev. Biochem.* **1997**, *66*, 717-749.
(14) Noji, H.; Yasuda, R.; Yoshida, M.; Kinosita, K. *Nature* **1997**, *386*, 299-302.
(15) Abrahams, J. P.; Leslie, A. G. W.; Lutter, R.; Walker, J. E. *Nature* **1994**, *370*, 621-628.
(16) Stock, D.; Leslie, A. G. W.; Walker, J. E. *Science* **1999**, *286*, 1700-1705.
(17) Macnab, R. M. *Annu. Rev. Microbiol.* **2003**, *57*, 77-100.
(18) Morin, J. F.; Shirai, Y.; Tour, J. M. *Org. Lett.* **2006**, *8*, 1713-1716.
(19) Gould, S. L.; Tranchemontagne, D.; Yaghi, O. M.; Garcia-Garibay, M. A. *J. Am. Chem. Soc.* **2008**, *130*, 3246-3247.
(20) Winston, E. B.; Lowell, P. J.; Vacek, J.; Chocholousova, J.; Michl, J.; Price, J. C. *Phys. Chem. Chem. Phys.* **2008**, *10*, 5188-5191.
(21) Haidekker, M. A.; Theodorakis, E. A. *Org. Biomol. Chem.* **2007**, *5*, 1669-1678.
(22) de Jonge, J. J.; Ratner, M. A.; de Leeuw, S. W.; Simonis, R. O. *J. Phys. Chem. B* **2004**, *108*, 2666-2675.
(23) Rozenbaum, V. M. *Phys. Rev. B* **1996**, *53*, 6240-6255.
(24) Horansky, R. D.; Clarke, L. I.; Winston, E. B.; Price, J. C. *Phys. Rev. B* **2006**, *74*.
(25) Horansky, R. D.; Clarke, L. I.; Price, J. C.; Khuong, T. A. V.; Jarowski, P. D.; Garcia-Garibay, M. A. *Phys. Rev. B* **2005**, *72*, 014302.
(26) Clarke, L. I.; Horinek, D.; Kottas, G. S.; Varaksa, N.; Magnera, T. F.; Hinderer, T. P.; Horansky, R. D.; Michl, J.; Price, J. C. *Nanotechnology* **2002**, *13*, 533-540.
(27) Zheng, X. L.; Mulcahy, M. E.; Horinek, D.; Galeotti, F.; Magnera, T. F.; Michl, J. *J. Am. Chem. Soc.* **2004**, *126*, 4540-4542.
(28) Baber, A. E.; Tierney, H. L.; Sykes, E. C. H. *Acs Nano* **2008**, *2*, 2385-2391.
(29) Maksymovych, P.; Sorescu, D. C.; Dougherty, D.; Yates, J. T. *J. Phys. Chem. B* **2005**, *109*, 22463-22468.
(30) Gao, L.; Liu, Q.; Zhang, Y. Y.; Jiang, N.; Zhang, H. G.; Cheng, Z. H.; Qiu, W. F.; Du, S. X.; Liu, Y. Q.; Hofer, W. A.; Gao, H. J. *Phys. Rev. Lett.* **2008**, *101*.

(31) London, G.; Carroll, G. T.; Landaluce, T. F.; Pollard, M. M.; Rudolf, P.; Feringa, B. L. *Chem. Commun.* **2009**, 1712-1714.
(32) Michl, J.; Sykes, E. C. H. *Acs Nano* **2009**, *3*, 1042-1048.
(33) Bellisario, D. O.; Baber, A. E.; Tierney, H. L.; Sykes, E. C. H. *J. Phys. Chem. C* **2009**, *113*, 5895-5898.
(34) Aswal, D. K.; Lenfant, S.; Guerin, D.; Yakhmi, J. V.; Vuillaume, D. *Anal. Chim. Acta* **2006**, *568*, 84-108.
(35) Cerofolini, G. F.; Romano, E. *Appl. Phys. A* **2008**, *91*, 181-210.
(36) Ulman, A. *Chem. Rev.* **1996**, *96*, 1533-1554.
(37) Love, J. C.; Estroff, L. A.; Kriebel, J. K.; Nuzzo, R. G.; Whitesides, G. M. *Chem. Rev.* **2005**, *105*, 1103-1169.
(38) Katsonis, N.; Lubomska, M.; Pollard, M. M.; Feringa, B. L.; Rudolf, P. *Prog. Surf. Sci.* **2007**, *82*, 407-434.
(39) Balzani, V.; Credi, A.; Venturi, M. *Chem. Phys. Chem* **2008**, *9*, 202-220.
(40) Chechik, V.; Crooks, R. M.; Stirling, C. J. M. *Adv. Mater.* **2000**, *12*, 1161-1171.
(41) Haensch, C.; Hoeppener, S.; Schubert, U. S. *Chem. Soc. Rev.* **2010**, *39*, 2323-2334.
(42) Li, J.; Thiara, P. S.; Mrksich, M. *Langmuir* **2007**, *23*, 11826-11835.
(43) Lummerstorfer, T.; Hoffmann, H. *J. Phys. Chem. B* **2004**, *108*, 3963-3966.
(44) Kolb, H. C.; Finn, M. G.; Sharpless, K. B. *Angew. Chem. Int. Ed.* **2001**, *40*, 2004-2021.
(45) Wu, P.; Fokin, V. V. *Aldrichimica Acta* **2007**, *40*, 7-17.
(46) Kolb, H. C.; Sharpless, K. B. *Drug Discov. Today* **2003**, *8*, 1128-1137.
(47) Binder, W. H.; Kluger, C. *Curr. Org. Chem.* **2006**, *10*, 1791-1815.
(48) Binder, W. H.; Sachsenhofer, R. *Macromol. Rapid Commun.* **2007**, *28*, 15-54.
(49) Nandivada, H.; Jiang, X. W.; Lahann, J. *Adv. Mater.* **2007**, *19*, 2197-2208.
(50) Collman, J. P.; Devaraj, N. K.; Chidsey, C. E. D. *Langmuir* **2004**, *20*, 1051-1053.
(51) Lee, J. K.; Chi, Y. S.; Choi, I. S. *Langmuir* **2004**, *20*, 3844-3847.
(52) White, M. A.; Johnson, J. A.; Koberstein, J. T.; Turro, N. J. *J. Am. Chem. Soc.* **2006**, *128*, 11356-11357.
(53) Prakash, S.; Long, T. M.; Selby, J. C.; Moore, J. S.; Shannon, M. A. *Anal. Chem.* **2007**, *79*, 1661-1667.
(54) Chelmowski, R.; Kafer, D.; Koster, S. D.; Klasen, T.; Winkler, T.; Terfort, A.; Metzler-Nolte, N.; Woll, C. *Langmuir* **2009**, *25*, 11480-11485.

(55) Pollard, M. M.; Lubomska, M.; Rudolf, P.; Feringa, B. L. *Angew. Chem. Int. Ed.* **2007**, *46*, 1278-1280.
(56) Kanan, S. A.; Tze, W. T. Y.; Tripp, C. P. *Langmuir* **2002**, *18*, 6623-6627.
(57) Smith, E. A.; Chen, W. *Langmuir* **2008**, *24*, 12405-9.
(58) Angst, D. L.; Simmons, G. W. *Langmuir* **1991**, *7*, 2236-2242.
(59) Silberzan, P.; Leger, L.; Ausserre, D.; Benattar, J. J. *Langmuir* **1991**, *7*, 1647-1651.
(60) Alvarez, S. G.; Alvarez, M. T. *Synthesis-Stuttgart* **1997**, 413-414.
(61) Kessel, C. R.; Granick, S. *Langmuir* **1991**, *7*, 532-538.
(62) Fryxell, G. E.; Rieke, P. C.; Wood, L. L.; Engelhard, M. H.; Williford, R. E.; Graff, G. L.; Campbell, A. A.; Wiacek, R. J.; Lee, L.; Halverson, A. *Langmuir* **1996**, *12*, 5064-5075.
(63) Heise, A.; Stamm, M.; Rauscher, M.; Duschner, H.; Menzel, H. *Thin Solid Films* **1998**, *327*, 199-203.
(64) Wollman, E. W.; Kang, D.; Frisbie, C. D.; Lorkovic, I. M.; Wrighton, M. S. *J. Am. Chem. Soc.* **1994**, *116*, 4395-4404.
(65) Collman, J. P.; Devaraj, N. K.; Eberspacher, T. P. A.; Chidsey, C. E. D. *Langmuir* **2006**, *22*, 2457-2464.
(66) Devadoss, A.; Chidsey, C. E. D. *J. Am. Chem. Soc.* **2007**, *129*, 5370-5371.
(67) Durfor, C. N.; Turner, D. C.; Georger, J. H.; Peek, B. M.; Stenger, D. A. *Langmuir* **1994**, *10*, 148-152.
(68) Moon, J. H.; Kim, J. H.; Kim, K.; Kang, T. H.; Kim, B.; Kim, C. H.; Hahn, J. H.; Park, J. W. *Langmuir* **1997**, *13*, 4305-4310.
(69) Coleman, A. C.; Areephong, J.; Vicario, J.; Meetsma, A.; Browne, W. R.; Feringa, B. L. *Angew. Chem. Int. Ed.* **2010**, *49*, 6580-6584.
(70) Wu, S. *Polymer Interface and Adhesion;* Marcel Dekker: New York: **1982**.
(71) Peanasky, J.; Schneider, H. M.; Granick, S.; Kessel, C. R. *Langmuir* **1995**, *11*, 953-962.
(72) Pollard, M. M.; Klok, M.; Pijper, D.; Feringa, B. L. *Adv. Funct. Mat.* **2007**, *17*, 718-729.
(73) Harris, A. L.; Rothberg, L.; Dubois, L. H.; Levinos, N. J.; Dhar, L. *Phys. Rev. Lett.* **1990**, *64*, 2086-2089.
(74) Barrett, C.; Natansohn, A.; Rochon, P. *Macromol.* **1994**, *27*, 4781-4786.
(75) Wasserman, S. R.; Whitesides, G. M.; Tidswell, I. M.; Ocko, B. M.; Pershan, P. S.; Axe, J. D. *J. Am. Chem. Soc.* **1989**, *111*, 5852-5861.
(76) Hudalla, G. A.; Murphy, W. L. *Langmuir* **2009**, *25*, 5737-5746.

(77) Wang, L.; Tian, Y.; Ran, Q.; Hu, Z.; Xu, J.; Xian, Y.; Peng, R.; Jin, L. *Electrochem. Commun.* **2009**, *11*, 339-342.
(78) Devaraj, N. K.; Decreau, R. A.; Ebina, W.; Collman, J. P.; Chidsey, C. E. D. *J. Phys. Chem. B* **2006**, *110*, 15955-15962.
(79) Tatiana Fernández Landaluce, forthcoming PhD Theis, University of Groningen

Chapter 5
Functionalized altitudinal molecular motors on surfaces

In this chapter the synthesis of molecular motors containing functional groups in their rotor part is presented. In an attempt to control the wetting properties of solid surfaces a hydrophobic perfluorobutyl chain and a relatively hydrophilic cyano-group were introduced to the rotor part of the motor. To test the effect of the functional groups on the rotary motion, photochemical and thermal isomerization studies were performed in solution. Preliminary results on the influence of the functional groups on surface wettability are described.

5.1 Introduction

Control of the assembly and arrangement of molecules on surfaces potentially allows for interfaces with tailored properties to be created. Modifications of surfaces with self-assembled monolayers[1] (SAMs) give opportunities to create interfaces exhibiting various properties including hydrophilicity/hydrophobicity,[2-5] conductance,[6,7] catalytic activity,[8,9] chirality,[10-12] etc. Amongst the SAM-forming molecules, especially interesting are those that are able to switch reversibly between distinct geometrical forms accompanied with changes in physical properties such as dipole moment or conductance.[13-15] Such reversible changes in chemical and physical character would facilitate the fabrication of multi-functional interfaces that could allow for reversible switching from one desired property to another.

Azobenzenes and spiropyrans have been widely used to reversibly modulate surface free energy by light[13-15] (Scheme 1). Azobenzenes can undergo *cis* → *trans* photoisomerization, which induces a change in dipole moment, which in turn determines the hydrophilic and hydrophobic nature of the isomers[16] (Scheme 1a). Spiropyrans can be switched photochemically between a relatively hydrophobic spirocyclic isomer and a hydrophilic zwitterionic merocyanine isomer[17] (Scheme 1b).

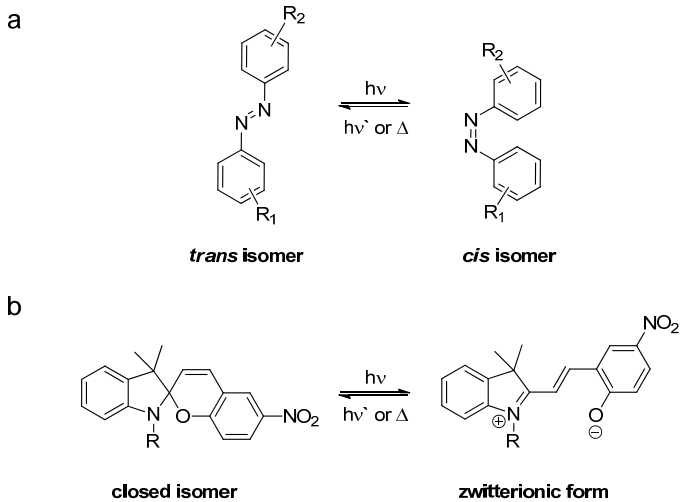

Scheme 1 Reversible photoisomerization of (a) azobenzenes and (b) spiropyrans. The photochemical isomerizations result in large geometrical/structural and polarity changes.

Given the inherent changes in polarity that accompany structural changes, azobenzenes and spiropyrans can affect surface free energy in monolayer assemblies[18,19] without an additional functional group being required to ensure sufficient polarity change. Nevertheless, additional functional groups[19-21] and surface-pretreatment[22,23] can enhance the effect of isomerization.

Molecular rotary motors based on overcrowded alkenes[24] are a unique class of compounds that can undergo repetitive unidirectional rotary motion upon irradiation with UV-light. In a surface bound ensemble of rotary motors two types of rotary motion can be distinguished in terms of orientation: azimuthal[25,26] (Figure 1a) and altitudinal[27,28] (Figure 1b). In comparison to azimuthal rotation, application of altitudinal rotary motion related to the modulation of surface properties is more readily apparent.

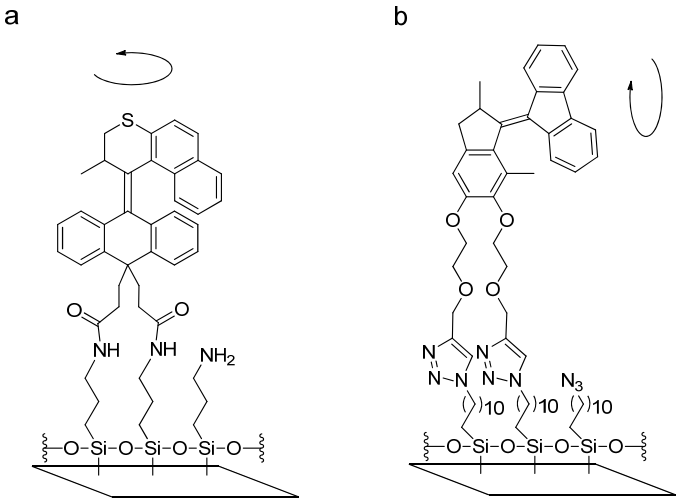

Figure 1 Azimuthal (a) and altitudinal (b) rotary motors. In order to exploit the rotary motion, the introduction of functional groups is required.

However, compared to azobenzenes and spiropyrans, altitudinal motors containing symmetric rotor units do not provide a sufficient change in polarity upon rotation that could affect macroscopic surface properties. To develop rotary motor based interfaces that undergo cyclical changes in polarity, functional groups have to be introduced to the rotor half.

In the previous chapters the focus was on establishing a robust and reproducible surface modification strategy. Among the procedures tested,

interfacial 1,3-dipolar cycloaddition was found to be the most reliable method that allows for the attachment of molecular motors to solid substrates without the need for activation to increase reactivity and the use of less stable intermediates or extreme care with reaction conditions (including temperature, air humidity, concentration, etc.).[27,28]

In this chapter the synthesis of molecular motors containing functional groups in the rotor part is presented. To test the effect of the functional groups on the rotary motion, photochemical and thermal isomerization studies were performed in solution. Preliminary results on the influence of the functional groups on surface wettability are shown.

5.2 Synthesis of functionalized molecular motors

5.2.1 Molecular motor with perfluoroalkyl-chain

To attach different functional groups to the rotor part of the motor, a brominated derivative of 9-fluorenone was prepared *via* oxidation of 2-bromofluorene (**5.1**) to 2-bromo-9-fluorenone (**5.2**)[29] (Scheme 2).

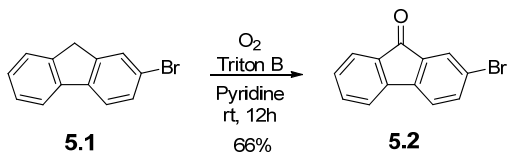

Scheme 2 Synthesis of 2-bromo-9-fluorenone (**5.2**) *via* the oxidation of 2-bromofluorene.

A possible way to introduce hydrophobicity into the motor is to functionalize the rotor part with a perfluoroalkyl chain. Copper-mediated cross-coupling reactions between aryl halides and perfluoroalkyl iodides have been used successfully to synthesize perfluoroalkylated aryl compounds.[30,31] Using this approach, perfluoroalkylation of 2-bromo-9-fluorenone (**5.2**) with perfluorobutyl iodide *via* a perfluorobutyl-copper intermediate gave product **5.3** in 72% yield (Scheme 3).

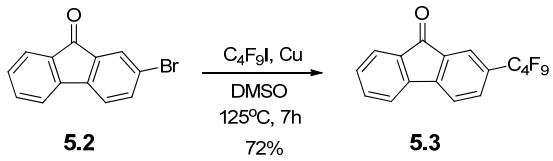

Scheme 3 Copper mediated fluoroalkylation of **5.2** for the introduction of a hydrophobic chain.

Ketone **5.3** was subsequently transformed into the corresponding hydrazone with hydrazine monohydrate, and was obtained as a mixture of *cis* and *trans* isomers (Scheme 4). Preparation of hydrazone **5.4** requires lower temperatures compared to the hydrazone derived from symmetric 9-fluorenone or 2-bromo-9-fluorenone. At reflux in MeOH, the hydrazone is expected to undergo Wolff-Kishner reduction yielding the corresponding fluorene.
Hydrazone **5.4** was converted to the diazo-derivative by oxidation with manganese oxide (MnO_2) in THF providing 2-perfluorobutyl-9-diazofluorene (**5.5**), which was used immediately in the following diazo-thioketone coupling step (Scheme 5).

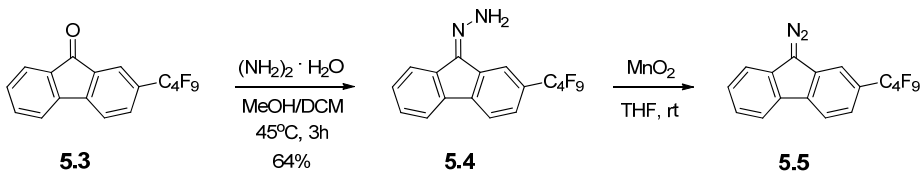

Scheme 4 Synthesis of the rotor-part diazofluorene **5.5**, which was used immediately in the next reaction step.

The Barton-Kellogg coupling reaction[32,33] between the upper half thioketone **2.23** and the lower half diazo compound **5.5** was performed in toluene at 75 °C for 3 h (Scheme 5). The formation of the corresponding episulfide **5.6** was followed by ^{1}H NMR spectroscopy as a shift of the upper-half aromatic proton from 6.66 ppm in the thioketone **2.23** to 6.34 and 6.39 ppm in the *cis*/*trans* isomers of the episulfide **5.6** in $CDCl_3$. Addition of 2 eq PPh_3 to the reaction mixture followed by an additional 2 h stirring at 75 °C yielded the overcrowded alkene in 70% yield after purification by column chromatography as a mixture of *cis*/*trans* isomers (1.4 : 1).

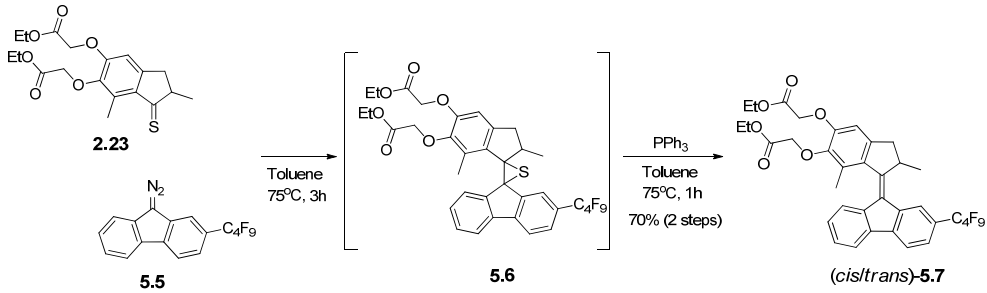

Scheme 5 Synthesis of fluoroalkylated motor **5.7** *via* a diazo-thioketone coupling.

The reduction of the ester groups in **5.7** was carried out with $LiBH_4$ in THF at 50 °C yielding the corresponding diol derivative **5.8** as a mixture of *cis* and *trans* isomers (Scheme 6). Separation of the two isomers was possible at this stage by column chromatography over silica gel (Et_2O).

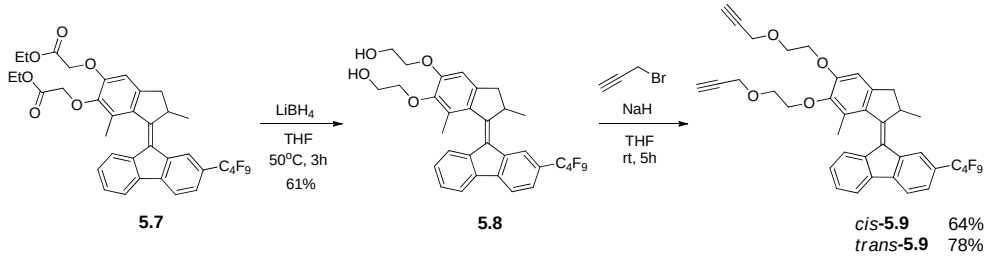

Scheme 6 Introduction of terminal alkyne groups in order to attach the motor to azide functionalized surfaces *via* interfacial 1,3-dipolar cycloaddition reaction. The *cis* and *trans* isomers of **5.8** could be separated and alkylated further to obtain *cis*-**5.9** and *trans*-**5.9**.

The *cis* and *trans* isomers of diol **5.8** were assigned by comparison of their ^1H NMR spectra ($CDCl_3$) (Figure 2) with that of previously reported structurally similar molecular motors. It was found in all the cases of previously reported motors bearing desymmetrized fluorene lower halves,[34-37] that the singlet or doublet absorption of H_a in the *cis* isomer appears at higher field compared to H_a in the *trans* isomer. This difference is attributed to the shielding effect of the aromatic upper-half in the *cis* isomer.

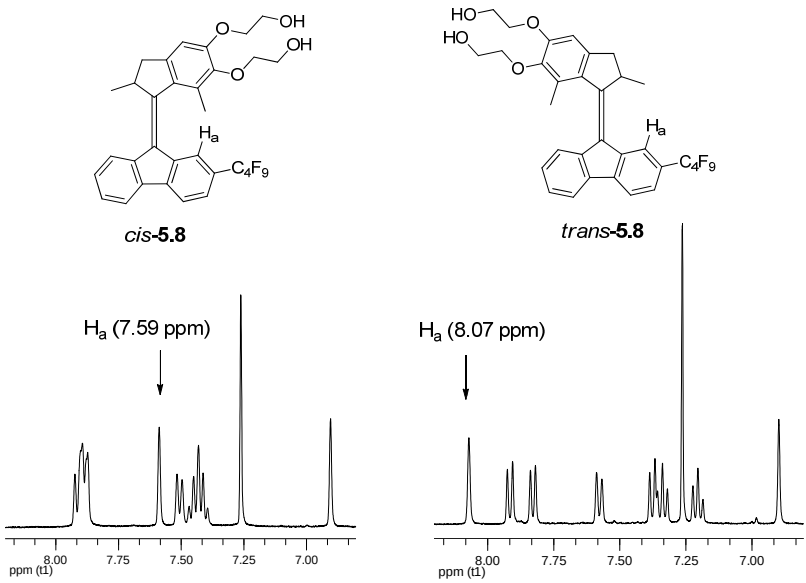

Figure 2 Partial ^{1}H NMR spectra of *cis*-**5.8** and *trans*-**5.8** in $CDCl_3$. *Cis* and *trans*-**5.8** were assigned based on the singlet absorption of H_a of the aromatic lower half. In previously reported motors containing substituted fluorene lower halves the absorption of H_a appears at higher field in the *cis*-form compared to the *trans* isomer.

Next, the two isomers of **5.8** were alkylated with propargyl bromide in the presence of NaH in THF to obtain the *cis* and *trans* isomers of motor **5.9** in 64% and 78% yields, respectively (Scheme 6).

A different approach to introduce the perfluorobutyl chain to the rotor part would be the coupling between perfluorobutyl iodide and the bromo-functionalized motor **5.13** (Scheme 9). To this end 2-bromo-9-fluorenone (**5.2**) was converted to the corresponding hydrazone (**5.10**) by heating at reflux in MeOH in the presence of hydrazine-monohydrate (Scheme 7) followed by oxidation to the diazo derivative **5.11** with MnO_2 in THF. The product was used in the subsequent diazo-thioketone coupling step without further purification.

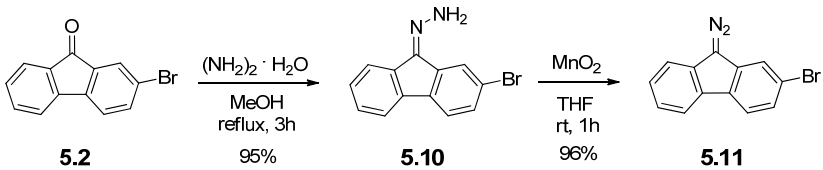

Scheme 7 Synthesis of 2-bromo-9-diazofluorene (**5.11**).

The Barton-Kellogg coupling (Scheme 8) was performed similarly as in the previous case. The upper half thioketone **2.23** and the lower half diazo-compound **5.11** were heated at 75 °C in toluene for 4 h. After most of the thioketone was converted to the episulfide **5.12** (the absorption of the upper half aromatic protons appear at 6.35 ppm and 6.37 ppm in $CDCl_3$), 2 eq PPh_3 was added to the mixture, and stirred at 75°C for an additional 2 h to yield motor **5.13**. One of the isomers (*cis*-**5.13**) of the motor could be precipitated from Et_2O at this stage, however, the mixture of the isomers was used in the next step.

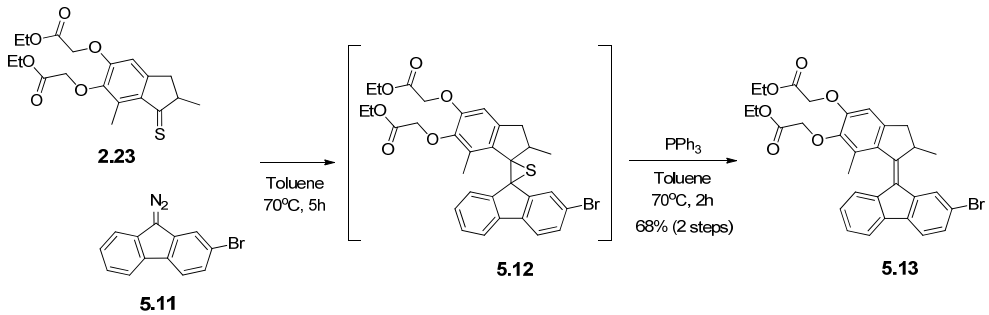

Scheme 8 Synthesis of motor **5.13** containing a brominated lower half for the introduction of a fluoroalkyl chain. Episulfide **5.12** and motor **5.13** were formed as a mixture of *cis*/*trans* isomers.

The resulting (*cis*/*trans*)-bromo-motor **5.13** was subjected to perfluoroalkylation under the same conditions as 2-bromo-9-fluorenone (**5.2**) and the desired product **5.7** could be obtained without observing any degradation of the motor (Scheme 9).

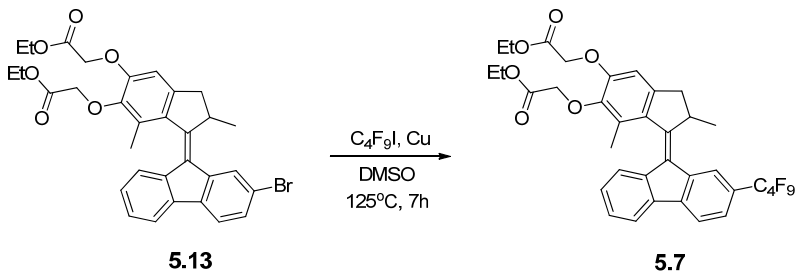

Scheme 9 Copper-mediated fluoroalkylation of bromo-motor **5.13**.

A drawback of this functionalization method is, however, that it is not possible to completely separate the unreacted starting material **5.13** from the perfluoroalkylated product **5.7** in any stage of the synthesis towards dialkyne motor **5.9**. A possible way to overcome this difficulty is to use a longer perfluoroalkyl chain for alkylation, which might increase the difference in polarity leading to better separation.

5.2.2 Molecular motor with cyano-group

Cyano-substituted motor **5.14** was prepared *via* palladium-catalyzed cyanation of bromo-motor **5.13** using the protocol of Confalone (Scheme 10).[38] This methodology has already been applied successfully for the introduction of the cyano functional group to molecular motors.[39] As expected, the reaction gave the product **5.14** in high yield without affecting the other functional groups present in the molecule.

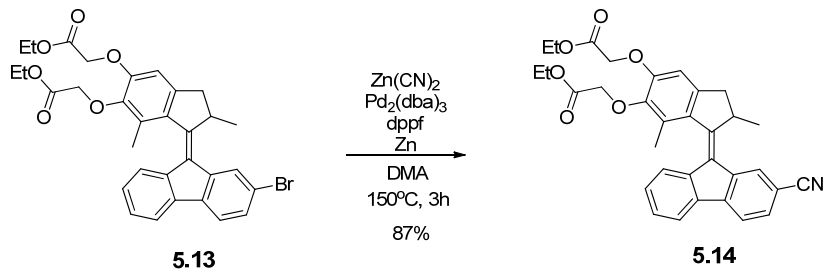

Scheme 10 Synthesis of cyano-functionalized motor **5.14** *via* palladium-catalyzed cyanation of bromo-motor **5.13**.

Reduction of the ester groups in **5.14** with $LiBH_4$ yielded the corresponding diol derivative **5.15**. When more than 1.1 eq of reducing agent was used in this reaction step an unidentified by-product was formed, which was not the result of the reduction of the cyano-group. This impurity resulted to be inseparable from the desired product **5.15** by column chromatography and recrystallyzation.
Finally, the terminal alkynes, necessary for reaction with azide functionalized surfaces, were introduced in the system by deprotonation of the primary alcohols in **5.15** with NaH and subsequent alkylation with propargyl bromide in THF.

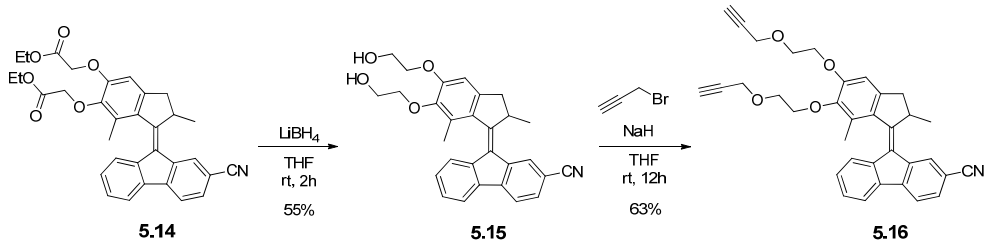

5.14 5.15 5.16

Scheme 11 Synthesis of **5.16** containing terminal alkyne groups. *Cis* and *trans*-**5.16** could be separated by column chromatography.

Cis and *trans* isomers of alkene **5.16** could be separated by column chromatography over silica using a toluene/Et_2O (20/1) eluent mixture. The structures of the isomers were assigned by comparison of their ^1H NMR spectra ($CDCl_3$) with that of previously reported structurally similar molecular motors[34-37] as described in section 5.2.1.

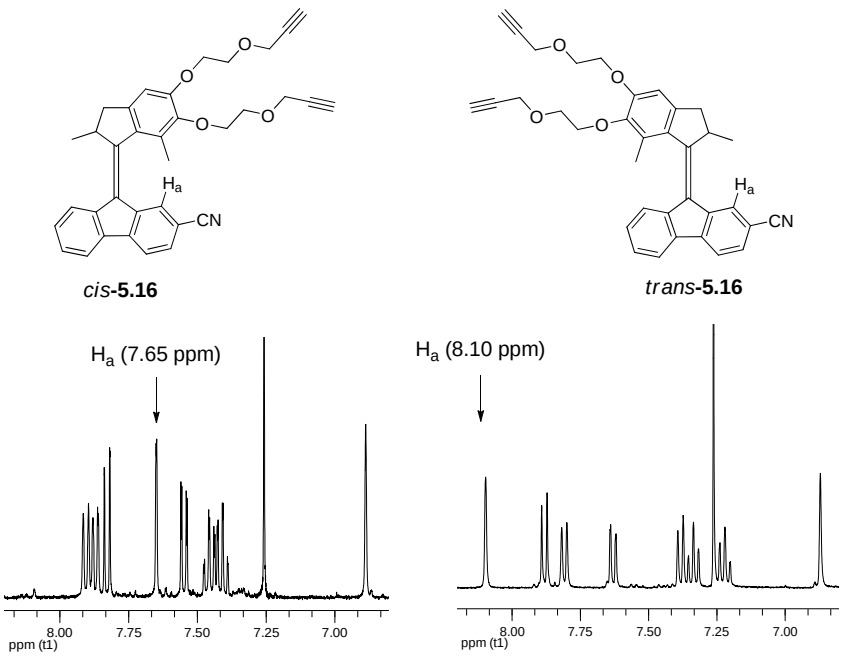

cis-**5.16** *trans*-**5.16**

Figure 3 *Cis* and *trans*-**5.16** were assigned based on the absorption of H_a of the aromatic lower half in $CDCl_3$. In previously reported motors containing substituted fluorene lower halves the absorption of H_a appears at higher field in the *cis*-form compared to the *trans* isomer.

5.3 Photochemical and thermal isomerization studies in solution

To show that **5.9** and **5.16** operate as molecular motors,[24] photochemical and thermal isomerization studies were carried out in solution using low-temperature UV-vis and ^{1}H NMR spectroscopy.

5.3.1 UV-vis spectroscopy: perfluorobutyl motor 5.9

The UV-vis spectra of a sample of *cis*-**5.9** and *trans*-**5.9** in MeOH at -20°C show absorption bands centered at 388 nm and 389 nm, respectively (Figure 4 and Figure 5, solid line). Compared to motors **2.20**, **2.25**, **2.27**, **2.30** and **2.31** with symmetric fluorene moieties reported in Chapter 2, the introduction of the fluorinated alkyl chain resulted in a slight red-shift of the UV-vis absorption. Such shifts have already been observed upon the introduction of electron donating or electron withdrawing substituents to molecular motors,[39] azobenzenes and stilbenes.[40-42]

Irradiation of a sample of stable-*cis*-**5.9** and stable-*trans*-**5.9** in MeOH solution at -20°C with UV-light (λ_{max}= 365 nm) led to a red-shift and broadening of their UV-vis absorptions at 407 nm and 400 nm, respectively, indicating the photochemically induced formation of the unstable isomers (Figure 4 and Figure 5, dashed line). During irradiation, clear isosbestic points were observed in both cases, indicating that the photochemical isomerization from the stable to unstable form proceeds cleanly. Both samples were irradiated until no further changes were observed. Allowing the solutions to warm to room temperature led to reversion of the spectra consistent with thermal relaxation yielding stable-*trans*-**5.9** and stable-*cis*-**5.9**, respectively (Figure 4 and Figure 5, ▲).

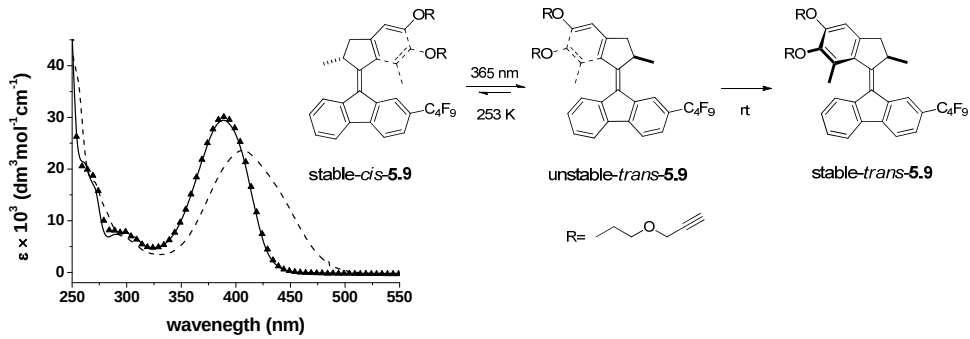

Figure 4 UV-vis spectra of stable-*cis*-**5.9** (solid line), the PSS mixture of stable-*cis*-**5.9** and unstable-*trans*-**5.9** after irradiation (dashed line) at λ_{max}= 365 nm at 253 K, and the mixture of stable-*cis*-**5.9** and stable-*trans*-**5.9** after thermal conversion upon standing at rt for 15 min (▲).

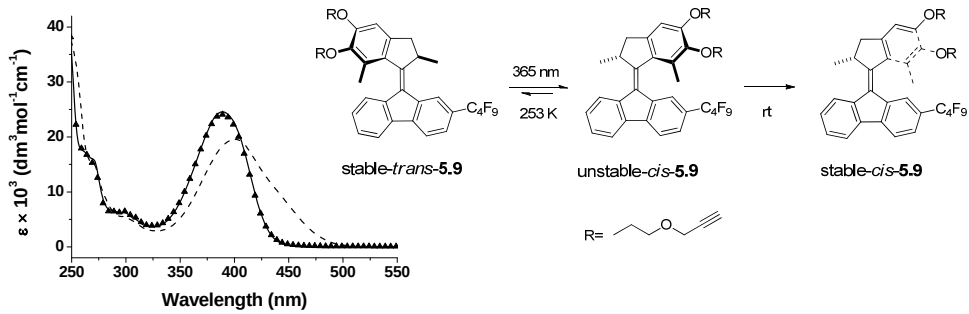

Figure 5 UV-vis spectra of stable-*trans*-**5.9** (solid line), the PSS mixture of stable-*trans*-**5.9** and unstable-*cis*-**5.9** after irradiation (dashed line) at λ_{max}= 365 nm at 253 K, and the mixture of stable-*trans*-5.9 and stable-*cis*-5.9 after thermal conversion upon standing at rt for 15 min (▲).

The conversion of unstable-*cis*-**5.9** and unstable-*trans*-**5.9** to the corresponding stable isomers was monitored by UV-vis spectroscopy at 440 nm as a function of time at different temperatures ranging from 253 K to 273 K. From the first-order rate constants the Gibbs free energy of activation ($\Delta^{\ddagger}G°$) could be determined with the Eyring equation (see Figure 6a and b for the Eyring plots) and was calculated to be 83.3 kJ/mol for the unstable-*cis* → stable-*cis* and 84.0 kJ/mol for unstable-*trans* → stable-*trans* thermal conversions. By extrapolation of the kinetic data half-lives ($t_{1/2}$) of 81 s and 102 s were calculated for the unstable-*cis* → stable-*cis* and unstable-*trans* → stable-*trans* processes, respectively. These values are similar to those obtained for structurally related motors,[27,28,36,37,43] indicating that the

introduction of the perfluoroalkyl chain does not have significant influence on the thermal isomerization step.

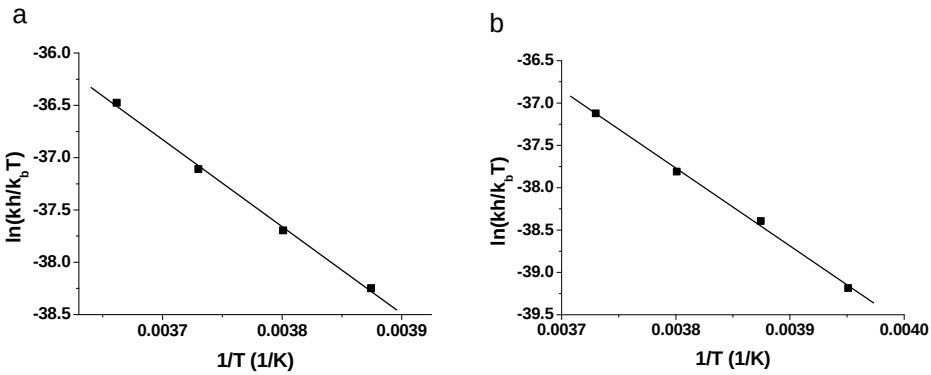

Figure 6 (a) Eyring plot of the conversion of unstable-*trans*-**5.9** to stable-*trans*-**5.9** and (b) Eyring-plot of the conversion of untable-*cis*-**5.9** to stable-*cis*-**5.9** *via* thermal helix inversion.

5.3.2 ^{1}H NMR-spectroscopy: perfluorobutyl-motor 5.9

In order to characterize further the unstable isomers and determine the PSS, low temperature ^{1}H NMR spectroscopic measurements were performed. Irradiation (λ_{max}= 365 nm) of a sample of stable-*cis*-**5.9** and stable-*trans*-**5.9** in CD_2Cl_2 at -55°C resulted in the appearance of new absorptions in their ^{1}H NMR spectra. The identity of the unstable isomers was evident from the downfield shift of the doublet absorptions of the stereogenic methyl groups of the *cis* and *trans* stable forms from 1.29 ppm to 1.41 ppm (unstable-*trans*-**5.9**) and 1.46 ppm (unstable-*cis*-**5.9**). These shifts are consistent with the conformational change of the stereogenic methyl substituents from the preferred pseudo-axial to the unfavored pseudo-equatorial orientation upon photo-isomerization.[27,36,37,43] The relative integration of the absorptions of the stable and unstable isomers revealed a PSS composition of 1 : 2.5 for the stable-*cis* → unstable-*trans* and 1 : 1.5 for the stable-*trans* → unstable-*cis* isomerization processes. When the samples, containing the PSS mixtures, were allowed to warm to rt for 30 min, the ^{1}H NMR spectra showed quantitative conversion of the unstable isomers to the corresponding stable isomers.

A summary of the full unidirectional rotary cycle of motor **5.9** is shown in Scheme 12.

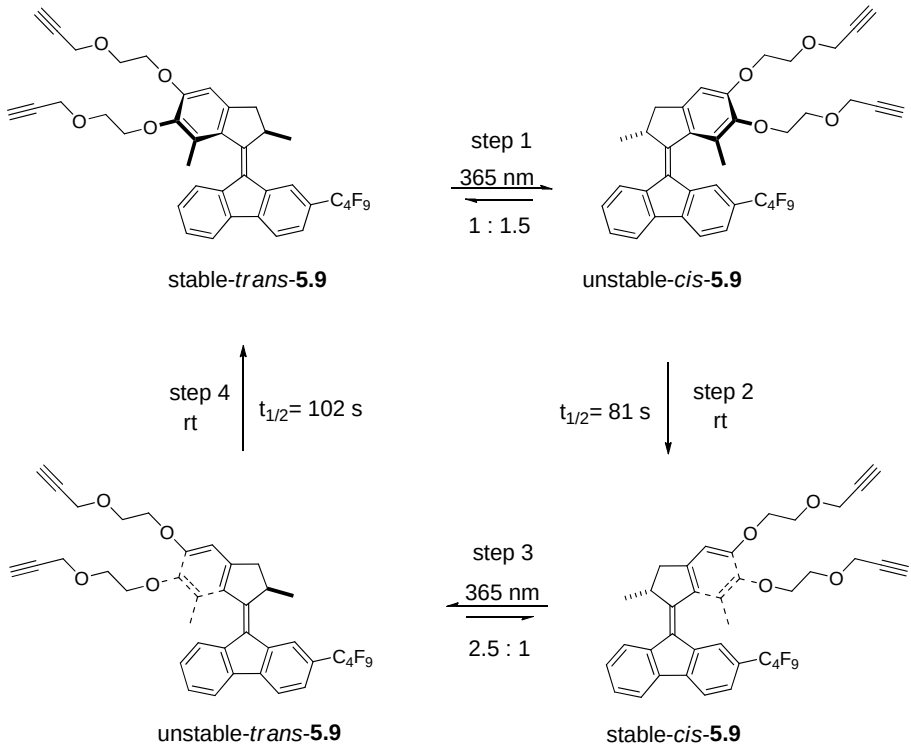

Scheme 12 Summary of the photochemical and thermal isomerization steps in the unidirectional rotary cycle of perfluorobutyl-substituted molecular motor **5.9**.

5.3.3 UV-vis spectroscopy: cyano–motor 5.16

UV-vis spectroscopic studies were performed under identical conditions as in the case of motor **5.9**. In the case of the *cis* and *trans* cyano-substituted motor **5.16**, the maxima of the major absorption band of the stable isomers (396 nm for stable-*cis*-**5.16**, 395 nm for stable-*trans*-**5.16**) in MeOH (Figure 7 and Figure 8) are more red-shifted compared to that of the fluoroalkyl-motors (388 nm for stable-*cis*-**5.9**, 389 nm for stable-*trans*-**5.9**) (Figure 4 and Figure 5, solid lines). This shift is attributed to the stronger electron-withdrawing character of the cyano-group compared to the perfluoroalkyl chain.[39]

Samples of stable *cis* and *trans*-**5.16** in MeOH were exposed to UV-irradiation (λ_{max}= 365 nm) at -20°C. The formation of the unstable isomers was evident from the red-shift of the initial UV-vis absorptions (Figure 7 and Figure 8, dashed line). During the irradiation clear isosbestic points were maintained in both cases,

indicating that the photochemical isomerization proceeds cleanly. The samples were irradiated until no further changes were observed. Upon warming the samples to rt the shifts were reversed (Figure 7 and Figure 8, ▲) which were consistent with the thermal isomerization process that yields stable-*trans*-**5.16** and stable-*cis*-**5.16**.

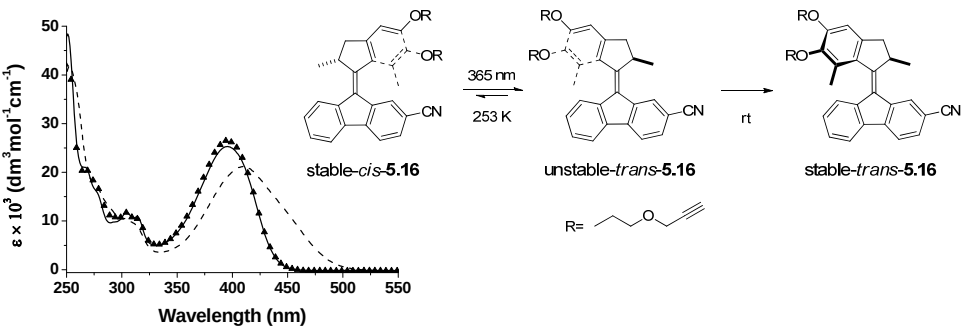

Figure 7 UV-vis spectra of stable-*cis*-**5.16** (solid line), the PSS mixture of stable-*cis*-**5.16** and unstable-*trans*-**5.16** after irradiation (dashed line) at λ_{max}= 365 nm at 253 K, and the mixture of stable-*cis*-**5.16** and stable-*trans*-**5.16** after thermal conversion upon standing at rt for 15 min (▲).

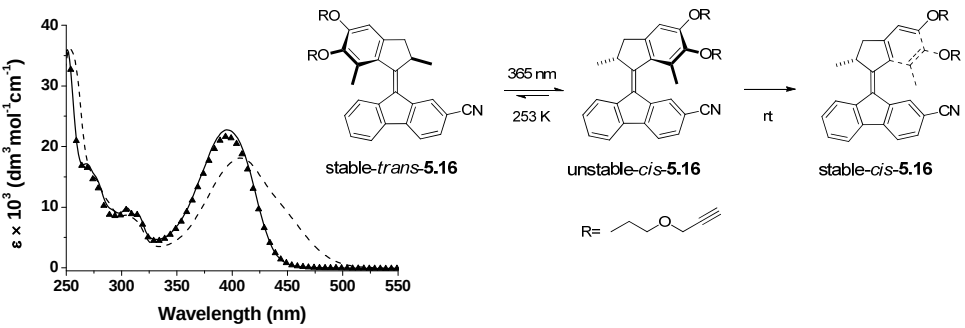

Figure 8 UV-vis spectra of stable-*trans*-**5.16** (solid line), the PSS mixture of stable-*trans*-**5.16** and unstable-*cis*-**5.16** after irradiation (dashed line) at λ_{max}= 365 nm at 253 K, and the mixture of stable-*trans*-**5.16** and stable-*cis*-**5.16** (▲) after thermal conversion upon standing at rt for 15 min.

The thermal isomerization of unstable-*cis*-**5.16** and unstable-*trans*-**5.16** to the corresponding stable isomers was monitored by UV-vis spectroscopy at 450 nm as a function of time at four different temperatures (253, 258, 263 and 268 K). Using the Eyring equation (see Figure 9 for the Eyring plots) the Gibbs free energy of

activation ($\Delta^{\ddagger}G°$) was calculated to be 82.2 kJ/mol for the unstable-*cis* → stable-*cis* and 82.5 kJ/mol for the unstable-*trans* → stable-*trans* thermal conversion. By extrapolation of the kinetic data half-lives ($t_{1/2}$) of 50 s and 57 s were calculated for the unstable-*cis* → stable-*cis* and unstable-*trans* → stable-*trans* processes, respectively. These values are similar to those obtained for the motors with symmetric lower halves (**2.20**, **2.25**, **2.27**, **2.30** and **2.31**), indicating that the introduction of the cyano group does not have a significant influence on the thermal isomerization step.

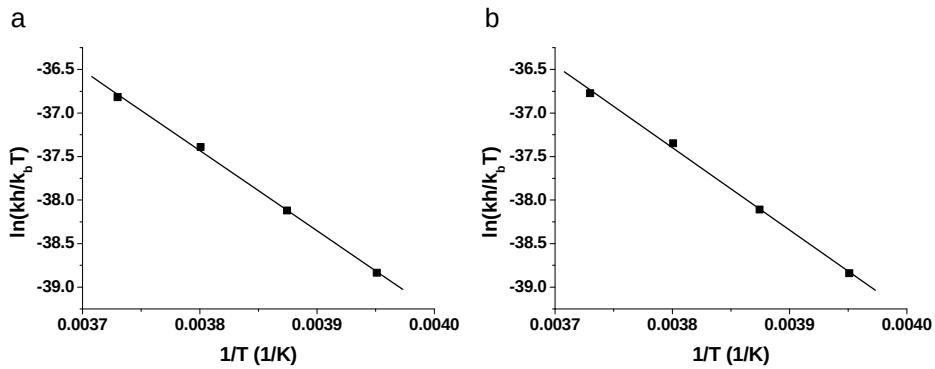

Figure 9 (a) Eyring plot of the conversion of unstable-*trans*-**5.16** to stable-*trans*-**5.16** and (b) Eyring-plot of the conversion of unstable-*cis*-**5.16** to stable-*cis*-**5.16** *via* thermal helix inversion.

5.3.4 ^{1}H NMR-spectroscopy: cyano-motor 5.16

Upon irradiaton (λ_{max}= 365 nm, -55°C) of a sample of stable-*cis*-**5.16** in CD_2Cl_2 solution, in its ^{1}H NMR spectrum at the photostationary (PSS) state a mixture of stable-*cis*-**5.16** and unstable-*trans*-**5.16** could be observed in a ratio of 1 : 5. Irradiation of stable-*trans*-**5.16** under identical conditions resulted in a mixture of stable-*trans*-**5.16** and unstable-*cis*-**5.16** in 1 : 3 ratio. The identity of the unstable isomers was evident from the downfield shift of the doublet absorptions of the stereogenic methyl groups upon irradiation. In stable-*cis*-**5.16** the absorption of the stereogenic methyl group appears at 1.28 ppm and shifts to 1.42 ppm in unstable-*trans*-**5.16**. Comparable changes were observed in the ^{1}H NMR spectrum of stable-*trans*-**5.16** upon irradiation. In this case, the absorption of the stereogenic methyl group shifted from 1.29 ppm to 1.44 ppm indicating the formation of unstable-*cis*-**5.16**. The observed changes in chemical shifts are consistent with the conformational change of the stereogenic methyl group from the favored pseudo-

axial to the less favored pseudo-equatorial orientation upon the formation of the unstable isomers.[27,36,37,43]

A summary of the full unidirectional rotary cycle of motor **5.16** is shown in Scheme 13.

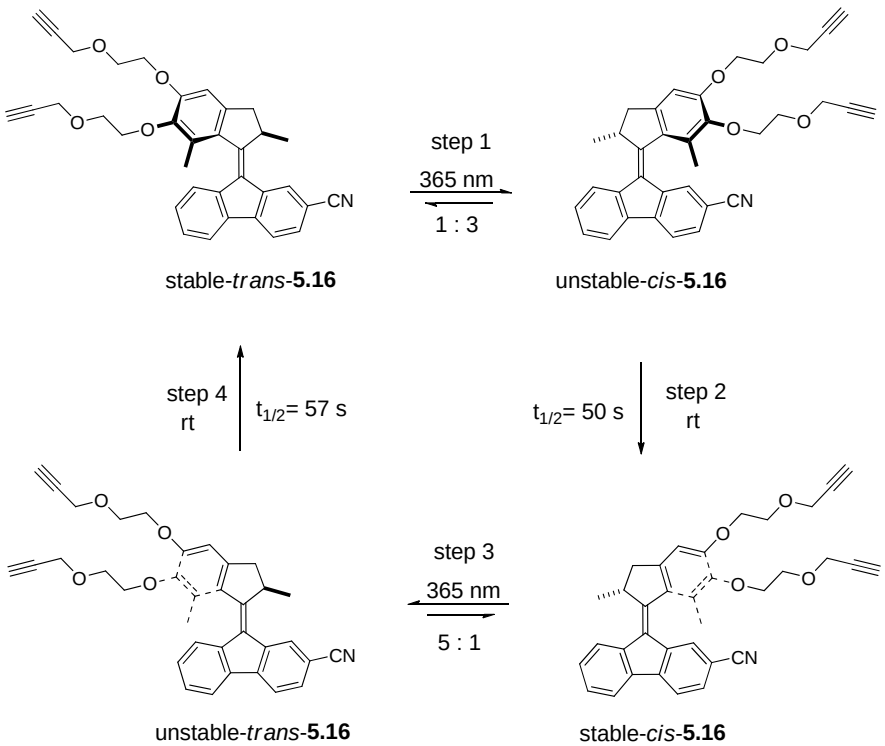

Scheme 13 Summary of the photochemical and thermal isomerization steps in the unidirectional rotary cycle of cyano-substituted molecular motor **5.16**.

5.4 Attachment to quartz surface

Molecular motors **5.9** and **5.16** were attached to quartz surfaces through interfacial 1,3-dipolar cycloaddition reactions[44-46] as developed and described for molecular motors with a non-functionalized rotor part.[27,28]

It was expected that the functional groups would not interfere with the copper-catalyzed coupling step and the functionalized motors will bind to quartz under identical reaction conditions used previously.[27,28]

To attach the alkyne-terminated motors to quartz surfaces through interfacial azide-alkyne cycloadditions, an azide-terminated monolayer was prepared using 11-azidoundecyltrimethoxysilane as described earlier[27,28] (Scheme 14).

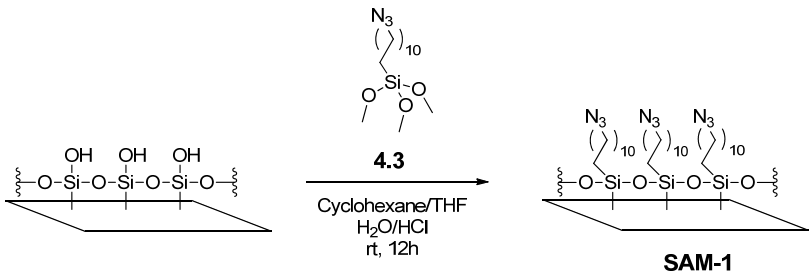

Scheme 14 Assembly of an azide-terminated monolayer on quartz surface.

Piranha-cleaned quartz slides were immersed in a cyclohexane/THF solution of azide **4.3** containing a small amount of water and acid to hydrolyze the methoxysilane groups to silanol groups. Under these conditions higher azide coverage was observed compared to the self-assembly of **4.3** from toluene solution.[27] Quartz slides were immersed in the hydrolysis solution for 12 h and then rinsed by sonication in toluene, DMF and MeOH (2 min in each solvent) and dried under a stream of argon.

Typical water contact angles for **SAM-1** prepared by this method were 83(±2)°, which is in agreement with contact angles reported earlier for azide functionalized surfaces.[27,28,47-49]

5.4.1 Perfluoralkyl-motor 5.9 on quartz

To test the effect of the substituent on the wetting properties of the modified surface, both the *cis* and the *trans* isomers of **5.9** were attached to quartz substrates (Scheme 15).

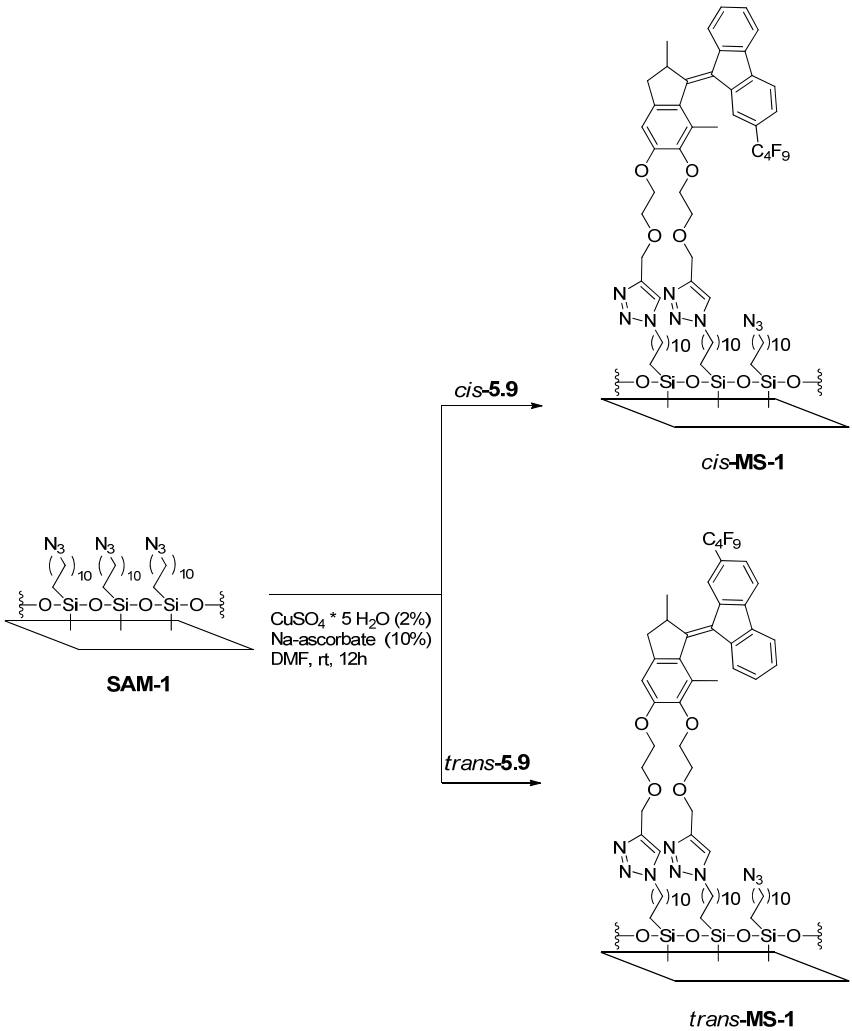

Scheme 15 Attachment of *cis*-**5.9** and *trans*-**5.9** to azide functionalized quartz surfaces through a copper-catalyzed interfacial azide-alkyne cycloaddition reaction.

The UV-vis spectra of the quartz substrates immersed in a 1 mM DMF solution of *cis*-**5.9** and *trans*-**5.9** in the presence of copper catalyst showed the characteristic absorption of the motors (Figure 10a and b, solid lines) which indicates that the attachment was successful. The maxima of the major absorption band and the absorption profile are similar to that observed in MeOH solution. As the attachment of *cis* and *trans*-**5.9** to a quartz surface did not cause any significant

changes in the UV-vis absorption profile and with the assumption that the molar absorptivity (ε) of stable-*cis*-**5.9** and stable-*trans*-**5.9** is the same in solution and on the surface, the surface coverage could be estimated.[50] Using the Lambert-Beer law, the relation between the absorption (A) and the surface-density (Γ) of the absorbing species can be written as follows:

$$A = \varepsilon \times \Gamma \qquad \textbf{Eq. 1}$$

Taking into account that both sides of the slides are functionalized, the surface coverage density is estimated to be 3.0×10^{-10} mol/cm^2 for *cis*-**5.9** and 3.9×10^{-10} mol/cm^2 for *trans*-**5.9** for a single side, which is in agreement with the values obtained for monolayers of overcrowded alkenes reported elsewhere recently.[51]

Irradiation of the functionalized slides at λ_{max}=365 nm at -5°C resulted in a shift of the UV-vis absorption similarly as observed in MeOH-solution indicating the formation of the unstable form of the surface-bound motors (Figure 10a and b, dashed line). Upon leaving the sample overnight at room temperature, the UV-vis absorption reversed, which is consistent with the thermal isomerization process (Figure 10a and b, ▲).

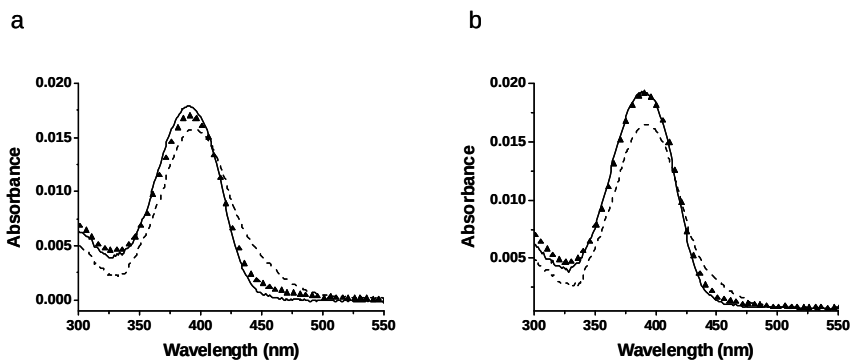

Figure 10 UV-vis spectra of (a) stable-*cis*-**MS-1** and (b) stable-*trans*-**MS-1** (solid lines) on quartz. Both isomers undergo photochemical isomerization upon irradiation at λ_{max}= 365 nm at -5°C (dashed lines) and thermal isomerization upon standing at rt overnight (12 h) (▲).

Contact angle measurements were performed on quartz surfaces modified with *cis* and *trans*-**5.9**. In the case of *trans*-**MS1**, where the perfluorobutyl chains are exposed to the interface, a contact angle of 92(±1°) was obtained (Figure 11b)

which is due to the hydrophobic character (low surface energy) of the fluoroalkyl chains. A somewhat lower contact angle, 80(±2°), was measured for the *cis* isomer, where the perfluorobutyl chain is likely hidden from the interface (Figure 11a). The effect of the substituent on the wettability of the surface is evident when compared to the motor with a symmetric rotor part, for which a water contact angle of 67(±2°) was measured.[27] The higher contact angle in the case of *cis*-**MS-1** compared to the symmetric motor is probably due to the shielding of the more polar ethylene glycol units and triazol moieties beneath the chromophore by the fluoroalkyl chains. The fluorinated chains decrease the free volume in the interface, minimizing the interactions between water and the hydrophilic components.

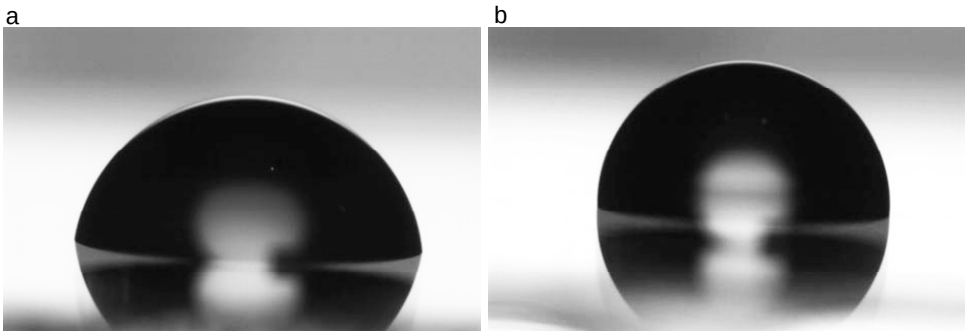

Figure 11 Water droplets on quartz surfaces modified by the attachment of perfluorobutyl-motor *cis*-**5.9** (a) and *trans*-**5.9**.(b). Water contact angles of 80(±2°) and 92(±1°) were measured for *cis*-**5.9** and *trans*-**5.9** isomers, respectively.

As a comparison, the difference in water contact angle between the more polar *cis* and the less polar *trans* geometry of unsubstituted or *para*-alkylazobenzenes was reported to be 2-9°.[19,52] In one case, where the azobenzenes were *para*-substituted with a perfluorooctyl-chain, a contact angle of 104(±1°) was obtained for the *trans* isomer.[52] However, in contrast to the *para*-alkylazobenzenes no change ($\Delta\theta \sim 0.5°$) in wettability was observed upon their photo-isomerization.[52] Since it was shown that the perfluorooctylazobenzenes still undergo switching on the surface (the authors report that 65% of the azobenzenes undergo *E*-to-*Z* isomerization), this result suggests that the fluorinated chains remain exposed to the interface.

Table 1 Contact angles of water and diiodomethane on *cis* and *trans*-**MS-1**, and the surface energies calculated based on the contact angles by the harmonic-mean equation (Wu-method).

	Contact angle (°)		
Surface	H_2O	CH_2I_2	Surf. Energy[a] (mN/m)
cis-**MS-1**	80(±2)	43(±1)	43.9
trans-**MS-1**	92(±1)	52(±1)	36.3

[a] Calculated based on the harmonic-mean equation developed by Wu.[53,54] The errors in estimating the surface energies were less than 1 mN/m.

Using the contact angles of water and diiodomethane, surface energies of 43.9 mN/m and 36.3 mN/m were calculated by the Wu-method for *cis*-**MS-1** and *trans*-**MS-1**, respectively (Table 1). The Wu-method uses water and diiodomethane as testing liquids and the harmonic mean equation for the calculation.[53,54] It has been compared to experimental data for a wide range of polymers and gives good predictions for the surface energy of polymer films[53] and used for surface energy calculations of SAMs[5,53] as well. As a comparison, the surface energy, calculated by the same method, of a perfluorodecyl-SAM on Si/SiO_2 substrate was reported to be 16 mN/m, while oligoethyleneglycol chains gave a surface energy value of 58 nM/m.[5] Surface energies for polyhexafluoropropylene, polytetrafluoroethylene and polytrifluoroethylene films are 17.0, 22.5 and 27.3 mN/m, respectively.[53]

Irradiation (λ_{max}=365 nm) of quartz slides cis-**MS-1** and trans-**MS-1** with a drop of water (2 μL) deposited on top produced no changes in contact angle until evaporation become significant.

5.4.2 Cyano-motor on quartz

As in the case of motor **5.9**, *cis* and *trans*-**5.16** were attached to quartz surfaces from a 1 mM DMF solution using a copper-catalyzed azide-alkyne cycloaddition reaction.[27,28] Quartz slides were immersed into 1 mM motor solutions in DMF for 12 h and rinsed by sonication in DMF, toluene and MeOH solvents (2 min in each) and dried in a stream of argon.

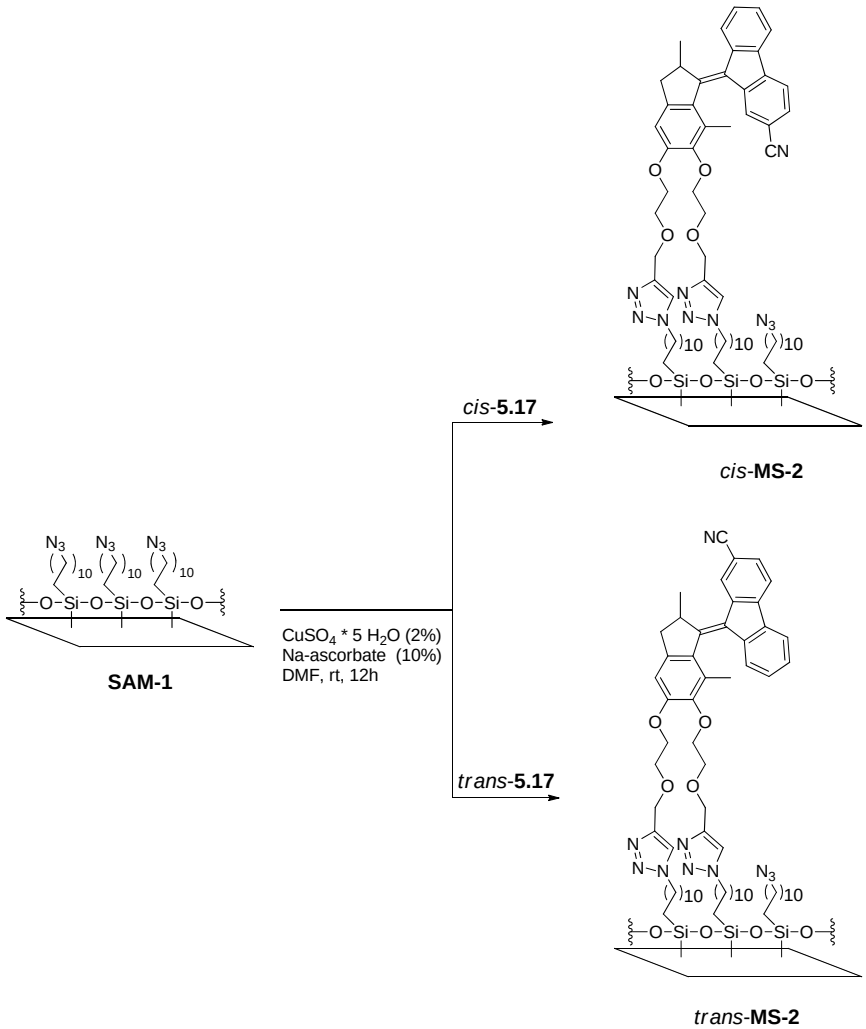

Scheme 16 Attachment of *cis*-**5.16** and *trans*-**5.16** to azide functionalized quartz surfaces through a copper-catalyzed interfacial azide-alkyne cycloaddition reaction.

As with slides **MS-1**, the presence of the cyano-motors **5.16** on quartz was evident from their characteristic absorption profile (Figure 12a and b, solid lines), which was similar to that observed in MeOH solution. As the attachment to quartz did not alter significantly the UV-vis absorption profile of the motors, the surface density was estimated to be 3.7×10^{-10} mol/cm^2 for *cis*-**MS-2** and 4.0×10^{-10} mol/cm^2 for *trans*-**MS-2** for a single side, based on the assumptions[50] described in section

5.4.1. Similar values were obtained for monolayers of overcrowded alkenes reported elsewhere recently.[51]

To show that the motors still undergo photochemical and thermal isomerizations while attached to quartz, the slides were irradiated with UV-light (λ_{max}=365 nm) at -5°C. As with previously described surface-bound molecular motors a moderate shift in the UV-vis absorption was observed, consistent with the formation of the unstable forms via photochemical *cis*/*trans* isomerization[27, 28] (Figure 12a and b, dashed lines). Reversion of the absorption upon leaving the sample at rt overnight is indicative of the thermal isomerization step (Figure 12a and b, ▲).

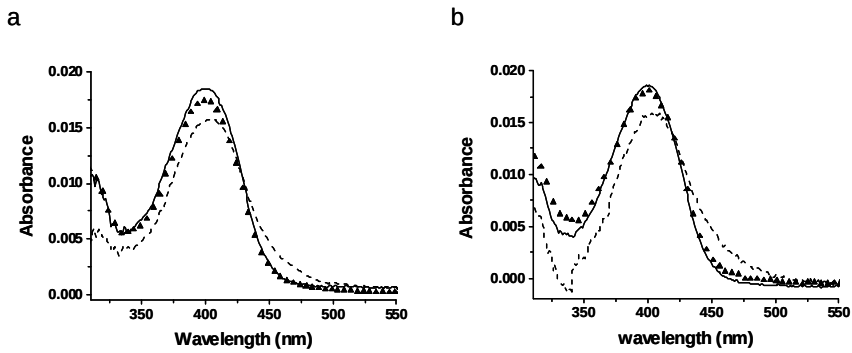

Figure 12 UV-vis spectra of (a) stable-*cis*-**MS-2** and (b) stable-*trans*-**MS-2** (solid lines). Both isomers undergo photochemical isomerization upon irradiation at λ_{max}= 365 nm at -5°C (dashed lines) and thermal isomerization upon standing at rt overnight (12 h) (▲).

Both *cis*-**MS-2** and *trans*-**MS-2** showed lower water contact angles compared to *cis* and *trans*-**MS-1** indicating higher surface energies. When the CN-group was displayed at the interface, as in *trans*-**MS-2,** the measured water contact angle was 60(±1°), while for the hidden cyano-group in *cis*-**MS-2** the value increased to 67(±1°). The contact angle value for *cis*-**MS-2** is the same as that obtained for the unsubstituted motor **2.30** on quartz (see Chapter 4 and ref. 27), indicating that it does not change the surface energy considerably, probably due to its small size and comparable polarity to the hydrophilic ethylene glycol units beneath the motor.

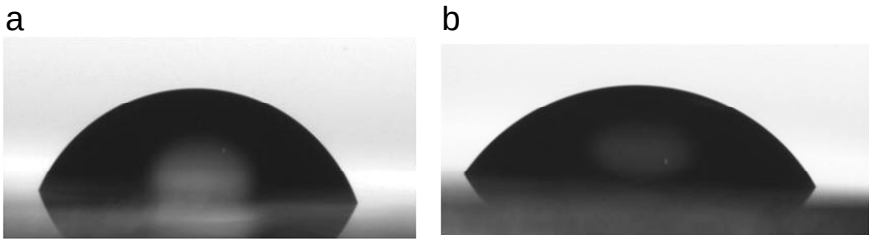

Figure 13 Water droplets on quartz surfaces modified by the attachment of (a) *cis*-**5.16** and (b) *trans*-**5.16** containing a cyano-group on the rotor part. Water contact angles of 67(±1°) and 60(±1°) were measured for *cis*-**5.16** and *trans*-**5.16** isomers, respectively.

Table 2 Contact angles of water and diiodomethane on *cis* and *trans*-**MS-2**, and the surface energies calculated based on the contact angles by the harmonic-mean equation (Wu-method).

	Contact angle (°)		
Surface	H_2O	CH_2I_2	Surf. Energy[a] (mN/m)
cis-**MS-2**	67(±2)	19(±2)	56.9
trans-**MS-2**	60(±1)	29(±1)	57.5

[a] Calculated based on the harmonic-mean equation developed by Wu.[53,54] The errors in estimating the surface energies were less than 1 mN/m.

Surface energies for *cis* and *trans*-**MS-2** based on the contact angles of water and diiodomethane were calculated by the Wu-method[53,54] (Table 2). The calculated values of 56.9 and 57.5 mN/m for *cis* and *trans*-**MS-2** are higher compared to those obtained for *cis* and *trans*-**MS-1**, which is consistent with the stronger hydrophilic character of the cyano-functionalized motors, compared to the fluoroalkyl motors on the surface.

5.5 Discussion and conclusions

From the above experimental observations it can be concluded that molecular motors containing perfluorobutyl- and cyano-substituents were successfully synthesized and attached to quartz surfaces using an interfacial 1,3-dipolar cycloaddition reaction. Furthermore, it was evident by UV-vis spectroscopy, that the rotary function of the motors is preserved while confined at the interface. It has been also shown that the surfaces functionalized with the *cis* and *trans* isomers of

the substituted motors **5.9** and **5.16** provided different water contact angles depending on the polarity and orientation of the substituents (Table 3).

Table 3 Water contact angle values obtained for *cis* and *trans* **MS-1** and **MS-2**.

	H_2O contact angle (°)
cis-**MS-1**	80(±2)
trans-**MS-1**	92(±1)
cis-**MS-2**	67(±1°)
trans-**MS-2**	60(±1°)

Despite the difference in contact angles of water on the different substrates, preliminary attempts to modify the wettability of the surfaces *in situ* did not show substantial effects.

This could be due to the observed lower photoconversion in the case of monolayers **MS-1** and **MS-2** compared to the motors in solution, as indicated by the smaller red-shift of the long wavelength absorption band in their UV-vis spectra (Figure 4 and Figure 5 vs. Figure 10; Figure 7 and Figure 8 vs. Figure 12). The smaller photoconversion is probably due to the intermolecular interactions between the motors within the monolayer. The increased steric crowding in the interface has already been shown to influence the dynamic behavior of the surface-bound motors by slowing down the thermal isomerization step considerably (see Chapter 4 and ref. 28).

Design elements that should be considered for future experiments towards switching the wettability of solid surfaces are discussed in the following section.

5.5.1 Switching of wetting properties

To date, azobenzene and spiropyran based systems are amongst the best candidates to achieve reversible photo-controlled wetting of molecularly engineered surfaces.[13-15] The dominant reasons for the observed behavior are that both molecules can undergo rapid and reversible switching between two geometrical forms upon irradiation with different wavelengths of light, and that both forms are sufficiently long-lived so as to enable exploitation of their hydrophilic/hydrophobic characters.

To achieve reversible wetting of solid surfaces using overcrowded alkene based systems, the application of photochemically bi-stable switches with two

thermally stable states or molecular motors with longer half-lives at rt bearing appropriate (hydrophilic/hydrophobic) functional groups may be needed.

In addition to the structure of the photochromic molecule, other important aspects of wettability-control are the local environment of the attached molecules on the surface and the roughness of the surface the molecules are bound to. It has been reported that a sufficient free-volume is required for efficient isomerization on the surface.[18,55,56] This could be achieved by diluting the surface coverage of the photo-active molecule with diluents that do not interfere with photochemical processes. Another possible way, which is under investigation in our group, would be to use more bulky anchoring units that decrease the concentration of the molecular switch/motor at the interface (Figure 14).

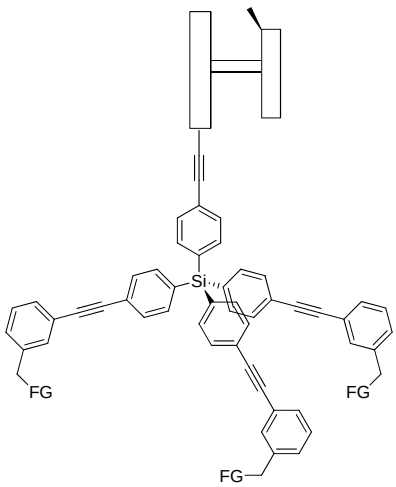

Figure 14 Molecular motor with a bulky anchoring unit. The tripod structure may provide sufficient free volume for more efficient isomerization. (FG= functional group for covalent attachment to solid surfaces.)

It is noted, however, that although the lower surface coverage might contribute to higher photoconversions by providing a larger free volume for the isomerization of the motors, it may also decrease the difference in contact angle between the *cis* and *trans*-motor functionalized surfaces, lowering the possible effect on wettability.

It has been shown for both azobenzene and spiropyran functionalized surfaces that a rough surface morphology significantly amplifies the light induced change in water contact angle compared to smoother surfaces.[22,23] The contribution of nano-

and microscopic pockets of air trapped below the liquid drop have been attributed to the increased hydrophobicity.[57-59] The most significant changes in wettability involve the reversible switching of superhydrophilic (water contact angle ~ 0°) and superhydrophobic (water contact angle ~ 150°) surfaces and have been achieved with molecular switches attached to nano/microstructured surfaces.[22,23] The combination of overcrowded alkene based motors and switches with similar materials should be considered.

5.6 Acknowledgement

The optimization of the synthesis and spectroscopic characterization of compound **5.16** and the preparation and characterization of *cis* and *trans*-**MS-2** was performed by Kuang-Yen Chen who is acknowledged for his contribution. Tom van Leeuwen is acknowledged for his assistance with the characterization of compounds **5.2**, **5.10** and **5.11**.

5.7 Experimental

5.7.1 General remarks

For general remarks on the synthesis and characterization of compounds and intermediates see Chapter 2. For general remarks on surface characterization see Chapter 3.

5.7.2 Experimental procedures for surface modification

11-Azidoundecyltrimethoxysilane monolayer on quartz

Quartz microscope slides (UQG Optics) were cut into pieces so as to fit into the measurement cell of the UV/Vis spectrometer. They were cleaned using a 3/7 ratio of 30% H_2O_2 in H_2SO_4 (*Caution! This mixture is extremely corrosive and reactive toward organics*) at >90 °C. These samples were then rinsed with doubly destilled water (3 times) and with MeOH and dried under a stream of Ar.

1.25 mL of a hydrolysis solution containing 0.04 g 11-azidoundecyltrimethoxy silane **4.3**, 6 ml distilled THF, 31 µl double-distilled H_2O and 4 µl 37% aq. HCl were added to 25 mL cyclohexane to give a slighty hazy solution. The piranha-cleaned quartz slides were immersed into this solution overnight at rt. After the

assembly the slides were sonicated in DMF, toluene and MeOH for 2 min each and dried under a stream of Ar.

Procedure for interfacial 1,3-dipolar cycloadditon reaction (MS-1 and **MS-2)**
Compounds **5.9** and **5.16** were grafted to the azide monolayer by immersing the slide into a 1 mM solution of *cis* and *trans* **5.9** and **5.16** in DMF containing 1 mol% $CuSO_4$•$5H_2O$ and 5 mol% sodium-ascorbate relative to the alkyne moieties. The azide functionalized slides were immersed for 12 h at rt. The modified quartz substrates (**MS-1** and **MS-2**) were sonicated in DMF, water and MeOH for 2 min each and then dried under a stream of Ar.

5.7.3 Synthesis of compounds and intermediates

2-Bromo-9H-fluoren-9-one (5.2)

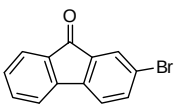

5.2 was prepared based on a method described in the literature.[29] Triton B (5 mL, 40 % in MeOH) was added to a stirred solution of 2-bromo-9*H*-fluorene **5.1** (10 g, 40 mmol) in pyridine (50 mL), upon which the reaction mixture turned red. Air was bubbled through the reaction mixture via a needle for 10 hours. The progress of the reaction can be followed by TLC (SiO_2, *n*-heptane : EtOAc = 8 : 1, $R_{f,product}$ = 0.49, $R_{f,starting\ material}$ = 0.81.). The green solution was poured into 10 % aq. HCl (100 mL) and the precipitate was filtered and recrystallized twice from EtOH yielding **5.2** (7.9 g, 76%) as yellow needles. Mp 146-147°C (lit[29]: 145-147°C); ^{1}H-NMR (400 MHz, $CDCl_3$) δ 7.70 (s, 1H), 7.61 (d, *J* = 7.4 Hz, 1H), 7.56 (d, *J* = 7.9 Hz, 1H), 7.47 (m, 2H), 7.33 (d, *J* = 7.9 Hz, 1H), 7.31–7.25 (m, 1H); ^{13}C NMR (APT, 50 MHz, $CDCl_3$) δ 192.6, 143.6, 142.9, 137.0, 135.7, 135.0, 133.6, 129.4, 127.5, 124.6, 122.9, 121.7, 120.4.
HRMS (APCI): calcd for $C_{13}H_7OBr$ 258.97530 (MH^+), found 258.97518; Anal calcd for $C_{13}H_7OBr$: C 60.26 %, H 2.72 %, found: C 60.22 %, H 2.64 %.

2-(Perfluorobutyl)-9H-fluoren-9-one (5.3)

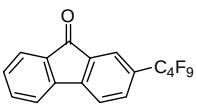

Compound **5.3** was prepared based on a method described in the literature.[31] A suspension of Cu-bronze (2.6 g, 40.6 mmol) in DMSO (30 mL, dried over 4 Å molecular sieves for 12 h) was heated at 125 °C for 15 min under an inert atmosphere (N_2). Iodononafluorobutane (3.5 mL, 20.3 mmol) in DMSO (5 mL) was added dropwise

and the mixture was stirred for 45 min at 125 °C. Next, 2-bromofluorenone **5.2** (1.0 g, 3.9 mmol) in DMSO (10 mL) was added dropwise and the mixture was stirred for an additional 6 h at the same temperature. The mixture was diluted with diethyl ether (50 mL), and was filtered over celite to remove Cu-bronze. The organic phase was washed with water (5 × 100 mL) and brine, dried (Na_2SO_4) and concentrated under reduced pressure. The crude product was purified by flash chromatography (SiO_2, *n*-heptane : dichloromethane 10 : 1 → 5 : 1, dry-loaded on celite) to give **5.3** as yellow crystals (1.1 g, 2.8 mmol, 72 %). Mp 96-97 °C; ^{1}H NMR (400 MHz, $CDCl_3$) δ 7.40 (t, *J* =7.1 Hz, 1H), 7.57 (t, *J* = 7.4 Hz, 1H), 7.63 (d, *J* = 7.4 Hz, 1H), 7.7 (d, *J* = 7.8 Hz, 1H), 7.74 (d, *J* = 7.7 Hz, 2H), 7.88 (s, 1H); ^{13}C NMR (100 MHz, $CDCl_3$) δ 120.4, 121.2, 122.7 (t, *J* = 6.5 Hz), 124.7, 129.6 (t, *J* = 24.6 Hz), 130.3, 133.2 (t, *J* = 6.5 Hz), 134.3, 134.4, 135.1, 142.9, 147.7, 192.1. Peaks corresponding to *C*F_3 are not observed due to to the low intensity of the peaks in the region they are expected (~ 115 ppm). (See also the supporting information of ref. 31.)
HRMS (APCI) calcd for $C_{17}H_8F_9O$ 399.0433 (MH^+), found 399.0423.

(*E*/*Z*)-(2-(Perfluorobutyl)-9H-fluoren-9-ylidene)hydrazine (5.4)

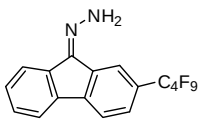

To a solution of 2-(perfluorobutyl)-9H-fluoren-9-one (**5.3**) (1.0 g, 2.5 mmol) in MeOH : DCM (4:1, 25 mL), $(NH_2)_2$ × H_2O (8 mL) was added and the solution was heated at 45°C for 3 h. Addition of water (10 mL) to the hot mixture followed by cooling to room temperature resulted in the precipitation of a pale yellow solid. The solid was filtered, washed with cold MeOH and dried in air. The product **5.4** (151 mg, 0.37 mmol, 64 %) was obtained as a mixture of *E*/*Z* isomers (~ 1 : 1.5) as a pale yellow solid and was used without further purification. ^{1}H NMR (300 MHz, $CDCl_3$) δ 6.52 (br s, 2H, major), 6.58 (br s, 2H, minor), 7.36-7.42 (m, 2H, major), 7.43-7-53 (m, 2H, minor), 7.56 (d, *J* = 8.0 Hz ,1H, minor), 7.67 (d, *J* = 8.0 Hz, 1H, major), 7.71-7.74 (m, 1H, major), 7.76-7.79 (m, 1H major, 1H minor), 7.87 ($t_{apparent}$, *J* = 8.7 Hz, 1H major, 1H minor), 7.94 (d, *J* = 7.1 Hz, 1H, minor), 7.98 (s, 1H, minor), 8.07 (s, 1H, major). ^{13}C NMR (100 MHz, $CDCl_3$) δ 119.4 (t, *J* = 5.6 Hz), 119.5, 120.3, 120.4, 121.0, 121.3, 123.3 (t, *J* = 6.3 Hz), 125.3, 126.7 (t, *J* = 6.6 Hz), 128.3 ($d_{apparent}$, *J* = 7.1 Hz), 128.7, 128.9, 129.2, 129.8, 130.0, 130.6, 136.9, 138.0, 138.4, 139.6, 141.4, 143.4, 143.8, 144.5
HRMS (ESI) calcd for $C_{17}H_{10}F_9N_2$ 413.0695 (MH^+), found 413.0690.
Minor-isomer was isolated (SiO_2, *n*-heptane : EtOAc 5 : 1):

^{1}H NMR (400 MHz, $CDCl_3$) δ 6.58 (br s, 2H) 7.44-7.53 (m, 2H), 7.56 (d, *J* = 8.2 Hz, 1H), 7.78 (d, *J* = 7.9 Hz, 1H), 7.86 (d, *J* = 7.9 Hz, 1H), 7.94 (d, *J* = 7.6 Hz, 1H), 7.98 (s, 1H)

Diester-perfluorobutyl motor (5.7)

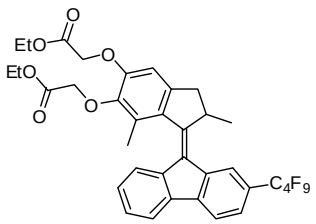

MnO_2 (0.5 g, 5.75 mmol) was added to a stirred solution of hydrazone **5.4** (760 mg, 1.84 mmol) in THF (10 mL) after which the color of the solution turned to red. The mixture was stirred for an additional 30 min and then filtered over a plug of celite. The solvent was removed under reduced pressure and the solid was dissolved in toluene (5 mL) and added to a solution of thioketone **2.23** (560 mg, 1.47 mmol) in toluene (10 mL). The mixture was heated at 75°C for 3 h. The formation of the episulfide was monitored by ^{1}H NMR spectroscopy by following the shift of the absorption of the aromatic proton of the thioketone from 6.66 to 6.34 and 6.39 ppm in the episulfide isomers. After the conversion of the thioketone was complete, PPh_3 (0.8 g, 3.05 mmol) was added to the episulfide solution, followed by an additional 1 h stirring at 75°C. The mixture was cooled to rt and the solvent was evaporated under reduced pressure. The crude product was dissolved in Et_2O and CH_3I (2 mL, 32 mmol) was added. The solution was stirred for 2 h at rt, the precipitate was filtered and the solvent was removed *in vacuo*. The crude product was purified by column chromatography (SiO_2, *n*-heptane → *n*-heptane : Et_2O 3 :1) to give **5.7** as a mixture of isomers (1.4 : 1) as a yellow oil (792 mg, 1.08 mmol, 73%).

^{1}H NMR (400 MHz, $CDCl_3$) δ 1.28-1.36 (m, 9H major, 9H minor), 2.21 (s, 3H major), 2.25 (s, 3H minor), 2.56 (d, *J* = 14.8 Hz, 1H major), 2.58 (d, *J* = 14.7 Hz, 1H minor), 3.32 (dd, *J* = 4.7, 14.8 Hz, 1H major, 1H minor), 4.06-4.18 (m, 1H major, 1H minor), 4.24-4.34 (m, 4H major, 4H minor), 4.52 (d, *J* = 15.6 Hz, 1H major), 4.68 (d, *J* = 15.8 Hz, 1H minor), 4.75 (s, 2H major, 2H minor), 4.87 (d, *J* = 15.8 Hz, 1H major), 4.92 (d, *J* = 16.1 Hz, 1H minor), 6.77 (s, 1H minor), 6.79 (s, 1H major), 7.24 (t, *J* = 7.4 Hz, 1H minor), 7.34 (t, *J* = 7.4 Hz, 1H minor), 7.39-7.46 (m, 3H major, 1H minor), 7.50 (d, *J* = 7.9 Hz, 1H major), 7.56-7.59 (m, 1H major, 1H minor), 7.81 (d, *J* = 7.6 Hz, 1H minor), 7.85-7.91 (m, 2H major, 1H minor), 8.06 (s, 1H minor).

^{13}C NMR (100 MHz, $CDCl_3$) δ 13.7, 13.8, 13.9, 15.5, 16.1, 18.5, 18.6, 41.2, 41.3, 44.8, 44.9, 60.6, 60.7, 61.1, 61.2, 65.5, 65.6, 69.1, 69.3, 108.0, 108.4, 115.6-116.6

(m, *C*F_3), 119.1, 119.4, 119.8, 120.3, 121.5 (t, *J* = 6.9 Hz), 121.8 (t, *J* = 6.4 Hz), 123.6, 123.7, 124.8 (t, *J* = 6.2 Hz), 125.1 (t, *J* = 4.8 Hz), 126.0 (t, *J* = 23.7 Hz), 126.3 (t, *J* = 23.6 Hz), 126.8, 127.1, 127.7, 127.9, 128.0, 128.2, 131.6, 132.1, 133.7, 133.9, 137.5, 137.9, 138.2, 139.3, 139.9, 142.2, 142.7, 143.6, 143.9, 145.0, 145.5, 151.3, 151.9, 153.3, 153.7, 168.2, 169.1, 169.4,
HRMS (ESI) calcd for $C_{36}H_{31}F_9O_6Na$ 753.6039 (MNa^+), found 753.1856.

Dihydroxy-perfluorobutyl motor (5.8)

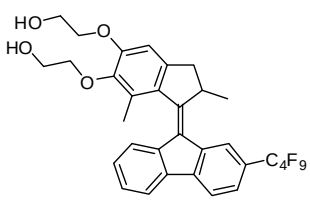

A suspension of $LiBH_4$ (66 mg, 3 mmol) in THF (5 mL) was added to a solution of motor **5.7** (660 mg, 0.9 mmol) in THF (15 mL) and the mixture was heated at 40 °C for 3 h. The reaction was quenched with H_2O (10 mL) and the mixture was extracted with EtOAc until the aqueous phase was colorless. The combined organic layers were washed with water and brine and dried (Na_2SO_4). The solvent was evaporated under reduced pressure. The crude product was purified by column chromatography (SiO_2, Et_2O → EtOAc). One of the isomers could be precipitated by adding Et_2O to the product mixture. The rest of the *E* and *Z* isomer mixture was separated by column chromatography (SiO_2, Et_2O)
***Cis*-5.8** (140 mg, 0.22 mmol, 24 %) was obtained as a yellow solid.
^{1}H NMR (400 MHz, $CDCl_3$) δ 1.35 (d, *J* = 6.7 Hz, 3H), 2.18 (s, 3H), 2.59 (d, *J* = 14.7 Hz, 1H), 3.35 (dd, *J* = 5.6, 14.91 Hz, 1H), 3.37 (br s, O*H*), 3,75 (br s, O*H*), 3.86 ($t_{apparent}$, *J* = 10.4 Hz, 1H), 3.91-4.00 (m, 3H), 4.04-4.10 (m, 1H), 4.12-4.27 (m, 4H), 6.90 (s, 1H), 7.39-7.47 (m, 2H), 7.51 (d, *J* = 8.0 Hz, 1H), 7.59 (s, 1H), 7.87-7.92 (m, 3H).
The protons of the terminal OH-groups could be observed in DMSO-d_6:
^{1}H NMR (400 MHz, DMSO-d_6) δ 1.29 (d, *J* = 6.5 Hz, 3H), 2.07 (s, 3H), 2.61 (d, *J* = 14.8 Hz, 1H), 3.69 (br dd, *J* = 5.1, 9.7 Hz, 2H), 3.81 (br dd, *J* = 4.1, 8.6 Hz, 2H), 3.94-4.02 (m, 2H), 4.09 (q, *J* = 6.5 Hz, 1H), 4.12-4.18 (m, 2H), 4.75 (t, *J* = 5.3, O*H*), 4.93 (t, *J* = 5.2 Hz, O*H*), 7.13 (s, 1H), 7.47 (t, *J* = 7.4 Hz, 1H), 7.51-7.55 (m, 2H), 7.62 (d, *J* = 8.2 Hz, 1H), 7.93 (d, *J* = 7.9 Hz, 1H), 8.11 (d, *J* = 7.4 Hz, 1H), 8.18 (d, *J* = 8.2 Hz, 1H). (1H is not observed due to overlap with DMSO peak at 3.33 ppm)
^{13}C NMR (100 MHz, $CDCl_3$) δ 15.6, 18.9, 41.6, 45.1, 60.9, 61.8, 70.5, 74.4, 108.3, 119.3, 120.4, 121.6 (t, *J* = 7.1 Hz), 123.8, 125.3 (t, *J* = 5.3 Hz), 126.1 (t, *J* = 23.6

Hz), 126.9, 127.9, 128.1, 131.9, 133.3, 137.7, 138.0, 140, 2, 142.4, 144.6, 145.7, 153.2, 154.2,

***Trans*-5.8** (200 mg, 0.31 mmol, 34%) was obtained as a yellow solid.

^{1}H NMR (400 MHz, $CDCl_3$) δ 1.36 (d, *J* = 6.7 Hz, 3H), 2.21 (s, 3H), 2.62 (d, *J* = 14.7 Hz, 1H), 3.54 (dd, *J* = 5.7, 14.9 Hz, 1H), 3.73 (br s, O*H*), 3.91-4.24 (m, 9H), 6.89 (s, 1H), 7.20 (t, *J* = 7.6 Hz, 1H), 7.33 (t, *J* = 7.5 Hz, 1H), 7.37 (d, *J* = 7.9 Hz, 1H), 7.57 (d, *J* = 8.0 Hz, 1H), 7.83 (d, *J* = 8.0 Hz, 1H), 7.91 (d, *J* = 7.9 Hz, 1H), 8.07 (s, 1H)

The protons of the terminal OH-groups could be observed in DMSO-d_6:

^{1}H NMR (400 MHz, DMSO-d_6) δ 1.29 (d, *J* = 6.6 Hz, 3H), 2.09 (s, 3H), 2.63 (d, *J* = 15.1 Hz, 1H), 3.70 (q, *J* = 5.2 Hz, 2H), 3.79 (q, *J* = 5.0 Hz, 2H), 3.92-3.97 (m, 1H), 3.98-4.05 (m, 1H), 4.08-4.19 (m, 3H), 4.77 (t, *J* = 5.4 Hz, O*H*), 4.91 (t, *J* = 5.4 Hz, O*H*), 7.11 (s, 1H), 7.30-7.33 (m, 2H), 7.37-7.41 (m, 1H), 7.69 (d, *J* = 7.8 Hz, 1H), 8.02 (s, 1H), 8.04 (d, *J* = 7.6 Hz, 1H), 8.22 (d, *J*= 7.9 Hz, 1H). (1H is is not observed due to overlap with DMSO peak at 3.33 ppm.)

^{13}C NMR (100 MHz, $CDCl_3$) δ 15.9, 18.8, 41.6, 44.9, 61.0, 62.1, 70.5, 74.4, 108.1, 119.5, 120.0, 121.9 (t, *J* = 7.0 Hz), 123.4, 124.9 (t, *J* = 6.3 Hz), 126.6 (t, *J* = 23.7 Hz), 127.1, 127.6, 128.0, 132.1, 133, 5, 137.8, 138.5, 139.5, 142.6, 144.4, 145.6, 152.9, 153.7.

HRMS (ESI) calcd for $C_{32}H_{27}F_9O_4Na$ 669.5304 (MNa^+), found 669.1622.

trans-Dialkyne-perfluorobutyl motor (_trans_-5.9)

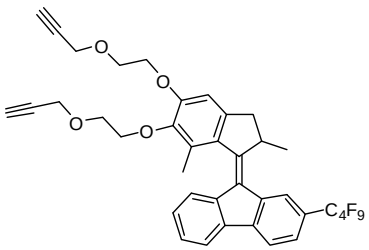

A suspension of NaH (100 mg, 50% in oil, 2.1 mmol) in THF (2 mL) was cooled to 0ºC and a solution of *trans*-**5.8** (90 mg, 0.14 mmol) in THF (4 mL) was added dropwise. Then, propargyl bromide (0.1 mL, 80 % in toluene, 0.9 mmol) was added to this mixture and the resulting solution was stirred at rt for 5 h. The reaction was quenched with water (10 mL) and the mixture was extracted with EtOAc until the yellow color of the aqueous phase had disappeared. The organic phase was washed with water (10 mL) and brine (10 mL) and dried (Na_2SO_4). The solvent was evaporated under reduced pressure and the crude product was purified by column chromatography (SiO_2, *n*-pentane : DCM 1 : 1 → 1 : 2) to give the product as a yellow solid (80 mg, 0.11 mmol, 78 %).

^{1}H NMR (400 MHz, $CDCl_3$) δ 1.35 (d, *J* = 6.7 Hz, 3H), 2.19 (s, 3H), 2.43 (t, *J* = 2.4 Hz, 1H), 2.49 (t, *J* = 2.4 Hz, 1H), 2.59 (d, *J* = 14.7 Hz, 1H), 3.33 (dd, *J* = 6.0, 14.6 Hz, 1H), 3.88-3.95 (m, 2H), 3.99 (t, *J* = 4.7 Hz, 2H), 4.06-4.17 (m, 3H), 4.22-4.37 (m, 2H), 4.30 (d, *J* = 2.4 Hz, 2H) 4.32 (d, *J* = 2.4 Hz, 2H), 6.87 (s, 1H), 7.20 (t, *J* = 7.5 Hz, 1H), 7.32 (t, *J* = 7.4 Hz, 1H), 7.38 (d, *J* = 7.8 Hz, 1H), 7.56 (d, *J* = 8.1 Hz, 1H), 7.81 (d, *J* = 7.4 Hz, 1H), 7.91 (d, *J* = 8.0 Hz, 1H), 8.07 (s, 1H); ^{13}C NMR (100 MHz, $CDCl_3$) δ 16.1, 18.9, 41.5, 44.9, 58.3, 58.6, 68.0, 68.2, 69.3, 71.6, 74.5, 74.7, 108.3, 119.5, 119.9, 121.9 (t, *J* = 7.1 Hz), 123.6, (t, *J* = 6.6 Hz), 126.5 (t, *J* = 23.8 Hz), 127.0, 127.7, 127.8, 132.0, 133.2, 137.6, 138.5, 139.5, 142.6, 143.7, 145.8, 153.1, 154.2
HRMS (APCI) calcd for $C_{38}H_{32}F_9O_4$ 723.2151 (MH^+), found 723.2152.

Irradiation experiment to generate unstable isomer of motor *trans*-5.9:
Motor *cis*-**5.9** (~2 mg) was dissolved in CD_2Cl_2 (~1 mL). This sample was placed in an NMR tube and irradiated at 365 nm at -50ºC at a distance of 2-3 cm from the centre of the lamp. ^{1}H NMR spectra of the sample were taken before, during and after irradiation at -50ºC. No further changes were observed after 7 h of irradiation. The relative integration of the absorptions from the two isomers revealed a photostationary state of stable-cis-**5.9** to unstable-*trans*-**5.9** of 1 : 2.5. After warming the sample to rt, only the stable form was observed by ^{1}H NMR spectroscopy.

stable-*cis*-**5.9** ^{1}H NMR (500 MHz, CD_2Cl_2, -50°C) δ 1.29 (d, *J* = 6.6 Hz, 3H), 2.06 (s, 3H), 2.52 (t, *J* = 2.3 Hz, 1H), 2.55-2.58 (m, 2H), 3.28 (dd, *J* = 5.3, 14.6 Hz, 1H) 3.79-3.85 (m, 2H), 3.9-4.0 (m, 4H), 4.10 (quin, *J* = 6.0 Hz, 1H), 4.14-4.25 (m, 2H), 4.26 (t, *J* = 2.4 Hz, 2H), 4.29 (d, *J* = 2.3 Hz, 2H), 6.88 (s, 1H), 7.39 (t, *J* = 7.3 Hz, 1H), 7.44 ($t_{apparent}$, *J* = 8.0 Hz, 1H), 7.48 (d, *J* = 8.5 Hz, 1H), 7.51 (s, 1H), 7.89-7.92 (m, 3H).
unstable-*trans*-**5.9** ^{1}H NMR (500 MHz, CD_2Cl_2, -50°C) δ 1.41 (d, *J* = 6.3 Hz, 3H), 1.95 (s, 3H), 2.50-2.51 (m, 1H), 2.55-2.59 (absorptions in this region could not be resolved due to overlap with remaining stable-*cis*-**5.9**), 3.40 (dd, *J* = 8.4, 16.1 Hz, 1H), 3.72-4.29 (absorptions in this region could not be resolved due to overlap with remaining stable-*cis*-**5.9**), 6.82 (s, 1H), 7.19-7.22 (m, 2H), 7.28-7.31 (m, 1H), 7.32-7.51 (absorptions in this region could not be resolved due to overlap with remaining stable-*cis*-**5.9**), 7.82 (s, 1H), 7.85 (d, *J* = 7.8 Hz, 1H), 7.89-7.94

(absorptions in this region could not be resolved due to overlap with remaining stable-*cis*-**5.9**)

cis-Dialkyne-perfluorobutyl motor (_cis_-5.9)

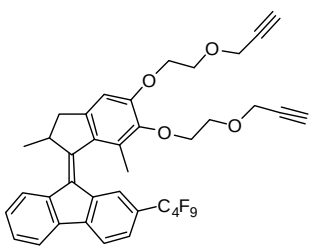

A suspension of NaH (100 mg, 50% in oil, 2.1 mmol) in THF (2 mL) was cooled to 0ºC and a solution of *cis*-**5.8** (140 mg, 0.22 mmol) in THF (5 mL) was added dropwise. Then, propargyl bromide (0.15 mL, 80 % in toluene, 1.35 mmol) was added to this mixture and the resulting solution was stirred at rt for 12 h. The reaction was quenched with water (10 mL) and the mixture was extracted with EtOAc until the yellow color of the aqueous phase had disappeared. The organic phase was washed with water (10 mL) and brine (10 mL) and dried (Na_2SO_4). The solvent was evaporated under reduced pressure and the crude product was purified by column chromatography (SiO_2, *n*-pentane : DCM 2 : 1 → 2 : 3) to give the product as a yellow solid (100 mg, 0.14 mmol, 64 %).

^{1}H NMR (400 MHz, $CDCl_3$) δ 1.33 (d, *J* = 6.7 Hz, 3H), 2.16 (s, 3H), 2.42 (t, *J* = 2.3 Hz, 1H), 2.49 (t, *J* = 2.3 Hz, 1H), 2.57 (d, *J* = 14.6 Hz, 1H), 3.33 (dd, *J* = 5.8, 14.41 Hz, 1H), 3.92 (t, *J* = 4.5 Hz, 2H), 3.99-4.01 (m, 2H), 4.07-4.18 (m, 2H), 4.23-4.37 (m, 7H), 6.88 (s, 1H), 7.38-7.46 (m, 2H), 7.50 (d, *J*= 7.9 Hz, 1H), 7.61 (s, 1H), 7.86-7.92 (m, 3H); ^{13}C NMR (100 MHz, $CDCl_3$) δ 15.6, 19.0, 41.5, 45.1, 58.3, 58.6, 67.9, 68.2, 69.2, 71.8, 74.2, 74.7, 108.5, 119.1, 120.4, 121.7 (t, *J* = 6.5 Hz), 123.8, 125.1 (t, *J* = 5.8 Hz), 126.1 (t, *J* = 23.2 Hz), 126.7, 127.5, 128.0, 131.7, 133.0, 137.7, 138.0, 140.2, 142.2, 144.0, 146.2, 153.5, 154.7.

HRMS (APCI) calcd for $C_{38}H_{32}F_9O_4$ 723.2151 (MH^+), found 723.2152.

Irradiation experiment to generate unstable isomer of motor _cis_-5.9:

Motor *trans*-**5.9** (~2 mg) was dissolved in CD_2Cl_2 (~1 ml). This sample was placed in an NMR tube and irradiated at 365 nm at -50ºC at a distance of 2-3 cm from the centre of the lamp. ^{1}H NMR spectra of the sample were taken before, during and after irradiation at -50ºC. No further changes were observed after 7 h of irradiation. The relative integration of the absorptions from the two isomers revealed a photostationary state of stable-trans-**5.9** to unstable-*cis*-**5.9** of 1 : 1.5. After warming the sample to rt, only the stable forms were observed by ^{1}H NMR spectroscopy.

stable-*trans*-**5.9** ^{1}H NMR (500 MHz, CD_2Cl_2, -50°C) δ 1.29 (d, *J* = 6.6 Hz, 3H), 2.09 (s, 3H), 2.52 (t, *J* = 2.3 Hz, 1H), 2.58 (d, *J* = 14.7 Hz, 1H), 2.59 (t, *J* = 2.5 Hz, 1H), 3.28 (dd, *J* = 5.6, 14.7 Hz, 1H), 3.77-3.86 (m, 3H), 3.94 (t, *J* = 3.9 Hz, 2H), 3.98-4.02 (m, 1H), 4.06 ($t_{apparent}$, *J* = 6.5 Hz, 1H), 4.17-4.32 (m, 2H) 4.24 (d, *J* = 2.0 Hz, 2H), 4.28 (d, *J* = 2.3 Hz, 2H), 6.87 (s, 1H), 7.20 (t, *J* = 7.6 Hz, 1H), 7.30-7.34 (m, 2H), 7.55 (d, *J* = 8.1 Hz, 1H), 7.84 (d, *J* = 7.4 Hz, 1H), 7.95 (d, *J* = 8.0 Hz, 1H), 8.00 (s, 1H).
unstable-*cis*-**5.9** ^{1}H NMR (500 MHz, CD_2Cl_2, -50°C) δ 1.46 (d, *J* = 6.2 Hz, 3H), 1.89 (s, 3H), 2.49-2.51 (m, 1H), 2.55-2.60 (absorptions in this region could not be resolved due to overlap with remaining stable-*trans*-**5.9**), 3.00 (dd, *J* = 5.7, 16.4 Hz, 1H), 3.41 (dd, *J* = 8.4, 16.3 Hz, 1H), 3.74-4.32 (absorptions in this region could not be resolved due to overlap with remaining stable-*trans*-**5.9**), 4.22 (s, 2H), 6.83 (s, 1H), 7.19-7.39 (absorptions in this region could not be resolved due to overlap with remaining stable-*trans*-**5.9**), 7.37 (s, 2H), 7.44 (d, *J* = 7.9 Hz, 1H), 7.74 (d, *J* = 7.7 Hz, 1H), 7.87 (d, *J* = 7.4 Hz, 1H), 7.92 (d, *J* = 7.8 Hz, 1H).

(*E*/*Z*)-2-Bromo-9*H*-fluoren-9-ylidene hydrazine (5.10)

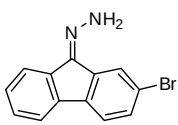

To a stirred suspension of 2-bromo-9*H*-fluoren-9-one **5.2** (3.0 g, 11.0 mmol) in MeOH (30 mL), hydrazine monohydrate (4 mL) was added and the reaction mixture was heated to reflux for 2 h, turning from yellow to orange. The reaction can be followed by TLC (SiO_2, petroleum ether : EtOAc = 5 : 1, $R_{f,\mathbf{5.10}}$ = 0,25 and 0.30 (*E* and *Z*), $R_{f,\mathbf{5.2}}$ = 0,75). The reaction mixture was poured into water (50 mL) and extracted with DCM (2×50 mL). The organic phase was dried ($MgSO_4$) and the solvent was evaporated under reduced pressure to give a pale brown solid. Recrystallization from cyclohexane yielded **5.10** as a mixture of *E* and *Z* isomers (2.73 g, 91%) as pale brown needles. Mp 139°C; ^{1}H-NMR (400 MHz, $CDCl_3$) δ 8.09 – 8.00 (d, *J*= 1.6 Hz, 1H), 7.86 (m, 2H), 7.78–7.66 (m, 2H), 7.65–7.57 (m, 2H), 7.56 (d, *J* = 1.7 Hz, 1H), 7.54–7.47 (m, 1H), 7.47–7.40 (m, 2H), 7.40–7.28 (m, 3H), 6.50 (s, 2H), 6.42 (s, 2H); ^{13}C NMR (50 MHz, $CDCl_3$) δ 144.2, 143.7, 140.2, 140.0, 137.5, 137.1, 132.3, 131.6, 131.1, 129.9, 129.7, 128.6, 128.4 , 128.2, 128.0, 125.3, 123.9, 121.7, 121.6, 121.0, 120.83, 120.80, 120.6, 119.6.
HRMS (ESI): calcd for $C_{13}H_9BrN_2$ 273.0017 (MH^+), found 273.0022; Anal calcd for $C_{13}H_9BrN_2$: C 57.17 %, H 3.32 %, N 10.26 % found: C 57.34 %, H 3.28 %, N 10.19 %.

2-Bromo-9-diazo-9H-fluorene (5.11)

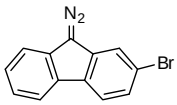

MnO_2 (3.8 g, 44 mmol) was added to a stirred solution of **5.10** (3 g, 11 mmol) in THF (100 mL) upon which the color changed from yellow to red. The resulting suspension was stirred for 5 min and filtered over a plug of sea sand and celite. The solvent was removed under reduced pressure giving **5.11** as a light red solid (2.9 g, 98%). The product was used in the next reaction step without further purification. Mp 121°C; ^{1}H NMR (400 MHz, $CDCl_3$) δ 7.89 (d, *J* = 7.6 Hz, 1H), 7.75 (d, *J* = 8.2 Hz, 1H), 7.60 (s, 1H), 7.52–7.35 (m, 3H), 7.32 (t, *J* = 7.4 Hz, 1H); ^{13}C NMR (50 MHz, $CDCl_3$) δ 134.7, 132.7, 130.5, 130.2, 127.6, 126.7, 124.8, 122.0, 121.0, 120.1, 119.2.
HRMS (APCI): calcd for $C_{13}H_7BrN_2$ ($MH^+ - N_2$) 242.9851, found 242.9803; Anal calcd for $C_{13}H_7BrN_2$: C 57.59 %, H 2.60 %, N 10.33 % found: C 57.49 %, H 2.50 %, N 9.94 %.

(*E*/*Z*)-Diester-bromo motor (5.13)

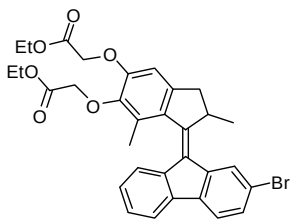

2-bromodiazofluorenone (**5.11**) (1.23 g, 4.7 mmol) was added to a solution of thioketone **2.23** (1.64 g, 4.3 mmol) in toluene (30 mL). The mixture was heated up to 55°C for 3 h. The formation of the episulfide was monitored by ^{1}H NMR spectroscopy by following the shift of the aromatic proton of the thioketone from 6.66 ppm to 6.35 and 6.37 ppm (*E*/*Z* isomers of the episulfide). After the conversion of the thioketone was complete, PPh_3 (1.2 g, 4.7 mmol) was added to the episulfide solution and the mixture was heated for an additional 2 h at 75°C. The reaction mixture was cooled to rt and concentrated *in vacuo.* EtOAc (60 mL) was added to the mixture, which resulted in the precipitation of PPh_3S as yellow crystals. The precipitate was filtered and the procedure was repeated once more. The solvent was removed under reduced pressure. The product was obtained as a mixture of *E* and *Z* isomers (42 : 58) after column chromatography (SiO_2, *n*-hexane : EtOAc = 4 : 1) as a yellow solid (1.6 g, 2.93 mmol, 68 %). ^{1}H NMR (400 MHz, $CDCl_3$) δ 1.30-1.34 (m, 9H major, 9H minor), 2.23 (s, 3H, major), 2.24 (s, 3H, minor), 2.54 (d, *J*= 14.7 Hz, 1H major, 1H minor), 3.29 (dd, *J* = 5.8, 14.76 Hz, 1H major, 1H minor), 4.04-4.15 (m, 1H major, 1H minor), 4.26-4.33 (m, 4H major, 4H minor), 4.67 (d, *J* = 15.8 Hz, 1H major), 4.70 (d, *J* = 15.7 Hz, 1H minor), 4.74 (s, 2H, major), 4.75 (s, 2H, minor), 4.83 (d, *J* = 15.7 Hz, 1H, minor), 4.90 (d, *J* = 15.8 Hz, 1H, major), 6.75 (s, 1H, major), 6.77 (s, 1H, minor), 7.17 (t, *J* = 7.6 Hz, 1H, major), 7.29 (t, *J* =

7.5 Hz, 1H, major), 7.32-7.41 (m, 1H major, 3H minor), 7.45-7.48 (m, 1H major, 1H minor), 7.61 (d, *J* = 8.1 Hz, 1H, minor), 7.66 (d, *J* = 8.1 Hz, 1H, major), 7.71 (d, *J* = 7.3 Hz, 1H, major), 7.76-7.79 (m, 1H, minor), 7.82-7.85 (m, 1H, minor), 7.95 (s, 1H, major)
^{13}C NMR (100 MHz, $CDCl_3$) δ 14.1, 14.2, 16.2, 18.8, 18.9, 41.3, 41.4, 44.7, 44.8, 60.9, 61.0, 61.4, 65.8, 65.9, 68.1, 69.3, 69.7, 108.2, 108.4, 119.1, 119.6, 120.2, 120.3, 120.4, 120.7, 123.6, 123.7, 126.4, 126.7, 126.8, 126.9, 127.0, 127.1, 128.1, 128.4, 129.3, 129.4, 131.9, 132.1, 134.0, 134.2, 137.4, 137.9, 138.4, 138.7, 139.2, 139.3, 141.3, 143.5, 143.7, 145.1, 145.6, 151.2, 151.7, 152.8, 152.9, 168.4, 168.5, 169.3, 169.5
HRMS (ESI) calcd for $C_{32}H_{32}O_6Br$ 591.1377 (MH^+), found 591.1379.
One of the isomers (*Z*) could be crystallized from Et_2O:
^{1}H NMR (400 MHz, $CDCl_3$) δ 1.29-1.35 (m, 9H), 2.23 (s, 3H), 2.55 (d, *J* = 14.9 Hz, 1H), 3.29 (dd, *J* = 5.5, 15.1 Hz, 1H), (quin, *J* = 6.5 Hz, 1H), 4.26-4.33 (m, 4H), 4.67 (d, *J* = 15.9 Hz, 1H), 4.74 (s, 2H), 4.90 (d, *J* = 15.8 Hz, 1H), 6.75 (s, 1H), 7.17 (t, *J* = 7.8 Hz, 1H), 7.29 (t, *J* = 7.2 Hz, 1H), 7.33 (d, *J* = 7.9 Hz, 1H), 7.47 (d, *J* = 8.1 Hz, 1H), 7.66 (d, *J* = 8.1 Hz, 1H), 7.71 (d, *J* = 7.4 Hz, 1H) 7.95 (s, 1H)
^{13}C NMR (100 MHz, $CDCl_3$) δ 14.1, 14.2, 16.2, 18.9, 41.4, 44.8, 60.9, 61.4, 65.8, 69.3, 108.2, 119.1, 120.5, 120.8, 123.6, 126.7, 127.0, 127.1, 128.5, 129.3, 132.1, 134.3, 137.5, 138.2, 138.5, 141.3, 143.5, 145.1, 151.3, 152.8, 168.5, 169.6.

(*E*/*Z*)-Diester-cyano motor (5.14)

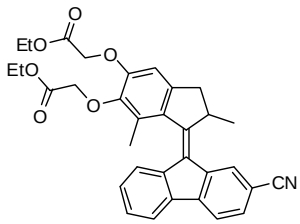

A solution of (*E*/*Z*)-**5.13** (546 mg, 1.00 mmol) in *N*, *N*-dimethylacetamide (22 mL) was added to a mixture of $Pd_2(dba)_3$ (18.5 mg, 0.02 mmol, 2 mol%), dppf (22.3 mg, 0.04 mmol, 4 mol%), Zn powder (13.1 mg, 0.20 mmol, 20 mol%) and $Zn(CN)_2$ (235.0 mg, 2.00 mmol, 200 mol%) flushed with argon and the mixture was heated at 150°C for 5 h. The reaction mixture was cooled to rt, diluted with EtOAc (50 mL), and washed with saturated aq Na_2CO_3 (60 mL), brine (20 mL), dried (Na_2SO_4) and concentrated *in vacuo*. Purification by column chromatography (SiO_2, *n*-hexane : EtOAc = 4 : 1) afforded the product as a mixture of *E* and *Z* isomers (~ 1 : 1) as a yellow solid (479 mg, 0.89 mmol, 89%).
E/*Z* mixture:
^{1}H NMR (400 MHz, CD_2Cl_2) δ 1.26-136 (m, 18H), 2.22 (s, 6H), 2.60 ($dd_{apparent}$, *J* = 3.2, 14.7 Hz, 2H), 3.31 (dd, *J* = 5.7, 14.7 Hz, 2H), 4.05-4.17 (m, 2H),

4.22-4.32 (m, 8H), 4.66 (d, *J* = 15.8 Hz, 1H), 4.77 (s, 4H), 4.81 (d, *J* = 13.6 Hz, 2H), 4.90 (d, *J* = 15.9 Hz, 1H), 6.80 (s, 1H), 6.81 (s, 1H), 7.26-7.49 (m, 5H), 7.58 ($d_{apparent}$, *J* = 7.9 Hz, 1H), 7.64-7.66 (m, 2H), 7.83-7.94 (m, 5H), 8.11 (s, 1H);
^{13}C NMR (125 MHz, $CDCl_3$) δ 14.1, 14.2, 16.2, 18.9, 19.2, 41.4, 44.9, 45.2, 60.9, 61.0, 61.5, 65.7, 65.9, 69.2, 69.3, 108.2, 108.5, 109.4, 109.5, 119.6, 119.8, 120.0, 120.1, 120.2, 120.6, 123.8, 123.82, 127.0, 127.1, 127.2, 127.3, 127.5, 127.6, 128.4, 128.5, 130.1, 130.4, 132.1, 132.3, 133.6, 133.9, 137.3, 137.7, 137.8, 138.3, 139.5, 140.1, 142.6, 143.3, 143.8, 143.9, 145.1, 145.4, 151.6, 151.8, 154.5, 154.7, 168.4, 169.5, 169.6.
HRMS (ESI) calcd for $C_{33}H_{31}NO_6Na$ 560.2044 (MNa^+), found 560.2022.
One of the isomers (*Z*) could be crystallized from Et_2O:
^1H NMR (400 MHz, $CDCl_3$) δ 1.30-1.36 (m, 9H), 2.23 (s, 3H), 2.58 (d, *J* = 14.8 Hz, 1H), 3.31 (dd, *J* = 5.9, 14.7 Hz), 4.07 (quin, *J* = 6.4 Hz, 1H), 4.30 (m, 4H), 4.68 (d, *J* = 15.9 Hz, 1H), 4.75 (s, 2H), 4.92 (d, *J* = 15.9 Hz, 1H), 6.76 (s, 1H), 7.26 (m, 1H), 7.35 (t, *J* = 7.8 Hz, 1H), 7.40 (d, *J* = 7.9 Hz, 1H), 7.63 (dd, *J* = 1.2, 7.9 Hz, 1H), 7.80 (d, *J* = 7.5 Hz, 1H), 7.88 (d, *J* = 7.9 Hz, 1H), 8.09 (s, 1H)
For further characterization of the isomers, a sample of the crystallized product (denoted as major) was irradiated (365 nm, rt, 5h) to generate the other isomer (denoted as minor). (Major : minor 2.3 : 1)
^1H NMR (400 MHz, $CDCl_3$) δ 1.29-1.36 (m, 9H major, 9H minor), 2.23 (s, 3H, major), 2.25 (s, 3H, minor), 2.57 (d, *J* = 14.8 Hz, 1H, minor), 2.58 (d, *J* = 14.8 Hz, 1H, major), 3.31 (dd, *J* = 5.7, 14.6 Hz, 1H major, 1H minor), 4.04-4.16 (m, 1H major, 1H minor), 4.26-4.34 (m, 4H major, 4H minor), 4.68 (d, *J* = 15.9 Hz, 1H, major), 4.75 (s, 2H, major), 4.76 (s, 2H, minor), 4.84 (d, *J* = 3.6 Hz, 2H, minor), 4.92 (d, *J* = 15.9 Hz, 1H, major), 6.76 (s, 1H, major), 6.79 (s, 1H, minor), 7.26 (m, 1H, major), 7.35 (dt, *J* = 1.0, 7.5 Hz, 1H, major), 7.40 (d, *J* = 7.7 Hz, 1H, major), 7.43-7.47 (m, 2H, minor) 7.57 (dd, *J* = 1.4, 7.9 Hz, 1H minor), 7.63 (dd, *J* = 1.3, 7.9 Hz, 1H, major), 7.65 (br s, 1H, minor), 7.80 (d, *J* = 7.3 Hz, 1H, major) 7.83 (d, *J* = 7.4 Hz, 1H, minor), 7.85-7.91 (m, 2H, minor) 7.88 (d, *J* = 7.9 Hz, 1H, major), 8.09 (s, 1H, major)

(*E*/*Z*)-Dihydroxy-cyano motor (5.15)

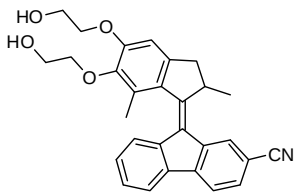

A solution of (*E*/*Z*)-**5.14** (339 mg, 0.63 mmol) in THF (22 mL) was added to a suspension of $LiBH_4$ (14.4 mg, 0.66 mmol) in THF (3 mL) and the mixture was stirred at rt for 90 min. The mixture was diluted with EtOAc (25 mL) and washed with H_2O (20 mL), brine (10mL), dried (Na_2SO_4) and concentrated *in vacuo*. Purification by flash column chromatography (SiO_2, EtOAc) afforded **5.15** as a mixture of isomers (1 : 1.7) as a yellow solid (152 mg, 0.34 mmol, 55%) ^{1}H NMR (500 MHz, $CDCl_3$) δ 1.36 (d, *J* = 6.6 Hz, 3H, minor), 1.37 (d, *J* = 6.7 Hz, 3H, major), 2.18 (s, 3H, minor), 2.19 (s, 3H, major), 2.61 (d, *J* = 14.9 Hz, 1H, minor), 2.62 (d, *J* = 14.8 Hz, 1H, major), 3.34 (dd, *J* = 5.70, 14.8 Hz, 1H major, 1H minor), 3.92-4.23 (m, 9H major, 8H minor), 4.28-4.32 (m, 1H, minor) 6.90 (s, 1H, major) 6.91 (s, 1H, minor), 7.22 (t, *J* = 7.6 Hz, 1H, major), 7.33-7.38 (m, 2H, major), 7.41-7.49 (m, 2H, minor), 7.56 (dd, *J* = 1.3, 7.9 Hz, 1H, minor), 7.63-7.65 (m, 1H major, 1H minor), 7.81-7.85 (m, 1H major, 1H minor), 7.87-7.89 (m, 1H, minor) 7.89 (d, *J* = 7.9 Hz, 1H, major), 7.91 (d, *J* = 7.8 Hz, 1H, minor), 8.10 (s, 1H, major); ^{13}C NMR (125 MHz, $CDCl_3$) δ 155.0, 154.8, 153.4, 153.0, 145.6, 144.6, 144.5, 143.2, 142.8, 140.2, 139.6, 138.5, 137.8, 137.4, 133.3, 133.0, 132.2, 131.9, 130.1, 129.985, 128.6, 128.1, 127.3, 127.3, 127.2, 127.1, 127.0, 123.8, 123.4, 120.7, 120.3, 120.2, 120.1, 119.9, 119.8, 109. 6, 109.1, 108.3, 108.1, 74.4, 74.3, 70.6, 70.6, 64.4, 62.2, 62.0, 61.0, 45.0, 44.8, 41.6, 41.5, 19.2, 18.9, 16.1, 15.9.
HRMS (ESI) calcd for $C_{29}H_{27}NO_4Na$ 476.1832 (MNa^+), found 476.1843.

(*E*/*Z*)-Dialkyne-cyano motor (5.16)

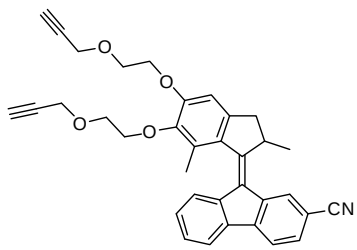

A solution of (*E*/*Z*)-**5.15** (160 mg, 0.35 mmol) in THF (14 mL) was added dropwise to the suspension of NaH (95%, 34.45 mg, 1.36 mmol) in THF (6 mL) and the mixture was stirred at rt for 30 min. To this mixture propargyl bromide (80 % in toluene, 170 µL, 1.53 mmol,) was added. The solution was stirred at rt for 12 h. The mixture was diluted with EtOAc (25 mL) and washed with H_2O (20 mL), brine (10 mL), dried (Na_2SO_4) and concentrated *in vacuo*. Purification by column chromatography (SiO_2, *n*-hexane : EtOAc = 4 : 1) afforded the product as a mixture of *E* and *Z* isomers as a yellow solid (118 mg, 0.22 mmol, 63%).

85 mg (0.16 mmol) of the *E*/*Z* mixture was separated by column chromatography (SiO_2, toluene : Et_2O 20 : 1).

***Cis*-5.16 (**26 mg, 0.05 mmol, 31%, R_f= 0.45) was obtained as a yellow solid.

^{1}H NMR (400 MHz, $CDCl_3$) δ 1.34 (d, *J* = 6.7 Hz, 3H), 2.16 (s, 3H), 2.41 (t, *J* = 2.4 Hz, 1H), 2.49 (t, *J* = 2.4 Hz, 1H), 2.58 (d, *J* = 14.8 Hz, 1H), 3.32 (dd, *J* = 5.7, 14.7 Hz, 1H), 3.92-3.94 (m, 2H), 4.00 (t, *J* = 4.77 Hz, 2H), 4.12 ($quin_{apparent}$, *J* = 8.0 Hz, 1H), 4.23-4.30 (m, 4H), 4.31-4.32 (m, 4H), 6.88 (s, 1H), 7.40 (dt, *J* = 1.1, 7.4 Hz, 1H), 7.45 (dt, *J* = 1.5, 7.6 Hz, 1H), 7.55 (dd, *J* = 1.4, 7.9 Hz, 1H), 7.65 ($d_{apparent}$, *J* = 0.8 Hz, 1H), 7.83 (dd, *J* = 0.5, 7.9 Hz, 1H), 7.87 ($dd_{apparent}$, *J* = 0.9, 7.3 Hz, 1Hz), 7.90 (d, *J* = 7.6 Hz, 1H).

^{13}C NMR (100 MHz, $CDCl_3$) δ 16.1 19.0, 41.5, 45.0, 58.4, 58.6, 68.1, 68.2, 69.3, 72.0, 74.4, 74.8, 108.5, 109.2, 119.7, 119.9, 120.7, 123.8, 126.8, 127.2, 128.5, 130.0, 131.8, 132.8, 137.7, 137.9, 140.2, 142.6, 144.0, 146.2, 153.7, 155.5.

***Trans*-5.16** (40 mg, 0.075 mmol, 47%, R_f=0.55) was obtained as a yellow solid.

^{1}H NMR (400 MHz, $CDCl_3$) δ 1.36 (d, *J* = 6.7 Hz, 3H), 2.18 (s, 3H), 2.43 (t, *J* = 2.3 Hz, 1H), 2.49 (t, *J* = 2.3 Hz, 1H), 2.59 (d, *J* = 14.8 Hz, 1H), 3.32 (dd, *J* = 5.9, 14.8 Hz, 1H), 3.89-3.93 (m, 2H), 3.99 (t, *J* = 4.7 Hz, 2H), 4.03-4.16 (m, 2H), 4.22-4.38 (m, 3H), 4.30 (d, *J* = 2.3 Hz, 2H), 4.32 (d, *J* = 2.4 Hz, 2H), 6.87 (s, 1H), 7.22 (t, *J* = 7.3 Hz, 1H), 7.33 (t, *J* = 7.3 Hz, 1H), 7.38 (d, *J* = 7.9 Hz, 1H), 7.63 (dd, *J* = 0.8, 7.9 Hz, 1H), 7.81 (d, *J* = 7.6 Hz, 1H), 7.88 (d, *J* = 7.9 Hz, 1H), 8.09 (s, 1H);

^{13}C NMR (125 MHz, $CDCl_3$) δ 16.0, 19.3, 41.5, 45.0, 58.3, 58.6, 68.0, 68.2, 69.3, 71.6, 74.6, 74.8, 108.3, 109.5, 120.0, 120.1, 120.3, 123.6, 127.1, 127.1, 127.2, 128.2, 130.0, 132.1, 133.0, 137.3, 138.6, 139.6, 143.2, 143.9, 145.8, 153.3, 155.3.

HRMS (ACPI) calcd for $C_{35}H_{31}NO_4$ 529.2253, found 530.2324 (MH^+)

Irradiation experiment to generate unstable isomers of motor *cis*-5.16:

Motor *trans*-**5.16** (~2 mg) was dissolved in CD_2Cl_2 (~1 mL). This sample was placed in an NMR tube and irradiated at 365 nm at -50ºC at a distance of 2-3 cm from the centre of the lamp. ^{1}H NMR spectra of the sample were taken before, during and after irradiation at -50ºC. No further changes were observed after 7 h of irradiation. The relative integration of the absorptions from the two isomers revealed a photostationary state of unstable-*cis*-**5.16** to stable-trans-**5.16** of 3 : 1. After warming the sample to rt, only the stable forms were observed by ^{1}H NMR spectroscopy.

stable-*trans*-**5.16** ^{1}H NMR (500 MHz, CD_2Cl_2, -50°C) δ 1.30 (d, *J* = 6.5 Hz, 3H), 2.09 (s, 3H), 2.52 (s, 1H), 2.57-2.60 (m, 2H), 3.28 (dd, *J* = 5.5, 14.7 Hz, 1H), 3.77-3.86 (m, 2H), 3.92-3.95 (m, 2H), 3.99-4.06 (m, 2H), 4.18-4.32 (m, 3H), 4.24 (s, 2H), 4.29 (s, 2H), 6.88 (s, 1H), 7.22 (t, *J* = 7.5 Hz, 1H), 7.3-7.34 (m, 2H), 7.65 (d, *J* = 7.9 Hz, 1H), 7.83 (d, *J* = 7.6 Hz, 1H), 7.91 (d, *J* = 7.9 Hz, 1H), 8.09 (s, 1H).
unstable-*cis*-**5.16** ^{1}H NMR (500 MHz, CD_2Cl_2, -50°C) δ 1.45 (d, *J*= 6.4 Hz, 3H), 1.92 (s, 3H), 2.48-2.50 (m, 1H), 2.55-2.60 (absorptions in this region could not be resolved due to overlap with remaining stable-*trans*-**5.16**), 2.98 (dd, *J* = 5.3, 16.0 Hz, 1H), 3.41 (dd, *J* = 8.2, 16.3 Hz, 1H), 3.74-4.31 (absorptions in this region could not be resolved due to overlap with remaining stable-*trans*-**5.16**), 4.22 (d, *J* = 2.2 Hz, 2H), 6.83 (s, 1H), 7.30-7.35 (absorptions in this region could not be resolved due to overlap with remaining stable-*trans*-**5.16**), 7.39 (t, *J* = 7.7 Hz, 1H), 7.47 (s, 1H), 7.53 (dd, *J* = 0.7, 7.9 Hz, 1H), 7.74 (d, *J* = 7.8 Hz, 1H), 7.87 (d, *J* = 7.8 Hz, 2H)

Irradiation experiment to generate unstable isomers of motor *trans*-5.16:
Motor *cis*-**5.16** (~2 mg) was dissolved in CD_2Cl_2 (~1 mL). This sample was placed in an NMR tube and irradiated at 365 nm at -50ºC at a distance of 2-3 cm from the centre of the lamp. ^{1}H NMR spectra of the sample were taken before, during and after irradiation at -50ºC. No further changes were observed after 7 h of irradiation. The relative integration of the absorptions from the two isomers revealed a photostationary state of unstable-*trans*-**5.16** to stable-cis-**5.16** of 5 : 1. After warming the sample to rt, only the stable forms were observed by ^{1}H NMR spectroscopy.

stable-*cis*-**5.16** ^{1}H NMR (500 MHz, CD_2Cl_2, -50°C) δ 1.29 (d, *J* = 6.5 Hz, 3H), 2.08 (s, 3H), 2.51 (s, 1H), 2.56-2.60 (m, 2H), 3.28 (dd, *J* = 5.4, 14.7 Hz, 1H), 3.80-3.88 (m, 2H), 3.95 (t, *J* = 3.6 Hz, 2H), 4.06-4.13 (m, 2H), 4.16-4.24 (m, 3H), 4.27 (s, 2H), 4.29 (d, *J* = 1.4 Hz, 2H), 6.89 (s, 1H), 7.40 (t, *J* = 7.3 Hz, 1H), 7.46 (t, *J* = 7.4 Hz, 1H), 7.57 (s, 2H), 7.85-7.91 (m, 3H).
unstable-*trans*-**5.16** ^{1}H NMR (500 MHz, CD_2Cl_2, -50°C) δ 1.43 (d, *J* = 6.4 Hz, 3H), 1.93 (s, 3H), 2.50-2.60 (absorptions in this region could not be resolved due to overlap with remaining stable-*cis*-**5.16**), 2.98 (dd, *J* = 5.30, 16.4 Hz, 1H), 3.42 (dd, *J* = 8.2, 16.3 Hz, 1H), 3.72-4.13 (absorptions in this region could not be resolved due to overlap with remaining stable-*cis*-**5.16**), 4.20 (d, *J* = 2.2 Hz, 2H), 4.21-4.25 (absorptions in this region could not be resolved due to overlap with remaining

stable-*cis*-**5.16**), 4.28 (d, *J* = 2.2 Hz, 2H), 6.83 (s, 1H), 7.19-7.23 (m, 2H), 7.30 (t, *J* = 7.7 Hz, 1H), 7.57 (d, *J* = 7.6 Hz, 1H), 7.84 (d, *J* = 7.7 Hz, 1H), 7.89 (d, *J* = 7.8 Hz, 1H), 7.98 (s, 1H).

5.8 References

(1) Ulman, A. *Chem. Rev.* **1996**, *96*, 1533-1554.
(2) Bain, C. D.; Whitesides, G. M. *J. Am. Chem. Soc.* **1988**, *110*, 3665-3666.
(3) Bain, C. D.; Whitesides, G. M. *J. Am. Chem. Soc.* **1988**, *110*, 5897-5898.
(4) Nuzzo, R. G.; Dubois, L. H.; Allara, D. L. *J. Am. Chem. Soc.* **1990**, *112*, 558-569.
(5) Janssen, D.; De Palma, R.; Verlaak, S.; Heremans, P.; Dehaen, W. *Thin Solid Films* **2006**, *515*, 1433-1438.
(6) Adams, D. M.; Brus, L; Chidsey, C. E. D.; Creager, S.; Creutz, C.; Kagan, C. R.; Kamat, P. V.; Lieberman, M.; Lindsay S.; Marcus, R. A.; Metzger, R. M.; Michel-Beyerle, M. E.; Miller, J. R.; Newton, M. D.; Rolison, D. R.; Sankey, O.; Schanze, K. S.; Yardley, J.; Zhu, X. Y. *J. Phys. Chem. B* **2003**, *107*, 6668-6697.
(7) Mantooth, B. A.; Weiss, P. S. *Proc. IEEE* **2003**, *91*, 1785-1802.
(8) Coperet, C.; Chabanas, M.; Saint-Arroman, R. P.; Basset, J. M. *Angew. Chem. Int. Ed.* **2003**, *42*, 156-181.
(9) Kakkar, A. K. *Chem. Rev.* **2002**, *102*, 3579-3587.
(10) Amabilino, D. B.; De Feyter, S.; Lazzaroni, R.; Gomar-Nadal, E.; Veciana, J.; Rovira, C.; Abdel-Mottaleb, M. M.; Mamdouh, W.; Iavicoli, P.; Psychogyiopoulou, K.; Linares, M.; Minoia, A.; Xu, H.; Puigmarti-Luis, J. *J. Phys.-Condens. Mat.* **2008**, *20*.
(11) Ariga, K.; Richards, G. J.; Ishihara, S.; Izawa, H.; Hill, J. P. *Sensors* **2010**, *10*, 6796-6820.
(12) Singh, A.; Myerson, A. S. *J. Pharm. Sci.* **2010**, *99*, 3931-3940.
(13) Browne, W. R.; Feringa, B. L. *Annu. Rev. Phys. Chem.* **2009**, *60*, 407-428.
(14) Katsonis, N.; Lubomska, M.; Pollard, M. M.; Feringa, B. L.; Rudolf, P. *Prog. Surf. Sci.* **2007**, *82*, 407-434.
(15) Wang, S. T.; Song, Y. L.; Jiang, L. *J. Photochem. Photobiol. C-Photochem. Rev.* **2007**, *8*, 18-29.
(16) Rau, H. In *Photoisomerization of azobenzenes;* in Rebek, J. F., (Ed.) Photochemistry and Photophysics; CRC Press: Boca Raton, **1990**.

(17) Berkovic, G.; Krongauz, V.; Weiss, V. *Chem. Rev.* **2000**, *100*, 1741-1753.
(18) Rosario, R.; Gust, D.; Hayes, M.; Jahnke, F.; Springer, J.; Garcia, A. A. *Langmuir* **2002**, *18*, 8062-8069.
(19) Siewierski, L. M.; Brittain, W. J.; Petrash, S.; Foster, M. D. *Langmuir* **1996**, *12*, 5838-5844.
(20) Demirel, G. B.; Dilsiz, N.; Cakmak, M.; Caykara, T. *J. Mater. Chem.* **2011**, *21*, 3189-3196.
(21) Min, M.; Bang, G. S.; Lee, H.; Yu, B. C. *Chem. Commun.* **2010**, *46*, 5232-5234.
(22) Lim, H. S.; Han, J. T.; Kwak, D.; Jin, M. H.; Cho, K. *J. Am. Chem. Soc.* **2006**, *128*, 14458-14459.
(23) Rosario, R.; Gust, D.; Garcia, A. A.; Hayes, M.; Taraci, J. L.; Clement, T.; Dailey, J. W.; Picraux, S. T. *J. Phys. Chem. B* **2004**, *108*, 12640-12642.
(24) Koumura, N.; Zijlstra, R. W. J.; van Delden, R. A.; Harada, N.; Feringa, B. L. *Nature* **1999**, *401*, 152-155.
(25) Pollard, M. M.; Lubomska, M.; Rudolf, P.; Feringa, B. L. *Angew. Chem. Int. Ed.* **2007**, *46*, 1278-1280.
(26) Carroll, G. T.; Pollard, M. M.; van Delden, R.; Feringa, B. L. *Chem. Sci.* **2010**, *1*, 97-101.
(27) London, G.; Carroll, G. T.; Landaluce, T. F.; Pollard, M. M.; Rudolf, P.; Feringa, B. L. *Chem. Commun.* **2009**, 1712-1714.
(28) Carroll, G. T.; London, G.; Landaluce, T. F.; Rudolf, P.; Feringa, B. L. *ACS Nano*, **2011**, *5*, 622-630.
(29) Pei, J.; Ni, J.; Zhou, X. H.; Cao, X. Y.; Lai, Y. H. *J. Org. Chem.* **2002**, *67*, 4924-4936.
(30) Facchetti, A.; Deng, Y.; Wang, A. C.; Koide, Y.; Sirringhaus, H.; Marks, T. J.; Friend, R. H. *Angew. Chem. Int. Ed.* **2000**, *39*, 4547-4551.
(31) Li, Y.; Tan, L.; Wang, Z. H.; Qian, H. L.; Shi, Y. B.; Hu, W. P. *Org. Lett.* **2008**, *10*, 529-532.
(32) Barton, D. H. R.; Willis, B. J. *J. Chem. Soc. Perkin Trans.* **1972**, *1*, 305-310.
(33) Buter, J.; Wassenaa.S; Kellogg, R. M. *J. Org. Chem.* **1972**, *37*, 4045-4060.
(34) Cnossen, A.; Pijper, D.; Kudernac, T.; Pollard, M. M.; Katsonis, N.; Feringa, B. L. *Chem. Eur. J.* **2009**, *15*, 2768-2772.
(35) Pijper, D.; Feringa, B. L. *Angew. Chem. Int. Ed.* **2007**, *46*, 3693-3696.
(36) Vicario, J.; Meetsma, A.; Feringa, B. L. *Chem. Commun.* **2005**, 5910-5912.

(37) Vicario, J.; Walko, M.; Meetsma, A.; Feringa, B. L. *J. Am. Chem. Soc.* **2006**, *128*, 5127-5135.
(38) Jin, F. Q.; Confalone, P. N. *Tetrahedron Lett.* **2000**, *41*, 3271-3273.
(39) Pollard, M. M.; Wesenhagen, P. V.; Pijper, D.; Feringa, B. L. *Org. Biomol. Chem.* **2008**, *6*, 1605-1612.
(40) Schultefrohlinde, D.; Gorner, H. *Pure Appl. Chem.* **1979**, *51*, 279-297.
(41) King, N. R.; Whale, E. A.; Davis, F. J.; Gilbert, A.; Mitchell, G. R. *J. Mater. Chem.* **1997**, *7*, 625-630.
(42) Lapouyade, R.; Czeschka, K.; Majenz, W.; Rettig, W.; Gilabert, E.; Rulliere, C. *J. Phys. Chem.* **1992**, *96*, 9643-9650.
(43) Pollard, M. M.; Meetsma, A.; Feringa, B. L. *Org. Biomol. Chem.* **2008**, *6*, 507-512.
(44) Lummerstorfer, T.; Hoffmann, H. *J. Phys. Chem. B* **2004**, *108*, 3963-3966.
(45) Chelmowski, R.; Kafer, D.; Koster, S. D.; Klasen, T.; Winkler, T.; Terfort, A.; Metzler-Nolte, N.; Woll, C. *Langmuir* **2009**, *25*, 11480-11485.
(46) Collman, J. P.; Devaraj, N. K.; Chidsey, C. E. D. *Langmuir* **2004**, *20*, 1051-1053.
(47) Prakash, S.; Long, T. M.; Selby, J. C.; Moore, J. S.; Shannon, M. A. *Anal. Chem.* **2007**, *79*, 1661-1667.
(48) Fryxell, G. E.; Rieke, P. C.; Wood, L. L.; Engelhard, M. H.; Williford, R. E.; Graff, G. L.; Campbell, A. A.; Wiacek, R. J.; Lee, L.; Halverson, A. *Langmuir* **1996**, *12*, 5064-5075.
(49) Heise, A.; Stamm, M.; Rauscher, M.; Duschner, H.; Menzel, H. *Thin Solid Films* **1998**, *327*, 199-203.
(50) Durfor, C. N.; Turner, D. C.; Georger, J. H.; Peek, B. M.; Stenger, D. A. *Langmuir* **1994**, *10*, 148-152.
(51) Coleman, A. C.; Areephong, J.; Vicario, J.; Meetsma, A.; Browne, W. R.; Feringa, B. L. *Angew. Chem. Int. Ed.* **2010**, *49*, 6580-6584.
(52) Ichimura, K.; Oh, S. K.; Fujimaki, M.; Matsuzawa, Y.; Nakagawa, M. *J. Incl. Phenom. Macrocycl. Chem.* **1999**, *35*, 173-183.
(53) Wu, S. In *Polymer Interface and Adhesion*, Marcel Dekker, New York, **1982**.
(54) Wu, S. *J. Polymer Sci. C* **1971**, 34, 19.
(55) Fujimaki, M.; Kawahara, S.; Matsuzawa, Y.; Kurita, E.; Hayashi, Y.; Ichimura, K. *Langmuir* **1998**, *14*, 4495-4502.
(56) Ichimura, K.; Oh, S. K.; Nakagawa, M. *Science* **2000**, *288*, 1624-1626.
(57) Dorrer, C.; Ruhe, J. *Soft Matter* **2009**, *5*, 51-61.

(58) Gao, X. F.; Jiang, L. *Nature* **2004**, *432*, 36-36.
(59) Tuteja, A.; Choi, W.; Ma, M. L.; Mabry, J. M.; Mazzella, S. A.; Rutledge, G. C.; McKinley, G. H.; Cohen, R. E. *Science* **2007**, *318*, 1618-1622.

Chapter 6
Light-induced control of protein translocation by the SecYEG complex

An azobenzene photoswitch was introduced into a protein-conducting pore. Reversible switching of the azobenzene unit between the trans and cis isomeric forms by irradiation with either visible or UV light resulted in the opening and closing of the protein-conducting pore.[*]

[*]This chapter has been published:
Bonardi, F.; London, G.; Nouwen, N.; Feringa, B. L.; Driessen, A. J. M. *Angew. Chem. Int. Ed.* **2010**, *49*, 7234-7238

6.1 Introduction

The convergence of research efforts in molecular biology and synthetic chemistry has opened new avenues so that much deeper insights into biological phenomena can be gained, including the reproduction, control and engineering of functions of natural occurring systems[1-3]. Recently, this synergistic approach has been extended to the exploration of biological motors and the incorporation of molecular switches into proteins. The use of biomolecular motors interfaced with synthetic systems,[4] the allosteric control of a glutamate sensitive protein *via* photochemical switching,[5] and the design of a light-actuated nanovalve derived from MscL that controls ion flow through a lipid bilayer[6,7] are all illustrative of this approach.

In nature, many proteins synthesized in the cell have to cross or to be incorporated into lipid bilayers. In bacteria, a membrane protein channel, SecYEG, together with a motor protein, SecA, accomplishes this task (Figure 1). Once a hydrophobic signal sequence-containing protein (preprotein) is synthesized,[8] it is brought by the molecular chaperone SecB to SecA. SecA then initiates cycles of ATP hydrolysis in order to translocate the preprotein across the SecYEG channel.[9]

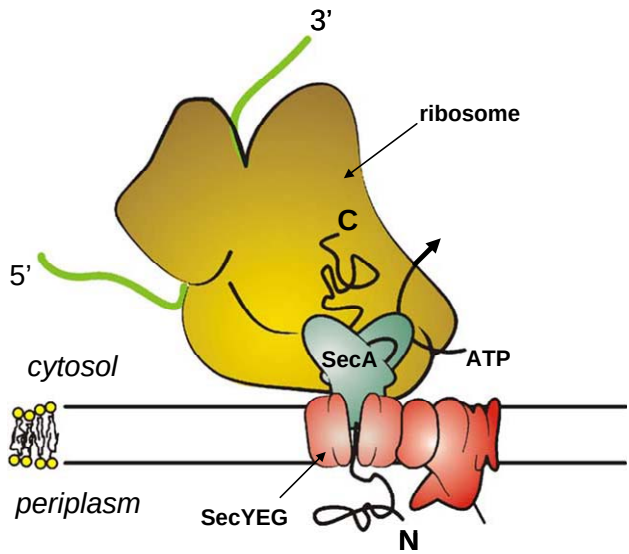

Figure 1 Schematic representation of the preprotein translocase of *E. coli*.

The main subunit of this complex, SecY, (Figure 2a) comprises two times five transmembrane segments (TM) that are arranged as a clamshell-like structure encompassing a central pore.[10-12]

The pore contains a lateral gate or hydrophobic crevice between the TM 2 and TM 7 segments (Figure 2 a) that provides an opening of the central pore to the interior of the lipid membrane. The lateral gate is believed to widen upon the binding of the motor protein SecA and the ATP-dependent insertion of the signal sequence and unfolded preprotein substrate into the translocation pore. Recently, it has been shown that when the lateral gate is constrained by specific introduction of a disulfide bridge or a chemical crosslink spanning 5 Å or less, the translocation activity of the SecYEG complex is blocked.[13] However, when cross-linkers are introduced with a span of 10 Å or larger, the pore is fully active,[13] suggesting that the lateral gate indeed needs to open during pre-protein translocation (Figure 2a).

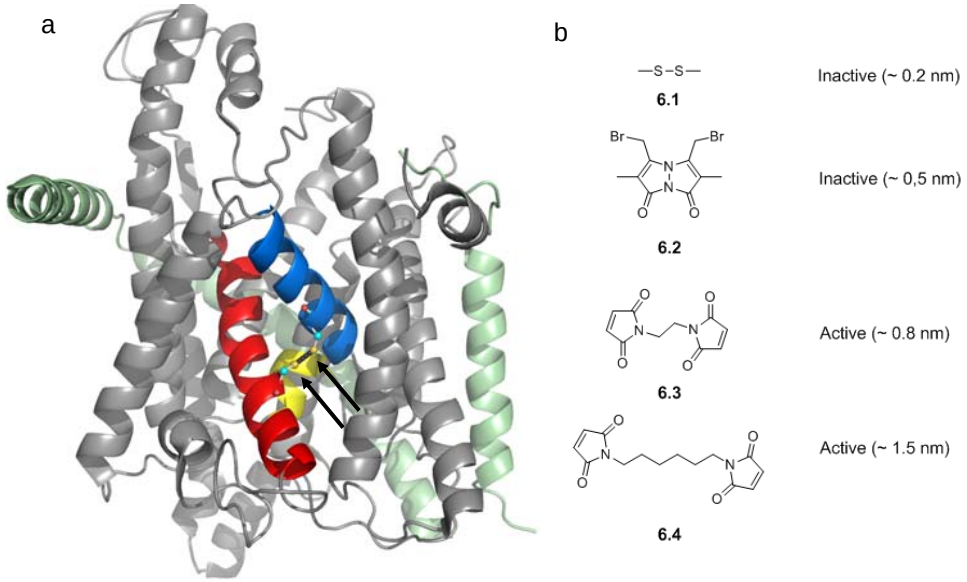

Figure 2 (a) Induced cysteine mutations (indicated by arrows) in TM2 (blue) and TM7 (red) segments of the lateral gate of SecY. (b) Introduction of cross-linkers spanning 0.5 nm or less blocks the translocation activity of the SecYEG complex.

Indeed, analysis of the SecY structure reveals that in the closed state the distance between the sulfur atoms of the introduced cysteines in the lateral gate is about 5 Å, while in the pre-open state it is about 13 Å (Figure 2a).[10-12] The disadvantage of such a chemical cross-linking approach is that the channel is irreversibly immobilized in a single and specific conformation. However, the proposed conformational switching behavior of the lateral gate of SecY makes it a good candidate for modification with an optical switch in order to control its activity and determine the overall channel flexibility in a reversible and non-invasive manner.

6.2 Control of protein translocation with an azobenzene photoswitch

Azobenzenes (Scheme 1) are very attractive to study light-driven experiments, since their photo-isomerization (*trans* (*E*)→*cis* (*Z*)) is one of the simplest photochemical processes known to date.[14] This process is fully reversible, so azobenzenes can undergo innumerable reaction cycles. Furthermore, the isomerization induces large structural changes in conformation and size, and in the dipole moment. Because of these particular properties azobenzenes have proven to be useful not only in material sciences[1, 2] but also for biological studies to induce changes in protein conformation.[15-18]

6.2.1 Structural considerations and synthesis of an azobenzene switch

A major advantage of azobenzene switches is the ease of their synthesis. However, an important drawback is that, depending on the substituent at the aromatic rings, they can undergo thermal *cis* → *trans* isomerization at significant rates.

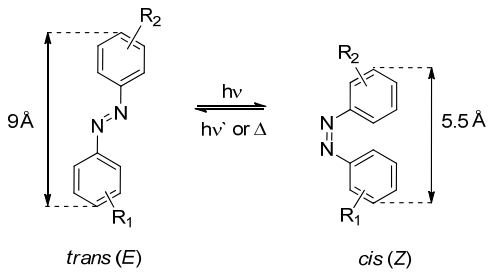

Scheme 1 Photo-isomerization of azobenzenes results in a large geometrical change in their structure.

The thermal isomerisation of the azobenzene unit is an important issue as the half-life of the thermal process determines the usefulness of the switch in certain applications. It has been shown in earlier studies that the metastable *cis*-azobenzene will thermally relax to the *trans* state on a timescale dictated by its ring-substitution pattern and local environment[19-21] (Scheme 2).

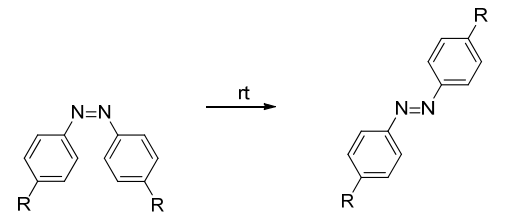

	R	$t_{1/2}$
6.5	CH_3	2-3 d
6.6	OCH_3	8-13 h

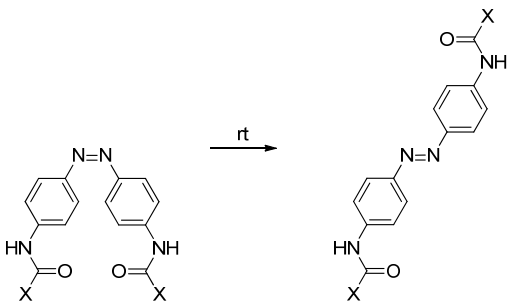

	X	$t_{1/2}$
6.7	$-H_2C-S(=O)(=O)-CH_3$	12 min
6.8	$-O-(CH_2)_2-S(=O)(=O)-CH_3$	80 s
6.9	$-N(H)-(CH_2)_2-S(=O)(=O)-CH_3$	11 s

Scheme 2 Lifetimes of *cis*-azobenzenes are strongly influenced by the substituents on the aromatic rings.

If electron-donating groups were attached at the *para*-positions the *cis*-to-*trans* thermal isomerization took place in a faster timescale (Scheme 2), which could be explained by the increased N-N single-bond character in the azobenzene (Scheme 3a).[19,21,22] However, when sp^3-carbon atoms were attached (Scheme 2), the possibility for extended delocalization was decreased and longer half-lives were obtained (Scheme 3).[19,21] Additionally, bulky substituents (e.g., polymers, oligo-peptides) on the aromatic rings also hinder the thermal back-reaction.[23,24]

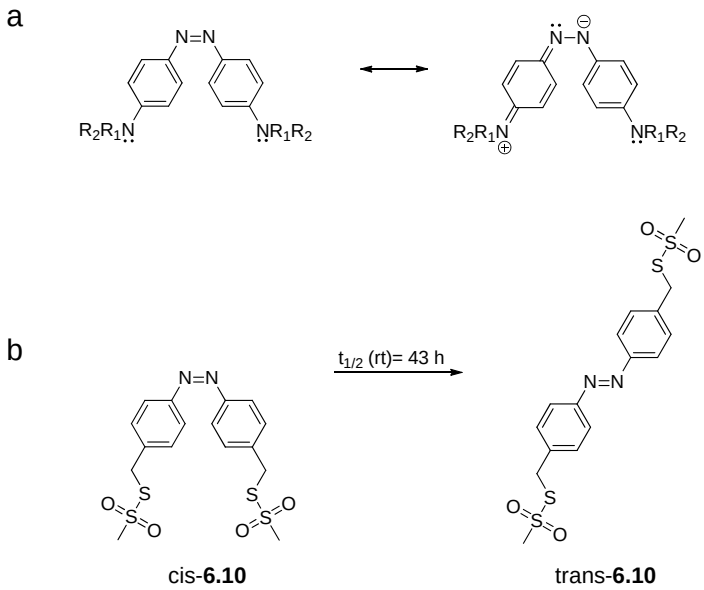

Scheme 3 (a) Two resonance forms of a *para*-substituted diaminoazobenzene. The increased single-bond carachter contributes to the faster *cis*-to-*trans* thermal isomerization. (b) Increased thermal stability of the *cis* form could be obtained by introducing sp^3-carbon atoms in the *para* positions due to the lack of extended delocalization.

Taking into account the above mentioned structural considerations an azobenzene derivative containing two bromine-atoms at benzylic positions, *para* to the azo-function was synthesized.[25-27]

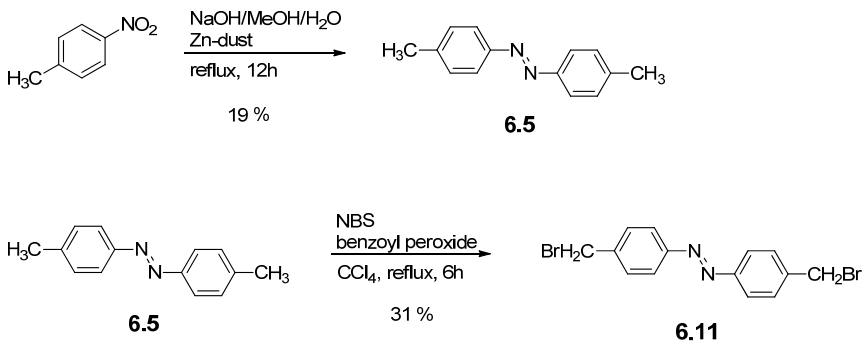

Scheme 4 Synthesis of 4,4'-bis(bromomethyl)azobenzene **6.10.**

The synthesis of the 4,4'-bis(bromomethyl)azobenzene **6.11**[25] was started from p-nitrotoluene which was treated with Zn-powder under basic conditions to yield 4,4'-dimethylazobenzene **6.5**. Bromination of **6.5** with NBS in the presence of benzoyl peroxide afforded **6.10** in 31 % yield.

6.2.2 Incorporation of the azobenzene switch into the SecYEG protein complex

Azobenzene **6.11** functionalized with two bromine atoms was expected to be able to form a cross-link between two specific cysteine positions engineered in TM2 and TM7 of SecY that are part of the lateral gate (Figure 2a). *Escherichia coli* inner membrane vesicles (IMVs) containing the SecYEG modified with two cysteines were incubated with increasing amounts of **6.11** After the treatment the efficiency of bifunctional modification of SecY was assessed by the use of a specific protease, OmpT.[13] This protease cleaves SecY at a double arginine motif, and a successful cleavage of SecY results in the formation of N- and C-terminal degradation products that can be identified by sodium dodecyl sulfate polyacrylamide gel electrophoresis (SDS-PAGE) and coomassie brilliant blue staining (Figure 3a, lane 3). In contrast, when the two cysteines in TM2 and TM7 are linked covalently by **6.11** the OmpT treated SecY protein migrates as a full-length protein on SDS-PAGE (Figure 3a, lane 2). Under the same conditions, the cysteine-less SecYEG complex is cleaved by OmpT both in the absence and presence of **6.11** showing that the OmpT activity is not blocked by the azobenzene. The maximal efficiency of modification was approximately 80% at a **6.11** concentration of 200 μM (Figure 3b).

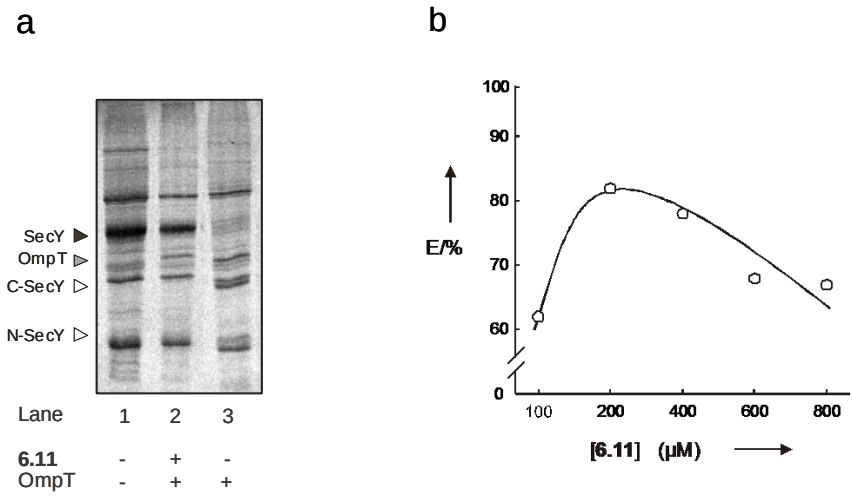

Figure 3 (a) OmpT assay performed on IMVs containing SecY(F286C/S87C)EG complex incubated with **6.11**. OmpT-treated SecY migrates as the uncleaved protein (lane 2). In the presence of tris(2-carboxyethyl)phosphane SecY is cleaved (lane 3). N-SecY and C-SecY indicate the N-terminal and C-terminal fragment, respectively. (b) Optimization of the crosslinking efficiency was performed with IMVs containing SecY(F286C/S87C)EG complex incubated with increasing amounts of **6.11** at 37°C for 2 h, followed by OmpT cleavage to determine the extent of the crosslinking.

6.2.3 Light-induced switching inside SecYEG protein complex

To analyze if the *cis/trans* isomerization takes place after the azobenzene was incorporated into SecY, the azobenzene-derivatized SecYEG complex was purified by Ni-NTA affinity chromatography and the protein was analyzed by UV/Vis spectroscopy. The absorbance spectrum of the free **6.11** in DMSO in the *trans* geometry has a characteristic absorbance at 340 nm that decreases in intensity upon UV irradiation (λ_{max}=365 nm) (Figure 4a). The absorption spectrum of the SecY-**6.11** complex shows the characteristic 340 nm maximum observed for the *trans* form of the free azobenzene in DMSO (Figure 4b), which decreases in intensity upon UV irradiation and re-appears upon irradiation with visible light[28,29] (Figure 4c) comparable with photochemical behavior of azobenzene-based peptides reported previously.[28-31] These results indicate that the light-induced *trans*/*cis* and *cis*/*trans* isomerizations of **6.11** are retained when the optical switch is conjugated to SecY.

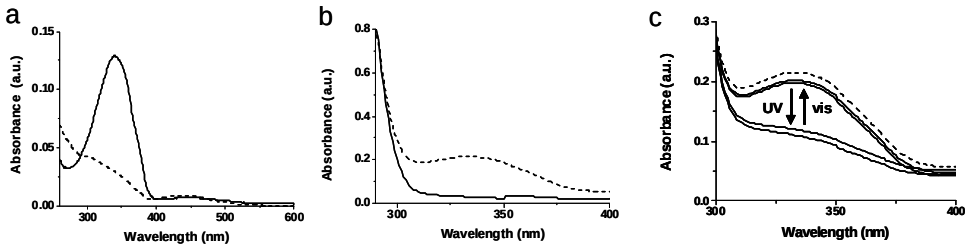

Figure 4 Spectral analysis of optical switching of **6.10** in solution and conjugated to SecY. a) UV-Vis spectra of the molecular switch **6.11** dissolved in DMSO when irradiated with white light (solid line) and after irradiation with 365 nm UV light (dashed line). b) UV-Vis spectra of purified SecYEG complex without (solid line) and with crosslinking with **6.11** (dashed line). c) Cycles of UV and visible light irradiation performed on the SecY-**6.10** complex (initial UV-vis absorption of the complex is indicated by dashed line).

6.2.4 Effect of isomerization on the translocation activity

In order to analyze the effect of the isomerization of **6.11** on the SecYEG translocation activity, IMVs containing the SecY-**6.11** conjugate were exposed to UV or to visible light and subsequently used in an *in vitro* translocation reaction employing fluorescein-labeled preprotein proOmpA as substrate (Scheme 5).

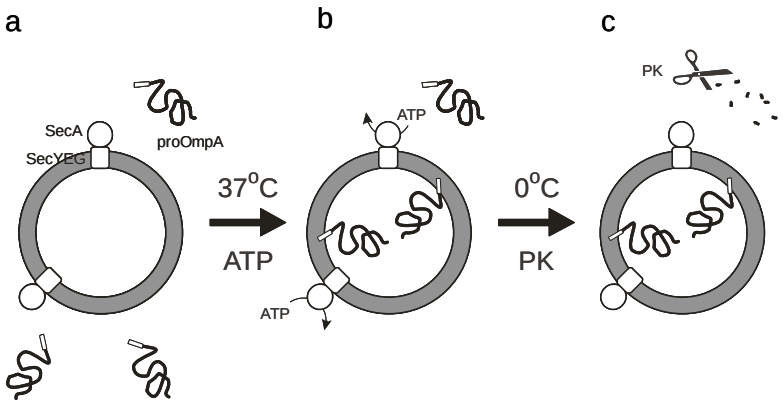

Scheme 5 Scheme of an *in vitro* translocation reaction. a) The fluorescein-labeled precursor of OmpA (proOmpA) is diluted into a buffer containing inner membrane vesicles (IMVs) of *E. coli* harboring the translocase complex (SecA ATPase motor protein and the SecYEG protein conducting channel). b) A fraction of the proOmpA is translocated into the IMVs upon adding ATP to fuel the reaction at 37 ºC. c) Once the reaction is completed, proteinase K (PK) is added that digests all non-translocated proOmpA whereas the translocated proOmpA is protected by the membrane.

The fluorescein-labeled precursor of OmpA (proOmpA) was diluted into a buffer containing inner membrane vesicles (IMVs) of *E. coli* harboring the translocase complex (SecA ATPase motor protein and the SecYEG protein conducting channel). Then the IMV suspension is heated to 37 ºC and ATP is added to fuel the reaction. A fraction of the proOmpA is translocated into the IMVs. Once the reaction was completed the IMV suspension is chilled on ice and proteinase K (PK) is added that digests all non-translocated proOmpA whereas the translocated proOmpA is protected by the membrane against proteinase K digestion. Next, the samples were analyzed on SDS-PAGE and the fluorescent proOmpA was visualized by in-gel fluorescence detection.

IMVs containing the *trans*-**6.11**-conjugated SecY translocated proOmpA with a similar efficiency as IMVs containing non-conjugated SecY (Figure 3a, lane 2 vs. 4). By contrast, UV irradiation of the IMVs containing *trans*-**6.11**-conjugated SecY resulted in a 3-5 fold decrease in the translocation of proOmpA due to the formation of excess *cis*-azobenzene, which causes the contraction of the channel (lane 3).

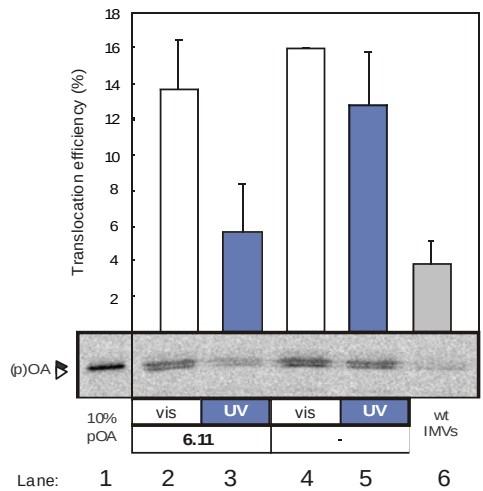

Figure 5 Light induced control of SecY lateral gate. Fluorescein-labeled proOmpA translocation performed with IMVs containing **6.11** cross-linked SecY when irradiated with white light (lane 2) and after irradiation with UV light (lane 3), and IMVs containing untreated SecY when irradiated with white light (lane 4) and after UV light (lane 5) irradiation. Translocation performed with IMVs containing wild type levels of SecY (lane 6) and 10% of fluorescent input proOmpA (lane 1).

Cis-**6.11** was found to be thermally stable under our measurement conditions[32]. UV irradiation of IMVs containing non-conjugated SecY did not significantly affect translocation (lane 5). These IMVs also contain endogenous levels of wild-type SecYEG complex which do not contain the cystein mutation, therefore do not cross-linked with azobenzene switches. The translocation activity of wild-type IMVs (lane 6) was similar to the activity of UV-irradiated IMVs containing the **6.11**-conjugated SecY (compare lane 6 vs. 3) suggesting that the low residual activity is largely due to the presence of endogenous wild type SecY that does not react with **6.11**. It has to be noted, however, that the incomplete *trans*/*cis* photostationary state can contribute to the residual activity as well, and that some photodegradation of the switch during the irradiation cycles can not entirely be excluded.[33]

To confirm that the reduction in translocation efficiency is indeed due to the *trans*/*cis* isomerization of **6.11** in the bifunctionally modified SecY subunit upon irradiation, we analyzed proOmpA translocation in IMVs which contained only one of the two cysteines (S87C or F286C) in the lateral gate of SecY. The single cystein was labeled with the optical switch 4-bromomethyl-4'-methylazobenzene (**6.12**)[25] containing only one reactive functional group. (Scheme 6)

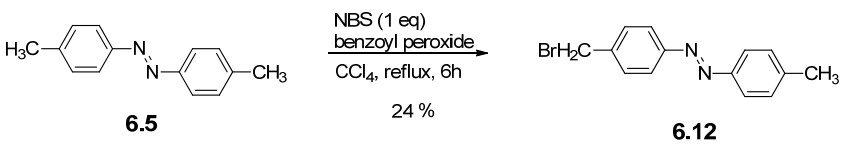

Scheme 6 Synthesis of 4-bromomethyl-4'-methylazobenzene (**6.12**).

Incorporation of **6.12** into the SecYEG complex had no effect on the translocation of proOmpA when irradiated with visible or UV light. As previously noted,[13] the introduction of the S87C mutation, however, slightly reduced the activity of the SecYEG complex as compared to the cysteine-less variant (Figure 6).

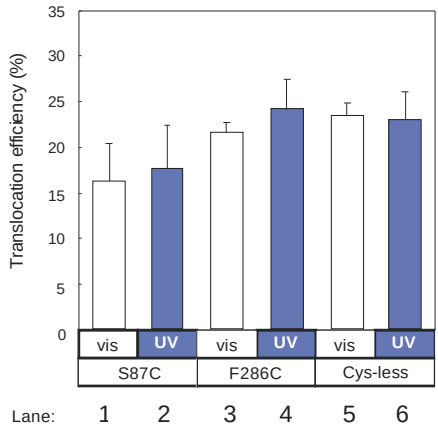

Figure 6 Control mutants SecY(S87C)EG, SecY(F286C)EG and cysteine-less SecY were labeled with 4-bromomethyl-4'-methylazobenzene (**6.12**) and tested for translocation after irradiation with UV and visible light.

The reversibility of the UV-induced inactivation of the protein translocation activity of **6.11**-conjugated SecY was also analyzed. To this end, IMVs containing the SecY-**6.11** hybrid were sequentially irradiated with visible and UV light and tested for translocation activity directly after each light exposure. After illumination with visible light (Figure 3c, lane 1), subsequent irradiation of SecY-**6.11** IMVs with UV light inhibits proOmpA translocation (lane 2). Next, illumination with visible light re-activates these IMVs for proOmpA translocation nearly to the original level (lane 3). A 2nd irradiation with UV light again inhibits proOmpA translocation (lane 4). These data show that the light induced opening and closing of the lateral gate is reversible.

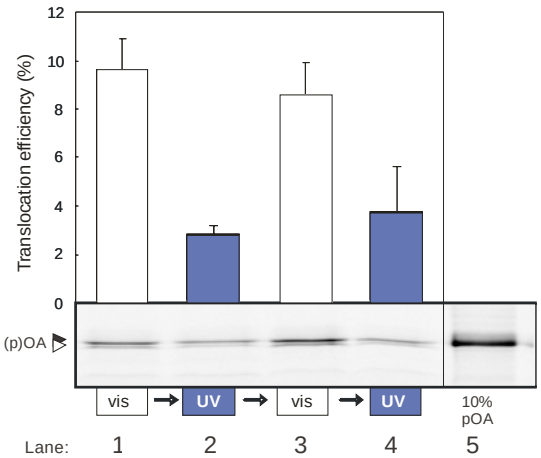

Figure 7 Multiple rounds of light induced opening and closing of SecY lateral gate. Translocation of fluorescein-labeled proOmpA was assayed with IMVs containing overexpressed levels of SecY(S87C/F286C)EG complex crosslinked with **6.11**, that in consecutive cycles were exposed to visible light (lanes 1 and 3) and 365 nm irradiation (lanes 2 and 4). The efficiency of translocation was quantified relatively to the 10% standard of fluorescein-labeled proOmpA (lane 5).

These observations demonstrate the importance of an opened lateral gate between TM2 and TM7 for translocation. When these two transmembrane segments are constrained relative to each other at a distance of ~ 5 Å as induced in the *cis* geometry of the optical switch, the translocation channel cannot open and therefore the translocation is blocked. The SecA motor utilizes ATP to drive pre-protein translocation, an activity termed translocation ATPase. When SecA was tested for the translocation of proOmpA, the translocation ATPase activity decreased in the case of the UV-induced closed conformation of the pore compared to the visible light induced open conformation or the non-crosslinked SecY. This reduction in ATPase activity is not as large as noted for cysteine containing SecYEG complex in which the lateral gate is maximally constrained by a disulfide bridge but compares well with a dibromobimane (**6.2**) crosslinked lateral gate.[13] Thus the presence of the bridging azobenzene switch in its *cis* configuration hinders the movement of the lateral gate to a sufficient extent so as to interfere with the activation of the SecA translocation ATPase. With the optical switch some flexibility seems to be retained to allow for a reduced ATPase activity but this is insufficient to support translocation.

6.3 Discussion

Introduction of cysteine mutants in TM2 and TM7 allowed for an efficient crosslinking of the lateral gate. The positions of the cysteine mutations, as shown in earlier studies[13], define a minimum spacer-length which is suitable for efficient crosslinking. Depending on the length of the cross-linker and the distance of a given pair of cysteine mutation, the gate can be either closed or opened. These characteristics of the pore set the requirements for the design of responsive molecules to control the opening and closing of the gate. The thiol groups of the introduced cysteins have to be accessible for crosslinking with switches, but also the geometrical isomerization upon switching has to be large enough to induce structural changes that can influence the translocation properties. The importance of the structure of the switch at a given set of cysteine mutations was demonstrated by the introduction of an azobenzene switch functionalized with two maleimide groups. Maleimides are known to react easily with sulphur nucleophiles through conjugate addition reactions.
Azophenyl-*p*-*N*,*N*'-dimaleimide was synthesized from 4,4'-diaminoazobenzene and maleic anhydride.[34]

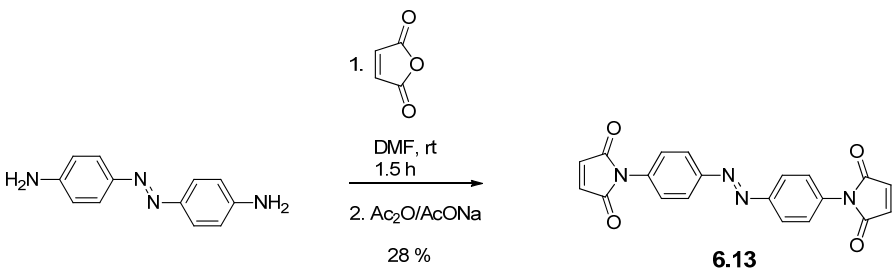

Scheme 7 Synthesis of azophenyl-*p*-*N*,*N*`-dimaleimide **6.13**.

Crosslinking cysteines introduced in the TM2 and TM7 transmembrane segments (Figure 2a) with **6.13** found to be challenging and provided the cross-linked protein in low yields. In a different approach to tune further the control over the functioning of the gate, cysteines was introduced to TM3 and TM7 (Figure 8) transmembrane segments. In this case, probably due to the better steric accessibility of this region of the protein by the switch, crosslinking was more

efficient. Optimization of the cross-linking process and photochemical studies of the system is currently ongoing.

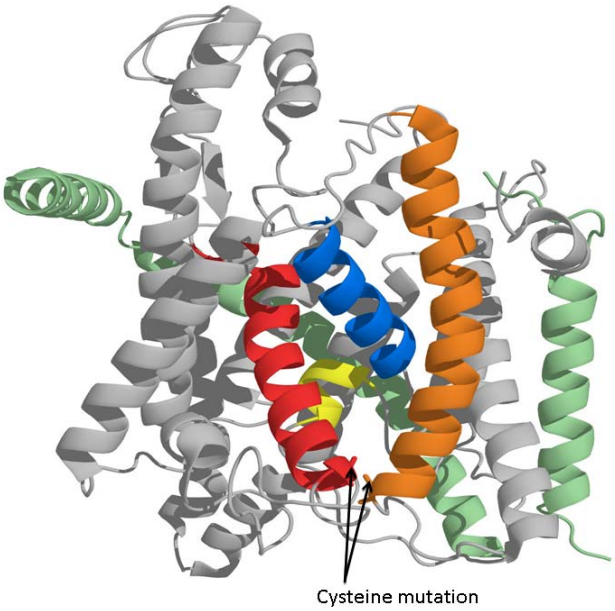

Figure 8 SecY subunit of the SecYEG protein translocation complex with cystein mutations (indicated by arrows) induced in TM3 (orange) and TM7 (red) transmembrane segments.

Further research related to the modification of the transmembrane channel at different positions with different photo-switches is conducted in collaboration with the Molecular Biology Department of the Groningen Biomolecular Sciences and Biotechnology Institute.

6.4 Conclusions

This study shows that the incorporation of a photoswitchable compound into the lateral gate of the protein conducting channel allows for reversible optical control of the SecY pore opening and closing, and therefore control of a translocation event. These results provide strong support for the requirement for an increase in the distance between TM2 and TM7 as an essential step during protein

translocation. Furthermore this is the first example of direct control of the activity of a membrane protein translocation channel. It represents a step forward in the direction of a biological system with added functionality, with potential applications in structural biology research that benefits from external control of conformational changes without perturbation of the system.

6.5 Acknowledgement

The incorporation of the azobenzene switches into the SecYEG protein complex and the protein translocation experiments described in this chapter were performed by Francesco Bonardi (University of Groningen) who is acknowledged for his contribution.

6.6 Experimental

6.6.1 General remarks

For general remarks related to the synthesis and characterization of compounds and intermediates see Chapter 2.

SecA[35] and SecB[36] were purified as described. Inner membrane vesicles (IMVs) containing overexpressed levels of SecY(F286C/S87C)EG, SecY(F286C)EG, SecY(S87C)EG and cysteine-less SecYEG complex were obtained from *E. coli* strain SF100 transformed with plasmid pFE-SecY16, pFESecY10, pFESecY5, and pEK20, respectively[13]. OmpT was expressed from plasmid pND9 in strain SF100 and expressed under its own temperature sensitive promoter.[37] The proOmpA cysteine mutant S245C was constructed with the QuickChange site-directed mutagenesis kit (Stratagene, La Jolla, CA) using pET2345 containing the cysteine-less proOmpA[38] as a template[39]. ProOmpA(S245C) was purified as described[40] and further referred to as proOmpA.

6.6.2 Synthesis of compounds and intermediates

4,4'-dimethylazobenzene (6.5)[25]

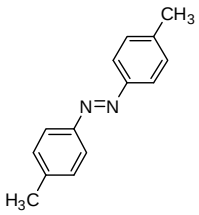

A solution of NaOH (4.5 g, 112.5 mmol) in H_2O (10 mL) and Zn dust (4 g, 61.2 mmol) was added to a stirred solution of *p*-nitrotoluene (3.5 g, 25.5 mmol) in methanol (30 mL). The reaction mixture was stirred and heated at reflux for 12 h and was filtered while still hot. Evaporation of the filtrate *in vacuo* gave an orange solid. Part of the product that remained in the filter was recovered by a subsequent extraction with methanol. The combined products were then stirred in 2% aq. HCl, and filtered. The product was washed with hot water (5×20 mL) and then recrystallized twice from ethanol to yield **6.5** as orange crystals (1 g, 4.76 mmol, 19%). Mp 142.1-143°C. ^{1}H NMR (400 MHz, $CDCl_3$) δ 2.43 (s, 6H), 7.3 (d, J = 8.4 Hz, 4H), 7.8 (d, J = 8.4 Hz, 4H); ^{13}C NMR (100 MHz, $CDCl_3$) δ 21.5, 122.7, 129.7, 141.2, 150.8. HRMS (EI) calcd for $C_{14}H_{14}N_2$ 210.1157, found 210.1150.

4,4'-bis(bromomethyl)azobenzene (6.11)[25]

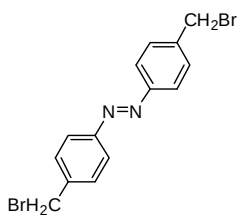

A mixture of **6.5** (0.82 g, 3.9 mmol), N-bromosuccinimide (2.14 g, 12 mmol) and benzoyl peroxide (50 mg, 0.21 mmol) in CCl_4 (50 mL) was heated at reflux for 6 h. The succinimide formed was separated by filtration of the hot mixture and washed with hot CCl_4. The organic phase was washed with hot water (2×30 mL), dried (Na_2SO_4) and concentrated *in vacuo*. The residue was recrystallized from CCl_4 and from butan-2-one to yield **6.11** as orange crystals (0.44 mg, 1.2 mmol, 31%). ^{1}H NMR (400 MHz, $CDCl_3$) δ 4.56 (s, 4H), 7.54 (d, J = 8.8 Hz, 4H), 7.89 (d, J = 8.4 Hz, 4H); ^{13}C NMR (125 MHz, $CDCl_3$) δ 32.7, 123.4, 129.9, 140.8, 152.2.HRMS (EI) calcd for $C_{14}H_{12}N_2Br_2$ 369.9327, found 369.9307.

4-bromomethyl-4'-methylazobenzene (6.12)[25]

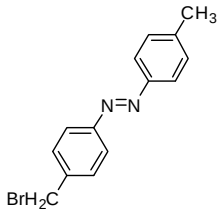

A mixture of **6.5** (0.29 g, 1.39 mmol), N-bromosuccinimide (0.25 g, 1.4 mmol) and benzoyl peroxide (10 mg, 0.042 mmol) in CCl_4 (20 mL) was heated at reflux for 2 h. The succinimide formed was separated by filtration of the hot mixture and washed with hot CCl_4. The organic phase was washed with hot water (2×30 mL), dried (Na_2SO_4) and concentrated *in vacuo*. The crude product was purified by flash chromatography (SiO_2, *n*-pentane : dichloromethane = 5 : 1). followed by recrystallization from EtOH to give orange crystals (95 mg, 0.33 mmol, 24%). ^{1}H NMR (400 MHz, $CDCl_3$) δ 2.44 (s, 3H), 4.56 (s, 2H), 7.32 (d, *J* = 8.4 Hz, 2H), 7.53 (d, *J* = 8.4 Hz, 2H), 7.83 (d, *J* = 8.4 Hz, 2H), 7.88 (d, *J* = 8.0 Hz, 2H); ^{13}C NMR (125 MHz, $CDCl_3$) δ 21.5, 32.8, 122.9, 123.1, 129.76, 129.84, 140.2, 141.9, 150.7, 152.4. HRMS (ESI) calcd for $C_{14}H_{13}N_2Br$ 289.03349, found 289.03333

Azophenyl-*p*-*N*,*N*`-dimaleimide (6.13)[34]

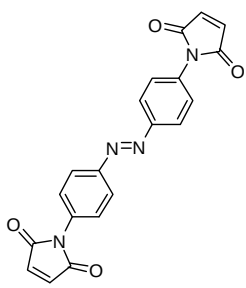

4,4`-Diaminoazobenzene (1 g, 4.71 mmol) was dissolved in dimethylformamide (DMF) (20 mL) and added to a solution of maleic anhydride (2.5 g, 25.5 mmol) in DMF (3 mL). After 1.5 h, the precipitated brown crystals were filtered, dried, and dissolved in acetic anhydride (200 mL) and sodium acetate (6 g, 73.2 mmol). The liquid was decanted, and its volume reduced under vacuum to 50 mL. Ice (~200 g) was added to the solution, and after 2 h the crystals were collected and washed with water. The crude product was purified by flash chromatography (SiO_2, *n*-heptane : EtOAc = 1 : 1) followed by recrystallyzation from dioxane/EtOH 1/1 to give orange crystals (0.49 g, 1.32 mmol, 28%). ^{1}H NMR (400 MHz, $CDCl_3$) δ 6.90 (s, 4H), 7.58 (d, *J* = 8.0 Hz, 4H), 8.04 (d, *J* = 8.0 Hz, 4H). ^{13}C NMR (100 MHz, $CDCl_3$) δ 123.7, 126.2, 133.6, 134.4, 151.2, 169.1. HRMS (EI) calcd for $C_{20}H_{12}N_4O_4$ 372.0859, found 372.0849.

6.6.3 ProOmpA labeling

ProOmpA (3 mg/ml) in 8 M urea and 50 mM Tris/HCl, pH 7 was treated with 1 mM tris-(2-carboxyethyl) phosphine (TCEP) for 30 min at room temperature and subsequently incubated with 2 mM fluoresceine-5-maleimide for 1 h at room

temperature, and recovered by trichloric acid precipitation as described elsewhere.[39]

6.6.4 Crosslinking of the lateral gate in SecY

IMVs (1 mg of protein/ml) were incubated for 2 h at 37 °C with a 10 mM solution of 4,4'-bis(bromomethyl)-azobenzene in DMSO at a final concentration of 0.1 to 1 mM. To test the efficiency of the crosslinking, IMVs were treated with 1 mg/ml OmpT in 50 mM Tris/HCl pH 7 and 0.1 % Triton X100 for 30 min at 37 °C. Samples were analyzed by SDS-PAGE (12% acrylamide) and coomassie brilliant blue staining. The intensity of the band at 37 KDa corresponding to the crosslinked SecY was compared to the intensity of the band corresponding to untreated SecY, in the presence or in the absence of the protease OmpT.

6.6.5 Translocation assays

In vitro translocation reactions (50 µl) were performed at 37 °C as described previously [41] using a solution containing 20 µg/ml of SecA, 32 µg/ml of SecB, 1 µg of urea-denaturated fluorescein-labeled proOmpA, 10 mM phosphocreatine and 50 mM creatine kinase in a buffer consisting of 50 mM Tris/HCl, pH 7, 30 mM KCl, 0.5 mM bovine serum albumin (BSA), 10 mM DTT and 5 mM $MgCl_2$. IMVs were added to a final concentration of 0.2 mg/ml. Reactions were started by adding 2 mM ATP and stopped after 10 min by chilling on ice. Samples were treated with proteinase K (1 mg/ml) for 30 min on ice, precipitated with 10% (w/v) TCA, washed with ice cold acetone and analyzed by 12% SDS-PAGE and fluorescent imaging using a Roche Lumi-Imager F1. Prior to translocation and to induce *cis-trans* isomerisation of the azobenzene unit, IMVs containing the SecY-**6.11** conjugate were irradiated with UV light (λ_{max}=365 nm, dose 150 mJ/cm^2) using a Select^{TM}XLE-1000 UV Crosslinker (Spectroline Corporation) or with visible light using a white light source for the same length of time. To prevent light-induced switching during translocation, the samples were protected from light sources during experiments.

6.6.6 ATPase assay

ProOmpA stimulated ATPase activity of SecA assay was performed as previously described[42, 43]. Briefly, the assay uses a solution of malachite green and ammonium

molybdate to detect the level of inorganic phosphate resulting from the enzymatic hydrolysis of ATP after 10 min of translocation reaction.

6.7 References

(1) Browne, W. R.; Feringa, B. L. *Annu. Rev. Phys. Chem.* **2009**, *60*, 407-428.
(2) Barrett, C. J.; Mamiya, J. I.; Yager, K. G.; Ikeda, T. *Soft Matter* **2007**, *3*, 1249-1261.
(3) van den Heuvel, M. G. L.; Dekker, C. *Science* **2007**, *317*, 333-336.
(4) Hess, H.; Bachand, G. D.; Vogel, V. *Chem. Eur. J.* **2004**, *10*, 2110-2116.
(5) Volgraf, M.; Gorostiza, P.; Numano, R.; Kramer, R. H.; Isacoff, E. Y.; Trauner, D. *Nat. Chem. Bio.* **2006**, *2*, 47-52.
(6) Kocer, A.; Walko, M.; Bulten, E.; Halza, E.; Feringa, B. L.; Meijberg, W. *Angew. Chem. Int. Ed.* **2006**, *45*, 3126-3130.
(7) Kocer, A.; Walko, M.; Meijberg, W.; Feringa, B. L. *Science* **2005**, *309*, 755-758.
(8) Blobel, G. *ChemBioChem* **2000**, *1*, 87-102.
(9) Driessen, A. J. M.; Nouwen, N. *Annu. Rev. Biochem.* **2008**, *77*, 643-667.
(10) van den Berg, B.; Clemons, W. M.; Collinson, I.; Modis, Y.; Hartmann, E.; Harrison, S. C.; Rapoport, T. A. *Nature* **2004**, *427*, 36-44.
(11) Zimmer, J.; Nam, Y. S.; Rapoport, T. A. *Nature* **2008**, *455*, 936-U32.
(12) Tsukazaki, T.; Mori, H.; Fukai, S.; Ishitani, R.; Mori, T.; Dohmae, N.; Perederina, A.; Sugita, Y.; Vassylyev, D. G.; Ito, K.; Nureki, O. *Nature* **2008**, *455*, 988-U72.
(13) du Plessis, D. J. F.; Berrelkamp, G.; Nouwen, N.; Driessen, A. J. M. *J. Biol. Chem.* **2009**, *284*, 15805-15814.
(14) Rau, H. In *Photoisomerization of azobenzenes;* Rebek, J. F., Ed.; Photochemistry and Photophysics; CRC Press: Boca Raton, **1990**.
(15) Zhang, F. Z.; Sadovski, O.; Woolley, G. A. *ChemBioChem* **2008**, *9*, 2147-2154.
(16) Fortin, D. L.; Banghart, M. R.; Dunn, T. W.; Borges, K.; Wagenaar, D.; Gaudry, Q.; Karakossian, M. H.; Otis, T. S.; Kristan, W. B.; Trauner, D.; Kramer, R. H. *Nature Methods* **2008**, *5*, 331-338.
(17) Banghart, M.; Borges, K.; Isacoff, E.; Trauner, D.; Kramer, R. H. *Nature Neuroscience* **2004**, *7*, 1381-1386.
(18) Zhang, J.; Wang, S. C.; Lee, C. T. *J. Phys. Chem. B* **2009**, *113*, 8569-8580.

(19) Pozhidaeva, N.; Cormier, M. E.; Chaudhari, A.; Woolley, G. A. *Bioconjug. Chem.* **2004**, *15*, 1297-1303.
(20) Renner, C.; Moroder, L. *ChemBioChem* **2006**, *7*, 869-878.
(21) Woolley, G. A. *Acc. Chem. Res.* **2005**, *38*, 486-493.
(22) Garcia-Amoros, J.; Martinez, M.; Finkelmann, H.; Velasco, D. *J. Phys. Chem. B* **2010**, *114*, 1287-1293.
(23) Lamarre, L.; Sung, C. S. P. *Macromolecules* **1983**, *16*, 1729-1736.
(24) Shirota, Y.; Moriwaki, K.; Yoshikawa, S.; Ujike, T.; Nakano, H. *J. Mater. Chem.* **1998**, *8*, 2579-2581.
(25) Guo, Q. P.; Zhong, Z. K. *Mater. Sci. Eng. C* **2000**, *7*, 91-98.
(26) Blank, M.; Soo, L. M.; Wassermann, N. H.; Erlanger, B. F. *Science* **1981**, *214*, 70-72.
(27) Wassermann, N. H.; Erlanger, B. F. *Chem. Biol. Interact.* **1981**, *36*, 251-258.
(28) White light was used for irradiation experiments. Literature examples show that white light or ambient daylight are good approximations for visible light ($\lambda > 400$ nm).Vollmer, M. S.; Clark, T. D.; Steinem, C.; Ghadiri, M. R. *Angew. Chem. Int. Ed.* **1999**, *38*, 1598-1601. See also ref. 26.
(29) Harvey, A. J.; Abell, A. D. *Bioorg. Med. Chem. Lett.* **2001**, *11*, 2441-2444.
(30) Prakash, H.; Shodai, A.; Yasui, H.; Sakurai, H.; Hirota, S. *Inorg. Chem.* **2008**, *47*, 5045-5047.
(31) Caamano, A. M.; Vazquez, M. E.; Martinez-Costas, J.; Castedo, L.; Mascarenas, J. L. *Angew. Chem. Int. Ed.* **2000**, *39*, 3104-3107.
(32) Based on our results, under the measurement timescales and conditions, the thermal stability of the switch is sufficient to obtain reproducible on-off switching of the translocation event. Additionally, a structurally similar azobenzene switch containing CysGly-dipeptide at the para-positions has been reported recently (See ref. 30) It served as a ligand in DNA-cleavage experiments which were performed at 37°C, the same temperature as our translocation experiments. The authors report thermal stability under their reaction conditions.
(33) Concerning the photostationary states upon irradiation with UV and visible light, it has to be noted that examples for photostationary states where 100% *cis*-form is present are rare. Generally, *trans*:*cis* ratios in the photostationary state range from 50:50 to 10:90 upon UV-irradiation. The incomplete *trans*-to-*cis* photostationary state is probably the reason for the additional

translocation compared to the wild-type protein. A structurally similar azobenzene switch containing CysGly-dipeptide at the para-positions has been reported recently (see ref. 30) which is a good model of our protein/azobenzene system. The authors report 70-80% trans-form in the trans-rich photostationary state upon irradiation of the *cis* form with visible light. Although the mother compound we used, 4,4'-dimethylazobenzene, has a *trans*:*cis* ratio of 20:80 at the photostationary state upon irradiation with 366 nm light (see also ref 28) the stabilization of the *cis*-form of azobenzenes is often observed when functionalized with peptide chains, leading to higher *cis*-content in the photostationary state. Literature examples of related systems report that irradiation with UV-light allow reversible switching between a *trans*:*cis* ratio of 0:100 to 70:30 (or higher). (See refs. 28-31).

(34) Kamenjicki, M.; Asher, S. A. *Macromolecules* **2004**, *37*, 8293-8296.
(35) Cabelli, R. J.; Chen, L. L.; Tai, P. C.; Oliver, D. B. *Cell* **1988**, *55*, 683-692.
(36) Weiss, J. B.; Ray, P. H.; Bassford, P. J. *Proc. Natl. Acad. Sci. U. S. A.* **1988**, *85*, 8978-8982.
(37) Kramer, R. A.; Dekker, N.; Egmond, M. R. *FEBS Lett.* **2000**, *468*, 220-224.
(38) Tomkiewicz, D.; Nouwen, N.; van Leeuwen, R.; Tans, S.; Driessen, A. J. M. *J. Biol. Chem.* **2006**, *281*, 15709-15713.
(39) de Keyzer, J.; van der Does, C.; Driessen, A. J. M. *J. Biol. Chem.* **2002**, *277*, 46059-46065.
(40) Crooke, E.; Brundage, L.; Rice, M.; Wickner, W. *EMBO J.* **1988**, *7*, 1831-1835.
(41) Cunningham, K.; Wickner, W. *Proc. Natl. Acad. Sci. U. S. A.* **1989**, *86*, 8630-8634.
(42) Lill, R.; Cunningham, K.; Brundage, L. A.; Ito, K.; Oliver, D.; Wickner, W. *EMBO J.* **1989**, *8*, 961-966.
(43) Henkel, R. D.; Vandeberg, J. L.; Walsh, R. A. *Anal. Biochem.* **1988**, *169*, 312-318.

Summary

The application of organic chemistry to create molecular and supramolecular systems that undergo switching processes has inspired the design of numerous systems that can be cycled between states through the application of various stimuli. A key theme has been the construction of chemical systems that mimic dynamic functions of macroscopic machines with the ultimate goal of creating molecular systems that can perform useful work.

This thesis focuses on the synthesis of light-driven molecular rotary motors and azobenzene switches and the study of their dynamic behaviour in confined environments. Confining such molecules at interfaces potentially allows for gaining control over different interfacial phenomena through the control of (sub)molecular motion.

Molecular motors based on overcrowded alkenes are a unique group of organic molecules that are able to undergo repetitive unidirectional rotation (Scheme 1). The unidirectional rotation around the central double bond (axis) is fuelled by light and heat energy and consists of two photochemical *cis/trans* isomerisations each followed by thermal helix inversion steps (Scheme 1).

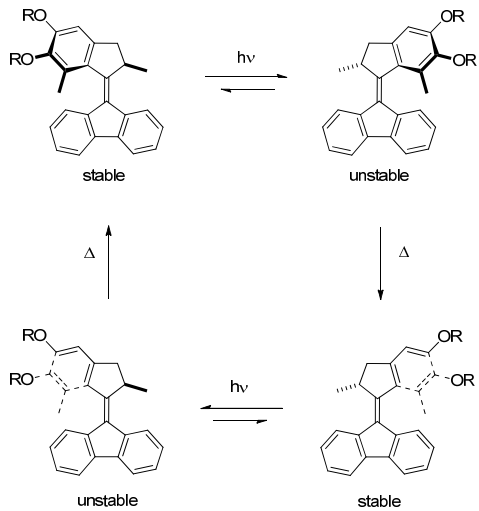

Scheme 1 The four step rotary cycle of light-driven molecular motors described in this thesis.

In order to harness the collective motions of rotary motors to perform useful tasks, it is expected that surface-confined systems will be the most relevant as these provide the opportunity to gain more order compared to solution-phase systems and minimize Brownian motion.

Two different types of surface-bound molecular rotary motors can be distinguished: azimuthal and altitudinal. In azimuthal motors the axis of rotation is perpendicular to the surface, while in altitudinal it is parallel to the surface (Figure 1).

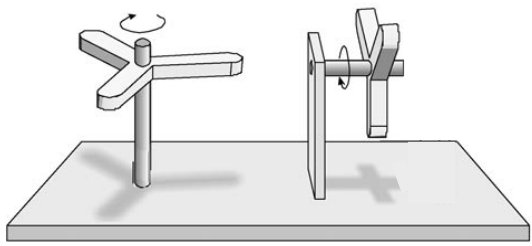

Figure 1 Left: Azimuthal rotation - the rotary axis is perpendicular to the surface; Right: Altitudinal rotation - the rotary axis is parallel to the surface.

Azimuthal rotation has been realized earlier experimentally in a monolayer of molecular motors on quartz and gold surfaces. However, molecular motors rotating in an altitudinal orientation relative to a surface (Figure 2, right) may have a larger impact on the construction of functional interfaces compared to the azimuthal versions. It is easy to envision altitudinal motors bearing different functional groups which could be exposed or buried in the interface upon isomerization. As a result of repetitive isomerization steps, reversible control over wettability, adhesion, friction or transport could be gained.

In the field of rotary motors, the major focus of our research was on the construction of self-assembled monolayers (SAMs) of altitudinal molecular motors and on the study of the dynamic behaviour of the surface-bound system. We synthesized molecular motors with a range of anchoring functions for different surface attachment strategies (Figure 2a). These include alkoxysilane-based coupling to quartz and silicon surfaces and interfacial 1,3-dipolar cycloadditions with a pre-formed organic coating containing terminal azides and alkynes. We found that the Cu-catalyzed 1,3-dipolar cycloaddition reaction provides a versatile approach to attach molecular motors to surfaces and is suitable for routine use to prepare such systems (Figure 2b).

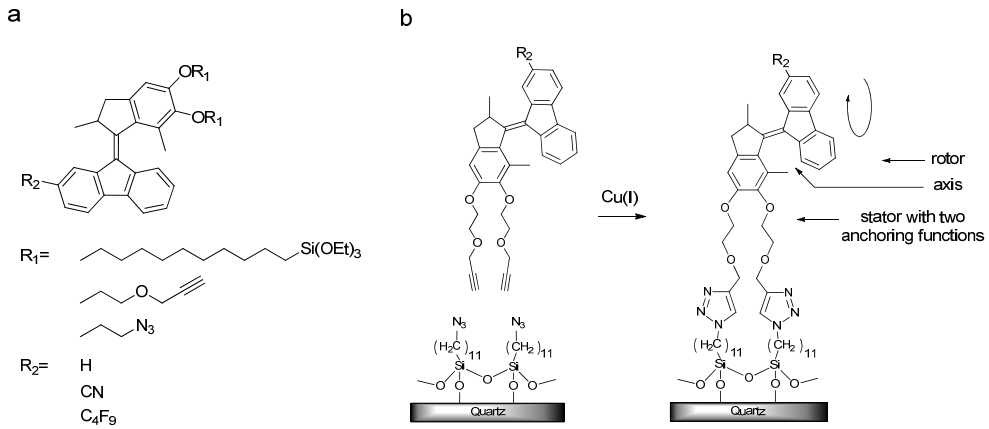

Figure 2 (a) Molecular motors with different substituents synthesized for controlled altitudinal rotation on solid surfaces. (b) Attachment of altitudinal motors to quartz surfaces *via* Cu-catalyzed interfacial 1,3-dipolar cycloaddition.

Surface-bound motors were found to undergo photochemical and thermal isomerizations consistent with unidirectional rotation in solution. In order to gain insight on the effect of surface attachment on the dynamic behaviour of the motors, we performed kinetic measurements on the surface-bound ensemble. We found that confinement at a surface reduces the rate of the thermal isomerization process. The rate of thermal isomerization was also dependent on the surface coverage of the motors. Additionally, from the kinetic measurements on motor films attached to quartz surfaces at least two half-lives could be derived that corresponds to at least two processes involved in the thermal step. This finding is pointing to significant intermolecular interactions between motors, effecting rotary speed. Both one and two-legged motors were attached to surfaces. The kinetics of thermal isomerization was not affected by the valency of attachment, indicating that the changes in kinetics from solution to surface systems are related to interactions between the surface-bound motors. These results contribute to a better understanding of the rotary cycle while the motor is confined at a surface and ultimately to the construction of interfaces with tailored properties. Furthermore, the first examples of altitudinal motors with a functionalized rotor part have been synthesized. The incorporation of functional groups onto one side of the rotor will allow for more advanced interfaces to be constructed in which surface properties can be reversibly transformed and patterned with photons.

In a collaborative effort we investigated the possibilities to interface photoswitches with biological systems. In nature, many proteins synthesized in the cell have to cross or be incorporated into lipid bilayers. In bacteria, a membrane protein channel, SecYEG, together with a motor protein, SecA, accomplishes this task. In order to reversibly photoregulate protein transport across the channel, azobenzene switches (Scheme 2) were synthesized and confined in the inner space of a transmembrane pore *via* covalent cross-linking.

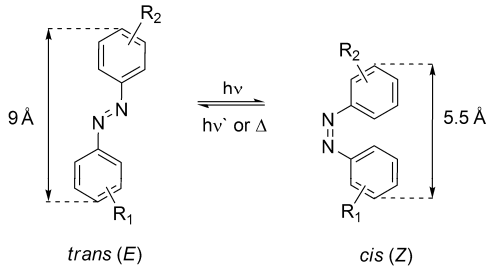

Scheme 2 Photoisomerization of azobenzenes. The large geometrical change could be used to control protein transport across a transmembrane channel by light.

We were able to show that through the reversible *cis/trans* photoisomerization of the switches the translocation event could be reversibly regulated. When the switches were in the extended *trans* geometry translocation could occur, while in the photoinduced *cis* geometry the azobenzenes dramatically reduced the translocation activity.

This research represents a step forward in the direction of a biological system with added functionality, with potential applications in structural biology research that benefits from external control of conformational changes without perturbation of the system.

Samenvatting

De toepassing van organische chemie in het ontwerp van moleculaire en supramoleculaire systemen die als schakelaars functioneren heeft geleid tot de ontwikkeling van talloze systemen die tussen meerdere toestanden kunnen schakelen door middel van verscheidene stimuli. Een belangrijk thema is de constructie van chemische systemen die de dynamische functies van macroscopische machines simuleren, met als uiteindelijk doel het maken van moleculaire systemen die werk kunnen verrichten.

Dit proefschrift richt zich op de synthese van door lichtaangedreven moleculaire motoren en azobenzeen schakelaars, en het bestuderen van de dynamische functies in een omgeving waar de bewegingsvrijheid van de moleculen beperkt is. Door deze moleculen op oppervlakken te plaatsen kan er controle worden verkregen over verschillende processen die zich hier afspelen door de controle over de beweging van (een deel van) de moleculen.

Moleculaire motoren die zijn gebaseerd op sterisch gehinderde alkenen zijn een unieke groep organische moleculen die een aangedreven draaibeweging rond een koolstof-koolstof binding kunnen verrichten. De rotatie rond de centrale dubbele binding (de rotatie-as) wordt aangedreven met behulp van licht en warmte en bestaat uit twee *cis/trans* isomerisaties, beiden gevolgd door een helix-inversie (Schema 1).

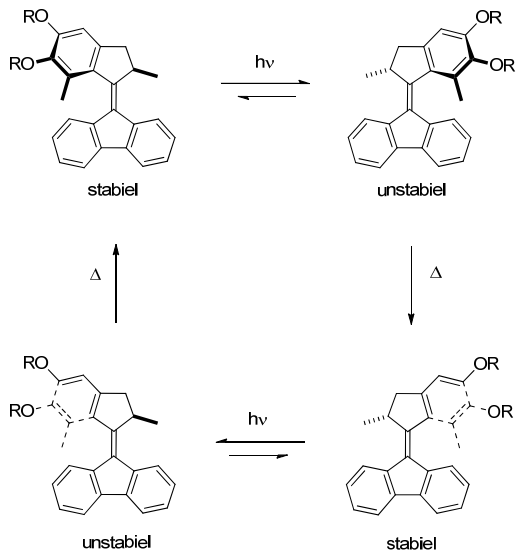

Schema 1 De vier stappen in één rotatie van een licht-aangedreven moleculaire motor, zoals beschreven in dit proefschrift.

Systemen die functioneren op oppervlakken bieden perspectief om de collectieve rotatie van meerdere motoren te gebruiken om nuttig werk te verrichten in vergelijking met systemen in oplossing, omdat er meer orde in het systeem is, en invloed van de Brownse beweging wordt geminimaliseerd.

Er kan onderscheid gemaakt worden tussen twee verschillende types oppervlakte-gebonden moleculaire motoren: horizontaal roterend en verticaal roterend. In de horizontale motoren staat de rotatie-as haaks op het oppervlak en bij de verticale motoren parallel aan het oppervlak (Figuur 1).

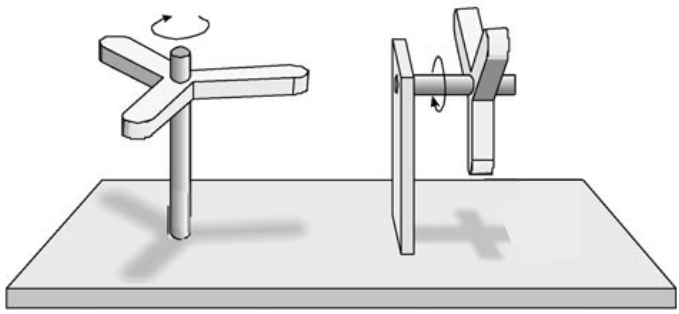

Figuur 1 Links: Horizontale rotatie – the rotatie-as staat haaks op het oppervlak. Rechts: Verticale rotatie – de rotatie-as ligt parallel aan het oppervlak.

Horizontale rotatie is eerder gerealiseerd in monolagen van moleculaire motoren op kwarts- en goudoppervlakken. In het geval van verticale rotatie heeft de beweging mogelijk een groter effect bij het creëren van functionele oppervlakken. Dit kan bijvoorbeeld door verticale motoren te voorzien van functionele groepen die ofwel uitsteken, ofwel teruggetrokken worden in de monolaag afhankelijk van de toestand van de motor. Op deze manier kan controle worden verkregen over de bevochtiging, adhesie en wrijving van oppervlakken, en mogelijk transport over oppervlakken.

Binnen het onderzoeksgebied van de moleculaire motoren stonden twee onderwerpen centraal: het maken van zelf-assemblerende monolagen van verticaal roterende moleculaire motoren en het bestuderen van de dynamische eigenschappen van deze systemen. Er werden verscheidene moleculaire motoren gesynthetiseerd met een scala aan groepen om deze aan verschillende oppervlakken te koppelen (Figuur 2a). Zo werd er gebruikt gemaakt van alkoxysilanen voor koppeling aan kwarts- en siliciumoppervlakken, en 1,3-dipolaire cycloadditie

reacties voor koppelingen aan oppervlakken die werden gecoat met alkynen en azides. Vooral de koper-gekatalyseerde 1,3-dipolaire cycloadditie bleek een veelzijdige methode om moleculaire motoren aan oppervlakken te koppelen (Figuur 2b).

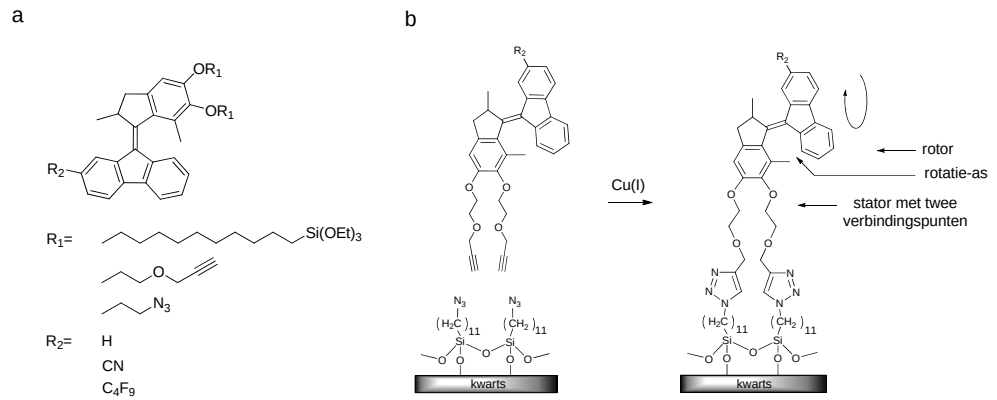

Figuur 2 Gesynthetiseerde moleculaire motoren met verschillende substituenten voor gecontroleerde verticale rotatie op oppervlakken. (b) Koppeling van verticale georienteerde motoren aan kwartsoppervlakken met een koper-gekatalyseerde 1,3-dipolaire cycloadditie.

Moleculaire motoren die aan een oppervlak waren gekoppeld ondergaan fotochemische en thermische isomerisatie in overeenstemming met rotatie in oplossing. Om meer inzicht te krijgen in het effect van het verbinden aan het oppervlak op de dynamische processen van de motoren werden kinetiek metingen verricht. De beperkte bewegingsvrijheid van de moleculen aan het oppervlak bleek de thermische isomerisatie te vertragen. De snelheid van deze thermische isomerisatie hangt ook af van de dichtheid van de motoren op het oppervlak. Uit kinetiekmetingen op het oppervlak bleek dat er minstens twee processen plaatsvinden in de thermische stap, met twee verschillende halfwaardetijden. De motoren werden zowel met een als met twee verbindingen aan het oppervlak gekoppeld. De snelheid van de thermische isomerisatie hangt niet af van het aantal verbindingen met het oppervlak, wat erop duidt dat de verandering in de kinetiek wordt veroorzaakt door interacties tussen de moleculen die aan het oppervlak zijn gekoppeld. Deze resultaten dragen bij aan een beter begrip van de rotatie van motoren aan oppervlakken en uiteindelijk aan de constructie van oppervlakken waarvan de eigenschappen kunnen worden gereguleerd. Ook werden de eerste verticale motor met gefunctionaliseerde rotors gesynthetiseerd. Door functionele

groepen aan één kant van de rotor te zetten, kunnen meer geavanceerde oppervlakken worden gemaakt, waarvan de eigenschappen reversibel kunnen worden veranderd en lokaal kunnen worden aangepast met licht.

In samenwerkingsverband werd de mogelijkheid onderzocht om met licht schakelbare moleculen te verbinden met biologische systemen. In de natuur worden vele eiwitten gemaakt in de cel die door een lipide bilaag moeten worden getransporteerd, of erin moeten worden opgenomen. In bacteriën wordt dit gedaan door een membraaneiwit, SecYEG, samen met een motoreiwit, SecA. Om het transport van proteïnes door het kanaal te kunnen reguleren met licht werden gefunctionaliseerde azobenzenen (Schema 2) synthetiseerd en met een covalente binding vastgemaakt een de binnenkant van een transmembraan kanaal.

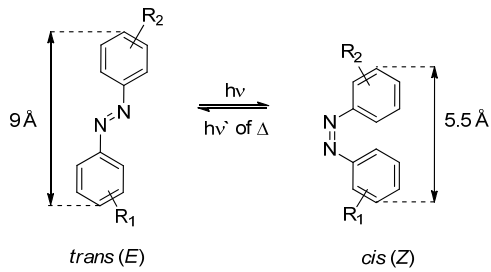

Schema 2 Fotoisomerisatie van azobenzenen. De grote geometrische verandering kan worden gebruikt om het transport van proteïnes door kanalen in een membraan te reguleren.

Er werd aangetoond dat de translocatie inderdaad kon worden gecontroleerd door *cis*/*trans* isomerisatie van deazobenzeen schakelaars. In de meer uitgestrekte *trans* configuratie kan translocatie plaatsvinden, maar in de meer samengetrokken *cis* configuratie was de translocatie sterk verminderd.

Dit onderzoek is een nieuwe stap in de richting van biologische systemen met toegevoegde functionaliteit. Potentiele toepassingen liggen in onderzoek in de structuurbiologie, waar externe controle over conformatieveranderingen zonder het systeem te verstoren van nut is.

Összefoglaló

Napjainkban a szintetikus szerves kémia egyik fókusz-területe olyan molekuláris és szupramolekuláris rendszerek létrehozása, melyek szerkezete valamilyen külső kémiai vagy fizikai hatás alkalmazásával irányítottan változtatható. Ezek közül is kiemelten érdekesek azok, amelyek képesek a makroszkópikus világból ismert gépek működését utánozni, igy várhatóan alkalmazhatók feladatok végrehajtására, munkavégzésre.

Tézisem tárgya az említett típusú rendszerek közül a fény-hajtású molekuláris rotációs motorok és azobenzol típusú molekuláris kapcsolók szintézise és fizikai-kémiai tulajdonságainak vizsgálata olyan környezetekben, ahol a molekulák egészének szabad mozgása gátolt. Molekuláris motorok és kapcsolók különböző határfelületekhez való rögzítése lehetőséget nyújthat határfelületi jelenségek befolyásolására a rögzített molekulák egyes szerkezeti egységeinek irányított mozgása révén.

A túlzsúfolt alkéneken alapuló rotációs motorok olyan szerves molekulák, melyek folyamatos egyirányú forgómozgásra képesek (Ábra 1). A központi kettős kötés, mint tengely körüli egyirányú rotaciót fény és hő energia biztosítja két fotokémiai *cisz-transz* izomerizációs és az ezeket követő termális hélix inverziós lépéseken keresztül.

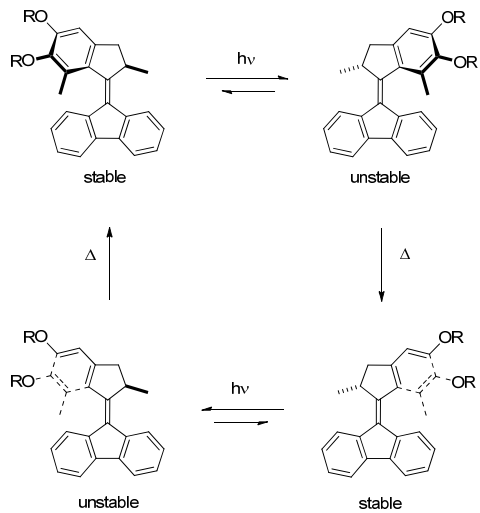

Ábra 1 Molekuláris motorok két fotokémiai és az azokat követő két termális izomerizációs lépésből álló rotációs mozgásának folyamatábrája.

Annak érdekében, hogy a rotációs motorok együttes forgómozgását munkavégzésre lehessen használni, határfelületekhez való kapcsolásuk az egyik legígéretesebb mód, mivel ezáltal a rendszer rendezettsége az oldatbelihez képest növelhető, a molekulák rendezetlen mozgása (Brown-mozgás) lecsökkenthető.

A felületekhez kötött molekuláris rotációs motoroknak két típusa különböztethető meg: horizontális és vertikális (Ábra 2). Horizontális motorok esetében a forgástengely a felületre merőleges, míg vertikális motoroknál a tengely párhuzamos a felülettel.

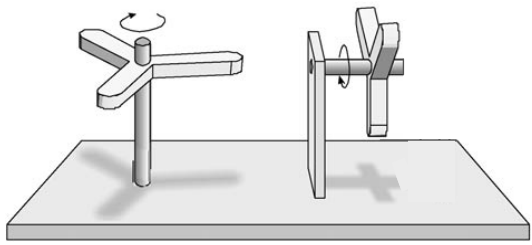

Ábra 2 Horizontális (bal) és vertikális (jobb) rotáció.

A korábban már előállított horizontális motorokhoz képest a vertikális elrendezésnek nagyobb szerepe lehet változtatható tulajdonságú határfelületek létrehozásában. Könnyen elképzelhető például, hogy a felülethez kötött verikális motor rotor eleméhez kapcsolt funkciós csoport az izomerizációs ciklusok során változtatja a felülethez viszonyított helyzetét, ezáltal ciklikusan változtatva a határfelület természetét. Ilyen módon, megfelelő funkciós csoportot választva, határfelületek nedvesedési, adhéziós vagy transzport sajátságai befolyásolhatók illetve iranyítottan változtathatók.

A motor molekulákkal kapcsolatos vizsgálatok középpontjában monomolekuláris rétegeik szilárd felületeken való létrehozása és a molekulák dinamikus sajátságainak ilyen környezetben való tanulmányozása állt. Ezen vizsgálatokhoz különböző felületkötő funkciós csoportokkal rendelkező molekulákat allítottunk elő, mely lehetővé tette különféle felületkapcsolási módozatok vizsgálatát (Ábra 3a). Ezek közé tartozik például alkoxiszilánok kapcsolása kvarc vagy szilícium (Si/SiO_2) felületekhez illetve határfelületi 1,3-dipoláris cikloaddíciós reakciók acetilén- és azid-terminális monomolekuláris rétegeken. Kísérleteink során a réz-katalizálta 1,3-dipoláris cikloaddíciós reakciókat találtuk a legreprodukálhatóbbnak valamint rutinszerűen

alkalmazhatónak bizonyultak a vizsgálandó molekuláris rétegek létrehozásában (Ábra 3b).

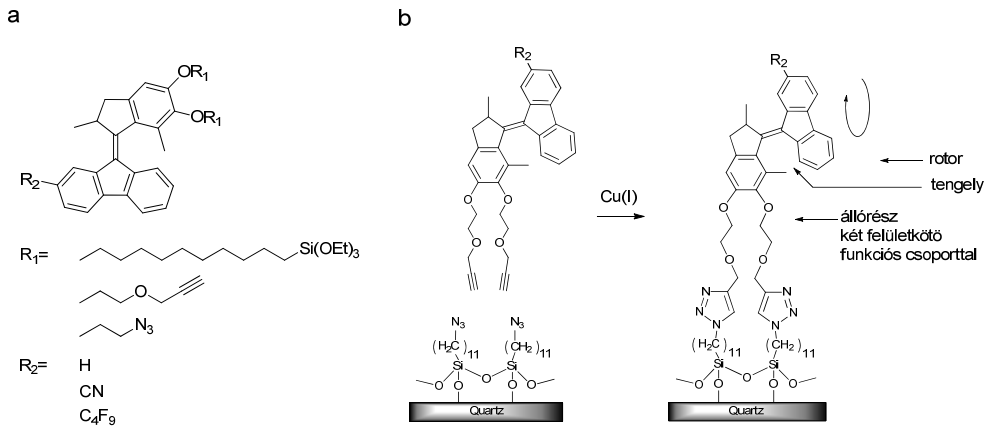

Ábra 3 (a) Vizsgálatainkhoz előállított, különböző felületkötő funkciós csoportokkal rendelkező molekuláris motorok. (b) Vertikális motorok rögzítése szilárd felületekhez réz-katalizálta határfelületi 1,3-dipoláris cikloaddíciós reakcióval.

Megmutattuk, hogy a szilárd felületekhez kapcsolt motor molekulák megőrzik motor funkciójukat, aktívak maradnak a fotokémiai és termális izomerizációs lépésekben. Kinetikai vizsgálatokkal tanulmányoztuk, hogyan befolyásolja a felülethez való kapcsolás a molekulák dinamikus sajátságait. Méréseinkből kiderült, hogy a rögzítés hatására a termális lépés sebessége lecsökken az oldatban mérthez képest, valamint, hogy a sebességcsökkenés mértéke függ a felületi borítottságtól. Az oldatban mérhető elsőrendű kinetikával ellentétben a felületi kinetikai mérésekből legalább két félélettartam ($t_{1/2}$) számítható, ami erős intermolekuláris kölcsönhatásokra utal, melyek hatással vannak a rotáció sebességére. Vizsgáltuk hogyan hat a rotációs mozgás sebességére a molekulákban talalható felületkötő funkciós csoportok száma. Az egy illetve két kovalens kötéssel rögzített motorok kinetikájában nem találtunk jelentős eltérést, ami arra utal, hogy a felülethez kötött és az oldatbeli molekulák kinetikájában mutatkozó eltérések elsősorban a felületen jelenlévő intermolekuláris kölcsönhatásoknak köszönhetők.Ezek az eredmények hozzájárulnak a szilárd felületekhez rögzített molekuláris motorok izomerizációs folyamatainak mélyebb megértéséhez, ezáltal változtatható tulajdonságokkal rendelkező határfelületek létrehozásához.

Előállítottuk továbbá az első, funkcionalizált rotorral rendelkező vertikális motorokat. Funkciós csoportok beépítése a forgó szerkezeti egységbe kulcsfontosságú a határfelületi jelenségek befolyásolásában.

Együttműködés keretében vizsgáltuk molekuláris kapcsolók biológiai rendszerekbe való beépítésének lehetőségét. Az élő sejtekben szintetizált fehérjék nagy része beépül vagy áthalad lipid kettősrétegeken. Baktériumokban ezeket a feladatokat a SecYEG csatornafehérje-komplex és a SecA motorfehérje együtt látják el.
Azobenzol típusú fotokémiai kapcsolókat (Ábra 4) állítottunk elő és építettünk be a csatornafehérjékbe abból a célból, hogy a csatornán keresztül zajló fehérjetranszportot reverzibilisen fotokémiailag tudjuk szabályozni.

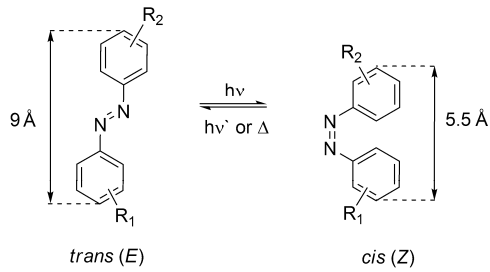

Ábra 4 Azobenzolok fotoizomerizációja. A számottevő méretváltozást kihasználva csatornafehérjék transzlokációs aktivitása befolyásolható.

Megmutattuk, hogy az azobenzol molekulák reverzibilis fotokémiai *cisz-transz* izomerizációját kihasználva a fehérjetranszport tetszés szerint ki-be kapcsolható.
A kapcsoló kiterjedtebb *transz* állapotában a fehérjék áthaladása a csatornán akadálytalan volt, míg az UV-besugárzással előállított *cisz* izomer jelenléte nagymértékben lecsökkentette a transzlokációs aktivitást.

Acknowledgements

Five years of research in the field of tiny rotary motors have come to an end. The Big Wheel, however, keeps on turning. But before the next round, I have to thank to a number of people without whom this thesis could not have been realized.

First of all I am grateful to my promoter, Professor Ben Feringa, who gave me the opportunity to be a member of his research group in the past years. Ben, thank you for your support and guidance and for providing such a working atmosphere that makes one feel that everything thinkable is also possible.

Most of the work described in this thesis was done with the help and collaboration of other members of the group. Mike, Greg, Tatiana and Francesco, it was a pleasure to work with you. I have to thank Wesley, Greg and Beatriz also for the critical reading of all the chapters and for their support throughout the writing period.

I would like to thank the members of my reading committee, Prof. Petra Rudolf, Prof. Gerard Roelfes and Prof. Arnold Driessen for their corrections and suggestions to improve my thesis.

Gratitude goes to all my past and present lab-mates who we were daily pushing the limits of science with, Arjen (acknowledged for the dutch translations also), Alex, Mahthild, Tatiana, Jos, Greg, Angela, Tony, Tom, Jiawen, Kuang-Yen, Martín, Sander, Norbert, Santi, Syuzi, Peter, Tibor, Steve, Robert.

I would like to thank all the past and present members of the Motor-Subgroup and the whole Feringa-group also for all their contributions to my research.

There are a number of people whose support was extended far beyond the professional and whose presence was very important to me. Tatiana, Greg, Angela, Mike, Barbara, Beatriz, Johan and Takashi thank you for all the time we have spent (and will spend) together.

Arjen and Tatiana, thank you for being my paranymphs!

A warm greeting goes to my office and coffee-mates Tom, Hans, Tony, Greg and Angela.

Finally, to all the group members and non-group members (especially Gerald and Antonio) for all the shared time either spent on science or other activities, thank you so much!

Csaba, az elmúlt öt év egyik nagy pozitívuma, hogy megismertelek! Durván nagyra értékelem a barátságod, arról nem is beszélve hogy mennyien kevesebbek lennénk egy-egy előhívó tankkal és rodinál szagú fürdőszobával nélküled.

Köszönet az otthoni barátoknak, hogy megmaradtak annak ellenére, hogy az utóbbi időben kevesebbet voltam otthon. Norbi és Kornél külön is köszönöm a szupportot! A családom folyamatos támogatása nélkülözhetetlen volt az utóbbi öt év során. Anyuka, Apuka, Mári, Gyerek, nélkületek ez nem lett volna lehetséges! Köszönöm!

Thank you!

g